Strathclyde Institute of Pharmacy and Biomedical Sciences
(SIPBS)

Investigating IKKα-dependent NF-κB signalling and gene regulation in a human bone cancer cell line

Kirsty Tinto

A thesis submitted in the fulfilment of the requirements for the degree of Doctor of Philosophy

November 2025

This thesis is the result of the author's original research. It has been composed by the author and had not been previously submitted for examination which has led to the award of a degree.

Signed: 

Date: 7.11.25

Acknowledgements

Throughout my PhD, I have been supported, inspired, and have ultimately loved my PhD project. The simultaneous guidance and freedom which my supervisors have given me has enabled me to flourish as an early career researcher. Therefore, I would first like to jointly thank my supervisors, Professor Robin Plevin and Dr Margaret Cunningham. By teaching me in my undergraduate degree with surmountable passion for their subjects, my supervisors have been instrumental in inspiring me to carry out further higher education. From believing in me enough to put me forward for the AJ Clark award, which funded my PhD, to the mock interviews and to the never-ending time which they make for me, they have completely changed my life. The scones along the way have been a delight, too! I know my case is a rarity, in that I have two devoted supervisors who are not only invested in my project, but invested in furthering my abilities, too. Both of you have given me support in countless opportunities, including conferences, meetings, training courses, supervising my first undergraduate summer students, a research trip to India and conferences in York, Harrogate and Germany. The fact that you both love your jobs and see them as a vocation rather than a chore has made my project so exciting. Thank you for the academic growth, personal growth, supervision, and friendship which I have gained, all down to you both. Making students feel like equals rather than part of a hierarchy is something you both do brilliantly, and it's because of people like you that research culture remains enjoyable and inspiring. As I finish my PhD, I know the science and experiences to come will be exciting, but ultimately, this will be bittersweet, as I realise this will bring an end to the best opportunity of my life.

Secondly, I would like to thank the British Pharmacological Society (BPS) for awarding me the AJ Clark studentship, which made this work possible. The support did not stop at funding my PhD; the BPS also nominated and funded me to represent the UK in the PhD Student Competition at the Dutch Medicines Days 2025. This incredible opportunity allowed me to present my bone cancer research during Bone Cancer Awareness Week, an experience that was both professionally rewarding and personally meaningful. I am deeply grateful to the BPS for their continued encouragement, recognition, and investment in my development as an early career pharmacologist.

I would like to thank Marco Bonfanti, my peer and close friend. Collaborating on RNA-sequencing and learning how to use ColabFold with you has been a blast, and I believe we have been the biggest cheerleader for one another over the duration of both our PhD journeys. Additionally, working with my close friend, Maheen Wahid has been an exceptional experience, and I would like to thank you, Maheen, for your endless support, contagious excitement for science, and friendship. I would also like to thank my friend Mohammad Farhan, who not only did I collaborate with on ideology to further my understanding, but we have worked closely in the laboratory since day one. A special thank you is attributed to those who have been involved in helping my initial understanding of techniques and those cheering me on; Professor Gwyn Gould for assisting me with subcellular fractionation, and Geraldine Buitrago and Grace Whelan with their help with RT-qPCR. Throughout this journey, I made some very special and supportive friends. For that, I would like to thank Graeme MacKenzie, Gayle McNeill and Nicholas Klemm, for the laughs and support when I needed it most.

Added post-viva: I would also like to sincerely thank the examination committee: internal examiner Ben Pickard, external examiner Sonia Rocha, and convener Trevor Bushell, whose thoughtful discussion, professionalism and genuine interest in the topic made the viva a thoroughly positive experience.

Before this PhD even began, there were people who believed I could achieve this (long before I believed it myself). I would like to thank Dr Mike Piper from BioAscent, and Sue Carr and Amy Cotterill from V Formation, because without your support and belief in me as a first-year undergraduate student and giving me an opportunity when all I had was a willingness to learn and a dream, I don't believe I would have ever gotten to PhD level. Mentoring me every summer during my undergraduate and giving me the opportunity of an internship in the drug discovery sector is an opportunity I will never forget. Thank you, Mike for encouraging me to apply for a PhD when I didn't believe in my own abilities. I will forever be grateful for your support and mentoring.

I would like to extend a special mention and massive thanks to Lily Tosh and Jia Wu, third year undergraduate students that I had the pleasure to mentor in the laboratory over the course of the summers in 2024 and 2025. This provided me with my first day-to-day supervisory experience, which has been undoubtedly transformative for my own academic and supervisory development.

My PhD research journey also took me beyond borders, and I'm incredibly grateful for the time I spent in the Systems Immunology Laboratory in New Delhi, India, under the supervision of Dr Soumen Basak. Thank you for hosting me for 2 months and teaching me EMSA techniques. Thank you to Naveen Sheoran, Bhawna Chugh and Nainy Goel, who made being away from home alone for the first time so much easier. The plethora of tools and insight which you provided me with has not only helped to form collaborations but also has given me clarity into the NF-κB dimers which form following exposure to a range of pro-inflammatory stimuli. Additionally, thank you to the University of Glasgow for the Mac Robertson travel scholarship which funded the entirety of this opportunity.

Last but certainly not least, I would like to extend a very special thank you to my friends and family. To my mum, daddy, Jillian and Luke, you have been so supportive over the past three years. To my mum especially, thank you for making sure I never went hungry and making my lunches for the past few years (and the previous 22 years before that), having your support took so much stress away. Being the first person in my family to undertake a PhD has certainly been a learning curve for us all, but we have learned and grown together along the way. Your patience, encouragement and curiosity in trying to understand what I actually do have meant the world to me, and I couldn't have done it without you. A very special thank you to Poppy (Pops), the dog that changed my life when she joined our family one month after I started my undergraduate degree. She has been the happiest part of my life ever since, bringing comfort, joy and a wagging tail through every stage of this journey. To Maria and Emily, I don't think I would have got through this experience without you. Thank you for always sharing my excitement, my highs, my lows and everything in between. You are my soul sisters. Emily, thank you for being there at two of the most important milestones of my PhD: receiving the AJ Clark studentship and submitting my PhD thesis. Ellis, thank you for being a constant ray of sunshine to me throughout my college, undergraduate and PhD journey, and for your unwavering positivity, encouragement and friendship over the years.

Finally, thank you to my boyfriend Paul, from supporting my high school endeavours, to college, an undergraduate degree and now a PhD, your support means more to me than words can say. The constant belief that you have in me, and the support through every chapter of this thesis, and every chapter of life does not go unnoticed.

***"Of course I'm happy, I'm a scientist."* – Robin Plevin, 2023**

Training and presentations

Oral presentations:

- **World congress pharmacology 2023, Glasgow, July 2023:** "TAK1 is an upstream kinase of IL-1β-mediated p100 phosphorylation."
- **6th European NF-kappaB Workshop in Marburg, Germany, September 2024:** "Bad to the bone: An RNA-sequencing study depicting the role of IKKα in osteosarcoma."
- **Dutch Medicines Days, 2025, Netherlands, October 2025:** "Bad to the Bone: IKKα in osteosarcoma."

Poster presentations:

- ECR day at Glasgow university, Glasgow, February 2023.
- Strathclyde Institute of Pharmacy and Biomedical Sciences Postgraduate research day, Glasgow, February 2023
- EMBL-EBI, Hinxton, November 2023
- Pharmacology 2024, Harrogate, December 2024

Education Funding Awarded

CULTURE-GAPS in STEM (£18.5k) - awarded January – December 2025

- Co-Principal Investigator on the CULTURE-GAPs in STEM project, which acquired internal pilot funding through the University of Strathclyde's Wellcome Trust Collaborative Research and Innovation Cultures award. I contributed to the proposal design and development, particularly the revisualisation of centrally collated ED&I data, and led the "inclusive assessment" focus group, using creative digital tools to explore student experiences and support inclusive teaching practices. I also supported the departmental ethics committee (DEC) application drafting for this project and facilitated other focus groups/workshops as part of this project.

British Pharmacological Society Education grant (£2000) - awarded 2024

- Co-Principal Investigator on a project developing a sustainable, low-cost human body-on-a-chip model and laboratory to support multi-level pharmacology education.

University of Strathclyde's AWERB award (£2000) - awarded 2024

- Co-Principal Investigator on an internally funded project to support a feasibility study exploring the use of killifish as a sustainable alternative model for multimorbidity research and life science education to replace the use of rodent models currently in use.

Scottish Alliance for Food (SCAF) pump priming award (£5000) - awarded 2024

- I was a Research Co-investigator on a collaborative project between SIPBS (Cunningham lab) and Swansea University (Murray lab), studying dietary fat and sex-based differences in muscle ageing using the African turquoise killifish model. The long-term goal is for this model to be established at Strathclyde for the purposes of research and teaching.

Other Research funding acquired

Bone Cancer Research Trust pilot grant (£35k) - awarded 2025

- This pilot project grant was awarded to my PhD supervisors. I contributed key findings from my PhD research and assisted in writing and completing costing for the proposal. A link to the details of our project: Researcher spotlight: Robin Plevin | Bone Cancer Research Trust

British Pharmacological Society Summer Intern Vacationship (£1480 / £1850) - awarded 2024 & 2025

- I co-wrote the research proposal and served as day-to-day supervisor for two third-year undergraduate students, Lily Tosh and Jia Wu, during 8- and 10-week vacationships in the Plevin laboratory (SIPBS, 2024 and 2025), gaining experience in project design, leadership and supervision.

University of Glasgow's MacRobertson Travel Grant (£4,000) - awarded 2023

- This grant allowed me to undertake a three-month laboratory research placement in Dr Soumen Basak's laboratory, a leading group studying IKKα and NF-κB, at the National Institute of Immunology (NII) in Delhi, India, from January to March 2024.

British Pharmacological Society AJ Clark Studentship (~£50k) and Strathclyde Student Excellence Award - awarded 2022

- I was awarded the competitive AJ Clark Studentship (British Pharmacological Society) and Strathclyde Excellence Award (~£100k total), jointly funding my PhD; the AJ Clark is awarded to one UK Pharmacology student annually through a competitive interview process.

Abstract

IKKα, a serine threonine kinase, has been consistently implicated in a range of inflammation-driven diseases and cancers. In the non-canonical NF-κB signalling pathway, IKKα homodimers function in a NIK-dependent manner, activated by specific members of the TNF superfamily, including lymphotoxin and LIGHT ligands. This activation led to phosphorylation of p100 and the subsequent nuclear translocation of the NF-κB heterodimer RelB:p52. In contrast, the canonical NF-κB pathway was activated by various pro-inflammatory stimuli, including IL-1β and TNFα, and relies on TAK1 and the IKK complex, which is composed of IKKβ, IKKα, and IKKγ. Within this complex, IKKβ plays the dominant role in initiating downstream signalling, resulting in phosphorylation and degradation of IκBα and the nuclear translocation of NF-κB dimers, most commonly p50:p65. Previously, a novel signalling mechanism was described in which IL-1β induced early p100 phosphorylation in an IKKα-dependent manner in human endothelial cells and in the human osteosarcoma cell line U2OS. In this study, potential downstream functions of p100 phosphorylation in this context were investigated, and IL-1β-mediated IKKα-dependent genes were explored.

This study validated that IL-1β-induced p100 phosphorylation is IKKα-dependent in U2OS cells and demonstrated the selectivity of two novel first-in-class IKKα inhibitors, SU1261 and SU1349, and their ability to inhibit this signalling mechanism. Furthermore, the TAK1 inhibitor 5Z-7-oxozeaenol was used to show that both p100 and IKKα phosphorylation was inhibited by TAK1 inhibition, and that this occurred at lower inhibitor concentrations than those required to suppress IKKβ-dependent responses following IL-1β stimulation. Additionally, downstream p52 and p65 nuclear translocation were inhibited at concentrations similar to those affecting IKKβ-dependent responses rather than IKKα-dependent responses, indicating that p52 was not downstream of IKKα-mediated p100 phosphorylation in this model. Therefore, Illumina RNA sequencing was subsequently employed to identify potential IKKα-dependent genes using IKKα CRISPR-Cas9 knockdown in this signalling system. These included the gene encoding the osteoclast-associated receptor, OSCAR, which was upregulated in the transcriptomic analysis of IKKα CRISPR-Cas9 knockdown cells but downregulated at the mRNA level following IKKα siRNA knockdown independently of IL-1β stimulation. The gene encoding DHCR7, a key enzyme in the final stages of cholesterol biosynthesis, was found to be downregulated in IKKα CRISPR-Cas9 knockdown U2OS cells in the transcriptomic data, which was also IL-1β-independent. This was subsequently validated by RT-qPCR, where similar findings were observed in both CRISPR-Cas9 and siRNA knockdown models. Red Amplex cholesterol assays also demonstrated significantly lower cholesterol production in IKKα CRISPR-Cas9 knockdown U2OS cells compared with wild-type cells. A smaller, yet significant, reduction in cholesterol production was also observed in IKKα siRNA-transfected cells compared with non-targeting siRNA controls. Finally, this study examined IL-1β-mediated expression of CXCL5, a gene associated with osteosarcoma progression and osteogenesis that contributed to tumour development. CXCL5 mRNA expression was shown to be IKKα-dependent using both IKKα CRISPR-Cas9 and siRNA knockdown methods, as well as through treatment with the novel IKKα inhibitors (SU1261 and SU1349). IL-1β-mediated CXCL8 expression was also investigated as a comparator, as it is a well-established as an IKKβ-dependent gene. Like CXCL5, CXCL8 binds to CXCR2 to promote osteogenesis and osteosarcoma progression. This study demonstrated that IKKα inhibition increased IL-

1β-induced CXCL8 mRNA expression, whereas treatment with a dual IKKα/IKKβ inhibitor, SU1266, decreased both CXCL5 and CXCL8 expression.
Collectively, this study provided the first evidence that CXCL5 is a bona fide downstream IKKα-dependent target and provides an insight into several other functional roles which IKKα may play in osteosarcoma cells.

Abbreviations

ACKR Atypical chemokine receptor

ARD Ankyrin Repeat Domain

BAFF B cell activating factor

BMSC Bone Marrow Stromal Cells

CAFs Cancer-Associated Fibroblasts

CRSP8 Mediator of RNA polymerase II transcription unit 27

c-Rel Cellular homolog of the avian retroviral oncoprotein v-Rel

DHCR7 7-DeHydroCholesterol Reductase

ECM Extracellular matrix

GCSRG Cholesterol Synthesis-Related Gene signature

GPCR G-protein coupled receptor

GRR Glycine Rich Repeat

HCT116 Human Colorectal Carcinoma 116

IKKα IKappaB Kinase alpha

IKKβ IKappaB Kinase beta

IKKγ IKappaB Kinase gamma

IL-1α Interleukin-1 alpha

IL-1β Interleukin-1beta

IL-2 Interleukin-2

IL-3 Interleukin-3

IL-6 Interleukin-6

IL-7 Interleukin-7

IL-8 Interleukin-8

IL-9 Interleukin-9

IL-10 Interleukin-10

IL-11 Interleukin-11

IL-12 Interleukin-12

IL-13 Interleukin-13

IL-15 Interleukin-15

IL-17 Interleukin-17

IL-18 Interleukin-18

IL-19 Interleukin-19

IL-20 Interleukin-20

IL-33 Interleukin-33

IP_3 Inositol trisphosphate

JNK c-Jun N-terminal Kinase

LPS Lipopolysaccharide

LZ Leucine Zipper

Maspin Mammary Serine Protease Inhibitor gene

MDSC Myeloid-derived suppressor cell

MEF Mouse embryonic fibroblast

NET Neutrophil extracellular trap

NF-κB Nuclear Factor-kappa B

NIK Nuclear Factor-kappa B-inducing kinase

OS Osteosarcoma

OSCAR Osteoclast-associated Receptor

RANK Receptor Activator of Nuclear Factor-kappa B

RANKL Receptor Activator of Nuclear Factor-kappa B Ligand

RHD Rel Homology Domain

RT-qPCR Real time quantitative polymerase chain reaction

Runx2 Runt-related transcription factor 2

SQLE Squalene Epoxidase

STAT3 Signal Transducer and Activator of Transcription 3

TAK1 Transforming growth factor-β-activated kinase 1

TAD Transactivation domain

TAM Tumour-associated macrophage

TAN Tumour-associated neutrophil

TM7SF2 Transmembrane 7 Super Family member 2

TME Tumour microenvironment

TMT Tandem Mass Tag

TNF-α Tumor necrosis factor alpha

Treg Regulatory T cell

UVB Ultraviolet B

BioRender Disclaimer

Illustrations and schematics throughout this thesis were created with BioRender.com with figures exported under a paid subscription (PI: Dr Margaret Cunningham; Lab Licence Seat: Miss Kirsty Tinto, University of Strathclyde). License numbers will be provided for any publications arising from this thesis.

Table of Contents

List of Figures

List of Tables

Chapter 1

General Introduction

Disclaimer: *Some figures within this chapter are adapted from my published article: [Tinto K, Cunningham M, Plevin R. Double trouble: cytosolic and nuclear IKKα in cancer. Open Biol. 2025. 15240375] under CCBY 4.0.*

1.1 The cellular basis of cancer

Cancer is a complex and multifactorial disease characterised by the uncontrolled growth and spread of abnormal cells (1). There are various environmental, genetic and lifestyle factors which contribute to cancer initiation. These include exposure to tobacco smoke, ultraviolet radiation, obesity, diet, chronic inflammation and infection. Between 80-90% of malignant tumours are suspected to be mediated by carcinogens, exemplifying the significant effects of external environmental factors on cancer incidence (2). These factors promote the accumulation of genetic mutations and epigenetic alterations which drive carcinogenesis, a multistep process initiated by these molecular alterations resulting in oncogene activation and or tumour suppression gene deactivation (3, 4). For example, carriers of the BRCA2 or TP53 gene mutations are more likely to develop specific types of cancer including osteosarcoma (OS), leukaemia and soft tissue sarcoma (5). These genetic and epigenetic processes disrupt normal regulatory events which maintain tissue homeostasis. This is followed by uncontrolled cell division and or inhibition of cell cycle arrest and programmed cell death (6). This disruption first manifests as increased cell number, known as hyperplasia. This can develop into dysplasia, characterised by abnormal cell morphology, including increased nucleus/cytoplasm ratio, decreased cell polarity and increased mitotic activity (7). Dysplasia represents a pre-malignant state, where cellular changes become apparent, but abnormal cells have not yet invaded surrounding tissue. In cases of untreated pre-malignant states, dysplastic lesions can result in early stages of cancer, including carcinoma *in situ (8)*. Consequently, the malignant tumour can grow, and migrate into lymph nodes and local organs and eventually to distant organs resulting in systemic metastasis, which is responsible for approximately 90% of cancer-related deaths (9). This progression highlights the clinical need for detection and intervention methods during pre-malignancy to prevent subsequent development and tumour metastasis.

1.2 The increasing global burden of cancer

The International Agency for Research on Cancer collated data from 185 countries and estimated that approximately 19.3 million new cancer cases and around 10 million cancer deaths took place in 2020 alone, and this expected to increase by 47% to 28.4

million cases by 2040 (10). This increasing trend in cancer diagnoses has been noted the past few decades, with a 0.8% annual increase on average in both men and women from 1994 to 2018 (11). There are various factors which make cancer an important research focus, particularly in the present and future. As the aging population continues to rise, cancer incidence will naturally increase as age is a major cancer risk factor (12). Therefore, some of the projected increases in cancer diagnoses can be attributed to the aging population. Additionally, it is expected that socioeconomic factors will contribute to cancer progression and mortality in the future, as it is predicted that countries with low or medium socioeconomic development will experience higher incidence of various cancers (13). Despite extensive efforts to conduct research into cancer aetiology, including the production of expansive data and relevant signalling networks of genes and proteins (14), cancer remains the leading cause of death in 57 countries (15). Therefore, cancer has an undeniable burden on health globally. Additionally, cancer has the highest economic burden globally out of the 15 highest causes of mortality (16). To overcome the detrimental effect which cancer places on the economy and health, more research and treatment options are required.

1.3 The histological characteristics of cancer

The tissue origin plays a key role in the classification and biological behaviour of cancers. Therefore, cancers are broadly categorised into different histological subtypes depending on the specific tissues and cells which they arise from (17). This classification is important in diagnosis but also gives insights into the potential associated prognosis and treatment options. The major histological types include carcinomas, sarcomas, lymphomas, leukaemias, myelomas and a combination of these categories can result in a mixed histological type (18). Carcinomas arise from epithelial cells, while sarcomas develop in mesenchymal tissues including bone, and soft tissue, which account for approximately 20% and 80% of sarcoma cases, respectively (19, 20). Lymphomas and leukaemias originate from immune cells and cells within blood, respectively (21, 22). Myelomas develop from antibody-producing plasma cells in the bone marrow (23). Neuroendocrine tumours are another type of tumour with its own characteristics, which develop from neuroendocrine cells, have nerve cell and hormone-producing traits and originate from tissue of diverse origin

(24). However, neuroendocrine tumours have not been recognised as a distinct histological tumour subtype separate from other tumour types. An outline of the histological subtype classification and origin of these cancers is shown in Figure 1.1.

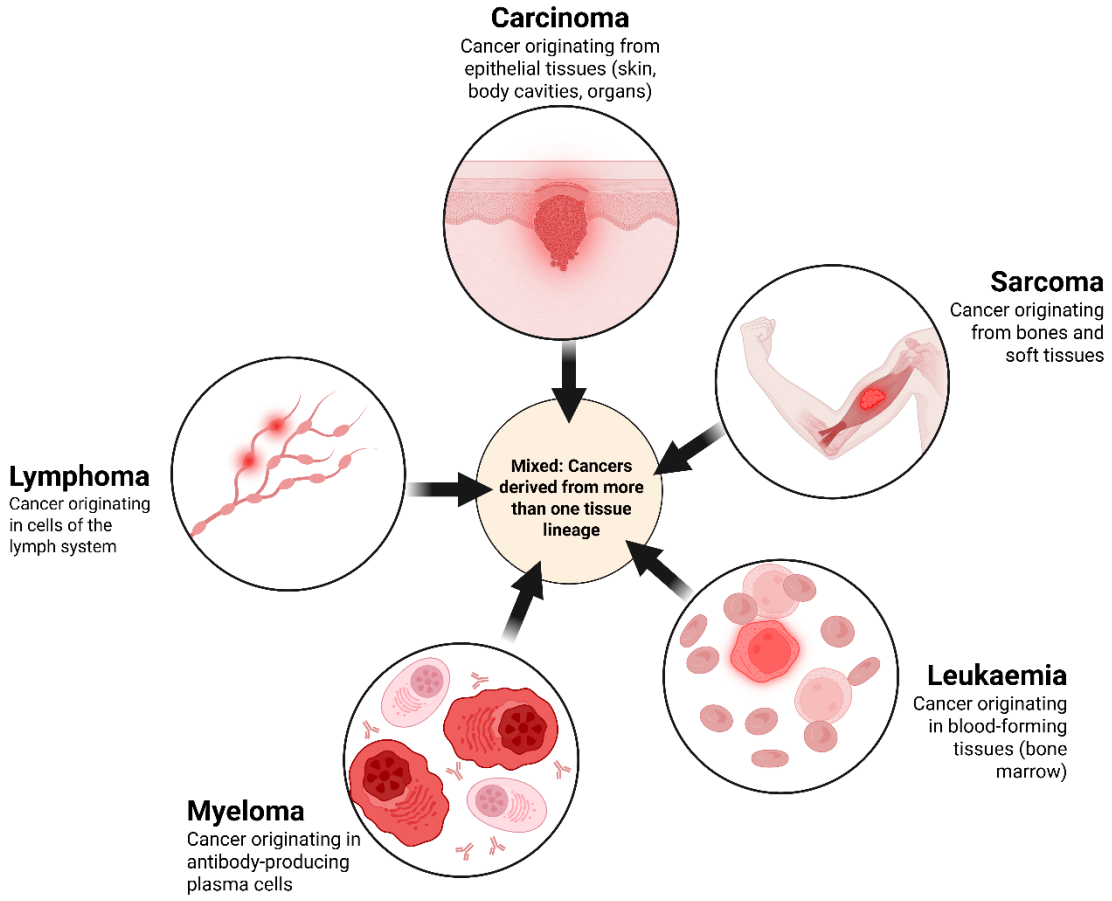

Figure 1.1. The histological types of cancer.
This schematic illustrates the primary histological classifications of cancer based on tissue of origin, including carcinoma, sarcoma, lymphoma, leukemia and myeloma. Figure created on BioRender.com.

1.4 The hallmarks of cancer

There are several hallmarks which initiate the complex and multifaceted processes involved in cancer development. Initially, the “hallmarks of cancer” was coined by Douglas Hanahan and Robert Weinberg in 2000 (25). This term was used to describe six essential capabilities which cancer cells utilise to promote cancer development: sustaining proliferative signalling, evading growth suppressors, resisting cell death,

enabling replicative immortality, inducing angiogenesis, and activating invasion and metastasis (25). In 2022, Hanahan proposed an additional two hallmarks of cancer and two enabling characteristics of cancer: reprogramming cellular metabolism and avoiding immune destruction, and genome instability and mutation and tumour-promoting inflammation, respectively (26). The eight characterised hallmarks of cancer are displayed in Figure 1.2.

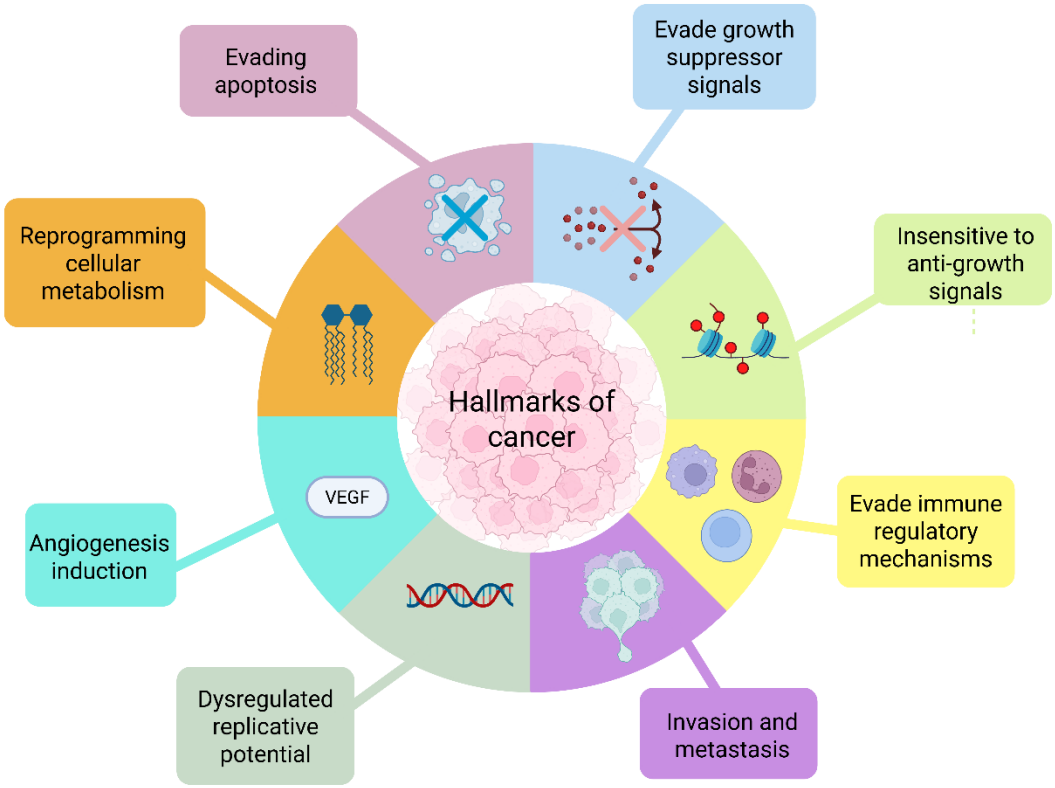

Figure 1.2. The hallmarks of cancer.
This schematic displays the currently recognised eight hallmarks of cancer, representing key biological capabilities acquired during tumour development. Figure created using Biorender.com, adapted from an original publication (27).

The eight hallmarks alongside the two enabling characteristics of cancer set a foundational framework to understand factors which rather than acting in isolation, operate collectively to shape cancer cell behaviour. In turn, these hallmarks contribute to the dynamic structure and function of the tumour microenvironment (TME).

1.5 An insight into the tumour microenvironment

Cancer cells cannot thrive in isolation; they exist within an intricate network of stromal, immune and extracellular-matrix components known collectively as the TME, which is essential for their survival, growth and progression (28). The TME plays a crucial role in cancer development. Within the TME, cancer cells recruit additional tumour-dependent stromal cells from surrounding tissue including endothelial cells, cancer-associated fibroblasts (CAFs), adipocytes and stellate cells (29). Blood vessels also contribute to the TME, as chronic hypoxia results in induction of VEGF and chemokines such as CXCL12, which directly promote tumour angiogenesis (30). Angiogenesis, the formation of new blood vessels, plays a continuous and vital role in physiological processes including bone remodelling, development, reproduction and wound healing (31). However, tumour cells develop a proangiogenic phenotype enabling them to promote dysregulated blood vessel formation (32). Due to tumour angiogenesis being a major driver in cancer development and metastasis, research efforts have explored the potential for utilising therapeutic drugs to downregulate tumour angiogenesis. Recently, anlotinib, a multi-tyrosine kinase inhibitor, was administered in combination with PD-L1/anti-PD-1 antibody immunotherapy treatments and shown to downregulate tumour angiogenesis in patients with high-grade serous ovarian cancer (33). The extracellular matrix (ECM) within the TME loses its normal physiological architecture in cancer contexts, as CAFs promote collagen and fibronectin deposition, which increases ECM stiffness (34). These modifications to the ECM enhance tumour cell proliferation, survival and invasion (34). Moreover, tumour-associated macrophages (TAMs) represent one of the most abundant immune cell types within the TME, which generally adopt M2-like characteristics, and release pro-tumourigenic mediators including IL-10, VEGF and TGF-β, which promote metastasis, immune evasion and angiogenesis (35). Collectively, several cell types including TAMs, endothelial cells and CAFs, shape the TME network by releasing chemokines and cytokines to promote an immunosuppressive environment where tumour growth can be maintained (36).

1.6 Chemokines in the tumour microenvironment

Chemoattractant cells produce a crucial subtype of small soluble secretory cytokines known as chemokines (8-12 kDa) which promote migration of several immune cells to the TME, which subsequently promote or inhibit tumour angiogenesis and metastasis (37, 38). The roles of chemokines are distinct, as different chemokines promote different immune cell types which can either support the immune response or elicit immunosuppressive functions. In the chemokine network, there are 50 chemokine ligands, 20 G-protein coupled receptor (GPCR) family members and four atypical chemokine receptors (ACKRs) (38-40). Conventional chemokine receptors couple to intracellular G-proteins and are typically found on immune cells, whereas ACKRs preferentially engage β-arrestin and are expressed on a broader range of cells, most notably endothelial cells (41). Consequently, ACKRs do not induce classical G-protein signalling but instead regulate chemokine levels through endocytosis, transcytosis, or degradation of their ligands (41).

Through binding to their cognate GPCRs, chemokines promote pro- or anti-tumorigenic effects by regulating immune cell trafficking and activity (38). Within the TME, dysregulated chemokine expression drives the infiltration of immunosuppressive cells such as regulatory T cells (Tregs), myeloid-derived suppressor cells (MDSCs), tumour-associated neutrophils (TANs), and tumour-associated macrophages (TAMs), which therefore supports tumour progression (38).

Chemokine ligands are classified into four subfamilies; C, CC, CXC and CX3C, which are distinctively identified by the sequence of conserved cysteine residues (42). The CXC chemokine subfamily has been particularly well studied in cancer, due to its central role in angiogenesis, immune cell recruitment and metastasis (43, 44). An outline of CXC chemokines, their respective receptors and the main purposes of the ligand-receptor signalling is depicted in (Table 1.1).

Table 1.1. A description of the CXC chemokine family, their specific receptors and the immune cell types which promote their production.

CXC Receptor	Main receptor purpose	Ligands	Immune cells which express CXC receptor	References
CXCR1	Neutrophil recruitment	CXCL6, CXCL8	Neutrophils, fibroblasts, vascular endothelial cells	(45-47)
CXCR2	Neutrophil recruitment	CXCL1, CXCL2, CXCL3, CXCL5, CXCL6, CXCL7, CXCL8	Neutrophils, fibroblasts, vascular endothelial cells, monocytes, natural killer cells, mast cells, endothelial cells	(45-47)
CXCR3	T cell migration	CXCL9 (Mig), CXCL10 (IP-10), CXCL11	Monocytes/macrophages, CD4+ T cells (mainly T helper type 1), CD8+ T cells, Treg cells, B cells, natural killer cells	(48-53)
CXCR4 (CD184)	Haematopoiesis	CXCL12, CXCL14	Dendritic cells, neutrophils, B cells, monocytes, CD4+ T cells (mainly T helper type 2), eosinophils	(54-59)
CXCR5	T cells/B cells	CXCL13	Treg cells, Th17 cells, B cells, follicular B helper T cells, macrophages, endothelial cells	(60-62)
CXCR6	T cells	CXCL16	Naïve CD8+ T cells (but does not appear to be important for CD8+ T cell priming/function), Memory CD4+ T cells, natural killer cells, natural killer T cells	(63-65)
CXCR7 (ACKR3)	T cells	CXCL11, CXCL12	CD4+ T cells, monocytes	(49, 54, 55, 66-68)
CXCR8 (GPR 35)	Monocytes	CXCL17	Monocytes	(69)

1.7 Bone Development and Remodelling

To understand how tumours arise or spread within the skeletal system, it is crucial to understand the unique and dynamic processes involved in healthy bone development and remodelling. Bone remodelling is a continuous and essential process to maintain optimal bone health. Bone remodelling is a tightly regulated process, influenced by genetic, environmental and hormonal factors (70). This process includes bone formation by osteoblasts, specialised mesenchymal cells which are situated within the bone marrow stroma and at periosteal surfaces (71). Bone remodelling also requires the degradation of old bone, which is mediated by osteoclasts predominantly derived from macrophages in the bone marrow (72). Crosstalk between osteoblasts and osteoclasts by direct cell-to-cell contact or indirect production of proteins aids bone homeostasis (73). However, dysregulated activation of osteoclasts can contribute inflammatory bone processes, including rheumatoid arthritis (74). Osteoclasts and osteoblasts have very distinct functions and characteristics, as osteoclasts originate from a haematopoietic stem cell lineage, whereas osteoblast differentiation is a multi-step process originating from mesenchymal stem cells. A description of cell differentiation leading to osteoclast and osteoblast cell types is highlighted in Figure 1.3.

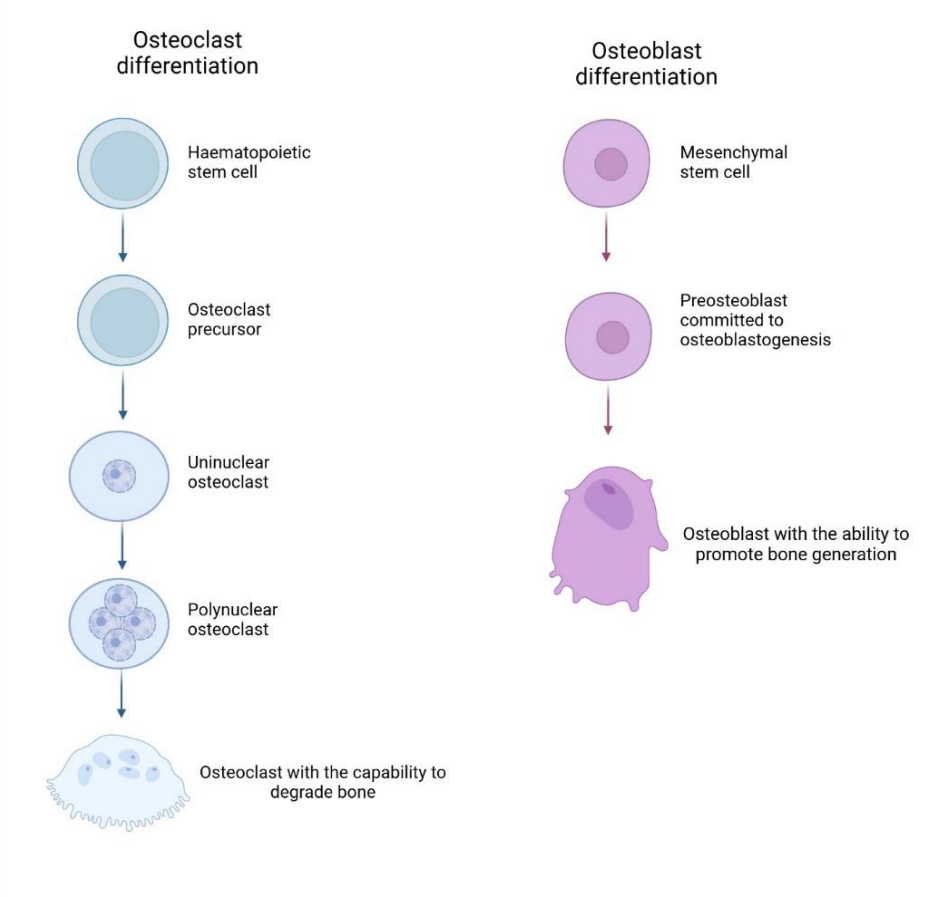

Figure 1.3. An outline of cell differentiation events leading to osteoclastogenesis and osteoblastogenesis.
Bone resorption cells, osteoclasts, originate from haematopoietic stem cells. Mesenchymal precursors can differentiate into eventual mature osteoblasts, which promote bone generation. Original figure created on BioRender.com with inspiration from (73).

1.8 Characterisation of osteosarcoma

When bone homeostatic processes become dysregulated, this can give rise to bone cancers. Bone cancers are rare but often are associated with having a poor prognosis and imposing detrimental effects on quality of life. OS is the most prevalent primary malignant bone tumour and is diagnosed in one to three individuals per million people every year worldwide (71, 75, 76). OS tumours are made up of osteoblast cells, promoting immature bone generation, resulting in disruption of bone homeostasis (71). Similarly, links have been demonstrated between OS and decreased osteoclastogenesis, where reduced osteoclastogenesis is more prominent in

chemoresistant OS patient samples (77). While most other cancers typically arise from a multi-step process including hyperplasia, dysplasia, carcinoma *in situ* and subsequent cancer invasion of tissues, primary OS does not have clearly defined premalignant lesions. Indeed, approximately 95% of OS cases arise as high-grade tumours with no known precursor lesions (78).

The bones frequently impacted by OS are long bones, including the humerus, femur and tibia (79, 80) as depicted in Figure 1.4. OS is marginally more common in males, and age-related incidence of OS is bimodal: the first peak is observed in 14-19 year-olds during puberty-related growth spurts with the majority of OS cases arising in individuals under the age of 25, and the second peak is detected in adults over the age of 65 (81, 82). There is a lack of research surrounding the bimodal nature of OS, and it is not well understood why these two age groups are predominantly affected by OS. However, an observation that can be made from these affected individuals is that OS preferentially affects those that are rapidly growing, while simultaneously targeting an age group where bone resorption is observed, associated with aging.

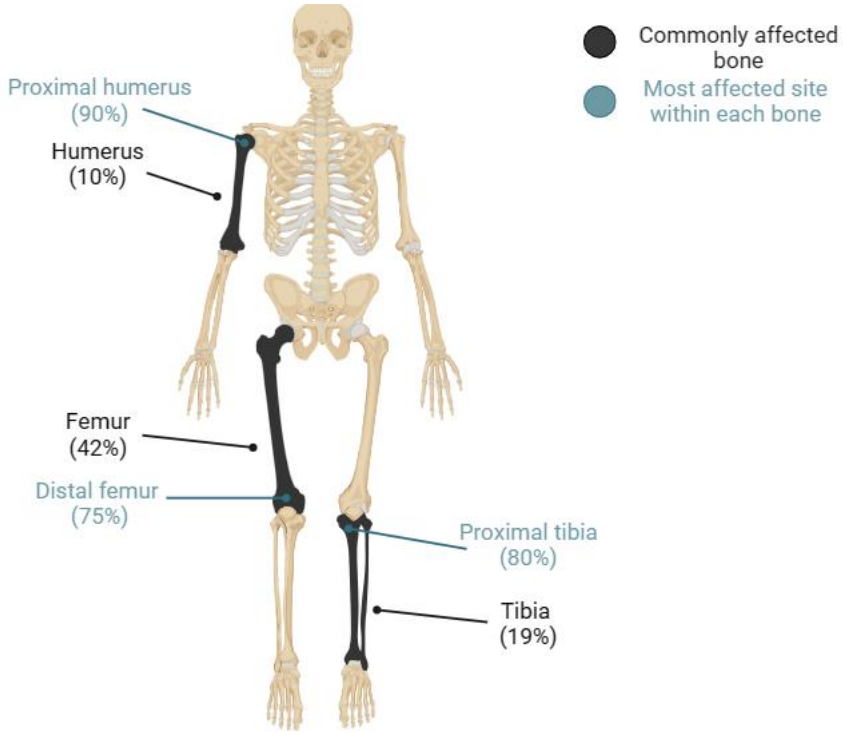

Figure 1.4. The commonly affected bones and specific sites in OS.
The proximal humerus, distal femur and proximal tibia as the most common sites of OS onset. Statistics used in this figure were obtained from (79). Figure created in BioRender.com.

The aetiology of OS is also not fully understood, but numerous research studies have been conducted to identify common factors which lead to poor prognosis. A meta-analysis study was conducted in 2020 collated information from 40 studies from the previous 10 years, including a total of 18126 patients which highlighted general themes affecting OS prognosis. Overall, this study identified several factors associated with poor prognosis including males, older in age, greater tumour size, tumour location being outwith extremities, proximal tumours, lack of response to chemotherapy, amputation surgery, and no surgical intervention (83). Additionally, in a study which utilised data from the Surveillance, Epidemiology, and End Results data base from 2008-2016, the 1-, 3- and 5-year survival rates following initial OS diagnosis were 87.3%, 67.2% and 58.0%, respectively (84). However, in another study which utilised data from Chinese patients under the age of 30 obtained between December 2012 and May 2019, the 5-year survival rates for nonmetastatic and metastatic OS patients were 52.1% and 2.6%, respectively (85). Additionally, OS is often a high-grade malignancy which is detected following lung metastases, which is observed in 74%

OS patients with metastases (86, 87). This demonstrates the poor prognosis for individuals with OS, particularly those with metastatic OS. OS is usually treated with surgical resection of the affected area and multi-drug chemotherapy which is successful in over 50% of patients (88). However, the result of surgical resection, and often amputation, can leave long-lasting negative effects on quality of life for adolescent patients, and improvement to the lack of treatment options and prognosis related to OS in the last 30 years have been marginal (89). The lack of targeted therapies and continued reliance on non-specific treatments like chemotherapy combined with the poor prognosis associated with OS demonstrates a clinical need for the discovery of novel therapeutic drug targets at a molecular level. This would further reduce the need for surgical resection, which can stunt growth and damage bones, a clear risk for OS patients, who are predominantly adolescents.

1.9 The TME in osteosarcoma

OS originates in bone and often arises during adolescent growth spurts, and therefore, certain features of its TME are uniquely shaped by these developmental and tissue-specific factors. The ECM is unique in bone cancers like OS, due to the mineralised bone tissue where OS arises. The increased stiffness of the ECM in OS promotes YAP/TAZ-dependent signalling, which is linked to OS development and metastasis (90). OS cells secrete increased matrix metalloproteinases including MMP-2 and MMP-9, which contribute to ECM remodelling, enabling metastasis, particularly to the lungs (91). Several components of the ECM in OS including increased collagen, fibronectin, laminin, and proteoglycans, promote OS development, metastasis and chemoresistance (92). Due to these factors, higher levels of collagens (collagen triple helix repeat containing 1 and collagen type I alpha 1 chain) are also correlated with an increase in mortality rate in OS (93). This makes signalling pathways involved in the ECM favourable pharmacological targets in OS.

The ECM acts as a reservoir to store chemokines, and tumour cells and stromal cells secrete chemokines to recruit immunosuppressive cells and promote metastasis. There are several chemokines which have been linked to OS progression, particularly CXCR1 and CXCR2 ligands. The first chemokine discovered was CXCL8 (IL-8), a

CXCR2 ligand. Since, CXCL3 and CXCL5 have been identified as the most and least potent CXCR2 ligands, respectively. Regardless, all CXCR2 ligands bind at low concentrations, considering the relatively high concentrations which would occur under pathophysiological responses observed in cancer. The CXCR2 axis is of particular interest in OS, as studies have demonstrated that CXCL5 expression is significantly increased in OS cell lines including U2OS cells, compared to non-cancerous osteoblast hFoB1.19 cells (94). Further, the study revealed that CXCL5 gene knockdown by siRNA in U2OS cells reduced U2OS cell infiltration and interestingly, overexpression of CXCL5 in hFoB1.19 cells resulted in increased U2OS cell infiltration (94). High CXCL5 mRNA expression and low CXCL5 mRNA expression in OS patients was linked to a difference in prognosis, with approximately 30% and 60% survival rate, respectively. This was further supported by a CXCL5-mediated effect on distant metastasis onset, which was reported in 10/18 (56%) OS patients with high CXCL5 expression and 4/20 (20%) OS patients with low CXCL5 expression.

CXCR1 and CXCR2 ligands also play a crucial role in lung metastasis in OS (95). Additionally, CXCL8 was found to upregulate OS progression in an OS cell line, MG-63, by increasing invasion and decreasing late-stage apoptotic activity (96). The CXCR2 axis in particular results in neutrophil recruitment, in particular tumourigenic N2 neutrophils and to date, several studies have demonstrated the key role of neutrophil extracellular traps (NETs) in enhancing metastasis in several cancers (97, 98). In the context of OS, a recent study identified 97 differentially expressed NETs-related genes between non-metastatic and metastatic OS patient tissue, therefore underpinning the importance of the CXCR2 axis in OS (99). The CXCR4 axis is also pivotal in the OS TME. Within the TME, cancer associated fibroblasts (CAFs) produce CXCL12 which preferentially binds to its highly conserved receptor, CXCR4, the most universally expressed G-protein coupled receptor (GPCR), or alternatively by binding to CXCR7, both of which are highly expressed on the surface of cancer cells and promote metastasis in several cancers (100-102). Additionally, previous meta-analysis studies have demonstrated a link between CXCR4 expression and poor prognosis in OS (103). Collectively, chemokines play a crucial role in the TME and ultimately enhance cancer development and metastasis.

1.10 Gene mutations in osteosarcoma

Like other cancers, OS is influenced by the hallmarks of cancer. However, different cancers are linked to distinct gene mutations, and some mutations can be either oncogenic or anti-oncogenic, depending on the cancer type and its location. OS is typically not associated with inherited genes, but instead, associated with epigenetic mutations due to radiation therapy or rapid cell proliferation (89, 104, 105). There are several studies which have highlighted where changes in gene expression, and gene mutations have been linked to OS onset and progression. For instance, mutations in the gene encoding tumour protein 53 (p53), typically a tumour suppressor, is the most mutated gene in OS. Mutations in other tumour suppressing genes have also been associated with promoting OS, including PTEN and retinoblastoma 1 (RB1) genes. Many of the defined epigenetic mutations and gene expression changes which have been linked to OS are summarised in Table 1.2.

Table 1.2. Gene expression changes and mutations in osteosarcoma.

Protein	Function	Prevalence
Tumour protein 53 (p53)	A tumour suppressor, p53 in its unaltered state is a negative modulator of osteoblastogenesis by downregulating Cbaf1, Osterix and Runx transcription factors (106). P53 is the most mutated gene in OS (107). However, studies have demonstrated lower numbers of secondary mutations when p53 is mutated in OS (108).	Gain of function mutations in p53 are observed in over 50% of OS cases (109).
Retinoblastoma 1 (RB1)	RB1 is a tumour suppressor gene which is altered in OS (108, 110).	RB1 mutations occur in 30-75% OS patients (111).
ATRX	Recurrent ATRX mutations have been associated with OS (112). Additionally, decreased ATRX expression is correlated with increased tumour growth, metastasis and NF-κB signalling in OS (113).	ATRX mutations which lead to a decrease in ATRX nuclear expression are found in 20-30% (114).
DLG2	DLG2 is an OS tumour suppressor, but DLG2 mutations enhance OS (112, 115).	DLG2 mutations have been found in 53% OS patients (116).
PTEN	PTEN acts as a tumour suppressor normally via negatively modulating the PI3K/AKT/mTOR signalling pathway, but decreased expression or gene mutations of PTEN result in amplified OS (112, 117).	PTEN is lost in 6-13% OS patients (118).
COPS3	COPS3 gene is upregulated in high-grade OS, and COPS3 mutations are also observed (112, 119).	An increase in COPS3 expression is observed in 31% OS cases (119).
PMP22	PMP22 mutations and increased PMP22 expression is associated with enhanced OS oncogenesis (112, 120).	Amplification of region 17p11.2~p12 containing PMP22 has been observed in 13-29% OS patients (121).
MAPK7	MAPK7 mutations were repeatedly identified in paediatric OS (112).	MAPK7 is within a region amplified (17p11.2~p12) in 13-29% OS patients (121).
NCOR1	NCOR1 is generally classified as a tumour suppressor but its mutations are associated with OS (122).	NCOR1 mutations were detected in 9/208 (4%) OS samples tested in the COSMIC catalogue (112, 122).
UBB	UBB mutations are associated with OS (112).	UBB is within the region alongside MAPK7, COPS3, PMP22, NCOR1 which is increased in OS patients (116).

		The incidence of UBB mutations is not widely reported, however amplification of this region is increased in 13-29% OS patients as outlined above.
LSAMP-AS3	LSAMP-AS3 mutations are associated with OS (112).	LSAMP gene expression has been shown to be reduced in approximately 60% of OS samples (123).
CCNE1	CCNE1 mutations have been observed in OS patients at varying incidences across studies (112, 124).	One study reported incidence of CCNE1 mutations in OS, while another study utilising 63 samples from 54 OS patients demonstrated that 33% patients displayed amplified CCNE1 expression (112, 124). In another study, 10.64% OS patients possessed CCNE1 mutations (125).
RECQL1	Mutations in the RECQL1 have been identified in OS (126).	Mutations in the RECQL1 was observed in 32% OS patients in a cohort study (126).
GNAS	There appears to be a low incidence of GNAS mutations observed in OS patients, particularly those with low-grade OS (127)(128).	Sequencing from a pool of 9 parosteal OS patients showed GNAS activating mutations in 5 patients, 4 of which were R201C mutations (where arginine is substituted with a cysteine at position 201) and 1 which was an R201H mutation (where arginine is replaced with a histidine at position 201) (127). This mutation does not appear to be particularly prominent in OS as another study showed no GNAS mutations in parosteal and low-grade OS (128).

1.11 Challenges in therapeutic drug treatment development in osteosarcoma

Given the rarity of OS and bone cancers in general, there is limited research directed to identifying new therapies for OS treatment. Additionally, due to the limited knowledge in the fundamental causes of OS development, insufficient progress has been made in the development of effective diagnostic methods, and late diagnosis is in fact common, thus developing a viable therapeutic drug remains challenging. There are additional challenges, including sample sizes in most studies, significant heterogeneity and inconsistencies across clinicals, all of which make it very difficult to apply research findings in clinical practice (129). Furthermore, the therapeutic inhibitors and monoclonal antibodies which have progressed to clinical testing have shown limited efficacy in OS patients (130-132).

1.12 Metastases to the bone (Secondary bone cancer)

Metastases to the bone are generally characterised as the third most common secondary cancers (133). Bone is the most common site of metastasis in late-stage breast cancer patients, as observed in 75% of late-stage breast cancer patients (134). Bone metastases are complex, exhibiting osteoclastic or osteoblastic characteristics depending on radiographic appearance of lesions: osteoblastic and osteoclastic secondary tumours appear as dense lesions and lesions showing localised bone resorption, respectively (135). This demonstrates the multifaceted characteristics of secondary OS. Therefore, more research is required at a molecular level to understand the mechanisms by which signalling pathways promote both primary OS, and metastasis to the bone.

1.13 Cytokine-mediated cell signalling in osteosarcoma

To understand OS within a molecular context basis, understanding the cytokines which promote an imbalance in bone homeostasis is crucial. Additionally, it is important to understand the cellular signalling pathways which are promoted by specific cytokines, and how these effects within the bone are involved in OS development. Therefore, the immune cells which release distinct cytokines and their roles in osteoblast function, osteoclast function and OS development are summarised in Table 1.3.

Table 1.3. A table depicting the role of cytokines in osteoblast function, osteoclast function, and in OS.

Cytokine	Immune cells which release cytokine	Impact on osteoblast function	Impact on osteoclast function	Impact on OS
IL-1α	Macrophages, dendritic cells (136)	The c-Jun N-terminal Kinase (JNK) and p38 MAPK pathways mediate IL-1α-induced apoptosis and inhibit osteoblast differentiation (137).	IL-1 alone cannot induce osteoclastogenesis due to limited IL-1R on bone marrow-derived macrophages, but overexpression of IL-1R, allows IL-1 to activate NF-κB, JNK, p38, and ERK signalling pathways, promoting osteoclastogenesis (138). IL-1α upregulates cathepsin K, M-CSF and PGE2 and downregulates OPD expression on osteoblasts, promoting osteoclast formation (139-141).a	IL-1α promotes several cancers but has not been linked to OS directly (142-144).
IL-1β	Monocytes, macrophages and dendritic cells (145).	IL-1β stimulates mesenchymal stem cell differentiation into osteoblasts and reduces osteoblast infiltration (146, 147).	Bone is the most sensitive tissue to IL-1 (148). IL-1β promotes osteoclast precursor proliferation, osteoclast recruitment, differentiation and activation, and is required for TNF-α-induced bone degradation (148-150).	IL-1β produced by M2 macrophages enhances OS metastasis by NF-κB/miR-181a-5p/RASSF1A/Wnt signalling (151, 152). In breast cancer, bone marrow IL-1β promotes tumour growth by activating NF-κB and CREB pathways, resulting in Wnt signalling (153). IL-1β and its receptor, IL-1R1 are upregulated in bone-metastatic breast cancer cells in mice (154). IL-1β has been linked to OS drug resistance (155). IL-1β gene polymorphisms are associated with OS risk, with lower frequencies of -31 CC and IL-1B-511 TT genotypes and the -31C allele detected in OS patients (156).
TNF-α	Mainly macrophages, but several other cell types including vascular endothelial cells and T cells (157-159).	TNF-α reduces osteoblast differentiation by inducing Receptor Activator of NF-κB Ligand (RANKL) and suppressing Runt-related transcription factor 2 (RUNX2) and IGF-1 expression. However, TNF-α may also enhance osteoblastogenesis by canonical NF-κB signalling, increasing Bone	TNF-α enhances RANKL and Receptor Activator of NF-κB (RANK) expression and therefore, increases osteoclast differentiation and activation (161).	TNF-α has been shown to enhance OS by promoting ERK signalling, resulting in OS staying in an undifferentiated state (162).

		Morphogenetic Protein 2, RUNX2 and Osterix expression (160).		
IL-2	T lymphocytes mainly (163)	IL-2 has not been shown to influence osteoblast function.	Low doses of IL-2 have been shown to induce NF-κB phosphorylation resulting in decreased RANK via the JNK pathway to suppress osteoclastogenesis in a collagen-induced mice model (164).	IL-2 has been shown to increase natural killer cell therapy to patients with OS lung metastasis without inducing toxic adverse effects (165, 166).
IL-3	T lymphocytes, macrophages and stromal cells (167, 168)	IL-3 increases osteoblast-specific gene expression including osteocalcin, osteopontin, alkaline phosphatase, collagen type I, Runx-2 and osterix. IL-3 increases osteoblast differentiation via the JAK/STAT signalling pathway (169).	IL-3 inhibits osteoclast differentiation in monocytes from osteoporosis patients (170). IL-3 inhibits RANKL-dependent osteoclast differentiation by suppression of IκB phosphorylation and degradation, preventing NF-κB nuclear translocation (167). IL-3 also prevents TNF-α-induced osteoclast differentiation by downregulating TNF receptor 1 and TNF receptor 2 expression (171, 172). However, IL-3 likely enhances osteoclast activity in myeloma (173).	No specific link between IL-3 and OS has been described, which is surprising due to primary OS being driven by osteoblasts.
IL-6	Osteoblasts, bone marrow stromal cells (BMSCs), T cells, macrophages and fibroblasts (174-176)	IL-6 signalling has been shown in osteoblasts to promote bone formation in mice models throughout aerobic exercise (177). IL-6 is also produced by osteoblasts to induce osteoclastogenesis (178).	IL-6 activates osteoclasts in a RANK-independent manner but can also indirectly induce RANK-mediated osteoclastogenesis by enhancing RANKL production by osteoblasts and stromal cells (179-181). However, contradictory findings have also suggested IL-6 downregulates osteoclast differentiation (182).	A study revealed high IL-6 expression in 73% (11/15) of paediatric and 66.7% (12/18) of non-paediatric OS patients (183).
IL-7	BMSCs (184)	IL-7 release by osteoblasts is crucial for B cell development within bone marrow (185).	IL-7 mediates osteoclastogenesis which appears to be STAT5-dependent and RANKL-independent (186).	IL-7 and CXCR5 receptor being co-expressed has been demonstrated to enhance CAR-T cell therapy for OS treatment (187).
IL-8 (CXCL8)	Macrophages, epithelial cells, endothelial cells and airway smooth muscle cells (188)	TGF-β1 produced by osteoblasts enhances IL-8 production by AP-1 and NF-κB-dependent mechanisms (189).	IL-8 enhances differentiation of osteoclast progenitor cells into osteoclasts (190).	IL-8 enhances OS advancement by increasing OS cell proliferation and enhancing immune cell recruitment and activation (191). This includes innate immune cells such as basophils, eosinophils and neutrophils. Adaptive immune cells such as B cells and T cells are also recruited.
IL-10	T cells, B cells, NK cells, mast cells, neutrophils and eosinophils (192)	Murine model studies have identified a role for IL-10 in osteoblast differentiation by regulation of microRNA-7025-5p (193).	IL-10 suppresses the differentiation of osteoclast progenitors into preosteoclast-like cells in a rat bone marrow cell culture study (194).	Studies have demonstrated that utilising an anti-IL-10 antibody enhances efficacy of mitamurtide, an immunostimulant, resulting in increased OS cancer cell death and reduced metastasis in an in vivo mouse model (195).

IL-11	Osteoblasts, chondrocytes, BMSCs and fibroblasts in the bone (196, 197)	Stimulation of primary osteoblasts with IL-11 results in increased RANKL expression, demonstrating its role in osteoclastogenesis (198).	IL-11 enhances osteoclast-driven bone resorption (199).	IL-11Ra is upregulated in human OS (200, 201).
IL-12	Monocytes/macrophages, dendritic cells and B cells (202)	IL-12 has been shown to be expressed in human osteoblast-like cells (203).	IL-12 suppresses RANKL-dependent and Lipopolysaccharide (LPS)-dependent osteoclastogenesis in mice (204, 205). IL-12 appears to inhibit TNF-α-induced osteoclastogenesis in a T-cell independent manner (206).	IL-12 downregulates OS tumour development in human LM7 OS cells (207).
IL-13	T cells, B cells, mast cells and basophils (208)	IL-13 inhibits cyclooxygenase-2-mediated prostaglandin production in osteoblasts (209)	IL-13 suppression of cyclooxygenase-2-dependent prostaglandin production in osteoblasts results in decreases osteoclastogenesis (209).	The IL-13 receptor, IL-13Rα2, enhances chemotherapeutic resistance to doxorubicin in human OS cell lines (210).
IL-15	Monocytes/macrophages and dendritic cells (211)	IL-15 enhances apoptosis of osteoblasts by activating NK cells (212, 213).	IL-15 promotes osteoclast cell death by NK cell activation (213).	IL-15 has been shown to be produced in human OS studies (214). However, administering inhaled recombinant IL-15 to dogs with OS, which is known to be similar to human OS, has shown promising results (215).
IL-17	T helper 17 cells, $\gamma\delta$ T cells and natural killer T (NKT) cells (216)	IL-17 enhances mesenchymal stem cell proliferation and osteoblast differentiation, proliferation, motility and chemotaxis (217). This has similarly been shown in mice calvarial cells (218).	IL-17 induces osteoclastogenesis (217, 219).	The IL-17/IL17RA axis is crucial for OS development in mice (220).
IL-18	Macrophages, dendritic cells (221).	Osteoblasts produce IL-18 which act through granulocyte-macrophage colony-stimulating factor to downregulate osteoclast formation (222).	IL-18 suppresses osteoclast formation by granulocyte-macrophage colony-stimulating factor-dependent mechanisms (223).	IL-18 is linked to enhancing pain in bone cancer but has been shown to inhibit metastasis in a highly metastatic mouse OS cell line (LM8 cells) (224, 225).
IL-19	Monocytes/Macrophages and dendritic cells (226)	IL-19 does not have a well characterised role related to osteoblast function.	IL-19 suppresses osteoprotegerin expression in BMSCs to enhance bone degradation in an LPS-mediated bone resorption mouse model (227). However, IL-19 has also been shown to decrease RANKL-dependent NF-κB-mediated osteoclast differentiation (228).	IL-19 is produced by osteoclasts which bind to IL-20RB, resulting in activation of the JAK1/STAT3 cellular signalling pathway and subsequent increased bone tumour cell proliferation (229).
IL-20	Monocytes/macrophages, dendritic cells and epithelial cells (230)	IL-20 suppresses osteoblastogenesis by increasing sclerostin and decreasing osterix, RUNX2 and osteoprotegerin expression in vitro (231).	IL-20 promotes osteoclastogenesis by enhancing RANK expression resulting in NF-κB, STAT3, NFATc1 and c-FOS induction in osteoclast precursor cells (231). Anti-IL-20 monoclonal antibodies have also been shown to suppress osteoclastogenesis (231).	An IL-20 receptor subunit, IL-20RB has been shown to be expressed on OS cells and is linked to bone metastasis of lung cancer (229).

IL-33	Macrophages, mast cells, dendritic cells and epithelial cells (232).	IL-33 expression has been identified in human osteoblast cells, but is not linked to normal bone remodelling (233).	IL-33 is expressed in osteoclasts and appears to enhance osteoclast apoptosis (234).	IL-33 expression is increased in human OS cell lines, including U2OS cells, and plays a role in maintaining OS cell viability (235).

1.14 IL-1β in osteosarcoma

Undoubtedly, many cytokines contribute to cancer development. However, IL-1β sparks a particular interest due to its diverse, and central roles in cellular signalling pathways and OS. As observed in other malignancies, IL-1β plays a key role in oncogenesis in OS, particularly via its complex roles in mediating both osteoblastogenesis and osteoclastogenesis (148, 236-239). IL-1α and IL-1β were the first characterised members of the IL-1 family, which now has 11 family members (240). IL-1β was initially identified as an endogenous pyrogen in rabbits with fever in 1955 (241). Seven decades later, IL-1β is known to be a pleiotropic pro-inflammatory cytokine, mainly expressed on innate immune cells with a well-characterised role in inflammatory-based diseases and oncogenesis (242). In solid malignancies, *in vivo* studies have demonstrated that secretion of IL-1β within the TME induces an accumulation of MDSCs (243). Interestingly, MDSCs are regulated by nuclear factor kappa B (NF-κB) signalling in tumour development, as studies have demonstrated that NF-κB (p65) knockout mice decreases MDSCs in syngeneic glioblastoma (244). Therefore, IL-1β-induced NF-κB signalling has a prominent role in linking inflammation to cancer. The area of IL-1β-mediated NF-κB signalling in the context of OS is of particular interest as IL-1β mRNA expression is higher in the bone marrow compared to any other organ in the body and its association with drug resistance in OS (245). Ultimately, this demonstrates the relevance of IL-1β in inflammatory and cancer-related processes within bone.

1.15 Discovery of the nuclear factor kappa light chain enhancer of activated B cells (NF-κB) transcription factor family

NF-κB was initially discovered by Ranjan Sen in the Nobel Prize laureate, David Baltimore's laboratory by usage of Oct factors obtained from mobility shift assays to confirm its interaction with an 11-base pair sequence (GGGACTTTCC) within the light-chain enhancer (κ) of human B cells (246). Despite NF-κB not being the transcription factor family which they planned to find; this discovery has shaped today's researchers understanding of normal physiological, and inflammatory processes. Indeed, following their discovery of NF-κB, they later discovered that LPS can stimulate NF-κB in pre-B cells (247), which was believed to be an exclusive phenomena in B cells. However, researchers have since highlighted NF-κB induction in a variety of cell types, including endothelial progenitor cells and CAFs, both of which are important in initiation and development of several cancers and metastasis, including in OS (248, 249). NF-κB transcription family members influence disease onset and prognosis by promoting the expression of various genes involved in inflammatory and immune responses, often contributing to inflammatory-based diseases and cancer (250). Due to the role of NF-κB in regulating pro-inflammatory genes, and the detection of an NF-κB family member, p65 in endothelial cells, macrophages, smooth muscle cells and T cells within atherosclerotic plaques, NF-κB is a potential drug target of interest for cardiovascular disease treatments (251, 252). Furthermore, through its inflammatory role, NF-κB signalling systems are also linked to the development and progression of rheumatoid arthritis, systemic lupus erythematosus and inflammatory bowel disease (253-256).

The NF-κB transcription factor family is now known to be composed of five inducible structurally analogous proteins, including NF-κB1 (p105/p50), NF-κB2 (p100/p52), RelA (p65), RelB and c-Rel. All five family members share a conserved 300 amino-acid long N-terminal Rel homology domain (RHD) (257). The RHD is required for site-specific DNA binding, inhibition of NF-κB protein binding, and enabling dimer formation between NF-κB family members (258). However, there are some notable structural differences between transcription factor family members including that p65, RelB and c-Rel share a transactivation domain (TAD) enabling them to bring about transcription, while this domain is absent in p50 and p52 (Figure 1.5). Therefore, p65, RelB, and c-Rel are more dominant NF-κB family members involved in gene induction, and p50

and p52 require a co-activator for transcriptional activity. NF-κB subunits form homo or heterodimers to bind to conserved κB sites in gene promoters to carry out their cellular functions in physiological processes (259, 260).

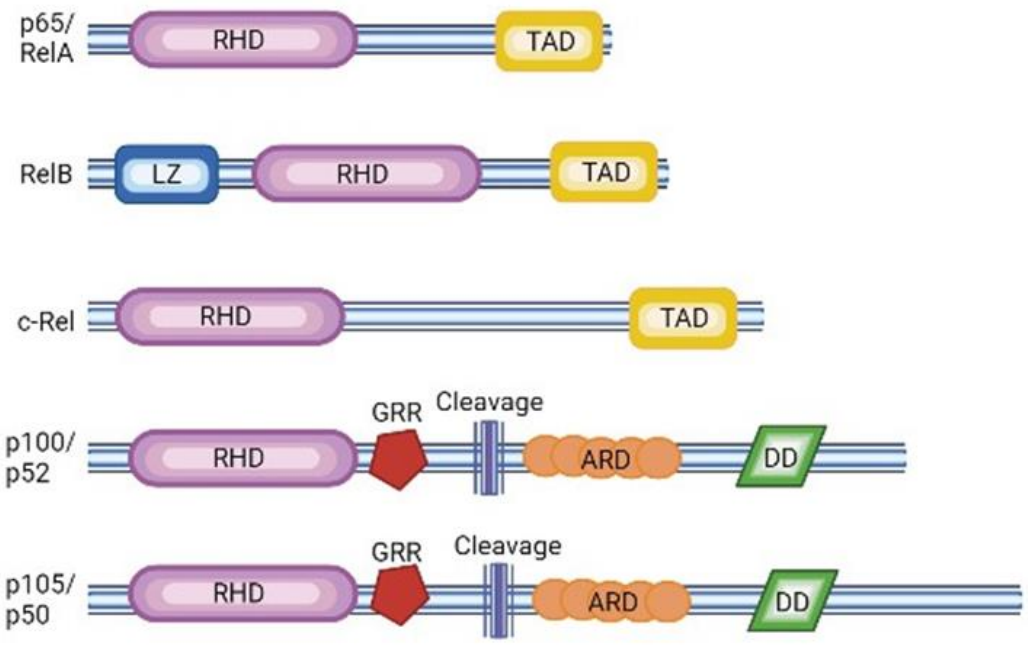

Figure 1.5. Structural representation of similarities and differences between the NF-κB transcription family members.
The conserved RHD is a structural similarity across all NF-κB transcription factors, TAD is shared across p65, RelB and c-Rel. NF-κB family isoforms, p100 and p105 additionally share a GRR, ARD and DD and are highly analogous to one another. P100 processing into p52 and p105 processing into p50 is displayed. TAD; transactivation domain, RHD; Rel homology domain, LZ; leucine zipper, GRR; glycine rich repeat, ARD; ankyrin repeat domain. Figure made with BioRender.com.

Despite there being five family members, early research largely focused on one specific transcriptional activity of one NF-κB heterodimer, which also exists as a heterotetramer, comprised of p50 and p65 subunits (261). These are inactive NF-κB complexes in the cytoplasm bound to inhibitory kappa B proteins, known as IκBs (262). However, a variety of stimuli have the potential to induce nuclear translocation of these heterodimers, inducing their transcriptional activity. Since the discovery of p50, its

synthesis has been shown to be dependent on proteasomal processing of its high molecular weight cytoplasmic precursor, p105 (263). This precursor protein is retained in the cytoplasm by its c-terminus, and is cleaved at the proteasome, resulting in p50 synthesis (263). David Baltimore's research laboratory have dominated this research area, by highlighting that the p105 c-terminus inhibits p50 transcriptional activity by its IκB properties, by preventing binding of p50-p50 homodimers to a κB motif on DNA, thereby limiting the ability of these dimers in gene induction (264).

The historic research focus on p50-p65 heterodimers has now drifted and expanded, as there are now 15 known possible NF-κB dimers, and a minimum of 12 of these can possess transcriptional activity and bind DNA (265). One NF-κB heterodimer which has become particularly interesting is p52-RelB. p52 preferentially binds RelB and p65, but not c-Rel or p50, whereas RelB only forms heterodimers with p105/p65 and p100/p52 NF-κB subunits (266). Similarly to p50, p52 is synthesised by proteasomal processing and c-terminal cleavage of a high molecular weight precursor protein, p100. P100 has IκB structural characteristics, and forms a heterodimer with RelB, which keeps RelB inactive in the cytoplasm. However, the inhibitory characteristics of p100 are not limited to p52:RelB responses, but can also prevent p65 nuclear translocation, and therefore inhibit transcriptional activity of p65 (267). The inhibitory mechanisms of p100 have been demonstrated by its ability to inhibit NF-κB binding to the IL-6 gene promoter, resulting in reduced IL-6 induction (268). IL-6 is known to be induced by p65, but also upstream mediators of p100 degradation, including NF-κB-inducing kinase (NIK) (269, 270). The proteasomal cleavage of p100 results in free p52:RelB transcriptionally active heterodimers. Therefore, p100 can act as an inhibitor of both p65 and p52:RelB-dependent gene induction. Additionally, early studies demonstrated that p100 knockout mice display gastric hyperplasia, leading to early postnatal death (271). This demonstrates that p100 is not only an important IκB protein but also has an important role in maintaining physiological function and survival. The dynamic and central role of p100 in regulating NF-κB subunits, collectively referred to as the NFkappaBsome, makes it an intriguing protein to study, particularly in disease contexts. The functional roles of p52 are also interesting, but p52 possesses opposing effects to p100, as p52 homodimers directly bind IκB-related oncoprotein, Bcl-3,

enabling construction of a ternary complex with DNA, which subsequently promotes oncogenesis (272).

To study the NF-κB paradigm is complex, and knockout of specific intermediate proteins, including p100 is not a feasible option due to physiological toxicity. Additionally, there are over 50 proteins involved in the tightly intertwined NF-κB signalling system with various protein complexes, which makes it a complicated system to fully study in a cellular environment. Therefore, alternative approaches out-with laboratory experiments have been developed to further understand the NF-κB system. Mathematical models have been constructed and introduced to aid the study of NF-κB dynamics and function in a cost-effective and efficient manner, which has been predominantly led by Alexander Hoffmann and Soumen Basak (273). These computational models have been revolutionary in NF-κB research, particularly for increasing understanding of the IκB family members and their differences in peak activation times. For example, IκBα mediates early NF-κB responses, whereas IκBβ and IκBε are associated with longer, sustained NF-κB-driven responses (274). This demonstrates that great progress has been made by utilising these models, and they may have great future potential in NF-κB-related research.

1.16 The IKKs

There are various kinases involved in NF-κB signalling, including the Inhibitor of Nuclear Factor Kappa-B Kinases (IKKs). In canonical NF-κB signalling, a trimeric IKK complex consisting of IKKα, IKKβ and IKKγ are indispensable (275). IKKβ is generally accepted as the main driver of canonical NF-κB signalling, but some studies have suggested that IKKα has a more prominent role in cell- and disease-specific contexts, including in colorectal cancer (276). Non-canonical NF-κB signalling is dependent on an IKKα homodimer, and is IKKβ- and IKKγ-independent (275). IKKα, IKKβ and IKKγ make up the classical IKKs, while there are IKK-related members of the family, such as IKKε and TBK1, which have a prominent role in antiviral signalling and interferon 3/7 activation (277, 278). The structure, homology and molecular weights of IKKα and IKKβ are similar at 85 kDa and 87 kDa, respectively, and both IKKα and IKKβ contain an N-terminal kinase domain which aids their catalytic activity, a scaffold dimerization domain, and a C-terminal NEMO-binding domain, which facilitates their binding to IKKγ (279, 280). IKKβ possesses an additional ubiquitin-like-domain (280). However, their cellular functions differ greatly as IKKβ is thought to be primarily cytosolic, but IKKα has a nuclear localisation signal (NLS) which enables it to traverse between the cytoplasm and nucleus (281). In addition to this, IKKα has a relatively newly discovered endosomal generated truncated form, p45-IKKα, which has primarily been identified and explored in DNA-damage and chemoresistance studies in colorectal cancer cell lines. Therefore, IKKα presents as an increasingly interesting and complex drug target in cancer, given its varied roles and differential subcellular localisation. The structural composition of the classical IKKs and p45-IKKα are outlined in Figure 1.6.

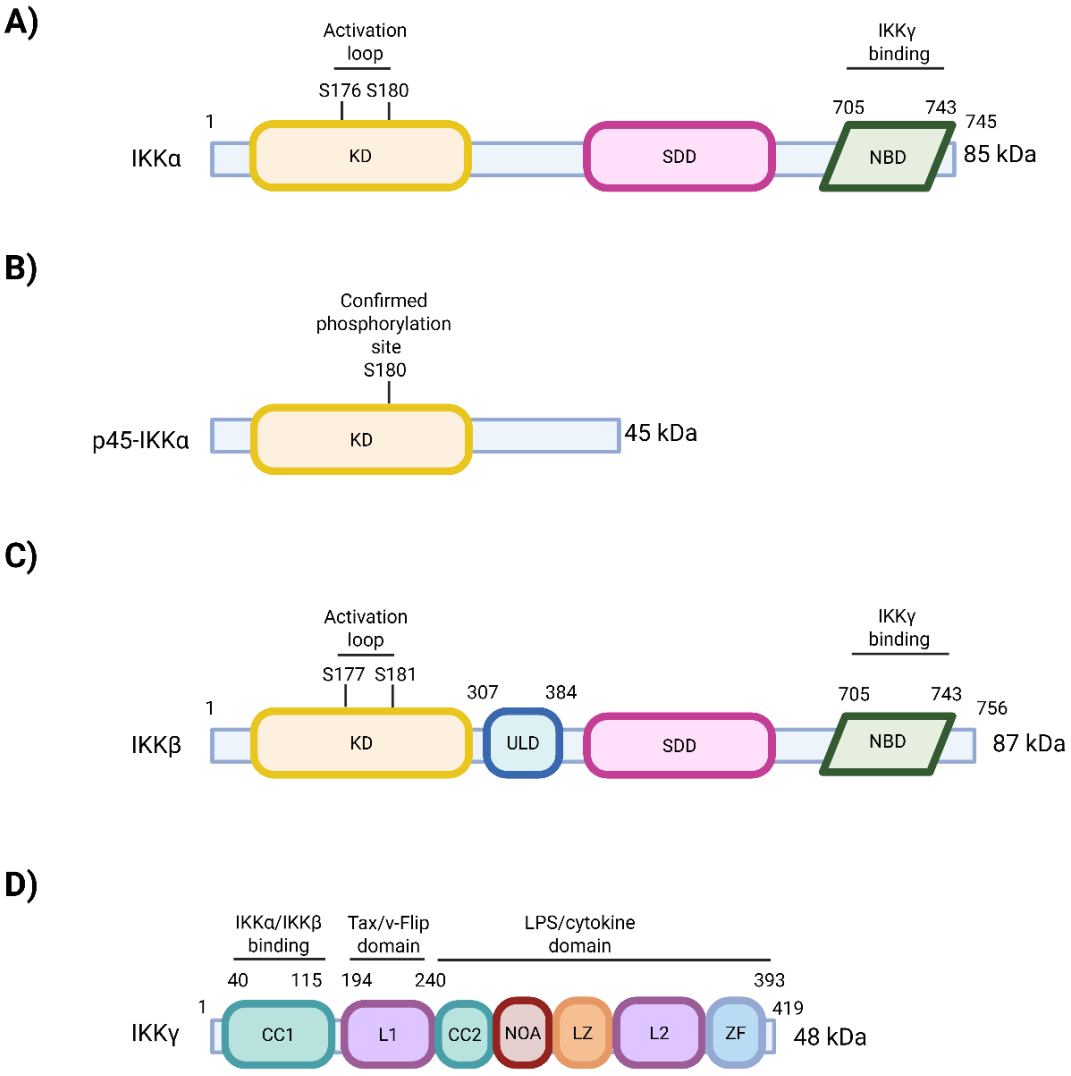

Figure 1.6. Diagrammatical representation of the structure of the IKK family members.

A) The structure of IKKα containing an N-terminal kinase domain with two phosphorylation sites within its activation loop, Ser176 and Ser180, a scaffold dimerization domain and a C-terminal NEMO-binding domain, which enables IKKα-IKKγ binding. **B)** The structure of a truncated endosomal-generated and nuclear active IKKα isoform, known as p45-IKKα. **C)** The structure of IKKβ containing an N-terminal kinase domain with two phosphorylation sites, Ser177 and Ser181, a ubiquitin-like domain, a scaffold dimerization domain and a C-terminal NEMO-binding domain. **D)** The structure of IKKγ is comprised of an N-terminal coiled coil 1 IKKα/IKKβ-binding domain, a Tax/v-Flip domain, and a LPS/cytokine domain made up of coiled coil 2, ubiquitin binding domain, leucine zipper, linker 2, and zinc finger, an additional ubiquitin binding domain. Figure created in BioRender.com, adapted from an original publication (27).

1.17 Canonical NF-κB signalling

The canonical NF-κB signalling pathway is rapidly activated by a plethora of pro-inflammatory ligands such as pathogen associated molecular patterns (PAMPs) and damage-associated molecular patterns (DAMPs) as well as pro-inflammatory cytokines including TNF-α and IL-1β (259, 282-284) (Figure 1.7). Specific binding of these pro-inflammatory ligands such as IL-1β to their relevant receptors (IL-1R1) induces rapid activation of the canonical NF-κB signalling cascade triggering downstream recruitment of adaptor protein complexes to the cytoplasmic receptor domains. This subsequently results in activation of Transforming growth factor-β-activated kinase 1 (TAK1) within 1-2 minutes and peak activation within 3-5 minutes after stimulation (285). TAK1 phosphorylates IKKβ, within the trimeric IKK complex resulting in phosphorylation, ubiquitination and proteasomal degradation of IκBα and in turn, nuclear translocation of p50 and p65 heterodimers. This NF-κB heterodimer binds to DNA encoding for anti-apoptotic and pro-inflammatory genes and subsequently results in generation of pro-inflammatory and anti-apoptotic proteins. Despite canonical NF-κB signalling-related studies predominantly focusing on IKKβ activation, IKKα similarly contributes to enhancing TNF-α-induced NF-κB1 (p65) activity, as measured by p65 phosphorylation, but IKKβ appears to play a greater role in IκBα degradation and processing (286).

1.18 Non-canonical NF-κB signalling

The non-canonical NF-κB arm is activated more slowly than the canonical NF-κB axis by specific TNF-α superfamily members (Figure 1.7). These ligands include RANKL, lymphotoxin, tumour necrosis factor superfamily member 14 also known as LIGHT, and CD40. By binding to their respective receptors, these ligands induce recruitment of adaptor protein TRAF3 which is bound to TRAF2 and cIAP1/2, to the receptor's cytoplasmic domain. In a basal state, cIAP1/2 ubiquitinates NF-κB-inducing kinase (NIK, also known as MAP3K14) at K48 within its TRAF3 binding domain which targets NIK to the proteasome resulting its degradation. However, when the non-canonical NF-κB arm is activated by ligand-receptor binding, this results in upregulated intracellular NIK levels, enabling liberated NIK to phosphorylate IKKα at Ser176 and

Ser180 within its activation loop, promoting activation of its kinase activity. The dependence on NIK protein synthesis and accumulation in non-canonical NF-κB signalling results in a notably slower signalling pathway than observed in the canonical NF-κB arm (287). NIK recruits IKKα to a large IκB p100 at conserved serine residues Ser866 and Ser870, facilitating p100 phosphorylation and post-translational processing (288, 289). In turn, this results in recruitment of the SCFβ-^{trcp} ubiquitin ligase complex, which subsequently induces ubiquitination at Lys856, the ubiquitin acceptor site on p100, leading to p100 degradation at the proteasome leading to p52 production. As a result, p52 can form an active heterodimer with RelB, which translocate to the nucleus to regulate specific anti-apoptotic and pro-inflammatory genes. The central role of NIK in the non-canonical pathway should not be overlooked. The non-canonical NF-κB cascade has crucial roles in physiological processes, which were originally thought to be limited to roles in B cell maturation, and germinal centre formation which contributes to lymphoid organ development (290). Indeed, researchers have shown that lymphotoxin-mediated non-canonical NF-κB signalling within stromal cells results in generation of CXCL13 and CCL2 chemokines, which play a key role in germinal centre development and maintenance and enhances proliferation of high affinity B cells to the B cell receptor (291). Another TNF-superfamily member which activates non-canonical NF-κB signalling, B cell activating factor (BAFF), is crucial for B cell activation, maturation, and autoimmunity (292, 293). Since these initial findings, there is now well-established evidence which demonstrates that non-canonical NF-κB signalling can induce development of inflammatory-based diseases. Additionally, there has been increasing evidence which suggests that DNA and RNA viruses can evade host immunity by upregulation of non-canonical NF-κB signalling. For example, microarray analysis studies have highlighted that NIK and TRAF2 expression are increased throughout initial stages of hepatitis B virus infection (294). Additionally, in chronic hepatitis B (CHB) patients, BAFF levels in serum are constitutively high, and therefore dysregulate the adaptive immune response by upregulation of B cell activation (292). Therefore, the non-canonical NF-κB signalling pathway plays a complex but important role in pathogenesis of inflammatory-based diseases. In relation to OS, NF-κB-inducing kinase (NIK), and therefore non-canonical NF-κB signalling has been implicated in enhancing bone formation (295). Furthermore, this identifies the non-canonical NIK- and IKKα-dependent NF-κB axis

another attractive target for inhibition of osteoblastogenesis, and therefore, a potential future signalling axis to target in OS.

1.19 Novel IL-1β-mediated non-canonical NF-κB (p100) signalling

Previously, IL-1β was exemplified to activate the canonical NF-κB pathway but had never been known to influence the non-canonical NF-κB arm. Recently, IL-1β and TNF-α was highlighted to induce phosphorylation of p100 in an OS cell line, U2OS cells, which is maximal by 15-30 minutes (296) (Figure 1.7). Interestingly, preincubation with 3 μM or 10 μM concentrations of the NIK-selective inhibitor, CW15337 did not inhibit IL-1β mediated p100 phosphorylation. Additionally, CRISPR/Cas9 IKKα deletion was used as a strategy to unravel the unknowns of IKKα-signalling, which demonstrated an IKKα-dependent mechanism for IL-1β-mediated non-canonical signalling. This indicates a novel NIK-independent mechanistic route of non-canonical NF-κB signalling. Due to the pivotal role of IKKα and downstream p100/p52 in inflammation and cancer, protein-protein interactions involved in IL-1β-mediated IKKα-dependent signalling would potentially uncover new drug targets (296).

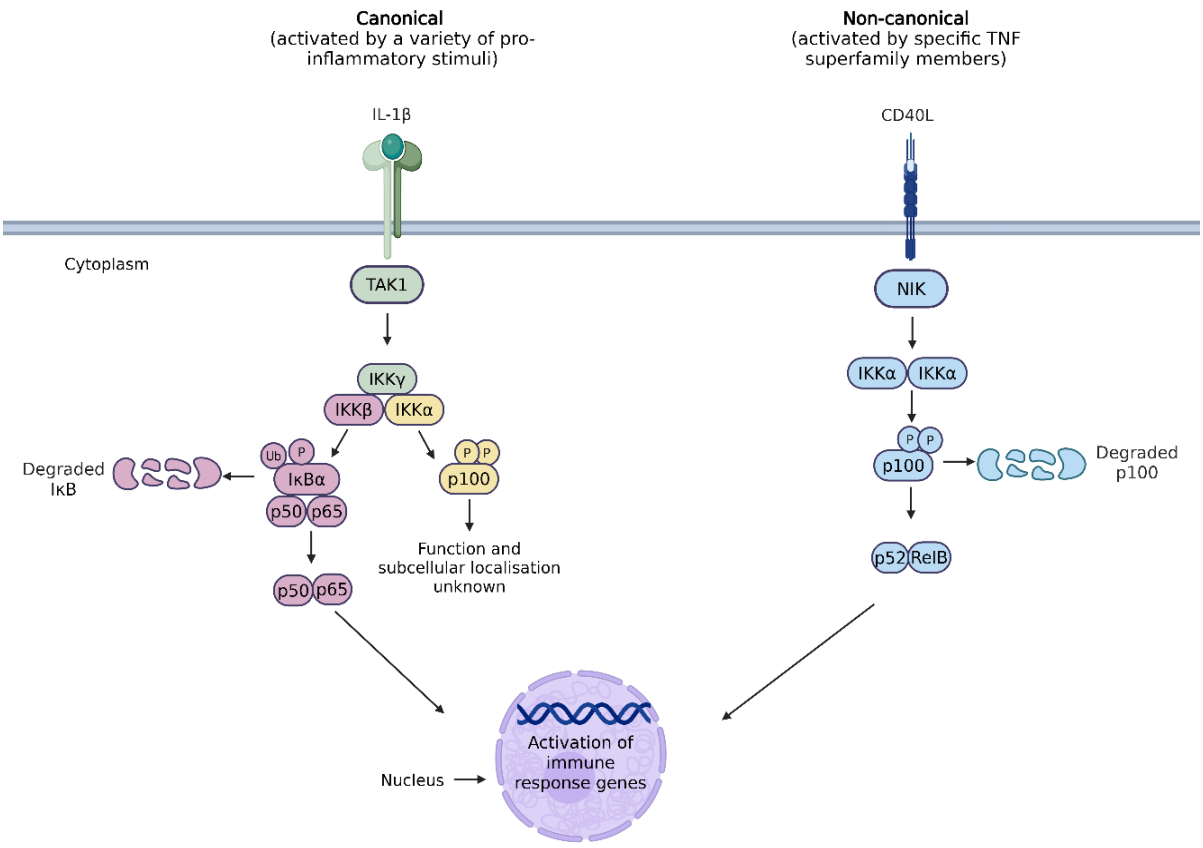

Figure 1.7. A diagrammatical representation of the current understanding of the NF-κB pathways.

Canonical NF-κB signalling (left) and non-canonical NF-κB signalling (right) are shown. The canonical NF-κB pathway is activated by a variety of pro-inflammatory stimuli, resulting in TAK1 activation, and subsequent activation of the IKK complex resulting in IKKβ-mediated IκBα phosphorylation and proteasomal degradation, resulting in p50/p65 heterodimers translocating to the nucleus. However, IL-1β-mediated and TNF-α-mediated canonical NF-κB signalling-dependent results in IKKα phosphorylation and further p100 phosphorylation, and no known subsequent p100 degradation leading to unknown p100 functions. Non-canonical NF-κB signalling is activated by TNF-superfamily members, leading to NIK accumulation, and IKKα homodimer phosphorylation followed by p100 phosphorylation and degradation into p52, which enables RelB and p52 heterodimers translocate to the nucleus. Both canonical, and non-canonical NF-κB signalling pathways result in activation of specific immune response-related genes. Figure created on BioRender.com, adapted from an original article (27).

1.20 NF-κB in osteosarcoma

Previous studies have highlighted that NF-κB activation, specifically the NF-κB p65 subunit is increased in metastatic human OS compared to primary human OS tissues (297). Other studies have identified increased NF-κB mRNA expression in OS tissue compared to adjacent tissues (298). Another research group has utilised single cell and bulk RNA-sequencing techniques to look at enrichment of genes which relate to signalling pathways within OS cells, which identified increased TNF-α-mediated NF-κB signalling compared to non-cancerous cells, as well as PI3K/AKT/mTOR and mTORC1 signalling pathways (299). Another study utilising a single cell RNA-sequencing dataset (Gene Expression Omnibus ID: GSE162454) which focused on eight identified cell types in OS utilised KEGG enrichment analysis to demonstrate heterogeneity in an NF-κB signalling pathway gene cluster in all eight cell types: B cells, CAFs, endothelial cells, myeloid cells, NK/T cells, osteoblastic OS cells, osteoclasts and plasmocytes (300). Additional studies have aimed to identify the relationship between NF-κB and other OS mediators, including GSK-3β which has a complex oncogenic or tumour suppressor role depending on disease context. The findings of this study included that OS patients who had high NF-κB and GSK-3β expression had a poorer prognosis (49.2 months) in comparison to OS patient tumours with low NF-κB and GSK-3β expression (109.2 months) (301). Further, the study identified that GSK-3β subsequently inhibits NF-κB signalling, therefore demonstrating the potential for future NF-κB-targeting therapeutic drugs in OS treatment.

1.21 IKKα in cancer

The gene which encodes IKKα, CHUK, has demonstrated to be expressed across many organs and cell types within the human body, with particularly high expression of CHUK RNA demonstrated in the kidney and bone marrow merit investigation into the role of IKKα in cancers which originate in these organs (302). Unsurprisingly, due to wide CHUK RNA expression, it has been demonstrated that IKKα has various roles in inducing cancer, cancer development and systemic metastasis (303). Notably, unlike IKKβ which is predominantly cytoplasmic, IKKα can traverse between the cytoplasm and nucleus and acts as an acetylase and chromatin kinase to modify

histones and therefore regulate chromatin structure and in turn, transcription of inflammatory genes and DNA repair (304-306). Some studies have attempted to uncover the complex roles of IKKα but have yet to demonstrate the nuclear transporter responsible for the shuttling of IKKα from the cytoplasm to the nucleus. However, the role of IKKα in regulation of oncogene expression is being increasingly studied. Researchers have employed western blotting and immunofluorescence techniques to an OS cell line, 143B cells, which identified that IKKα nuclear gene expression results in low expression of a highly conserved tumour suppressor gene, Mammary Serine Protease Inhibitor gene (maspin) (305). However, more research is required at a molecular level to fully explain how IKKα gene expression leads to cancer progression (305).

Researchers have also attempted to understand the role of IKKα in oncogenesis by studying the role of a truncated nuclear active form of IKKα, IKKα(p45). Studies have demonstrated that BRAF, TAK1 and p38-MAPK can mediate IKKα(p45) phosphorylation triggering its nuclear translocation as a consequence of DNA damage (303), which enhances tumour growth and possesses chemo-resistant properties (307). IKKα has been implicated in thyroid cancer, where mediator of RNA polymerase II transcription unit 27 (CRSP8), a highly expressed enzyme in anaplastic thyroid cancer cells, binds to the IKKα promoter region (residues 257 to 143) to downregulate its transcription (308). Additionally, IKKα knockdown has been demonstrated to decrease oral squamous cell carcinoma cell migration and invasion (309). However, CRSP8 knockdown was highlighted to prevent thyroid cancer by increasing IKKα transcription and signalling in a mouse model with human ATC (308). Additionally, NF-κB subunit p52 and its precursor p100 possess opposing effects as p100 downregulation and excessive p52 expression result in incidence of inflammatory diseases and breast cancer (271, 310). This exemplifies the complexity of non-canonical signalling components in disease states.

Due to the presence of IKKα in the IKK complex in canonical NF-κB signalling, the role of IKKα as a mediator of canonical NF-κB signalling in some cancers has been studied. Interestingly, it has been demonstrated that IKKα has a dominant role in

canonical signalling in an epithelial colorectal cell line, Human Colorectal Carcinoma 116 (HCT116) cells, as TNF-α- and IL-1α- induced phosphorylation of p65 at S468 and p65 nuclear translocation was extensively downregulated in IKKα KO HCT116 clones, but unaffected by IKKβ KO HCT116 clones (276). The authors suggest that the roles of the classical IKKs in canonical signalling are cell- and region-specific, as well as dependent on level of development (276). However, these effects could be artefactual due to complex disruption. Therefore, this justifies additional research into IKKα involvement in the canonical NF-κB cascade in cancer settings.

IKKα has various NF-κB-independent functions in cancer. An early example of this was demonstrated in mice keratinocytes, which highlighted that IKKα deletion results in skin squamous cell carcinoma (303). Specifically, IKKα expression is enhanced by its binding to chromatin at the 14-3-3 theta locus which downregulates CDC25, a phosphatase which regulates G2/M stages of the cell cycle and is involved in the transfer of accurate DNA information to daughter cells. In turn, insufficient CDC25 activity results in excessive cell proliferation and damaged or inaccurate DNA being transferred to daughter cells, which can enable induction and progression of skin squamous cell carcinoma. IKKα has also been demonstrated to be instrumental in ultraviolet B (UVB)-induced apoptotic responses in human keratinocytes and mouse embryonic fibroblasts (MEFs) in a p53/PERP dependent and NF-κB-independent manner. As UVB has a prominent role in UV skin damage due to its longer wavelength than UVA and UVC, IKKα may offer drug target validity in the future for skin cancer treatment (311). Findings from other research groups have highlighted that accumulation of nuclear IKKα displays a key NF-κB-independent role in prostate cancer progression by suppression of *Maspin* gene transcription (312). Cyclin D1, a key cell regulator predominantly located in the nucleus when inactive, is phosphorylated at residue T286 by IKKα leading to cyclin D1 dysregulation and wide subcellular distribution, which drives progression of lung and breast tumours (313-316). Due to the more prevalent overexpression of cyclin D1 compared to other D-type cyclins in human cancers, future research may focus on development of selective cyclin D1 antagonists for patients with specific types of cancer (317). Some of the mechanisms which IKKα has been shown to promote the hallmarks of cancer are summarised in Figure 1.8.

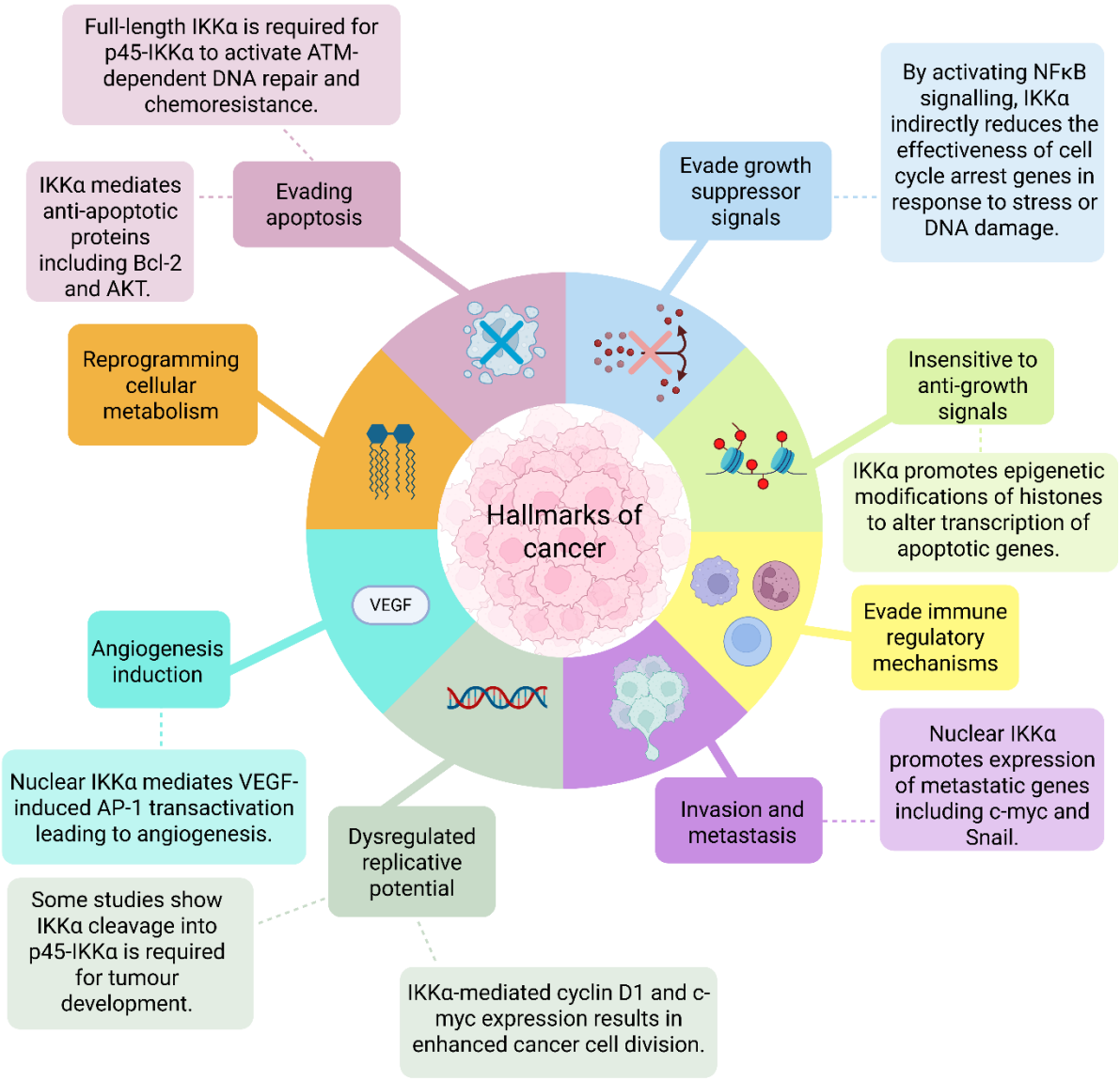

Figure 1.8. A schematic highlighting some oncogenic roles of IKKα in promoting several cancer hallmarks.

IKKα promotes dysregulated replicative potential, invasion and metastasis, angiogenesis induction, increases insensitivity to anti-growth signals, evasion of growth suppressor signals and evasion of apoptosis. Figure was created on BioRender.com, and adapted from an original publication (27).

1.22 The benefit of IKKα inhibition in a cancer setting

Initially, IKKβ dominated the IKK research field, given its prominent role in canonical NF-κB signalling. Therefore, there were several efforts to develop selective ATP-competitive inhibitors. Despite great efforts and substantial funding to develop and trial

selective IKKβ antagonists, including PS-1145, these inhibitors consistently promoted systemic toxicities. To date, there are still no FDA-approved IKKβ antagonists used for therapeutic purposes. Due to the lapse in success in developing therapeutic drugs targeting IKKβ which could successfully tip the balance in favour of benefit compared to risk, the global research focus within the IKK field somewhat shifted to the role of IKKα in inflammatory processes and cancer. This has since enabled several breakthroughs, and a greater understanding of the roles of IKKα in promoting cancer, many of which are IKKβ- and NF-κB-independent.

The world's first-in-class selective IKKα inhibitor, SU1261, was developed by Ka Ho and others, and was studied for its effects on human umbilical vein endothelial cells (HUVECs) (318). This study was carried out as an alternative to IKKβ inhibition due to the previously reported toxic pro-apoptotic effects of IKKβ on the endothelium. SU1261 downregulated downstream non-canonical p100 phosphorylation in a concentration-dependent manner (0.3-3 μM), with no effects on IKKβ when tested up to 30 μM. Therefore, SU1261 possesses high IKKα selectivity. There are various other IKKα inhibitors available including ACHP and BMS-345541, but these inhibitors lack selectivity and act off target on IKKβ due to the structural similarity between the IKKs. Additionally, given the known systemic toxicity of IKKβ inhibition in disease settings, this highlights the need for inhibitors with higher selectivity towards IKKα (9). However, an inhibitor, BAY 32-5915, which has been claimed to be highly selective for IKKα, has recently been demonstrated to block LPS-induced pulmonary metastasis (9). Despite claims that this inhibitor is IKKα-selective, there is little evidence to demonstrate this inhibitor does not have off-target effects on IKKβ or other kinases and given the similarity between IKKα and IKKβ, this information is required to determine the selectivity of BAY 32-5915.

1.23 Osteogenesis signalling pathways

Osteoblast differentiation is a vital physiological process to retain bone health. However, as primary OS relies on excessive uncontrolled osteoblast differentiation, it is important to identify the cellular signalling events which result in osteoblast differentiation. Both the CXCL/CXCR2 axis and GAS7 directly binding to transcription

factor Runx2 are important events which ultimately result in increased alkaline phosphatase, osteocalcin and osteopontin production, and subsequently, an increase in osteoblast differentiation. A proposed mechanism by which these signalling events occur is highlighted below (Figure 1.9).

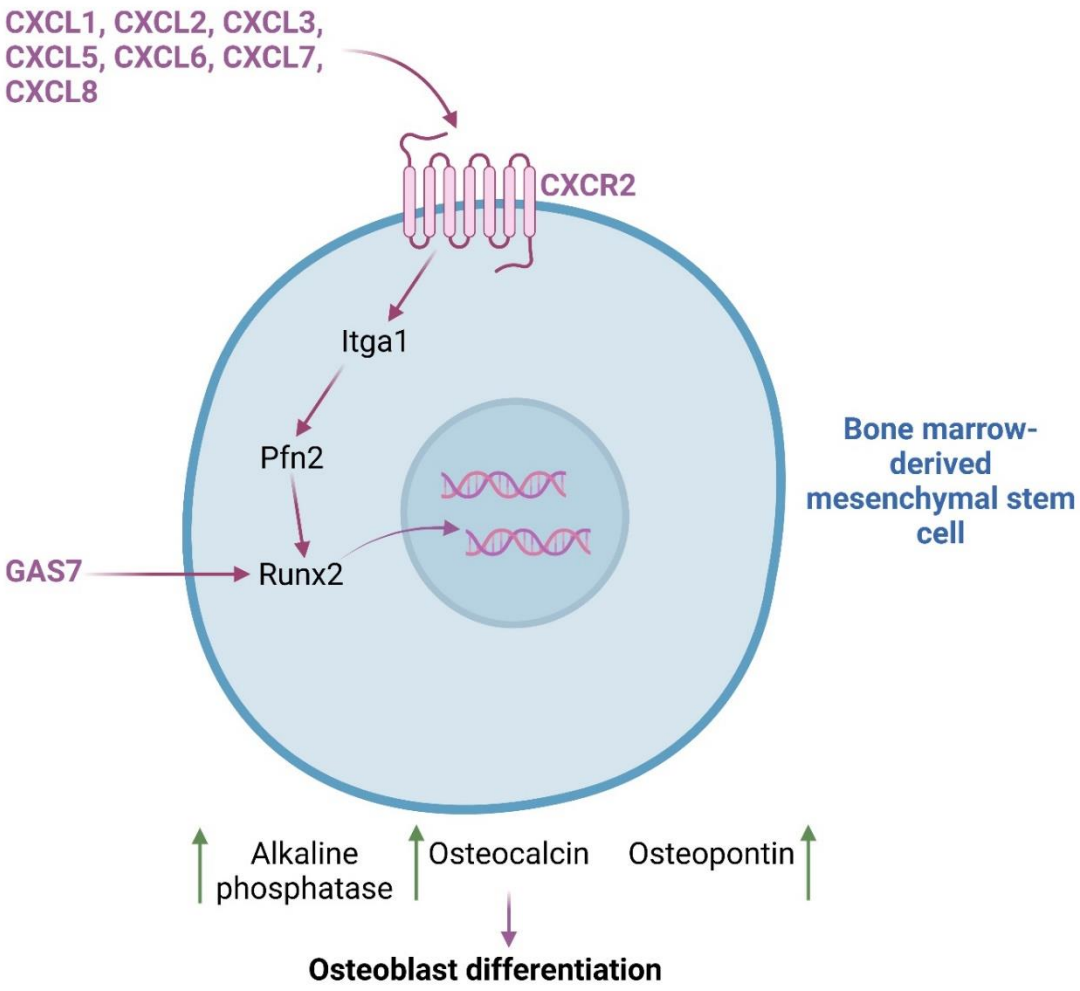

Figure 1.9. An illustration of cellular signalling pathways which result in osteoclast differentiation.

CXCR2 agonists, including chemokines such as CXCL1, CXCL2, CXCL3, CXCL5, CXCL6, CXCL7, CXCL8 all promote CXCR2-dependent signalling. CXCR2 signalling in bone marrow-derived mesenchymal stem cells results in activation of Runx2, resulting in Runx2-dependent osteoblast differentiation via increased expression of alkaline phosphatase, osteocalcin and osteopontin. GAS7 can also directly increase Runx2 expression resulting in Runx2 -dependent osteoblast differentiation. Figure was created using BioRender.com.

Understanding the molecular mechanisms which underpin osteogenesis presents an exciting and unique opportunity to uncover the pro-inflammatory signalling pathways responsible for secretion of CXCL chemokines, particularly to suppress recruitment of TANs and the osteogenesis process. A deeper understanding of these signalling

pathways would enable identification of potential upstream drug targets for novel OS treatments.

1.24 Osteoclastogenesis signalling pathways

Several signalling pathways tightly regulate osteoclast bone resorption, and osteoblast bone generation including RANKL-induced NF-κB signalling (highlighted in non-canonical NF-κB signalling in Figure 1.7) and canonical Wnt signalling (319, 320). Indeed, it has been exemplified that inhibition of RANKL-induced NF-κB signalling, and RANKL/RANK deletion prevents osteoclastic bone resorption. There are two main receptors which are crucial in osteoclast differentiation, RANK and Osteoclast-associated receptor (OSCAR). While RANK results in the enhancement of downstream signalling pathways, including canonical and non-canonical NF-κB signalling, and osteoclastogenesis, OSCAR plays an instrumental auxiliary role to promote RANK-mediated osteoclastogenesis. OSCAR is an immunoglobulin-like receptor activated mainly by collagen types I-III. This subsequently results in downstream phosphorylation of Fc receptor common γ chain (FcRγ), an ITAM-containing adaptor protein by Syk, and thereby, Syk auto-phosphorylates itself leading to PLCγ phosphorylation. Phosphorylated PLCγ increases inositol trisphosphate (IP_3) production leading to increased release of calcium from the endoplasmic reticulum which indirectly results in increased NFATc1 expression, and NFATc1 directly binding to several genes in the nucleus to promote osteoclastogenesis (Figure 1.10).

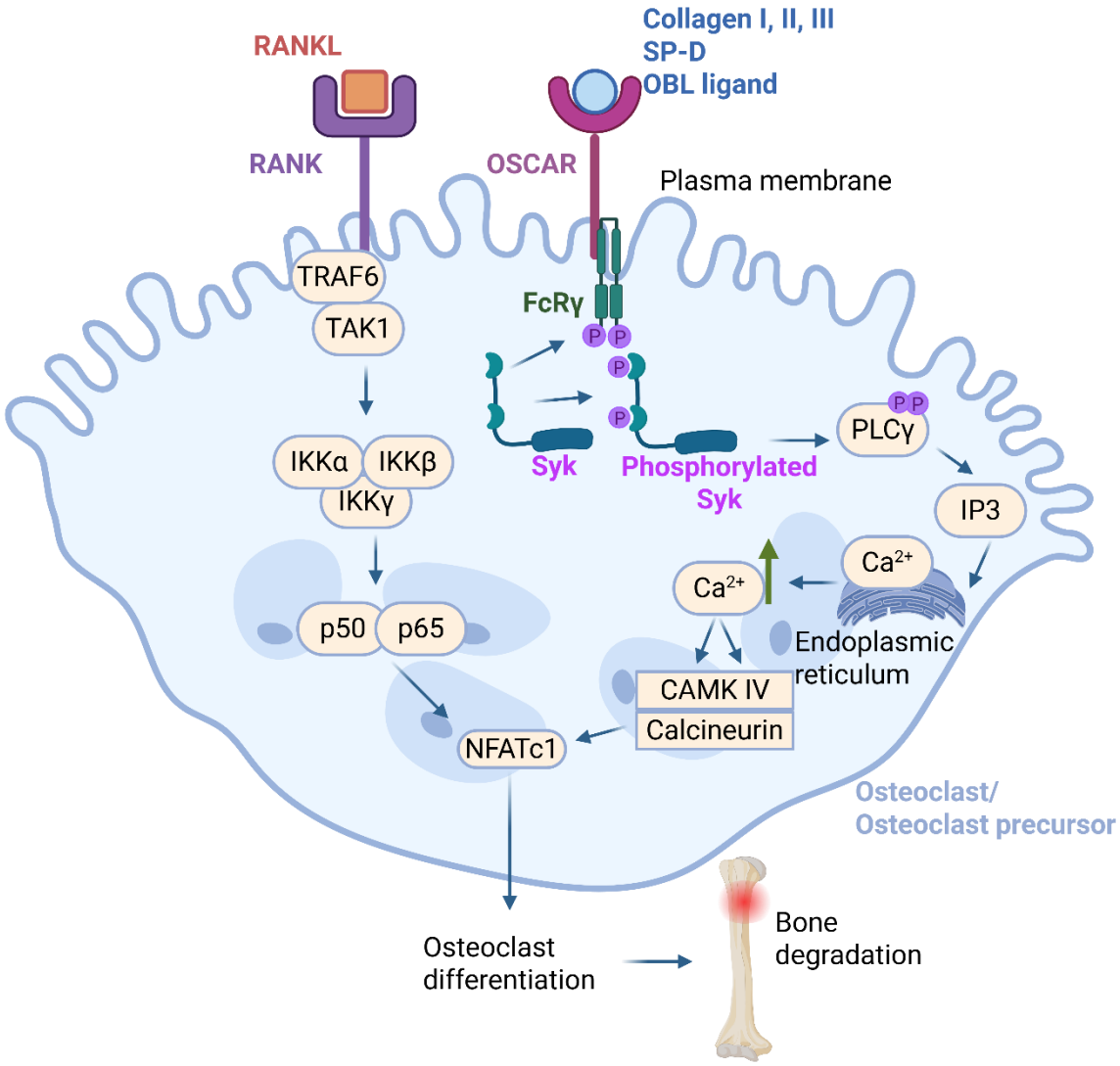

Figure 1.10. An illustration of cellular signalling pathways which result in osteoclast differentiation.
Osteoclast-associated receptor is activated by collagen I, II, III, SP-D, and OBL ligand, resulting in a Syk-dependent signalling pathway, resulting in subsequent, PCLg phosphorylation, resulting in IP_3-mediated increased Ca2+ expression, and downstream NFATc1 expression. This, in turn, results in osteoclast differentiation and therefore, bone degradation. Figure was created using BioRender.com.

1.25 Cholesterol biosynthesis in osteosarcoma

A considerable amount of evidence has demonstrated the importance of cholesterol production in OS development and prognosis. Lipid droplets, which serve as reservoirs for cholesterol esters were first discovered in an ultrastructural study of human OS in 1981 (321). Additionally, Synvinolin (MK-733), a selective antagonist of HMG-CoA reductase, the rate-limiting enzyme in cholesterol biosynthesis, was shown to reduce

metastatic potential in BN472 rat tumour cells, a model of chemically-induced OS in 1989 (322). However, the significance of lipids including sterols in OS was overlooked for several decades. In recent years, studies have highlighted an intriguing, but complex relationship between lipids and OS. A study which has utilised OS patient data (88 samples) from The Cancer Genome Atlas highlighted that by eight years, OS patients with high glycolysis and cholesterol synthesis-related gene signature (GCSRG) and low GCSRG have a survival probability of approximately 0.25 and 0.8, respectively (323). Additionally, high GCSRG may correlate to OS tumour growth, as patients with high GCSRG had significantly higher tumour purity and lower immune score than low GCSRG patients, indicative of a higher ratio of cancerous cells to non-cancerous cells in tumours. Further studies have identified an increase in cholesterol biosynthesis-related genes in OS cells compared to healthy cells (299). Despite the cholesterol biosynthetic pathway not being fully characterised in the context of OS, treatment with simvastatin, and atorvastatin reduced these properties, and reduced KLF4 expression in a dose-dependent manner. Interestingly, KLF4 increased spheroid formation, which was reversed by statin administration, indicating statins may target KLF4 (324). Future studies into OS therapeutic drug targets may reveal ways in which the cholesterol biosynthesis pathway can be downregulated by targeting upstream mediators, including specific cellular signalling pathways.

Several studies have previously demonstrated that cholesterol and mediators of cholesterol biosynthesis play an integral role in long bone growth and growth plate disorganisation and disruption. Indeed, expression of endoplasmic reticulum localised genes which mediate cholesterol biosynthesis, SREBP cleavage-activating protein, and HMGCR, are significantly downregulated in the hypertrophic zone (HZ) compared to proliferative zone (PZ) in E16.5 embryo distal femur chondrocytes (325). Additionally, hedgehog signalling promotes genes involved in the cholesterol biosynthetic pathway, and mutually, intracellular cholesterol also regulates hedgehog signalling (325, 326). In a cancer setting, hedgehog signalling has been linked to osteoblast regulation in OS by overexpression of the YAP-1 gene and long-coding RNA, H19 (327). Several antagonists including ATO, vismodegib and GANT61 which target the hedgehog/GLI2 signalling pathway have shown promising therapeutic potential in OS, by downregulating invasion and metastasis of OS cells (328).

Therefore, this implicates a role for genes which enhance cholesterol biosynthesis in OS development and migration. In support of this, a recent study utilised open access datasets to identify four distinct groups of OS patients based on their median gene expression into a glycolysis, cholesterol, quiescent and mixed subgroup. This study identified that the cholesterol and mixed OS patient subtypes displayed the worst prognosis in relation to patient survival (329). In addition, other studies have highlighted some cholesterol biosynthetic enzymatic genes including SQLE and TM7SF2 in a prognostic OS gene model (330).

1.26 The use of transcriptomics in cellular signalling and osteosarcoma

Without a fundamental understanding of the downstream consequences of cellular signalling pathways on gene expression, it is of little clinical relevance to study these cellular signalling pathways. Therefore, it is essential to study the genes which are increasingly induced because of IL-1β-mediated, IKKα-dependent signalling to identify the extent of the role which IKKα partakes in inflammatory processes. One way which this can be achieved in an unbiased, selective, and large-scale manner is to conduct a transcriptomics study, otherwise known as RNA-sequencing. Genomics has become a particularly intriguing subject over the past few decades. The genomics world was revolutionised following the completion of the Human Genome Project, an ambitious and collaborative effort which spanned 13 years, from 1990 to 2003, which resulted in sequencing approximately 92% of the human genome (331-333). The human genome project utilised Sanger sequencing, which was the first DNA sequencing method reliant on sequencing one DNA fragment at a time (334). The novelty, and large quantity of data which this project unveiled has revolutionised the field of genomics and wider, and ultimately, increased knowledge of human genetics, and the fundamental role of gene mutations in disease onset (335, 336). Following the human genome project, several attempts have been made to design methods which can measure the expression of all genes in samples to prevent the need for measuring expression of singular genes by laboratory techniques such as real time quantitative polymerase chain reaction (RT-qPCR). Next generation sequencing (NGS) was developed to overcome these challenges. Illumina sequencing, a short-read method (~50-300 base

pairs per read) has since become the most utilised short-read RNA sequencing platform, and has several advantages over other NGS methods, including the highest accuracy and affordability. Illumina RNA sequencing represents a powerful and high-throughput approach for comprehensive transcriptome analysis, enabling the identification of genes that are differentially expressed in response to specific signalling pathways. Therefore, this methodology enables a deeper understanding of the molecular mechanisms regulated by these pathways and offers insights into the functional significance of key pathway kinases, supporting future studies to identify their validity as potential therapeutic targets.

To study OS specifically, transcriptomics provides unique opportunities for studying distinct cellular signalling pathways which are integral to oncogenesis. The ability to screen for every human gene simultaneously would benefit OS researchers greatly, as it is a poorly funded and researched area. Transcriptomics also provides an unbiased experimental approach, by preventing the need to study genes individually which may be important to cell processes in OS cells. Therefore, transcriptomics could provide a starting point for future gene studies related to OS at a molecular level, and depending on experimental set up, may provide a variety of important genes involved in OS onset and progression.

1.27 U2OS cell line as a model for osteosarcoma

Due to the rarity of OS, and therefore the ongoing challenge to obtain human OS tissue samples, as well as the focus on the molecular mechanisms which underpin OS, it is favourable to study OS in human cell lines. The U2OS cell line was one of the first cancer-derived cell lines, initially obtained from the tibia of a 15-year-old white female OS patient in 1964. Due to their genetic stability, responsiveness to extracellular stimuli and ease to maintain in cell culture, these cells remain a widely utilised model not just for OS research but also for cell signalling responses. U2OS cells have epithelial-like homology, and display upregulated RUNX2 gene expression compared to healthy osteoblasts (300). This demonstrates the ability of U2OS cells to not only elicit osteoblastic responses, but also to upregulate osteoblast differentiation, which would be expected in primary OS.

1.28 Summary of rationale and aims

Cancer research to date has rarely examined the molecular pathways disrupted in OS, and therefore, more studies are required at a molecular level to identify new therapeutic targets for OS patients. Previous research has highlighted that IKKα is instrumental in cancer development and metastasis in NF-κB-dependent and NF-κB-independent manners. However, in the context of OS, IKKα has been continuously overlooked, and its role on downstream gene expression has yet to be identified. Therefore, to further understand the role of IKKα in regulation of oncogenes, bulk RNA-sequencing studies are a sensitive, and reliable method to identify IKKα-dependent genes. Additionally, as IL-1β-mediated non-canonical NF-κB signalling has recently been identified to be IKKα-dependent, it is important to understand the upstream kinase which regulates IKKα in this novel signalling arm, and also the downstream binding partners of p100, which will give an indication into potential pathways which may be regulated by the IL-1β/IKKα/p100 axis specifically.

The key aims of this investigation are outlined below:

1. To carry out short-read RNA-sequencing on OS cell line samples with and without IKKα CRISPR-Cas9 knockdown, and to validate these findings with laboratory techniques.
2. To characterise the use of novel selective IKKα inhibitors in IKKα-dependent signalling.
3. To identify the MAP3 kinase responsible for IL-1β-induced, IKKα-dependent signalling in U2OS cells.

The main hypotheses of this thesis are highlighted below:

Given the established pro-oncogenic role of IKKa in other cancer types, it is hypothesised that IKKa regulates the expression of multiple genes that promote oncogenesis in OS. Additionally, it is hypothesised that IL-1b-induced IKKa-dependent signalling occurs in a TAK1-dependent manner.

Chapter 2

Materials and Methods

2.1 Materials

2.1.1 Key laboratory reagents

All materials and reagents were obtained from Sigma-Aldrich Chemical Company Ltd. (Poole, Dorset, UK), unless otherwise specified.

Supplier	**Reagent(s)**
Barnford Laboratories	Ethanol
Boehringer Mannheim Ltd (East Sussex, UK)	Dithiothreitol (DTT)
Bio-Rad Laboratories (Hertfordshire, UK)	SDS-PAGE molecular weight markers
Carl Roth GmbH + Co. KG (Karlsruhe, Germany)	Acrylamide Rotiphorese Gel 30.
Corning B.V (Buckinghamshire, UK)	Cell culture flasks, plates, and pasteur pipettes
Insight Biotechnology Ltd (Middlesex, UK)	Recombinant human IL-1β and LIGHT agonists
MRC PPU Reagents and Services (Dundee, UK)	plasmid DNA (HA-p100 construct)
Sarsredt AG & Co. Ltd (Leicester, UK)	5 mL and 10 mL serological pipettes
Thermo Fisher Scientific UK Ltd (Leicestershire, UK)	Bovine Serum Albumin (BSA, L-Glutamine (Gibco™), Penicillin-Streptomycin, Dithiothreitol (DTT), Trypsin, Fetal Bovine Serum (Gibco™), McCoy's 5A Medium, 2-mercaptoethanol and 4'6-diamidino-2-phenylindole (DAPI).
Whatmann (Kent, UK):	Nitrocellulose Membrane, Whattman blotting paper.

2.2 Methods

2.2.1 U2OS cell line

Human OS epithelial cells (U2OS cell line) cells were used throughout this study (passages 3-20) and were initially obtained from American Type Culture Collection (ATCC). Most experimental work was carried out in U2OS cells, except for tissue work and Electrophoretic Mobility Shift Assay (EMSA) experiments. All cell culture work throughout this study was conducted under aseptic conditions in a class II cell culture hood (Haraeus Instruments).

2.2.2 IKKα CRISPR/Cas9 knockout cells

CRISPR/Cas9 targeting CHUK (IKKα) was designed using in silico sgRNA selection tools to identify high-efficiency target sites within the CHUK coding sequence. Three independent 20-bp sgRNAs targeting distinct regions of CHUK were selected based on predicted on-target efficiency and minimal off-target effects and obtained as validated lentiviral constructs from Addgene. Cas9 was expressed using lentiCas9-Blast or lentiCas9n (D10A)-Blast vectors, enabling stable expression following lentiviral transduction. The three sgRNAs which were designed to target IKKα, were as follows: CHUK gRNA (BRDN0001149372) (Plasmid #77033), CHUK gRNA (BRDN0001149269) (Plasmid #77034), CHUK gRNA (BRDN0001148194) (Plasmid #77035). These gRNAs were pooled together to promote maximal efficiency of IKKα knockout.

2.2.2 Maintaining Cell culture

U2OS wildtype and U2OS IKKα CRISPR/Cas9 knockout cells were seeded and maintained in T-75cm^2 flasks in 10 mL McCoy's 5A media with 10% v(v) foetal bovine serum, 1% penicillin streptomycin and 1% (v/v) L-glutamine. This media was replaced every other day. Cells were routinely stored in incubators at 37 °C, with 5% CO_2. Selection and IKKα gene knockout were maintained in McCoys 5A medium, with the addition of 5 μg/mL blasticidin and 0.4 μg/mL puromycin every 2-3 cell passages.

2.2.3 Passaging cells

Cells were enabled to proliferate until flasks were approximately 90% confluent, and then media was aspirated from the flask. Cells were washed with 1.5 mL 0.5% trypsin solution, and then 3 mL 0.5% trypsin solution was added to the flask for approximately 3 minutes. Trypsin solution was aspirated off and then 10 mL pre-incubated McCoy's 5A media was added to the flask. The flask was tapped on the bench 4-5 times whilst being kept upright throughout. Cells were resuspended in the media by use of a 10 mL stripette. Cells were generally split 1:5 from this, where 4:5 media containing cells were placed in tissue culture plates to be used for experiments or discarded.

2.2.4 Quiescing cells

Prior to carrying out experiments, cells which were seeded into appropriate tissue culture plates were enabled to grow to 90-95% confluency. Following this, the media containing 10% FBS, 1% penicillin streptomycin and 1% L-glutamine was aspirated and replaced with McCoy's medium which was not supplemented with FBS. The cells were routinely maintained in this serum free media for 24 h prior to stimulations with agonists and or collecting the cell samples for experimental procedures.

2.2.5 Cell stimulation

Quiescent U2OS Cells were stimulated throughout with recombinant IL-1β recombinant protein (10 ng/mL) and LIGHT ligand (50 ng/mL) throughout this study.

2.2.6 Cell sample collection for RNA-sequencing and RT-qPCR

Firstly, wildtype and IKKα CRISPR/Cas9 knockout U2OS cells were counted by application a haemocytometer. Approximately 100,000 cells per 6 cm dish were added and enabled to adhere and proliferate until confluent. For each passage of both IKKα CRISPR-Cas9 knockout and wildtype U2OS cells, three dishes were prepared. This was carried out for three different passages for each cell type, resulting in three independent stimulations and a total of 18 dishes: 9 dishes per cell type. Once confluent, cells were incubated in serum free media, to induce quiescence. This was

carried out for 8 h prior to the first stimulation being added, with one of the three dishes per passage being treated with IL-1β (10 ng/mL) 24 h prior to cell lysis. Following this, another dish per passage for each cell type was treated with IL-1β (10 ng/mL) 8 h before cell lysis. The final dish per group of dishes was unstimulated, which acted as a negative control for each sample set. Following the timed stimulations, all three dishes containing cells were placed on ice to maximise RNA stability and directly lysed by application of 350 μL RLT containing 10 μL β-mercaptoethanol per 1 mL of RLT buffer prepared and stored at -80 °C. This preparatory process is illustrated in Figure 2.1.

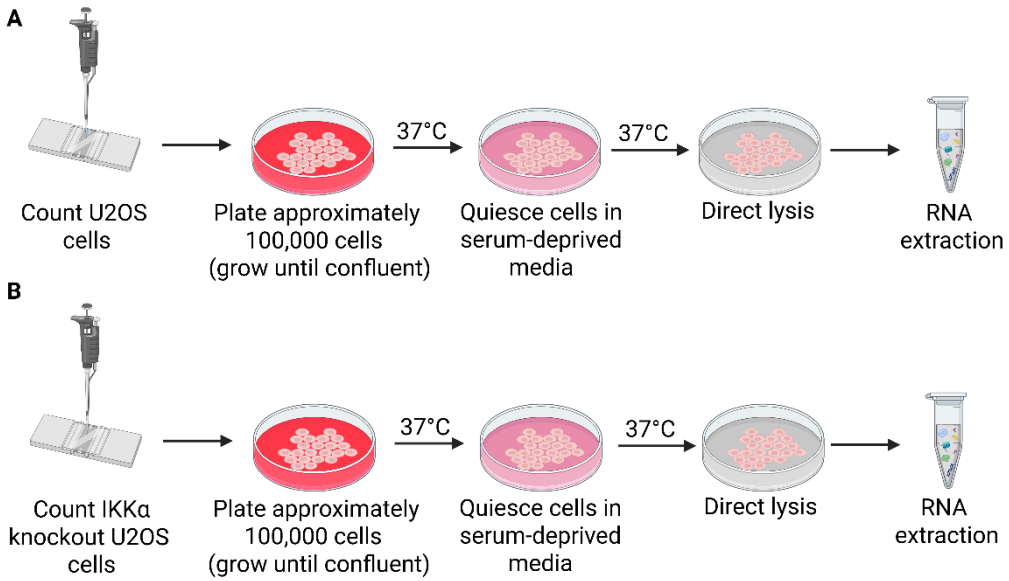

Figure 2.1. A schematic diagram highlighting the process of cell preparation for RNA extraction.
U2OS wildtype or IKKα CRISPR/Cas9 knockout U2OS cells were counted and plated into a dish. The cells were enabled to differentiate until confluent and then incubated in quiescent media. Cells were then untreated or treated with IL-1β (10 ng/mL) for 8 h or 24 h, and then directly lysed. These cells were stored at -80 °C prior to RNA extraction. Figure was created by using BioRender.com.

2.2.7 RNA extraction

To carry out RNA extraction (RNeasy mini kit by Qiagen), the cell lysates were retrieved, and the surroundings were sprayed with RNAseZap (Invitrogen by Thermo

Fisher Scientific). The prepared cell lysates were defrosted fully on ice. Cells were resuspended with a syringe. Then, all the sample (350 μL) was taken up by the syringe and placed into a 1.5 mL Eppendorf tube. 350 μL ethanol was added to the tube, and the contents were mixed with pipetting. The contents of the tube were then added to a fresh tube containing a detachable spin column containing a filter and centrifuged for 15 seconds (10000 RPM). The flow through was discarded and the spin column was placed back into the tube. The RNA was washed by addition of 350 μL RWI buffer and centrifuged for 15 seconds at 10000 RPM. The flow through was then discarded. A DNase I and Buffer RDD mixture was created consisting of 10 μL and 70 μL, respectively per sample and added to the spin columns. This was left to incubate at room temperature on the bench for 15 min. Following this, 500 μL Buffer RPE, a wash buffer with ethanol was then added and then the tube was centrifuged for 15 seconds at 10000 RPM. Flow through was discarded again. The RPE wash was repeated as before, but centrifugation was carried out for 2 min at 10000 RPM, and flow through was discarded. Finally, 30 μL RNAse-free water was added to the tube via the filter and centrifuged for 1 min at 10000 RPM to elute the RNA. A diagrammatical representation of the RNA extraction method used can be seen in Figure 2.2.

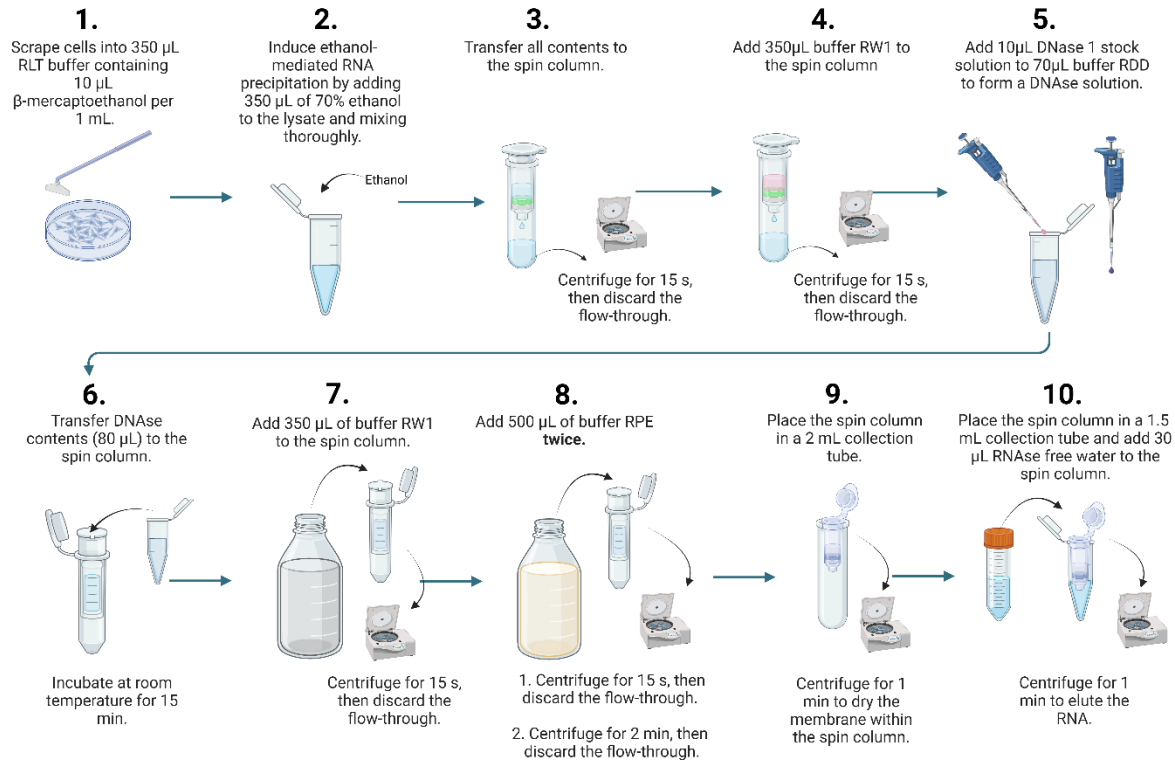

Figure 2.2. Workflow overview of RNA extraction from U2OS cells using the RNeasy Mini Kit.

The schematic illustrates the step-by-step procedure for isolating total RNA from cultured U2OS cells. Briefly, adherent cells were first lysed directly in the culture dish using RLT buffer containing β-mercaptoethanol to ensure complete disruption and inactivation of RNases. The lysate was then homogenised and transferred to a silica-membrane spin column, allowing selective binding of RNA. Following several wash steps to remove contaminants such as proteins and genomic DNA, high-purity RNA was eluted in RNase-free water. Figure created on BioRender.com.

2.2.8 RNA quantification

Following RNA extraction, 2 µL was immediately removed from the tube and added to another Eppendorf for quantification. RNA yield and purity (A260/A280, A260/A230) were determined using a NanoDrop spectrophotometer (Thermo Fisher Scientific). The remaining RNA was stored at -80 °C for future reverse transcription and RT-qPCR or sent to Genewiz at Azenta Life Sciences on dry ice for Illumina RNA-sequencing.

2.2.9 Reverse transcription

Prior to carrying out RT-qPCR experiments, complementary DNA (cDNA) was synthesised from total RNA using the Applied Biosystems High-Capacity cDNA Reverse Transcription Kit (Thermo Fisher Scientific UK Ltd, Leicestershire, UK), following the manufacturer's instructions. For each reaction, 1 μg of total RNA was used. The required volume of RNA was calculated, and sterile, nuclease-free water was added to make the volume up to 10 μL.

To reach a total reaction volume of 20 μL, 10 μL of reverse transcription master mix was prepared and added to each sample. The composition of the master mix is detailed in Table 2.1.

Table 2.1. Composition of the reverse transcription master mix used in each 20 μL reaction.

Reagent	Volume per reaction
10× RT Buffer	2 μL
25× dNTP Mix (100 mM)	0.8 μL
10× RT Random Primers	2 μL
MultiScribe™ Reverse Transcriptase	1 μL
Nuclease-free Water	4.2 μL

Thermal cycling was carried out under the following conditions: 25 °C for 10 min, 37 °C for 120 min, 85 °C for 5 min, followed by a hold at 4 °C until samples were collected. The complementary DNA synthesised was stored at -20 °C.

2.2.10 RT-qPCR

RT-qPCR was routinely applied to measure gene expression under different stimulations (IL-1β) at different time points, with different conditions including siRNA-mediated knockdown and or treatment with specific inhibitors.

2.2.10.1 RT-qPCR primers

Primers for RT-qPCR were either designed *de novo* using the target FASTA sequences inserted into the NCBI Primer-BLAST tool or selected based on previously published sequences. In the latter case, the primers were validated using NCBI BLAST to confirm specificity and ensure they were not off target. The primer sequences utilised for targets of interest in this study are outlined in Table 2.2, with HPRT1 being used as a reference gene for all RT-qPCR experiments.

Table 2.2. Primer sequences utilised for RT-qPCR.

Target of interest	Forward Primer	Reverse Primer
CXCL5	5'-CAG ACC ACG CAA GGA GTT CAT C-3'	5'-TTC CTT CCC GTT CTT CAG GGA G-3'
CXCL8	5'-ATG ACT TCC AAG CTG GCC GTG GCT-3'	5'-TCT CAG CCC TCT TCA AAA ACT TCT-3'
CXCL12	5'-CTC CGC TGT CAC CTT CCC-3'	5'-TGT GCC CTT CAG ATT GTA GCC-3'
DHCR7	5'-TCC ACA GCC TGA CCA ATG C-3'	5'-CGA AGT GGT CAT GGC AGA TGT C-3'
DHCR24	5'-CTC CTG CCG CTC TCG CTT ATC-3'	5'-GTC TTG CTA CCC TGC TCC TTC C-3'
GAS7	5'-CTC TCA GAA CTC GGC TTC AC-3'	5'-GTT CTC ACG GAA GTT CAT CAG GG-3'
HPRT1	5'-CAT TAT GCT GAG GAT TTG GAA AGG-3'	5'-CTT GAG CAC ACA GAG GGC TAC A-3'
IKKα	5-TCT GGA ACA GCG TGC CAT TGA TCT-3'	5'-ATT ACT GAG GGC CAC TTC CAC CTT-3'
IKKβ	5'-CGC CCA ATG ACC TGC CCC TG-3'	5'-GGC ACC TTC CCG CAG ACC AC-3'
OSCAR	5'-ACA TCA CTC CGT CTG TGG C-3'	5'-GTC CAA ATC TCC AAG CGG GT-3'

2.2.10.2 RT-qPCR preparation

Prior to running RT-qPCR, the 20 μL containing 1 μg of cDNA was thawed on ice. The master mix used for reverse transcription was diluted 1:10 by adding 180 μL of nuclease-free water to each sample. SybR Green was also thawed on ice.

A volume of 5 μL of the diluted DNA was added to the appropriate wells of a 96-well plate (Applied Biosystems). Each sample was assayed in triplicate for each target to ensure accuracy and reliability. A mastermix was prepared for each target gene of interest, with enough volume to add 15 μL per well. The composition of the RT-qPCR mastermix is outlined in Table 2.3.

Table 2.3. The composition of the RT-qPCR mastermix for each reaction.

Reagent	Volume
SybR green	10 μL
Forward primer	0.9 μL
Reverse primer	0.9 μL
Nuclease-free water	3.2 μL

2.2.10.3 RT-qPCR instrumentation and cycling parameters

A QuantStudio5 PCR machine (Thermo Fisher Scientific, UK) was used, with the following settings: holding stage at 95 °C for 15 seconds, followed by a PCR stage of 40 amplification cycles consisting of three steps: 95 °C for 15 seconds, 58 °C for 30 seconds, and 72 °C for 15 seconds. A melt curve was conducted during initial primer validation to assess amplification specificity.

2.2.10.4 RT-qPCR data normalisation and analysis

All RT-qPCR data were analysed relative to the target gene of interest and the housekeeping gene HPRT1, which was used for normalisation throughout. Mean threshold cycle (Ct) values were obtained for each sample, and delta Ct values were calculated using the following equation:

$$\Delta Ct = Ct_{target} - Ct_{HPRT1}$$

Relative changes in gene expression were determined using the delta delta Ct method, calculated as:

$$\Delta\Delta Ct = \Delta Ct_{treated} - \Delta Ct_{control}$$

Fold change in gene expression was calculated as:

$$Fold\ change = 2^{-\Delta\Delta Ct}$$

For genes with very low basal expression levels that were robustly induced by IL-1β stimulation, fold-change values were disproportionately large and not biologically informative. Therefore, for these genes, expression levels were additionally normalised to the maximal observed response and expressed as percentage of maximum response (% max). In this approach, the highest IL-1β-induced fold change value for each gene was set to 100%, and all other values were expressed relative to this maximum.

2.2.11. RNA quality for RNA sequencing analysis

To determine whether RNA was of adequate quantity from obtained total RNA extracted from cellular samples, RNA concentration was measured initially by utilisation of a ThermoFisher Scientific Nanodrop. To rule out sample quantification overestimation which can be influenced by contaminants when using the Nanodrop, Sample RNA was quantified again more sensitively by use of RNA Qubit assay techniques following shipment of samples to Genewiz at Azenta Life Sciences (Essex, UK).

2.2.12. Illumina RNA-sequencing

The sample RNA was initially quantified, and quality controls were carried out using a NanoDrop spectrophotometer (ThermoFisher Scientific). The RNA concentrations and 260/280 ratios were measured and within the range of 1.9-2.1 prior to sample transportation. RT-qPCR, library preparation, bridge amplification, library sequencing and read alignment to the human genome was carried out by Genewiz at Azenta Life Sciences. The workflow of the RNA-sequencing carried out is illustrated in Figure 2.3.

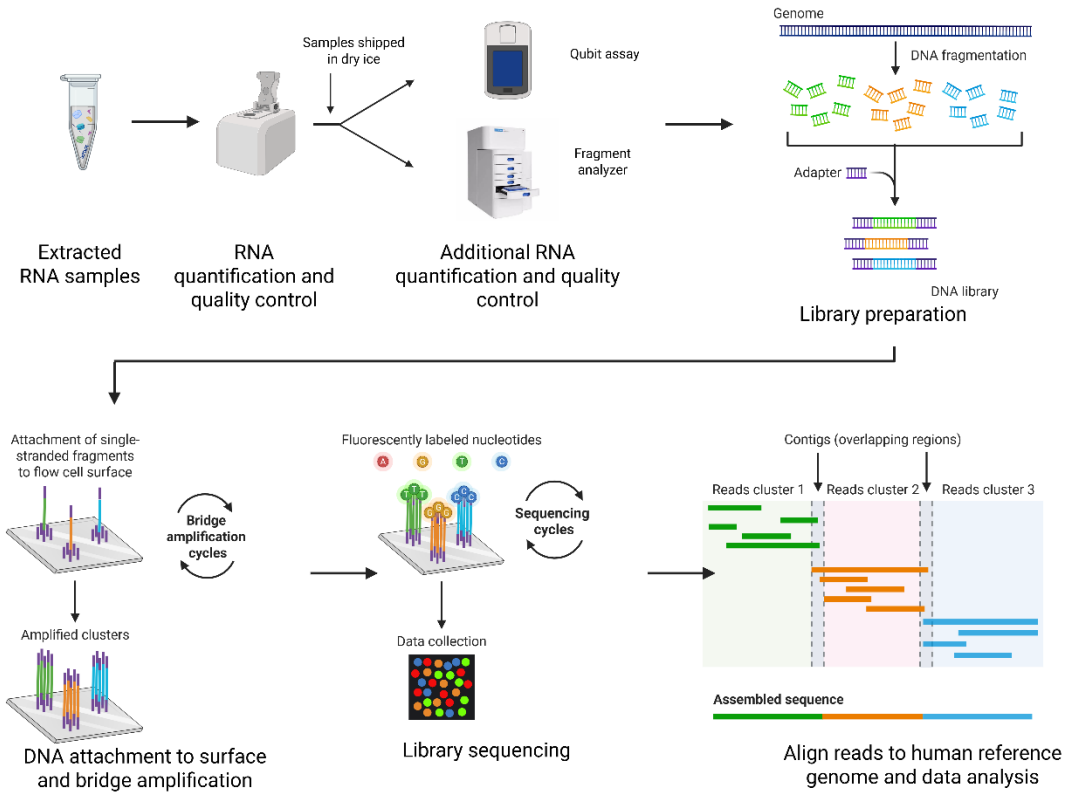

Figure 2.3. Overview of the RNA sequencing workflow used in this study. Sample preparation and handling, RNA extraction, quantification and quality control were conducted in-house, before shipment of samples to Genewiz where RT-PCR, library preparation and subsequent steps were conducted**.** Figure 2.3 was created on BioRender.com.

Each sample was independently repeated three times and grouped dependent on treatment conditions. This is outlined in Table 2.4.

Table 2.4. A demonstration of combination of the SampleIDs grouped for differential gene analysis.

Group name	Samples
WT Unstimulated	WT control 1, WT control 2, WT control 3
WT 8 hours	WT 8hr 1, WT 8 hr 2, WT 8 hr 3
WT 24 hours	WT 24hr 1, WT 24hr 2, WT 24hr 3

ND33 Unstimulated	ND33 control 1, ND33 control 2, ND33, control 3
ND33 8 hours	ND33 8hr 1, ND33 8hr 2, ND33 8hr 3
ND33 24 hours	ND33 24hr 1, ND33 24hr2, ND33 24hr3

To carry out the differential gene analysis required to determine differences between genes expressed in different treatment conditions, group comparisons were selected to be compared. This is highlighted in Table 2.5.

Table 2.5. A description of sample groups compared in differential gene analysis.

First group for comparison	Second group for comparison
WT Unstimulated	WT 8 hours
WT Unstimulated	WT 24 hours
WT 8 hours	WT 24 hours
ND33 Unstimulated	ND33 8 hours
ND33 Unstimulated	ND33 24 hours
ND33 8 hours	ND33 24 hours
WT Unstimulated	ND33 Unstimulated
WT 8 hours	ND33 8 hours
WT 24 hours	ND33 24 hours

2.2.13 Indirect Immunofluorescence

Cells were fixed in 3.6% PFA, washed in PBS and then incubated in 0.25% triton solution in PBS for 10 min. Cells were washed and incubated in 1% BSA in PBS for 30 min. Cells were then washed, and appropriate primary antibodies (1:100) were applied overnight in a humidity chamber at room temperature. Cells were washed 3 times and then incubated in 1:100 Alexa-488 Rabbit (Insert where from) or 1:100 Alexa-555 Mouse (Insert where from) secondary antibodies in 1% BSA in PBS for 1 h without exposure to light. The cells on coverslips were washed 3 times again and incubated in DAPI nuclear stain (1 μM) for 10 min. Coverslips were mounted onto microscope slides by use of Mowiol mounting media. Immunofluorescence was detected by use of a Leica SP8 confocal microscope.

2.2.14 EMSA

2.2.14.1 Origin of Mouse Embryonic Fibroblasts

WT and gene-deficient C57BL/6 mice were utilised and aligned with the National Institute of Immunology, Delhi, India Institutional Animal Ethics Committee (approval no. #258/11). Mouse Embryonic Fibroblasts (MEFs) derived from E13.5 embryos were immortalised as detailed previously (337). The gene-deficient MEFs utilised in this study include *IKK*$\alpha^{-/-}$ and *NIK*$^{-/-}$ knockout MEFs. These cells were primarily utilised in this study for EMSA experiments.

2.2.14.2 Cell culture 3T3 cells

3T3 cells were cultured in DMEM (Gibco) containing 10% FBS, 1% L-glutamine and 1% penicillin streptomycin. Cells were passaged by trypsinisation as described in Section 2.2.3. Cells were seeded into 6 cm^2 culture dishes for EMSA.

2.2.14.3 Nuclear protein sample preparation

3T3 cells in 6 cm^2 culture dishes were washed with 1 mL PBS (1x). Then, 1 mL ice cold PBS + EDTA (1 mM) was added, and cells were scraped using a sterile cell scraper. Cells were centrifuged (13000 RPM for 10 min) and then supernatant was discarded. Cells were resuspended in 100 μL cytoplasmic extract buffer. Cells were vortexed for 2 min and then placed on ice for 3 min. This was repeated for a total of 3 times. Samples were centrifuged (13000 RPM for 10 min) at 4 °C then cytoplasmic extract buffer was discarded. The pellet was then resuspended gently in 20 μL nuclear extract buffer. Samples were then placed in dry ice for 90 seconds, heated in a 30 °C water bath for 30 seconds, vortexed for 3 min and then placed on ice for 3 min for a total of 3 times. The samples were centrifuged (13000 RPM 10 min) at 4 °C. Supernatant was collected in separate microcentrifuge tube and the pellet was discarded. The samples were stored at -80 °C. Before using the samples, the protein concentration of all samples was quantified by application of the detergent-compatible protein assay. This technique requires DC protein assay Reagent S (BioRad) and DC protein assay Reagent A (BioRad) to be made up to a 1:50 working solution. 25 μL working solution and 2.5 μL nuclear extract sample were incubated in an Eppendorf tube together at room temperature for 5 min. Following this, 200 μL DC protein assay Reagent B (BioRad) was added to the Eppendorf tube and stored in the dark for 15 min to promote a colorimetric reaction due to alkaline conditions which enable

formation of a protein-copper (II) ion complex. Protein concentrations were read by a BioPhotometer Plus (Eppendorf). Sets of samples were subsequently normalised in nuclear extract buffer by use of the following formula:

$$Volume\ of\ NE\ buffer\ added = \left(\frac{OD\ sample}{OD\ lowest\ concentration\ sample} - 1\right)\ x\ 17.5$$

2.2.14.4 EMSA gel preparation

EMSA gel was prepared in a 100 mL beaker using the components and quantities listed in Table 2.6.

Table 2.6. Composition of EMSA gel preparation.

Reagent	Volume
Tris-Glycine-EDTA	36.7 mL
Acrylamide	8.35 mL
50% Glycerol	5 mL
10% Ammonium Persulphate	500 μL
N,N,N',N'-Tetramethylethylenediamine	25 μL

EMSA gel was then cast into a glass plate and a well comb was placed into the top of the gel. The gel was enabled to set for 1 h. The comb was removed, and wells were cleaned with distilled water. Wells were drawn on with a permanent marker on the outside of the glass, and the EMSA gel plate was placed into a tank filled with Tris-Glycine-EDTA in the middle section to fill the wells.

2.2.14.5 Probe labelling for EMSA

To prepare the probe for electrophoretic mobility shift assay (EMSA), 2.5 μL of nuclear extract was combined with 3 μL of binding buffer and 0.5 μL of ^{32}P-labelled probe in a microcentrifuge tube. The double-stranded oligonucleotide probe contained two consensus NF-κB binding sites with the following sequences: (Forward: 5′-GCTACAAGGGACTTTCCGCTGGGGACTTTCCAGGGAGG-3′; Reverse: 5′-

CCTCCCTGGAAAGTCCCCAGCGGAAAGTCCCTTGTAGC-3′). A free oligonucleotide control was prepared by mixing 5.5 μL of binding buffer with 0.5 μL of ^{32}P-labelled probe, to serve as a reference for unbound radioactivity. All mixtures were incubated for 20 min at room temperature before further analysis.

2.2.14.6 Gel running, transfer and imaging

While the samples incubated in the radioactive probe, the gel was pre-run for 20 min at 200 V. Following this, the gel running was paused, and the sample mixtures (6 μL) were added to the wells. The gel was run for 2 h at 200 V. The gel was removed from the running tank and placed on thick white paper. The gel was covered with clingfilm and then placed into a model 583 gel dryer (BioRad) set at 80 °C for 2 h. The gel was placed in a cassette and transferred onto a membrane for 16 h. The gel was removed, and the membrane was scanned on a Typhoon scanner.

2.2.15 pcDNA transfection

A mixture of 5 μL polyethyleneimine, 1 μg HA-p100 (Figure 2.4) and 100 μL McCoys 5A media were added to an Eppendorf tube for each well in a 12-well plate being transfected. This was upscaled for multiple wells, and the mixture was incubated at room temperature for 15 min. Fresh media was applied to each well containing 60-70% confluent U2OS cells and the pcDNA solution was applied to the U2OS cells in sterile conditions. The media was replaced after 24 h, and cells were used for SDS-Polyacrylamide Gel Electrophoresis (SDS-PAGE) samples, or for immunofluorescent samples.

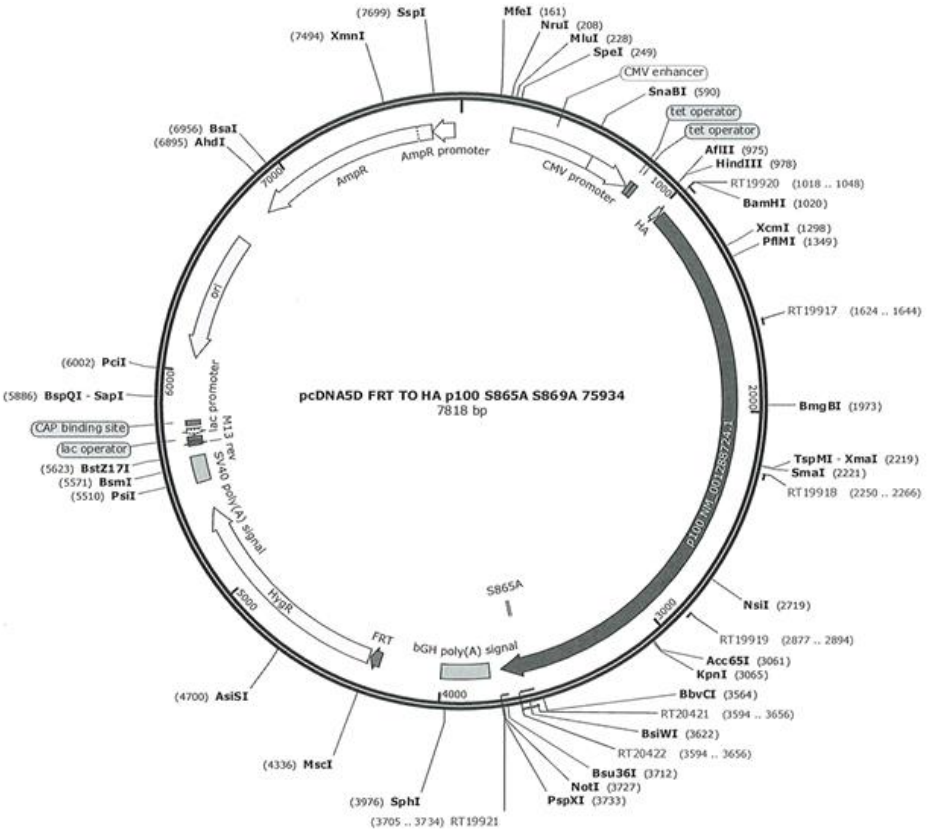

Figure 2.4. Map of the HA-p100 expression construct used for transfection of U2OS cells.
Schematic representation of the mammalian expression vector encoding the HA-tagged p100 protein.

2.2.16 Gene silencing with siRNA transfection

Small interfering RNA (siRNA) oligonucleotides were purchased from ThermoFisher Scientific (Dharmacon product line). Transfection was carried out using Lipofectamine RNAiMAX reagent following the manufacturer's guidelines, with minor modifications tailored for either 12-well or 6-well plate formats. For each transfection, the siRNA-lipid complexes were prepared fresh and scaled according to the number of wells used. The siRNA target genes and sequences are displayed in Table 2.7.

Table 2.7. siRNA Target genes, sequences and source information.

Target gene	Target sequence	Catalogue details
IKKα (CHUK)	GCGUGAAACUGGAAUAAU	Human CHUK Cat.no: J-003473-09
IKKβ (IKBKB)	GAGCUGUACAGGAGAUAA	Human IKBKB Cat.no: J-003503-13
Non-target	UGGUUUACAUGUCGACUAA	Non-target Cat.no: D-001810-01-20

2.2.16.1 Complex Formation

Tube A (siRNA Solution): For each well of a 12-well plate, 5 μL of siRNA stock was diluted in 95 μL of Opti-MEM I Reduced Serum Medium (ThermoFisher). For each well of a 6-well plate, 7.5 μL of siRNA was diluted in 142.5 μL of Opti-MEM. This tube was gently flicked to mix and incubated at room temperature for 5 min.

Tube B (Lipofectamine Solution): For each well of a 12-well plate, 2 μL of Lipofectamine RNAiMAX reagent was diluted in 98 μL of Opti-MEM. For each well of a 6-well plate, 3 μL of Lipofectamine RNAiMAX was diluted in 147 μL of Opti-MEM. This tube was also gently mixed and incubated at room temperature for 5 min. The contents of Tube A (siRNA solution) were then gently added to Tube B (Lipofectamine solution) and gently mixed. The combined mixture was incubated at room temperature for 20 min to allow lipid–siRNA complexes to form. For experiments involving multiple wells, the volumes listed were scaled accordingly to create a transfection mastermix, minimizing pipetting variability between wells.

2.2.16.2 Cell Preparation and Transfection

While the siRNA-lipid complexes were incubating, adherent cells plated in 12- or 6-well plates were prepared for transfection. The culture media were aspirated, and the wells were washed once with 1X Opti-MEM. Then, 800 μL of Opti-MEM was added to each well in a 12-well plate, and 1.7 mL to each well in a 6-well plate. Following incubation, the siRNA-lipid complexes were added directly to the wells: 200 μL of the siRNA-

Lipofectamine complex mixture was added to each 12-well plate well (final volume: 1 mL per well) or 300 μL was added to each 6-well plate well (final volume: 2 mL per well). The plates were gently rocked side to side to evenly distribute the complexes.

2.2.16.3 Incubation and Post-Transfection Culture

The cells were incubated with the siRNA-containing media for 18-20 h at 37°C in a CO_2 incubator. After incubation, the media were carefully aspirated and replaced with fresh complete McCoy's 5A growth medium. Cells remained in culture for 72 h post-transfection before being harvested for downstream assays (e.g., RNA extraction, lipid extraction or protein semi-quantification by SDS-PAGE and western blot analysis).

2.2.16.4 Preparation of cell samples for SDS-PAGE and western blot analysis

Cells were split into a 12-well plate. When ~95% confluent, the media was replaced with serum-free quiescent media to prevent excessive cell division for 24 h. Cells were then pre-treated and/or stimulated where applicable. 12-well plates were placed on ice, washed twice in ice cold PBS and cells were lysed in sample buffer (63 mM Tris-HCL, 2 mM $Na_4P_2O_7$, 5 mM EDTA, 10% (v/v) Glycerol, 2% (w/v) SDS, 0.007% Bromophenol Blue, 50 mM DTT). Individual wells were scraped, and samples collected using a syringe and placed into Eppendorf tubes. Sample tubes were then placed in a sterile boiling water bath for 5 min and then frozen at -20 °C until time of use.

2.2.17 Subcellular fractionation

WT U2OS cells and IKKα CRISPR-Cas9 knockout U2OS cells were grown in 100 mm^2 dishes and grown until 90% confluency and subsequently quiesced in serum-free medium for 24 h. Each sample required 6 x 100 mm^2 dishes. Cells were washed 3 times with ice-cold HES buffer (20 mM HEPES, 1 mM EDTA, 250 mM sucrose, pH 7.4). Cells were scraped in 4 mL HES/Inhibitor Buffer (HES buffer with 1 phosphatase and 1 protease inhibitor per 10 mL added on the day of the experiment). All cells were transferred into a 15 mL falcon tube and centrifuged at 200 x g for 5 min. The supernatant was removed, and the pellet was resuspended in 1 mL HES/Inhibitor Buffer and transferred into a 1.5 mL Eppendorf and homogenised with a syringe. The lysate was transferred into a 5 mL ultracentrifuge tube and centrifuged at 8000 RPM in a TLA 100.4 rotor for 20 min. The supernatant was transferred into a fresh 5 mL

ultracentrifuge tube (which contains high-density membrane and low-density membrane cell organelles) and stored on ice. The pellet was resuspended in 1 mL HES buffer and layered on top of 1 mL HES/Sucrose Buffer (HES buffer with 1.12 mM sucrose instead of 250 mM sucrose) in a 2 mL ultracentrifuge tube. The 2 mL tubes were centrifuged at 25000 RPM in TLS 55 rotor for 60 min. The white layer above the sucrose cushion was collected using a syringe (containing the plasma membrane) and transferred into a fresh 5 mL ultracentrifuge tube and diluted 1:5 with HE Buffer (HES Buffer without sucrose) and stored on ice. The pellet at the bottom of this 2 mL tube, containing mitochondria and nuclei, was suspended in 200 μL HES buffer and stored on ice. The supernatant from earlier containing high-density and low-density membrane organelles was centrifuged at 16000 RPM in TLA 100.4 rotor for 20 min. The supernatant (low-density membrane organelles) was transferred into a fresh 5 mL tube and resuspended in 150 μL HES Buffer. The pellet containing high density membrane organelles was transferred into a 1.5 mL Eppendorf tube. The plasma membrane and low-density membrane fractions were centrifuged at 60000 RPM in TLA 100.4 rotor for 60 min. For the plasma membrane fraction, the supernatant was discarded, and the pellet was resuspended in 150 μL HES Buffer and transferred into a 1.5 mL Eppendorf, giving the final plasma membrane. For the low-density membrane fraction, the supernatant containing soluble protein was collected and transferred into a 1.5 mL Eppendorf, giving the final low-density membrane. All fractions were mixed with the appropriate volume of 4x sample buffer and boiled for 3 min. The samples were subsequently stored at -20 °C for future SDS-PAGE and western blotting experiments.

2.2.18 Nuclear extraction

Cells in a 6-well plate were washed twice in 200 μL ice cold PBS, then scraped into 1 mL of ice-cold PBS. Cells were recovered by centrifugation at 13000 x g for 1 min. The supernatant was aspirated, and cells were resuspended in 200 μL low salt buffer (Buffer 1, pH 7.9) to swell the cells and incubated on ice for 15 min. 25 μL of 10% (w/v) NP-40 was added, and vortexed at full speed for 10 seconds. Centrifugation was carried out at 13000 x g for 2 min, and the supernatant was aspirated. 50 μL Buffer 2 (pH 7.9) was added, vortexed briefly to loosen the pellet, and placed on a shaker for

20 min at 4 °C. Eppendorf tubes were sonicated in a bath sonicator in ice for 30 seconds, twice. Samples were centrifuged at 13000 x g for 15 min, and the supernatants containing nucleus were transferred to a sterile tube. Sample buffer (63 mM Tris-HCL, 2 mM $Na_4P_2O_7$, 5 mM EDTA, 10% (v/v) Glycerol, 2% (w/v) SDS, 0.007% Bromophenol Blue, 50mM DTT) was applied to prepare nuclear lysates for SDS-PAGE. Samples were boiled for 3 min in a boiling bath. Nuclear samples were subsequently stored at -20 °C until required for SDS-PAGE.

2.2.19 Immunoprecipitation

Immunoprecipitation was carried out for endogenous protein expression throughout this study. Initially, the U2OS cells were subcultured into 100 mm^2 dishes and grown until 95% confluent, and subsequently quiesced for 24 h.

2.2.19.1 Cell lysate collection and preparation for Immunoprecipitation

Cell lysis was conducted by the following steps: Cells were washed twice in PBS (2 mL each wash), then scraped in lysis buffer (50 mM Tris-HCL pH 7.4, 1% Triton X-100 plus 1 Roche Mini Protease Inhibitor cocktail tablet per 10 mL of lysis buffer added on the day of the experiment. 500 μL of lysis buffer was added per 100 mm^2 dish containing cells on ice. Cell lysates were syringed and transferred into 1.5 mL microfuge tubes on ice. The tube lids were secured and covered in parafilm to keep them shut and tubes were end-on-end rotated for 1 h at 4 °C in the cold room. 30 μL of cell lysate was obtained after rotation and frozen at -20 °C prior to centrifugation. Sample tubes with the remaining lysate were centrifuged at 10000 RPM at 4 °C for 10 min, and 30 μL of cell lysate was collected and frozen. The supernatant was collected and transferred to a fresh tube on ice.

2.2.19.2 Pre-clearing cell lysates

Pre-clearing of lysates was performed to remove non-specific protein binding to the beads. Briefly, 20 μL of Calbiochem Protein G Plus/Protein A Agarose suspension (Merck Millipore) was washed twice with 300 μL of fresh lysis buffer by centrifugation at 3000 RPM for 3 min at 4 °C. A 300 μL aliquot of cell lysate supernatant was then added to the washed beads and rotated end-over-end at 4 °C for 60 min. Samples

were centrifuged again (3000 RPM, 3 min, 4 °C), and the resulting supernatants were transferred to new tubes without disturbing the agarose pellet.

2.2.19.3 Incubation with primary antibody

The pre-cleared lysate was incubated with 2 μL anti-HA tag antibody and rotated at 4 °C overnight. As before, 30 μL sample was collected at this stage and frozen for later troubleshooting if required.

2.2.19.4 Bead binding

Following antibody incubation, Protein A/G agarose beads were prepared as before, by washing and centrifuged twice with lysis buffer. 25 μL of bead slurry was added to each antibody-bound lysate sample and rotated for 2 h at 4 °C. The samples were centrifuged at 3000 RPM for 3 min at 4 °C, and beads were washed 3 times in lysis buffer.

2.2.19.5 Sample Elution

Samples were mixed with 2x sample buffer containing DTT (50 mM) and boiled at 95 °C for 3 min for use in SDS-PAGE and western blot analysis.

2.2.20 SDS-PAGE and Western blot analysis

Thick 1.5 mm SDS-PAGE gels were prepared at acrylamide concentrations ranging from 8-10%, depending on the molecular weight of the proteins under analysis. The resolving gel formulation was adapted accordingly to optimise protein resolution. The composition of the gels utilised for SDS-PAGE are presented in Table 2.8.

Table 2.8. Composition of SDS-PAGE acrylamide resolving gels used in this study.

Recipes are sufficient to prepare either 4 medium (1.0 mm) gels or 3 thick (1.5 mm) gels using standard gel casting apparatus.

Reagent	8% gel	9% gel	10% gel
Autoclaved purified water	11.6 mL	10.8 mL	10 mL
Buffer 1 (90.75 g Tris base, 2 g SDS, 400 mL dH_20, pH 8.8)	6 mL	6 mL	6 mL
Acrylamide	6.4 mL	7.2 mL	8 mL
APS (10%)	200 µL	200 µL	200 µL
TEMED	20 µL	20 µL	20 µL

80µL 0.1% SDS was added following resolving gel to enable the gel to uniformly set. The gels were enabled to set for 30 min, and the SDS was poured out of the top of the gel. Stacking gel was prepared. The composition of the stacking gel is presented in Table 2.9.

Table 2.9. Composition of SDS-PAGE acrylamide stacking gels used in this study.

Recipes are sufficient to prepare 6 thick (1.5 mm) stacking gels using standard gel casting apparatus.

Reagent	Volume
Autoclaved purified water	9.75 mL
Buffer 2 (30.25 g Tris base, 2 g SDS, 400 mL dH_20, pH 6.8)	3.75 mL
Acrylamide	1.5 mL
APS (10%)	250 μL
TEMED	40 μL

Stacking gel and combs were added for 25 min until stacking gels set. 30 μL cell lysates were loaded into the wells of the gel and gels were run for electrophoresis at 125 V constant voltage for approximately 1 h and 45 min at room temperature. When the cell lysates have successfully ran off from the bottom of the gel, proteins were transferred onto a nitrocellulose membrane for 2 h and 30 min at room temperature at a constant current of 300 mA. To prevent non-specific protein bands forming, membranes were blocked in 15 mL 1% BSA in NATT buffer (4 L dH2O, 35 g NaCl, 9.6 g Tris base and 1200 μL Tween 20) for 2 h. Primary antibody was applied to 3 mL 0.2% BSA in NATT buffer in a falcon tube and placed in the cold room on the shaker overnight. The details of utilised primary antibodies for western blotting are outlined in Table 2.10.

Table 2.10. Primary antibodies utilised for western blot analysis.

Protein of Interest	Antibody Source	Species	Dilution used
Phospho-NF-κB2 (p100)	Cell Signalling Technology (4810S)	Rabbit polyclonal	1:3000
IKKα	Millipore Limited (14A231)	Mouse monoclonal	1:6000
pIKKα/β	Cell Signalling Technology (2697S)	Rabbit polyclonal	1:3000
JNK	Santa Cruz Biotechnology (Sc 571)	Rabbit polyclonal	1:6000
Phospho-JNK	Cell Signalling Technology (9251S)	Rabbit polyclonal	1:3000
NF-κB2 (p100/p52)	Millipore Limited (32538)	Mouse monoclonal	1:10000
HA	Invitrogen (26183)	Mouse monoclonal	1:10000
OSCAR	Invitrogen (PA5-144371)	Rabbit polyclonal	1:5000
GAPDH	Cell Signalling Technology (14C10)	Rabbit monoclonal	1:6000
Phospho-NF-κB1 (p65)	Cell Signalling Technology (3031S)	Rabbit polyclonal	1:3000

Membranes were washed with NATT buffer 3 times for 20 min per wash and were placed on a shaker at 35-40 RPM. 2 μL of appropriate species of secondary antibody (rabbit or mouse) was applied to 14 mL 0.2% BSA in NATT buffer and placed on the shaker at 35 RPM for 1 h 30 min. Membranes were washed again as before. Excess liquid was removed from containers with membranes, and membranes were applied

to 5 mL ECL-1 and 5 mL ECL-2 for 2 min to allow chemiluminescence. Photosensitive films were exposed to membranes by use of exposure cassettes in a dark room and then developed in a JP-33 automatic film processor. For removal of primary antibodies, membranes were stripped by use of 15 mL stripping buffer with 105 μL β-mercaptoethanol added and incubated at 60 °C at 50 RPM.

2.2.21 ELISA

The Human ENA-78/CXCL5 ELISA Kit (Invitrogen obtained through Thermo Fisher Scientific) was utilised for ELISA experiments within this study.

2.2.21.1 Sample preparation for ELISA

U2OS cells were grown to 90-95% confluency, serum-starved for 24 h, then treated with IL-1β (10 ng/mL) or left unstimulated for 8 or 24 h. Conditioned media were centrifuged (300 x g, 5 min, 4 °C) to remove debris and supernatants used for ELISA.

2.2.21.2 ELISA procedure

All contents of the ELISA kit were thawed on ice prior to beginning the experiments. The media was either undiluted or diluted 1:10 for initial experiments to validate the protein concentration of CXCL5 in the media using the standard curve, and 1:10 was used in subsequent experiments. The 96-well plate coated with Human CXCL5 antibody was obtained from the freezer, and 100 μL of samples or 100 μL of standards were added in duplicate to the appropriate wells (0-18000 pg/mL). The wells were covered, and the plate was incubated for 2.5 h at room temperature with gentle shaking. The solution in the wells was discarded, and wells were washed 4 times with 300 μL of 1x wash buffer using a multi-channel Pipette. The liquid was removed after every wash by inversion of the plate and vigorous tapping on clean blue roll. Following the last wash, any remaining wash buffer was aspirated carefully. Then, 100 μL of biotin conjugate was added to each well (stock biotin conjugate concentrate was diluted 80-fold with 1X Assay Diluent B prior to use) and incubated for 1 h at room temperature with gentle shaking. The solution was discarded, and the wash steps were repeated as previously described. Next, 100 μL of streptavidin-HRP solution was

added to each well (stock streptavidin-HRP solution was diluted 500-fold with 1X Assay Diluent B prior to use) and incubated for 45 min at room temperature with gentle shaking. The solution was discarded, and the wash steps were repeated as before. 100 μL of TMB substrate was added to each well and incubated for 30 min at room temperature in the dark with gentle shaking. Following the colour change (from blue to yellow), 50 μL of Stop Solution was added to each well to terminate the reaction. The sides of the plate were tapped to mix the contents before reading. The plate was read with absorbance at 450 nm on the Molecular Devices FlexStation3 multi-mode plate reader immediately after adding the stop solution and a standard curve was generated. The standard curve was used to determine the protein concentration of CXCL5 in conditioned medium using SoftMax Pro 7.1.2 software.

2.2.22 Intracellular cholesterol quantification

2.2.22.1 Sample preparation and lysate collection

Cells were seeded into a 6-well plate and grown until approximately 50% confluent and siRNA was performed (as previously described). Cells were quiesced for 24 h prior to cell collection. Cells were washed twice with 500 μL ice cold PBS. Cells were lysed with 350 μL Buffer A (10 mM HEPES, pH 7.4, 150 mM NaCl, 1 mM EGTA, 0.1 mM MgCl2, 0.5% Triton X-100, plus one Roche Mini Protease Inhibitor cocktail tablet per 10 mL added on the day of experiment). A cell scraper was used, and lysates were transferred into Eppendorfs (1.5 mL) and centrifuged for 30 min at 4 °C.

2.2.22.2 Protein normalisation by BCA Assay

Protein concentration in lysates was normalised by performing a BCA utilising a Pierce BCA Protein Assay Kit (Thermo Scientific, 23225). A standard curve was prepared using bovine serum albumin (BSA) at concentrations ranging from 0 to 2000 μg/mL in Buffer A. 5 μL of each standard or sample made up in Buffer A was added to individual wells in duplicate of a 96-well plate. Working BCA reagent was freshly prepared by mixing Reagent B with Reagent A at a 1:50 ratio was added to each well. Buffer A alone was used as a blank control.

The 96-well plate was covered in aluminium foil and incubated at 37 °C for 30 min in a humidified cell culture incubator with 5% CO_2. Absorbance was measured at 562 nm using the Molecular Devices FlexStation3 multi-mode plate reader. A standard curve

was generated using SoftMax Pro 7.1.2 software, and sample concentrations were interpolated from the curve following blank subtraction.

2.2.22.3 Lipid extraction

To extract lipid from the lysates, a modification of the Folch method was applied (338). 225 μL chloroform and 75 μL methanol (3:1 ratio) was added with 150 μL lysate. The organic phase (bottom phase) was extracted and transferred into a new tube and left overnight at room temperature in a safety cabinet to allow solvent evaporation.

2.2.22.4 Red Amplex Cholesterol Assay

Samples were resuspended in 110 μL 1 x Reaction Buffer from the Amplex Red Cholesterol Assay kit (Invitrogen/Thermofisher). A 20 mM Amplex Red Reagent stock solution was made by thawing one vial of Amplex Red reagent and DMSO. Immediately prior to the experiment, the Amplex Red reagent (1 mg) vial was dissolved in 200 μL DMSO. The stock solution was protected from light and stored at -20 °C until use. To prepare a working solution of 300 mM Amplex Red reagent for samples, 75 μL of Amplex Red reagent stock solution was prepared with 2 U/mL HRP (50 μL), 2 U/mL cholesterol oxidase (50 μL), 0.2 U/mL (5 μL) cholesterol esterase and 4.82 mL of 1X Reaction buffer to make a total volume of 5 mL. This was scaled down depending on the number of samples being used. Another Amplex Red reagent stock was prepared without the cholesterol esterase for standards. 50 μL of samples or standards (0 to 20 mM) was put into the wells in duplicate, with 1x reaction buffer being used as a negative control, and H_2O_2 (10 mM) was used as a positive control. 50 μL of the appropriate Amplex Red reagent stock was applied to the wells to make a total volume of 100 μL per well. The plates were incubated for 30 min at 37 °C. The fluorescence was measured using the Molecular Devices FlexStation3 multi-mode plate reader using the excitation of 560 nm and emission detection at 590 nm. A standard curve was produced by SoftMax Pro 7.1.2 software and the concentration of cholesterol within samples was determined by using the equation of the line produced, where y was the measured fluorescence intensity, m was the gradient of the line, x was the concentration of cholesterol within the sample and c was where the line intercepts the y axis:

$$y = mx + c$$

2.2.23 Animal subjects and ethical compliance

Adult male Sprague Dawley rats, 8-12 weeks of age, weighing 250-300 g were purchased from the Biological Procedures Unit (BPU) at the Strathclyde Institute of Pharmacy and Biomedical Sciences, University of Strathclyde, Glasgow. The animals were housed in cages of up to 4 rats, within the Home Office Code of Practice Stocking Density, on a cycle of 12 h light/12 h dark, with access to a standard chow diet and purified water. All animals were handled in strict accordance with good animal practice approved by The Animals in Science Regulation Unit. Each procedure was performed under sterile conditions and adapted by the Guide for the Care and Use of Laboratory Animals published by the US National Institutes of Health (NIH Publication No. 85-23. revised 1996) and Directive 2010/63/EU of the European Parliament. Euthanasia was performed by administration of general anaesthesia overdose (pentobarbital).

2.2.24 Bone tissue preparation

In this study, the rat bones were washed twice with PBS, fixed in 3.7% PFA for 48 h, and then maintained in 10% EDTA solution in PBS (pH 7.8), and EDTA solution was changed every 48-72 h for approximately 8 weeks and until bones would bend without resistance. This decalcification process was crucial, as the bones needed to soften to section them properly. Following decalcification, the bone tissue was dehydrated with an increasing ethanol concentration cycle, followed by clearing with Histoclear which makes the tissue more compatible with paraffin, and further dipped in paraffin wax before collecting the bones to embed them in paraffin.

2.2.25 AlphaFold

Protein structure predictions were performed using ColabFold v1.5.2, which implements AlphaFold2. Amino acid sequences were retrieved from UniProt, saved in a text file and renamed with the .fasta extension. Sequences were formatted in standard FASTA format, as shown in an example in Table 2.11.

Table 2.11. The FASTA format of IKKα utilised for AlphaFold2 predictions.

```
>IKKa

MESCYNPGLDGIIEYDDFKLNSSIVEPKEPAPETADGPYLVIVEQPKQRGFRFRYGCEGPSH
GGLPGASSEKGRKTYPTVKICNYEGPAKIEVDLVTHSDPPRAHAHSLVGKQCSELGICAVSV
GPKDMTAQFNNLGVLHVTKKNMMGTMIQKLQRQRLRSRPQGLTEAEQRELEQEAKELKKVMD
LSIVRLRFSAFLRASDGSFSLPLKPVISQPIHDSKSPGASNLKISRMDKTAGSVRGGDEVYL
LCDKVQKDDIEVRFYEDDENGWQAFGDFSPTDVHKQYAIVFRTPPYHKMKIERPVTVFLQLK
RKRGGDVSDSKQFTYYPLVEDKEEVQRKRRKALPTFSQPFGGGSHMGGGSGGAAGGYGGAGG
GGSLGFFPSSLAYSPYQSGAGPMGCYPGGGGGAQMAATVPSRDSGEEAAEPSAPSRTPQCEP
QAPEMLQRAREYNARLFGLAQRSARALLDYGVTADARALLAGQRHLLTAQDENGDTPLHLAI
IHGQTSVIEQIVYVIHHAQDLGVVNLTNHLHQTPLHLAVITGQTSVVSFLLRVGADPALLDR
HGDSAMHLALRAGAGAPELLRALLQSGAPAVPQLLHMPDFEGLYPVHLAVRARSPECLDLLV
DSGAEVEATERQGGRTALHLATEMEELGLVTHLVTKLRANVNARTFAGNTPLHLAAGLGYPT
LTRLLLKAGADIHAENEEPLCPLPSPPTSDSDSDSEGPEKDTRSSFRGHTPLDLTCSTKVKT
LLLNAAQNTMEPPLTPPSPAGPGLSLGDTALQNLEQLLDGPEAQGSWAELAERLGLRSLVDT
YRQTTSPSGSLLRSYELAGGDLAGLLEALSDMGLEEGVRLLRGPETRDKLPSTAEVKEDSAY
GSQSVEQEAEKLGPPPEPPGGLCHGHPQPQVH
```

The FASTA file containing the relevant amino acid sequence data was uploaded onto COSMIC[2]. Following this, ColabFold 1.5.2 was selected from the toolkit to predict the protein structures from the amino acid sequence text file. The FASTA file of interest was selected, and appropriate parameters were selected, as highlighted in Table 2.12.

Table 2.12. The parameters selected for AlphaFold2 predictions.

Parameter	Selection
Number of models	5
Number of recycles	10
pLDDT	90

Advanced parameters were also selected, as amber relaxation was applied. Following selection of parameters, the settings were saved and ran externally on a supercomputer via Cosmic[2]. Once the task was completed and the output data were available, the full output file was downloaded and extracted via 7-zip on Windows. The new file which was generated from the first extraction was then itself extracted to access the five structural model predictions for the proteins in separate .pdb files in a ranked order of highest pLDDT to lowest pLDDT. The predicted aligned error (PAE) .json files were then also available for the corresponding prediction files. These files were uploaded to PAE viewer, an open-source tool designed to evaluate the quality for monomeric and multimeric predictions by calculating mean pLDDT, pTM and in multimeric predictions only, ipTM. After gathering this information, the .pdb file containing the highest ranked predicted structure was uploaded to Molstar, another readily available tool. The space filled settings were applied to identify any potential residues between proteins that may interact. Once identifying visually residues which may interact with one another, the distance setting between the residues of interest was applied. Based on review of the available literature, 0-8.5 angstrom was applied as the range where interaction between amino acid residues from two different proteins was possible and could merit laboratory investigation.

2.2.26 Data analysis

Data analysis was performed where at least three independent repeated experiments were performed. For all wet laboratory experiments excluding RNA-sequencing, data analysis was carried out following normality assessment by application of the Shapiro-Wilk test. After confirmation of normalisation, One-Way ANOVA was utilised. All data analysis for wet laboratory experiments was carried out by using GraphPad Prism 8.0.2.

2.2.26.1 Densitometry for western blot analysis

Western blots were scanned using an Epson Perfection 1640SU scanner and cropped using Adobe Photoshop version 5.0.2. Densitometry was measured with the Scion Image Programme by drawing a rectangular box around the bands to obtain a quantitative value ranging from zero, representing white, to 256, representing black. A background value was taken from another area within the same sample lane and subtracted from the band intensity for the target protein. The same procedure was followed to measure the loading control protein.

For each sample, the value for the target protein was divided by the value for the loading control. The result from the control sample was then divided by itself to standardise it equalling one-fold, and the values from all other samples were divided by the control value to calculate the fold change.

2.2.26.2 RNA-sequencing analysis

Genewiz at Azenta Life Sciences conducted the analysis for the RNA-sequencing to identify significant differentially expressed genes between sample groups. This involved FASTQC to carry out quality control of the reads. Reads were trimmed utilising Trimmomatic where quality scores for base pairs were less than 30 (less than 99.9% accuracy), particularly at the end of the reads. STAR was utilised to align the reads with the reference *Homo sapien* genome. FeatureCounts was utilised to calculate the gene count hit. Subsequently, DeSeq2 was applied to carry out differential gene analysis with the aim to identify genes with statistically significant expression changes between comparable groups. Original figures were then created to visualise the RNA-sequencing data on R. Code is presented in Appendix 1.

2.26.3 Software applications

Table 2.13. Software applied throughout this project.

Software	Applications
BioRender	Construction of illustrations
EndNote 20	Reference measurement
GraphPad prism 8	Graph construction Statistical analysis Hill equation
ImageJ	Confocal image composition Corrected total cell fluorescence measurement
Microsoft Excel	Used for data management
Microsoft PowerPoint	Used for figure composition
R	Generation of scripts Visualisation of RNA-sequencing data
ScionImage	Western blot quantification

Chapter 3

IKKα-dependent regulation of non-canonical NF-κB signalling in IL-1β stimulated U2OS cells

3.1. Chapter Introduction

While IKKα-dependent signalling in non-canonical NF-κB signalling has been covered extensively (339), its role in canonical NF-κB signalling has been less characterised. IKKα is predominantly known for its central role in non-canonical NF-κB signalling, activated by TNF superfamily members and dependent on NIK accumulation, as covered in chapter 1. NIK phosphorylates IKKα and recruits IKKα to p100 to aid IKKα-dependent p100 phosphorylation, resulting in the degradation of p100, liberation of p52 and subsequent nuclear translocation of p52:RelB heterodimers. Traditionally, IKKα is thought to have a minor or redundant role in canonical NF-κB signalling, despite its presence within the IKKα, IKKβ and IKKγ trimeric IKK complex which facilitates downstream canonical NF-κB signalling. As stated in chapter 1, canonical NF-κB signalling is TAK1-dependent, mostly driven by IKKβ in the IKK complex, and results in IκBα phosphorylation, ubiquitination and proteasomal degradation, and subsequent nuclear translocation of p65-p50 heterodimers. Recent attempts have begun to challenge this paradigm and unravel the role of IKKα in canonical NF-κB signalling, with a particular focus on IL-1β-mediated signalling (296, 340). Recent literature is increasingly recognising that IκBα can also be phosphorylated by IKKα and therefore promote downstream canonical NF-κB signalling (341). Additionally, studies have now highlighted a role for IKKα in IL-1β-mediated NIK-independent p100 phosphorylation (296). Therefore, this chapter further validates this paradigm, by utilising various interventions, including CRISPR/Cas9 and several novel selective IKKα inhibitors. Subsequent experiments were conducted to investigate signalling events upstream of IKKα in the IL-1β-mediated IKKα/p100, with particular focus on identifying the upstream MAP3K responsible for regulating these events. to evaluate the upstream MAP3K which regulates these events. Additionally, experiments were performed to explore whether the IL-1β-mediated IKKα/p100 axis results in downstream NF-κB isoform regulation.

This chapter focuses on further depicting this pathway and validating it in U2OS cells, by the application of TAK1 inhibitor, 5Z-7-oxozaenol. Additionally, in this chapter, the effect of IKKα CRISPR/Cas9 knockout, and novel selective IKKα inhibitors on IL-1β-mediated non-canonical NF-κB signalling are explored on downstream p100 phosphorylation. Furthermore, overexpression of p100 by pcDNA transfection is

utilised to assess the effects of IL-1β stimulation on HA-p100 expression. This investigates a time point where p100 is shown to be phosphorylated in this chapter as well as well as a time point where p100 phosphorylation is back to basal levels following stimulation to understand whether p100 is degraded following phosphorylation in this pathway like in normal non-canonical NF-κB signalling, or alternatively, if it is likely to have a downstream effect which differs from non-canonical NF-κB signalling events.

One way in which IKKα-dependent effects has been commonly investigated is using mouse embryonic fibroblasts (MEFs) derived from IKKα$^{-/-}$ embryos (286, 342). Although IKKα knockout mice exhibit perinatal lethality due to severe developmental defects, including skin and skeletal abnormalities (343), MEFs isolated from these embryos can be maintained in culture and provide a valuable system for dissecting downstream signalling mechanisms. In this chapter, wildtype, NIK$^{-/-}$ and IKKα$^{-/-}$ MEFs were used to perform preliminary electrophoretic mobility shift assays (EMSAs) to assess the temporal dynamics of NF-κB-DNA binding activity following IL-1β stimulation.

In summary, this chapter aimed to:

1. Measure IKKα with indirect immunofluorescent techniques in rat tibia tissue and U2OS cells to ensure prominent IKKα expression is relevant to bone function.
2. Utilise IKKα CRISPR/Cas9 knockout and novel IKKα inhibitors to confirm an IKKα dependent phosphorylation of p100.
3. Evaluate the effects of a TAK1 inhibitor on IL-1β-induced IKKα-dependent p100 phosphorylation and compare this to the effects of TAK1 inhibition on canonical NF-κB and JNK signalling.
4. Utilise a computational approach, known as ColabFold, to predict IKKα structure and binding to another MAP3K of interest, and validate findings with immunoprecipitation experiments.
5. Assess potential downstream effects of IL-1β-induced IKKα-dependent signalling in U2OS cells, and measure NF-κB-DNA-binding activity in response to IL-1β in MEFs.

3.2 IKKα expression in rat bone tissue and U2OS cells

3.2.1. IKKα localisation in rat tibias

Whilst U2OS cells are a stable bone cancer cell line, they have significant limitations with respect to bone pathophysiology. Therefore, healthy rat bone tissue, which was available within the department, was utilised to determine the expression of IKKα in a healthy bone environment. While IKKα has been studied in various bone-related diseases, such as osteoarthritis and rheumatoid arthritis, there are no known reports of its protein levels being measured in bone using indirect immunofluorescence. This gap is particularly significant, as research on the role of IKKα in bone cancer remains limited. Establishing its detectability in healthy bone is essential for accurately interpreting its involvement in pathological conditions. After sectioning the tissue, attempts were made utilising a pressure cooker. Following optimisation of methods, where heating and rehydration of bone tissue led to tissue detachment from slides, methods with an antigen retrieval step and without an antigen retrieval step were assessed. Then indirect immunofluorescence was carried out for IKKα. Interestingly, but not surprisingly, the no antigen retrieval method was unsuccessful at unmasking the PFA and therefore, minimal antibody-binding was observed (Figure 3.1).

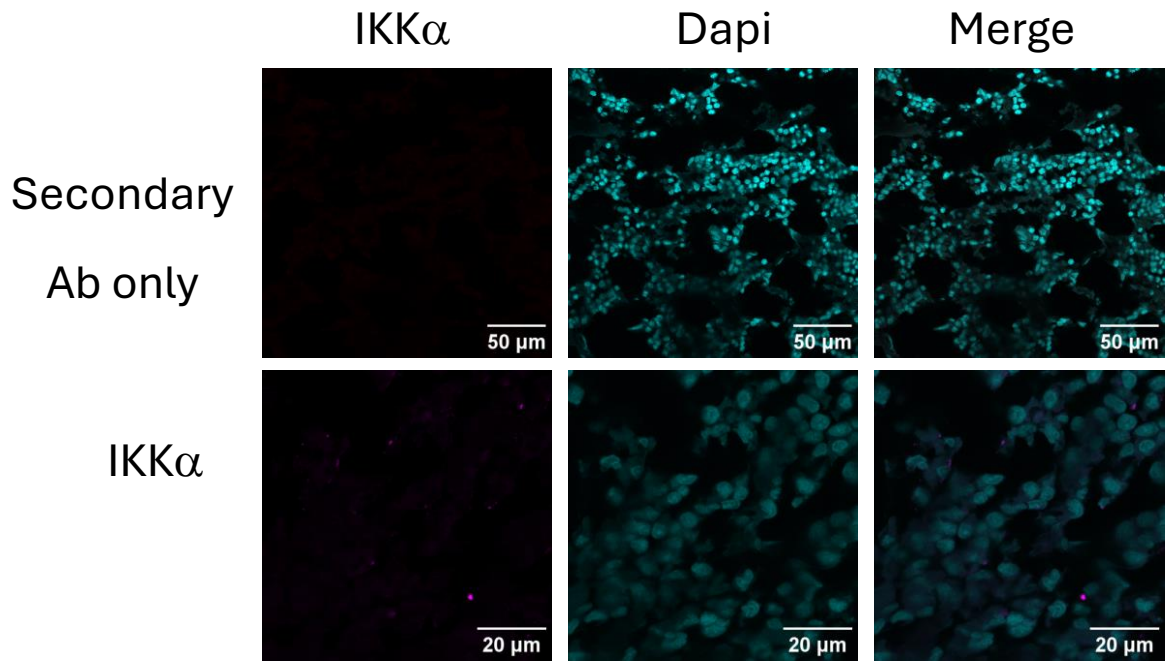

Figure 3.1. Lack of detection of IKKα in healthy rat tibia tissue using indirect immunofluorescence with no antigen retrieval.

To assess IKKα expression in healthy bone, rat bones were fixed in 3.7% PFA, decalcified in 10% EDTA for ~8 weeks until sufficiently softened, and embedded in paraffin. Sections were prepared and subjected to no antigen retrieval. Indirect immunofluorescence was performed to detect IKKα. Images were captured on a Leica SP8 confocal microscope, n=1.

However, the antigen retrieval method led to clear results, which showed a cytosolic localisation of IKKα (Figure 3.2).

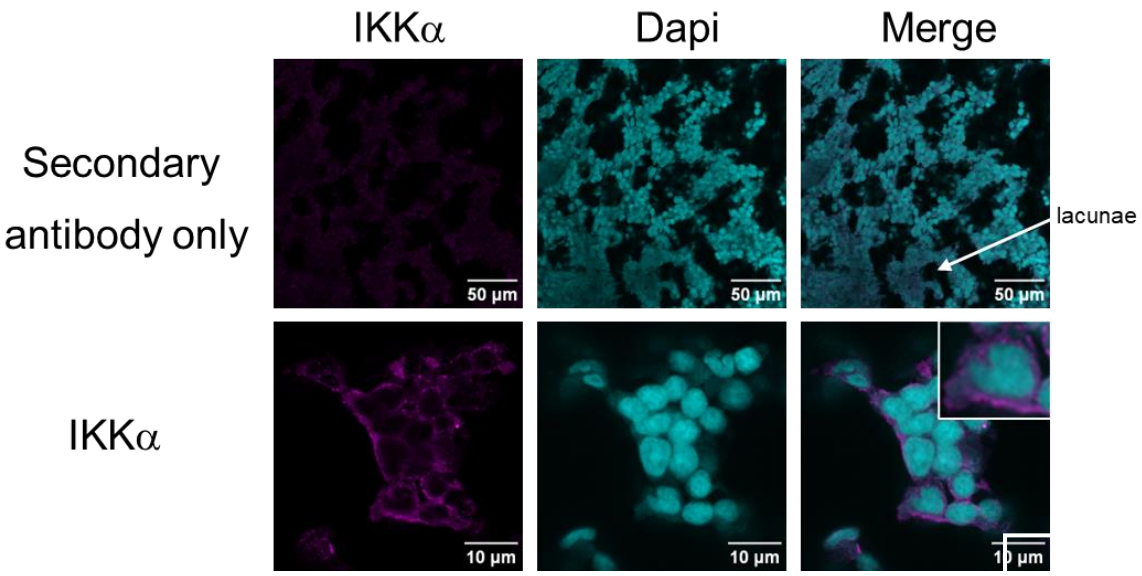

Figure 3.2. Detection of IKKα in healthy rat tibia tissue using indirect immunofluorescence with antigen retrieval.
Rat bones were fixed in 3.7% PFA, decalcified in 10% EDTA for ~8 weeks until sufficiently softened, and embedded in paraffin. Sections were prepared and subjected to EDTA-based retrieval using microwave heating (4.5 min on low heat, followed by 5 min at room temperature). Indirect immunofluorescence was performed to detect IKKα, by use of IKKα primary antibody (1:100) and Alexa-555 fluor anti-mouse secondary antibody (1:100). Images were captured on a Leica SP8 confocal microscope, n=3.

3.2.2 The expression and localisation of IKKα expression in U2OS cells

Using a standard preparation approach (see methods) the expression of IKKα in U2OS was examined. IKKα structure in U2OS cells similarly appears to be cytosolic. However, in some images (Figure 3.3), it is possible to detect nuclear IKKα in U2OS cells. This demonstrates that like in rat bone, IKKα protein expression can be detected in a human OS cell line.

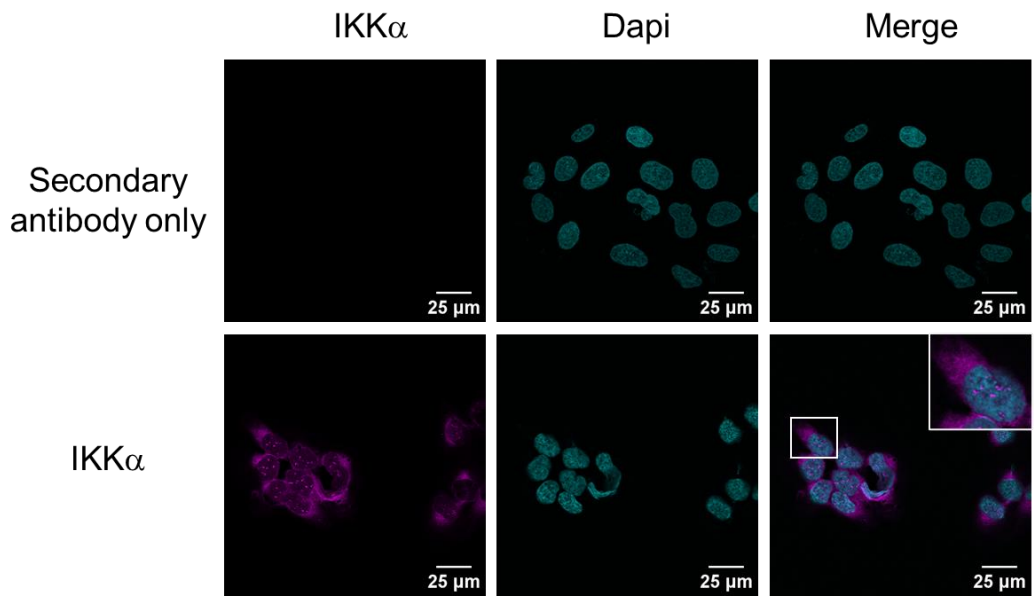

Figure 3.3. Expression and localisation of IKKα in U2OS cells.
U2OS cells were fixed in 3.7% PFA and blocked with 1% BSA in PBS. Cells were incubated with IKKα primary antibody (1:100) overnight at 4 degrees Celsius in a humidity chamber, followed by three washes with PBS. Alexa Fluor 555-conjugated secondary antibody was applied for 1.5 hours, followed by three additional washes. Nuclei were stained with DAPI for 10 minutes, and cells were mounted on slides using Mowiol. The zoomed in region highlights the nuclear and cytosolic localisation of IKKα, n=3.

3.3. IL-1β and LIGHT-induced phosphorylation of p100

Firstly, SDS-PAGE and western blotting analysis was utilised to semi-quantitatively measure p100 phosphorylation in response to canonical NF-κB ligand, IL-1β, and non-canonical NF-κB ligand, LIGHT across various time points (Figure 3.4). In response to LIGHT, maximal p100 phosphorylation (13.8-fold ± SEM) was observed after 2-4 hours stimulation. This aligns with several reviews and studies (265, 290, 344). In comparison, following IL-1β stimulation, earlier p100 phosphorylation was observed, and maximal p100 phosphorylation occurred after 30-60 minutes, measured at approximately 10.8- and 12.1-fold ± SEM, respectively. Additionally, p100 phosphorylation at 90 and 120 minutes of IL-1β stimulation was significantly lower than at 60 minutes, while remaining at approximately 3-fold and 2.6-fold compared with the control, respectively. Notably, while not quantified, there does not appear to be any total p100 degradation at any time point measured following IL-1β or LIGHT stimulation.

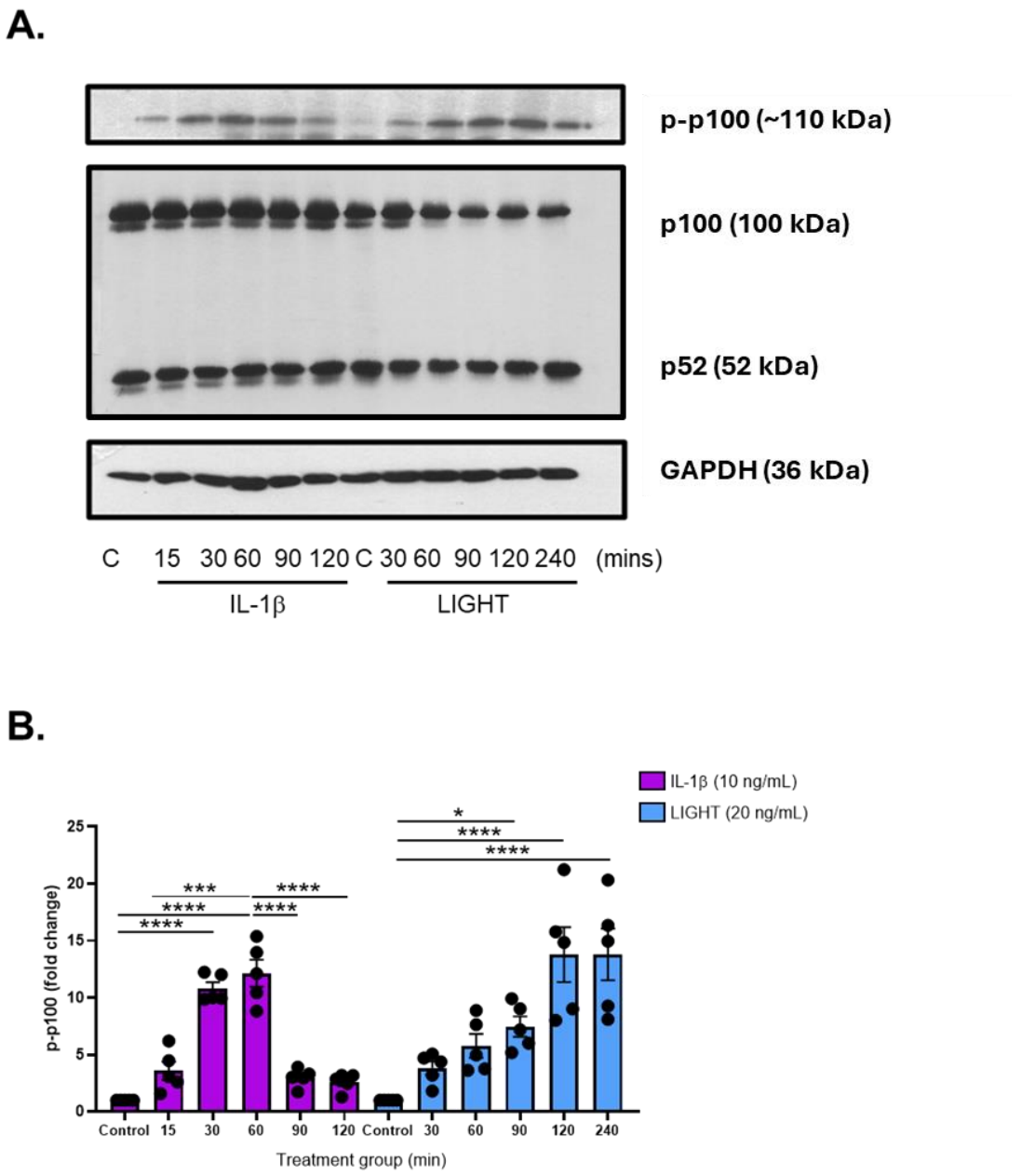

Figure 3.4. IL-1β and LIGHT ligands promote p100 phosphorylation in U2OS cells.

U2OS cells were either untreated or treated with IL-1β (10 ng/mL) or LIGHT (20 ng/mL) for the timepoints indicated. **A.** Phospho-p100 levels were measured in whole cell lysates by application of SDS-PAGE and western blot analysis using phospho-p100, p100 and GAPDH primary antibodies. **B.** Pixel density was quantified using ScionImage. A One-way ANOVA was performed to compare IL-1β-treated samples to the appropriate control, and IL-1β samples stimulated for 60 min were compared with all other samples in the relevant group (magenta). Additionally, the relevant control

was compared to each of the samples stimulated with LIGHT (blue). One-way ANOVA was conducted using GraphPad Prism 8, *p<0.05, ***p<0.001, ****p<0.0001 (n=5).

3.4. IL-1β- and IKKα-dependent p100 phosphorylation

Due to the early p100 phosphorylation induced by IL-1β, the following experiments focused on determining whether p100 phosphorylation is IKKα-dependent, similar to non-canonical NF-κB signalling mediated by TNF-superfamily members. This was explored by comparing p100 phosphorylation in wildtype U2OS and IKKα CRISPR-Cas9 knockout U2OS cells (Figure 3.5). The results in Figure 3.5 demonstrate p100 phosphorylation being effectively diminished in the absence of IKKα at time points between 15- and 120-min stimulation with IL-1β. Notably, the maximal p100 phosphorylation in wildtype U2OS cells within Figure 3.5 was approximately 9.6- and 9.8-fold ± SEM at 30 and 60 min, respectively. These data demonstrate similar results to those observed in Figure 3.4, demonstrating consistency with sample preparation. In all stimulated conditions (15, 30, 60, 90 and 120 min), IL-1β-induced p100 phosphorylation is diminished in IKKα CRISPR/Cas9 knockout U2OS cells. Additionally, p100 phosphorylation in IKKα knockout whole cell lysate samples were not significantly increased at any time point following IL-1β stimulation compared to the control. This exemplifies the IKKα-dependent nature of IL-1β-induced p100 phosphorylation. Additionally, IL-1β-mediated p100 phosphorylation does not appear to result in any p100 processing into p52 over the 120-minute time-period assessed.

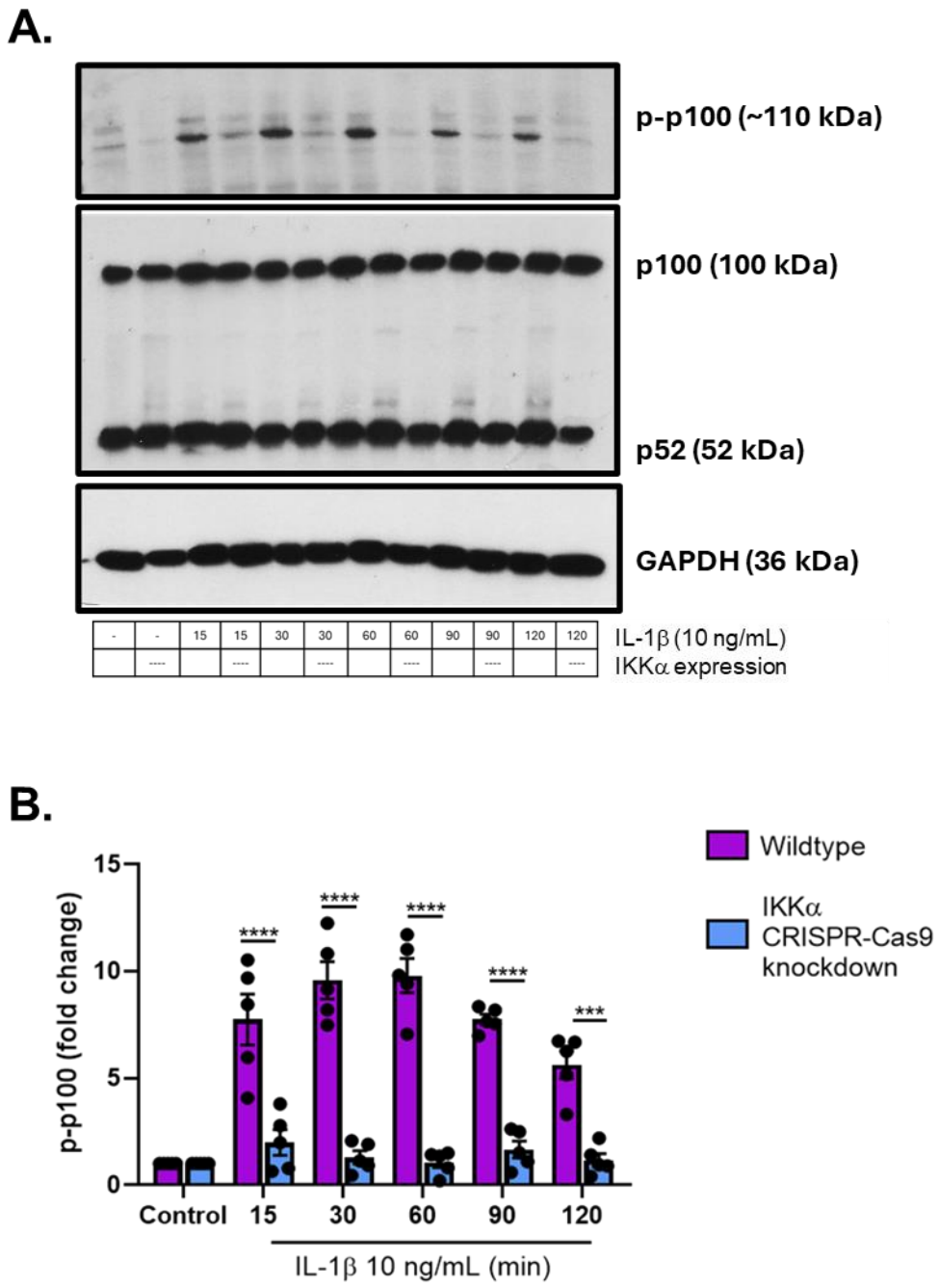

Figure 3.5. IL-1β-induced p100 phosphorylation is IKKα-dependent in U2OS cells.

A. Phosphorylation of p100 was measured in WT and IKKα CRISPR/Cas9 knockout U2OS cells by SDS-PAGE and western blot analysis techniques. P100 and GAPDH primary antibodies were used as total protein controls. **B.** Pixel density was quantified using ScionImage. One-way ANOVA analysis was carried out using GraphPad Prism 8, ***p<0.001, ****p<0.0001 (n=5).

3.5. The characterisation of the effect of novel IKKα inhibitors on IL-1β-mediated p100 phosphorylation

After establishing that phosphorylation of p100 is IKKα dependent using CRISPR-Cas9 in the U2OS cell system, novel IKKα inhibitors were applied to validate their effectiveness of inhibiting IKKα-mediated p100 phosphorylation. Firstly, SU1349, a novel and selective IKKα inhibitor was utilised. All concentrations tested in a low micromolar range (0.3 μM - 20 μM) of SU1349 resulted in a significant decrease in IL-1β-mediated phospho-p100 expression, and in a concentration-dependent manner (Figure 3.6).

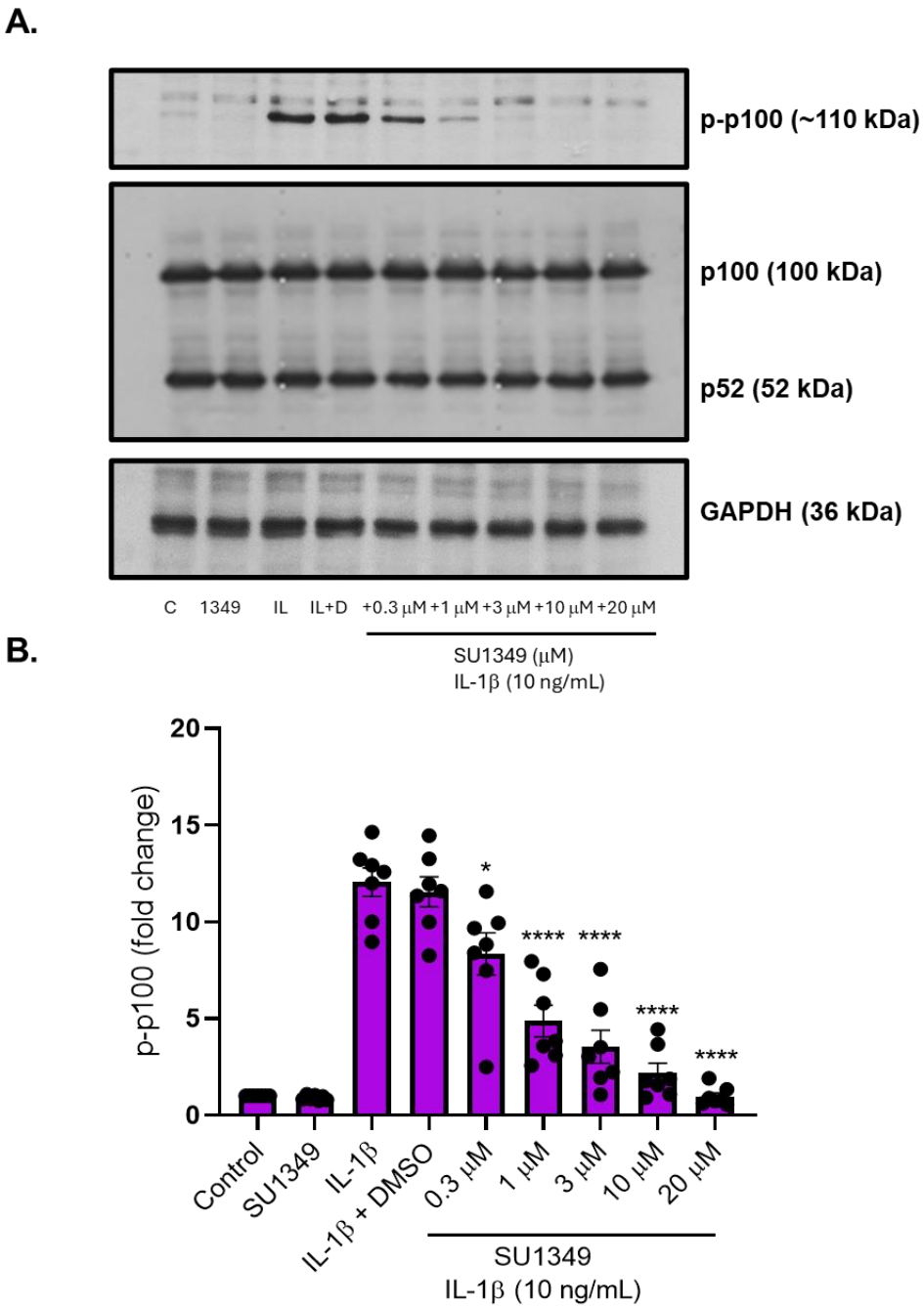

Figure 3.6. The effect of SU1349 on IL-1β-mediated p100 phosphorylation in U2OS cells.

Cells were seeded to 90-95% confluency before being maintained in serum-free media for 24 hours. Cells were untreated or pre-treated with SU1349 (0.3, 1, 3, 10 or 20 μM) prior to being unstimulated or stimulated with IL-1β (10 ng/mL) for 30 minutes. **A.** Cells were lysed and SDS-PAGE was carried out followed by western blot analysis. **B.** Statistical analysis was conducted by utilising one-way ANOVA on GraphPad Prism 8. Data represents mean p100 phosphorylation fold change compared to control ± SEM, n=7, *p<0.05, ****p<0.0001.

Another selective IKKα inhibitor, SU1261, was utilised to characterise its effect on IL-1β-induced non-canonical NF-κB signalling. SU1261 was applied at 1 μM, 3 μM, 10 μM and 20 μM. IL-1β and DMSO treatment resulted in a 11.6-fold increase in phospho-p100 expression, which was significantly decreased (*$p<0.05$) to approximately 7.3-fold, a 37 % reduction, with 1 μM SU1261 pre-treatment (Figure 3.7).

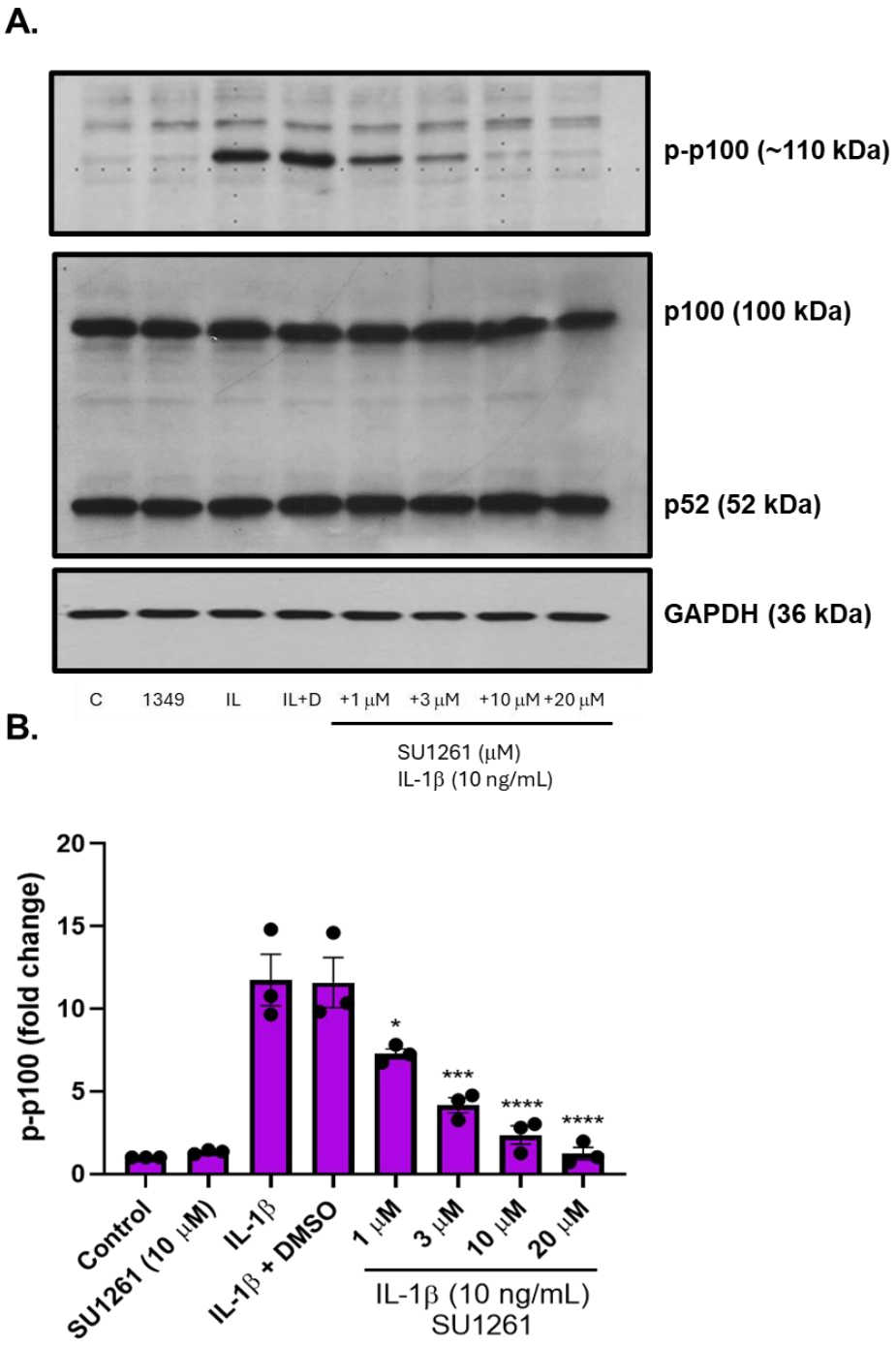

Figure 3.7. The effect of SU1261 on IL-1β-mediated p100 phosphorylation.
U2OS cells were seeded to 90-95% confluency before being maintained in serum-free media for 24 hours. Cells were untreated or pre-treated with SU1261 (1, 3, 10 or 20 μM) prior to being unstimulated or stimulated with IL-1β (10 ng/mL) for 30 minutes. **A.** Cells were lysed and SDS-PAGE was carried out followed by western blot analysis. **B.** Statistical analysis was conducted by utilising one-way ANOVA on GraphPad Prism 8. Data represents mean p100 phosphorylation fold change compared to control ± SEM, n=4, *p<0.05, ***p<0.001, ****p<0.0001.

A final novel IKKα inhibitor, SU1266 (318) which is a dual IKKα/IKKβ inhibitor but more potent towards IKKα, was tested for its effectiveness in suppressing IL-1β-mediated p100 phosphorylation (Figure 3.8). SU1266 appeared to be the most potent of the three novel IKKα inhibitors tested, reducing IL-1β-induced p100 phosphorylation from a 12.8-fold increase in IL-1β and DMSO-treated cells to 2.1-fold with 0.3 μM SU1266 pretreatment (****p<0.0001), and to 1.3-fold with 1 μM SU1266 (****p<0.0001).

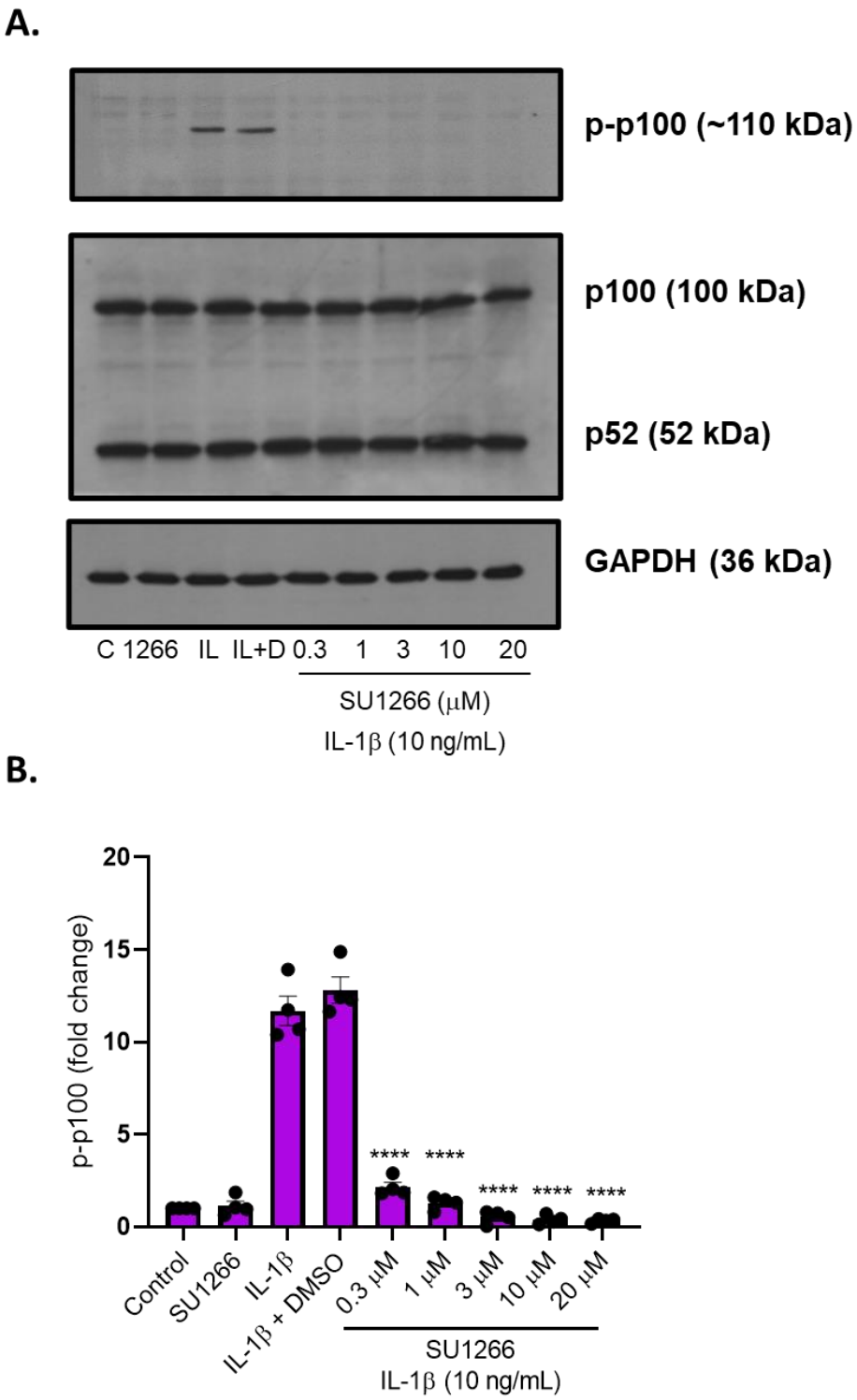

Figure 3.8. The effect of SU1266 on IL-1β-mediated p100 phosphorylation.
U2OS cells were seeded to 90-95% confluency before being maintained in serum-free media for 24 hours. Cells were untreated or pre-treated with SU1266 (0.3, 1, 3, 10 or 20 μM) prior to being unstimulated or stimulated with IL-1β (10 ng/mL) for 30 minutes. **A.** Cells were lysed and SDS-PAGE was carried out followed by western blot analysis. **B.** Statistical analysis was conducted by utilising one-way ANOVA on GraphPad Prism 8. Data represents mean p100 phosphorylation fold change compared to control ± SEM, n=4, *p<0.05, ****p<0.0001.

3.6. The characterisation of the effect of novel IKKα inhibitors on IL-1β-induced IκBα loss

To confirm selectivity for IKKα-mediated IL-1β-dependent signalling events, the inhibitors were also utilised to assess their effects on IKKβ-dependent IκBα expression. Initially, SU1261 was applied at various concentrations (1- 20 μM), where IL-1β-induced IκBα loss was not reversed at any of the tested concentrations (Figure 3.9). This implies SU1261 is not acting off target on IKKβ at the concentrations tested. This experiment was not extensively repeated as the main aim of this study was to look at IKKα-dependent responses, so this was simply applied as a proof-of-concept experiment.

SU1349 was also utilised at various concentrations (1- 20 μM), where IL-1β-mediated IκBα loss was not reversed at any of the concentrations applied (Figure 3.10).

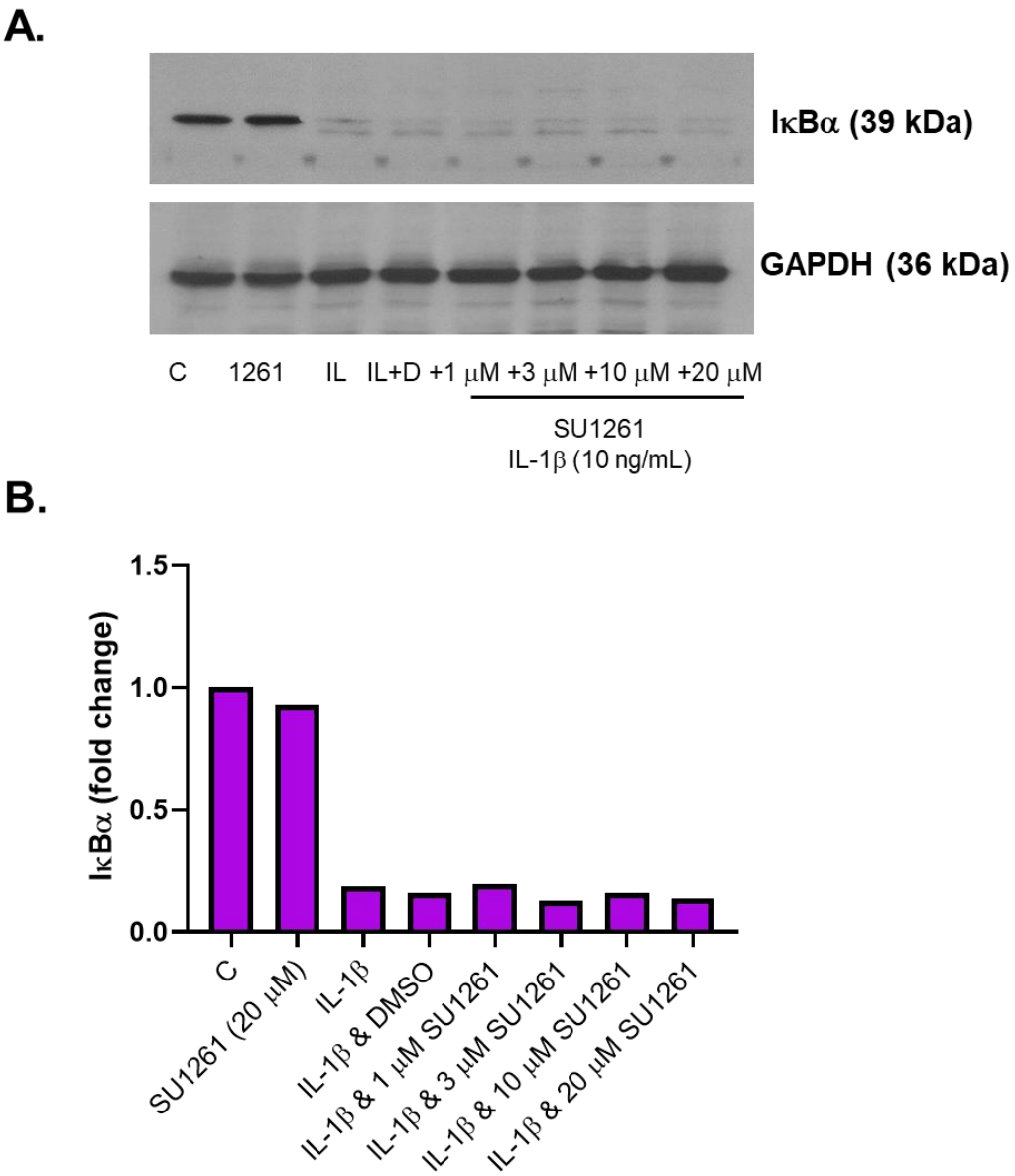

Figure 3.9. SU1261 has no effect on IL-1β-mediated IκBα loss.
U2OS cells were seeded to 90-95% confluency before being maintained in serum-free media for 24 hours. Cells were untreated or pre-treated with SU1261 (1, 3, 10 or 20 μM) prior to being unstimulated or stimulated with IL-1β (10 ng/mL) for 15 minutes. **A.** Cells were lysed and SDS-PAGE was carried out followed by western blot analysis with IκBα primary antibody. **B.** Data represents mean IκBα fold change compared to control, n=1.

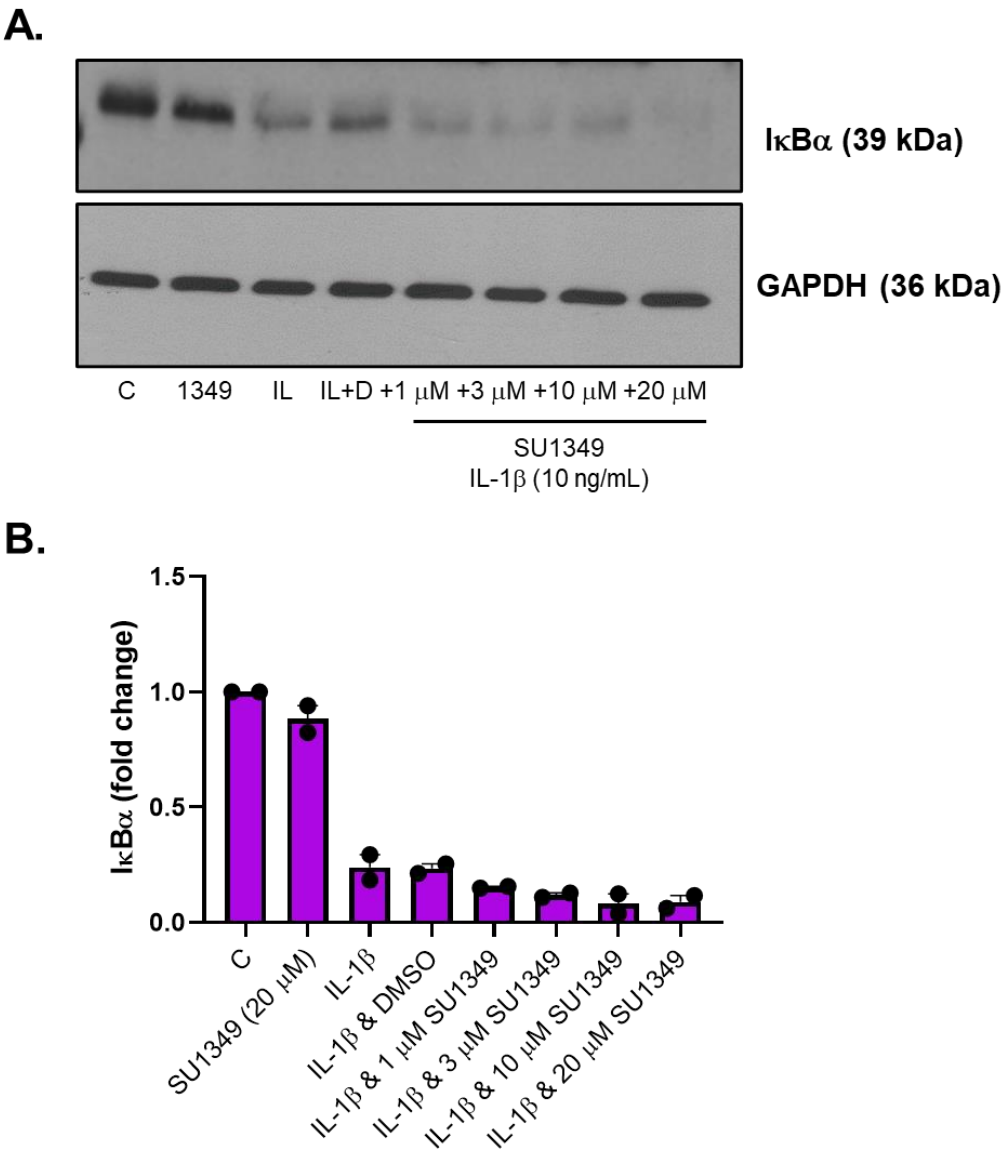

Figure 3.10. SU1349 has no effect on IL-1β-mediated IκBα loss.
U2OS cells were seeded to 90-95% confluency before being maintained in serum-free media for 24 hours. Cells were untreated or pre-treated with SU1349 (1, 3, 10 or 20 μM) prior to being unstimulated or stimulated with IL-1β (10 ng/mL) for 15 minutes. **A.** Cells were lysed and SDS-PAGE was carried out followed by western blot analysis with IκBα primary antibody. **B.** Data represents mean IκBα fold change compared to control ± SEM, n=2.

Finally, SU1266 was utilised at varying concentrations (1-20 μM), which highlighted that SU1266 can successfully reverse IL-1β-mediated IκBα degradation (Figure 3.11). This demonstrates that while the known selective IKKα inhibitors do not have any effects on IL-1β-mediated IκBα loss, SU1266 can reverse this by its dual role on IKKα and IKKβ at the concentrations tested.

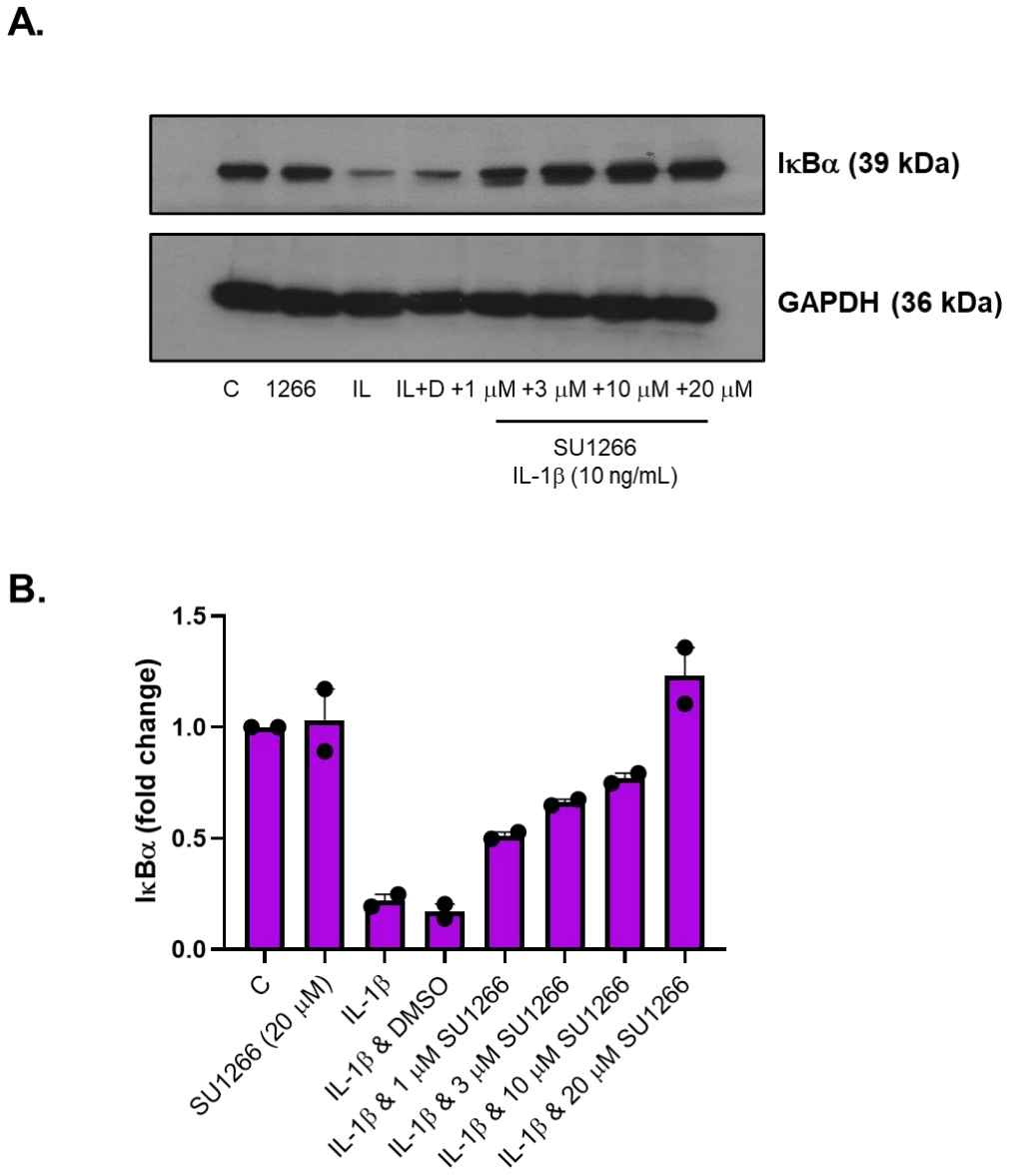

Figure 3.11. SU1266 reverses IL-1β-mediated IκBα loss.
U2OS cells were seeded to 90-95% confluency before being maintained in serum-free media for 24 hours. Cells were untreated or pre-treated with SU1266 (1, 3, 10 or 20 μM) prior to being unstimulated or stimulated with IL-1β (10 ng/mL) for 15 minutes. **A.** Cells were lysed and SDS-PAGE was carried out followed by western blot analysis with IκBα primary antibody. **B.** Data represents mean IκBα fold change compared to control ± SEM, n=2.

3.7. Investigation of HA-p100 expression levels following IL-1β stimulation

After determining IKKα-dependency of p100 phosphorylation and subsequently characterising novel IKKα inhibitors, another scientific question which should be addressed is understanding whether IL-1β-mediated p100 phosphorylation results in p100 proteasomal processing and degradation. Since there are no available antibodies which can detect endogenous p100 without also targeting p52, an HA-tagged p100 pcDNA construct was generated (University of Dundee) and utilised to effectively detect p100 specifically. Initially, three concentrations of HA-p100 were utilised to determine the optimal quantity of HA-p100 to use for further experimental validation. The three concentrations: 1 μg, 1.5 μg and 2 μg HA-p100 were all detectable by SDS-PAGE and Western blot analysis (Figure 3.12). Therefore, 1 μg was utilised going forward in further experiments.

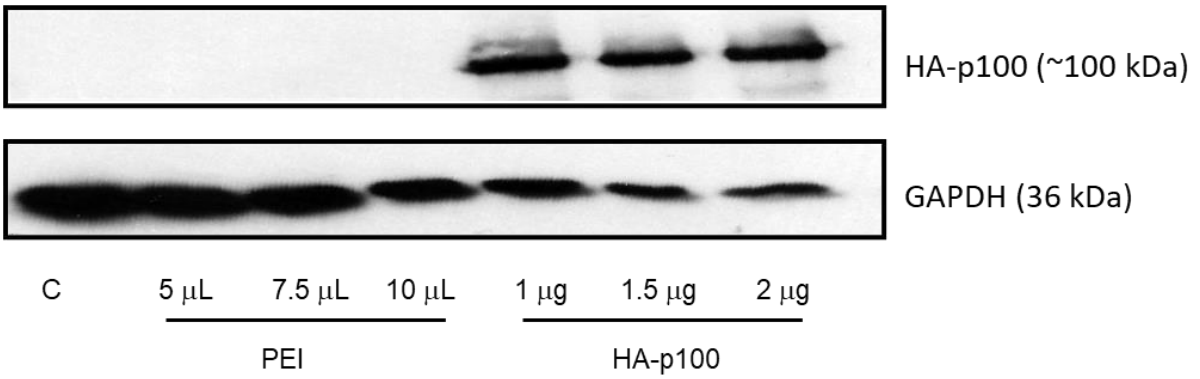

Figure 3.12. Representative of HA-p100 transfection optimisation.
Cells were incubated in media only or transfected with PEI alone (5 mL, 7.5 mL or 10 mL) or 1 μg, 1.5 μg or 2 μg with 5 μL PEI/μg pcDNA for 48 hours prior to cell lysis. Transfection was evaluated by SDS/PAGE and western blot techniques (n=3).

After optimisation of HA-p100 transfection, this construct was utilised to build on the current knowledge of the IL-1β-mediated phospho-p100 axis. U2OS cells were transfected with 1 μg HA-p100 and subsequently left unstimulated or were stimulated with IL-1β for 1 or 2 hours. Corrected total cell fluorescence was measured for these unstimulated and stimulated conditions, revealing that there is no statistically significant difference in HA-p100 across these three conditions (Figure 3.13). Therefore, it does not appear that overexpressed p100 is degraded in the presence of IL-1β stimulation. However, given the nature of overexpressing any protein and the natural variability in expression which can occur, this method cannot provide definitive evidence that p100 is not cleaved into the p52 NF-κB subunit.

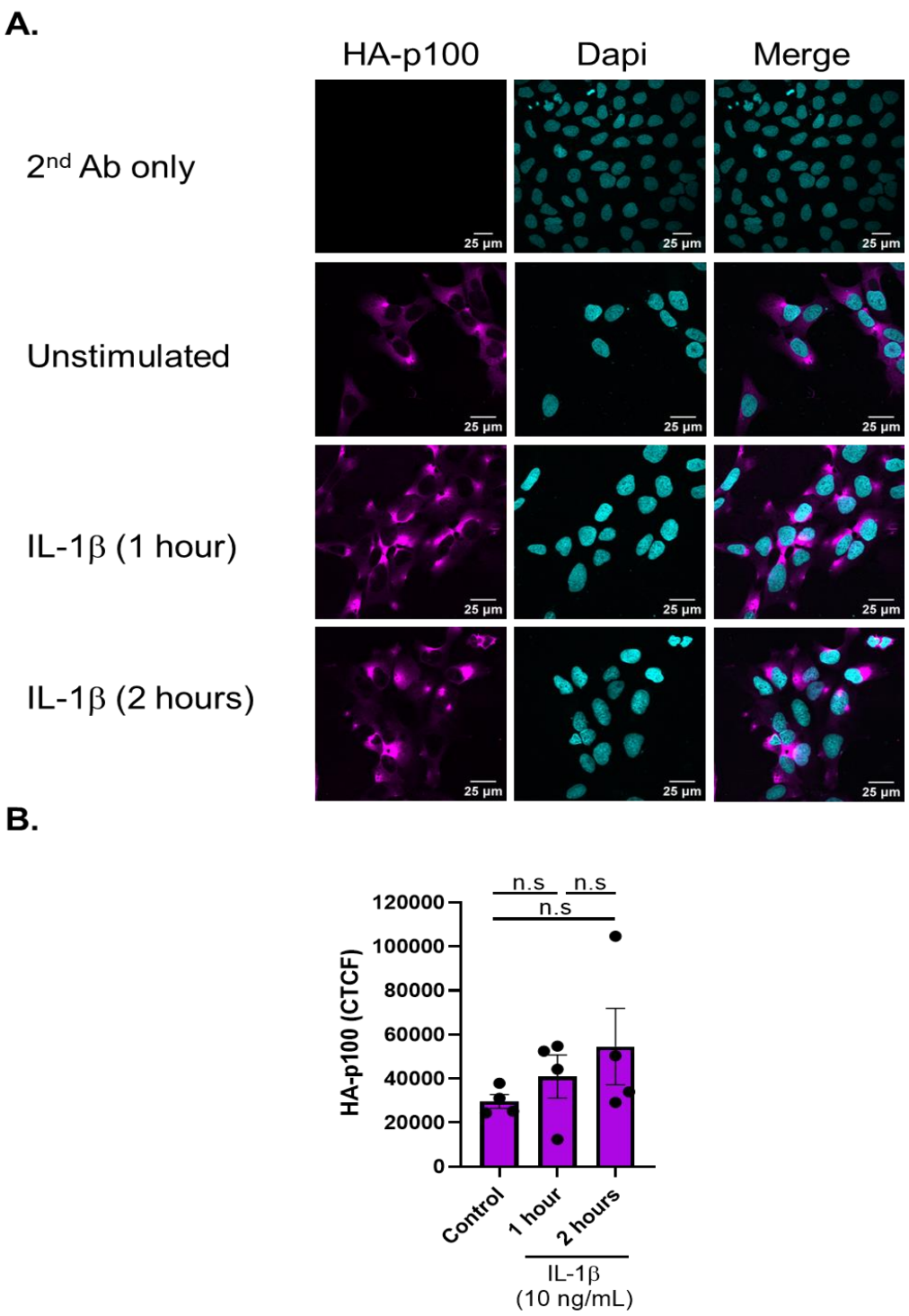

Figure 3.13. The effect of IL-1β on HA-p100 expression in U2OS cells.
A. Representative images taken on a Leica SP8 confocal microscope demonstrating HA-p100 expression in the absence and presence of IL-1β stimulation (1 and 2 hours). U2OS cells were transfected with HA-p100 (1 μg) and 5 μL PEI for 48 hours prior to stimulation with IL-1β. Indirect immunofluorescence was carried out by utilising an HA antibody to detect transfected HA-p100. **B.** Corrected total cell fluorescence for HA-p100 was determined using ImageJ software. Data represents n=4 ± SEM, p>0.05.

3.8. The effect of TAK1 inhibition on the IL-1β-mediated IKKα-dependent signalling axis

Building on the IKKα-dependent nature of p100 phosphorylation, it is important to validate the upstream MAP3K which is integral in this process. Given the background knowledge of canonical NF-κB signalling, this paradigm may be TAK1-dependent. Therefore, a selective TAK1 inhibitor, 5Z-7-oxozaeanol, was utilised to assess whether TAK1 inhibition can suppress the IL-1β-mediated IKKα-dependent p100 phosphorylation (Figure 3.14). While IL-1β and IL-1β plus DMSO increase p100 phosphorylation by 11.1- and 9.7-fold, respectively (****p<0.0001), phospho-p100 protein expression was significantly reduced by 1 μM, 5 μM, 10 μM and 20 μM (****p<0.0001).

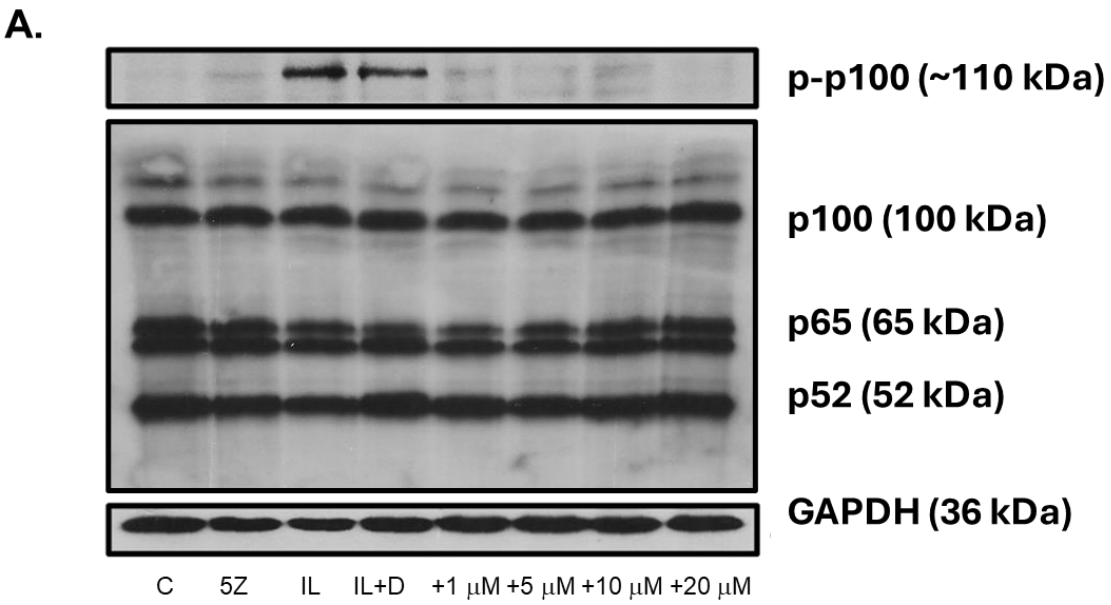

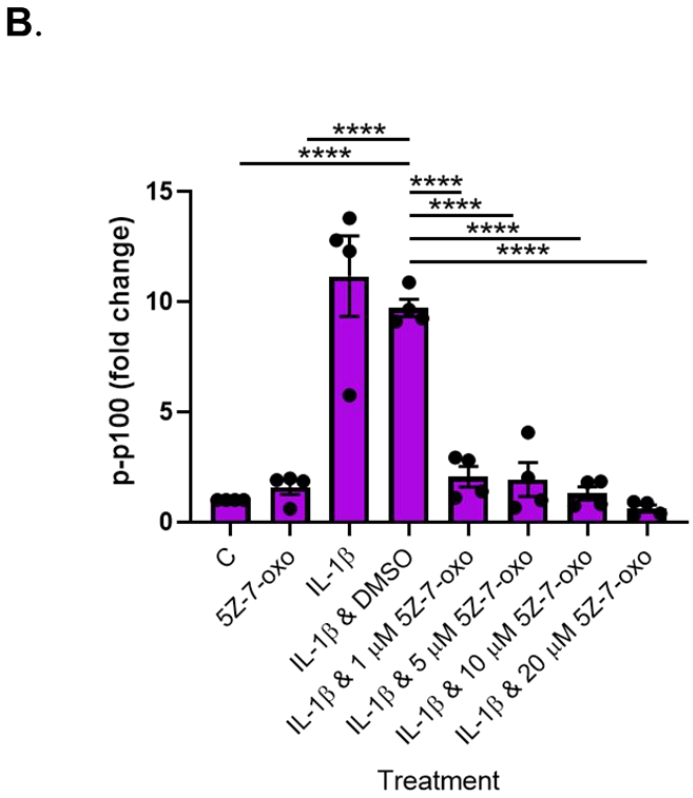

Figure 3.14. TAK1 inhibition diminishes IL-1β-mediated p100 phosphorylation. U2OS WT cells were untreated or pre-treated with 5Z-7-oxo at increasing concentrations (1-20 μM) or DMSO alone for 1 hour prior to IL-1β stimulation. Cells were stimulated with IL-1β for 60 minutes. **A.** Phosphorylation of p100 was evaluated by SDS/PAGE and western blot techniques. **B.** Pixel density was quantified using ScionImage. One-way ANOVA analysis was carried out using GraphPad Prism 8, ****$p<0.0001$ (n=4).

To evaluate concentration dependent effects on p100 phosphorylation, U2OS cells were treated with lower concentrations of 5Z-7-oxozeaenol for 2 hours prior to IL-1β stimulation; 0.1 μM, 0.3 μM, 1 μM, 3 μM and 5 μM (Figure 3.15 A). From this, fold change in phospho-p100 expression was translated into percent of maximal response, and a dose-response curve was constructed to understand the IC_{50} of 5Z-7-oxozeaenol on phospho-p100 expression (Figure 3.15 B). The IC_{50} calculated was 226.5 nM, and the Hill slope was equal to -3.428, demonstrating a steep inhibitory curve.

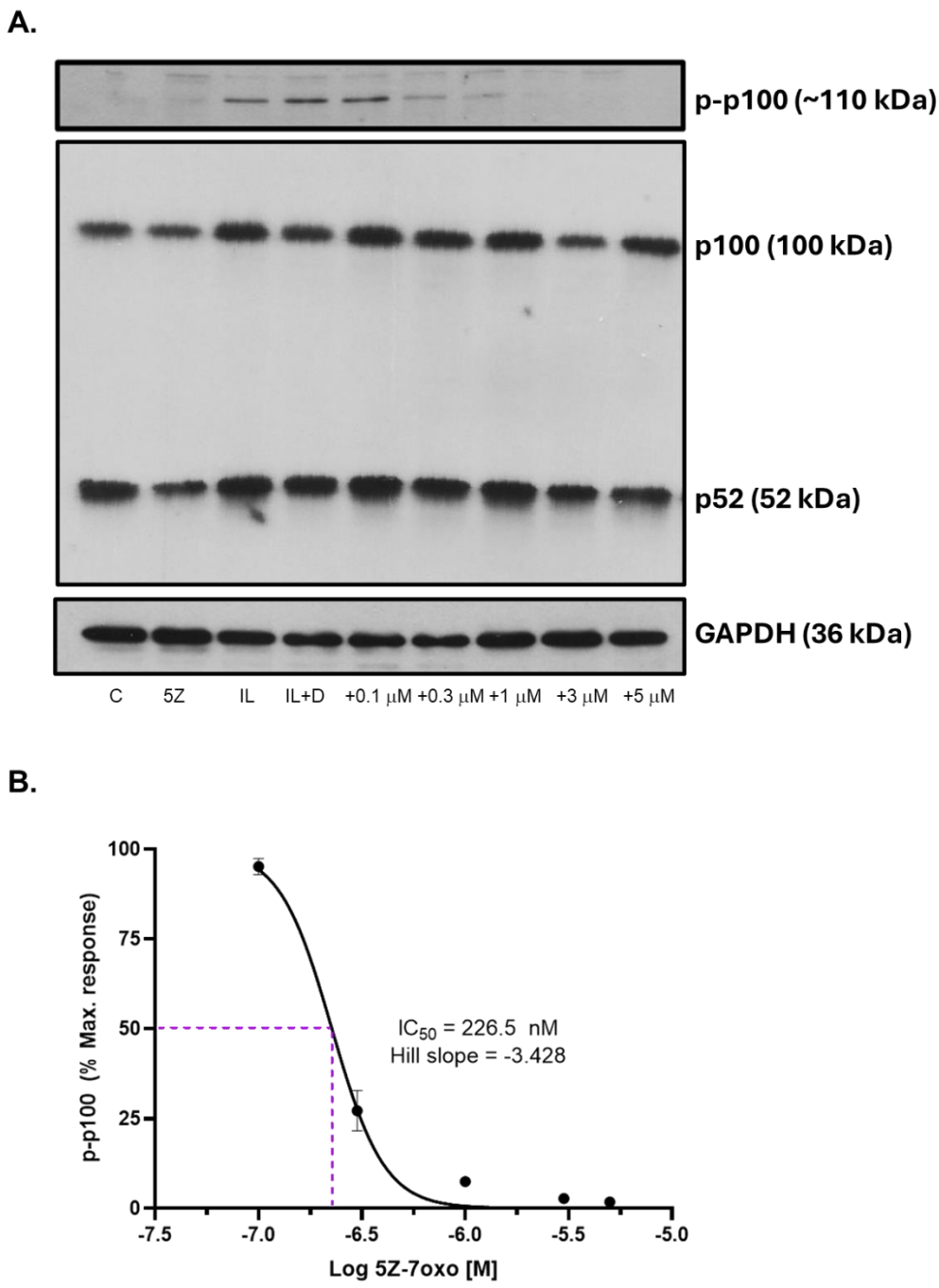

Figure 3.15. TAK1 inhibition decreases p100 phosphorylation.

U2OS wildtype cells were pre-treated and incubated with increasing concentrations of 5Z-7-oxo (100 nM-5 μM) for 2 hours, and IL-1β for a further 1 hour. **A.** SDS-page and western blotting analysis techniques were carried out. **B.** A concentration-response curve displaying the best-fit IC_{50} value and Hill slope of 5Z-7-oxo with respect to p100 phosphorylation. Graph was fitted using the Hill equation. Semi-quantification was carried out to measure pixel density by application of ScionImage software. IC_{50} measurement was carried out using GraphPad prism 8 software (n=3).

Following observation of a rapid decrease in p100 phosphorylation with low concentrations of 5Z-7-oxozeaenol being utilised for 2-hour pre-treatment, the effects of 5Z-7-oxozeaenol were assessed on IKKα phosphorylation (Figure 3.16). The IC_{50} calculated for phospho-IKKα was 252.5 nM, closely aligning with the IC_{50} calculated for phospho-p100 expression.

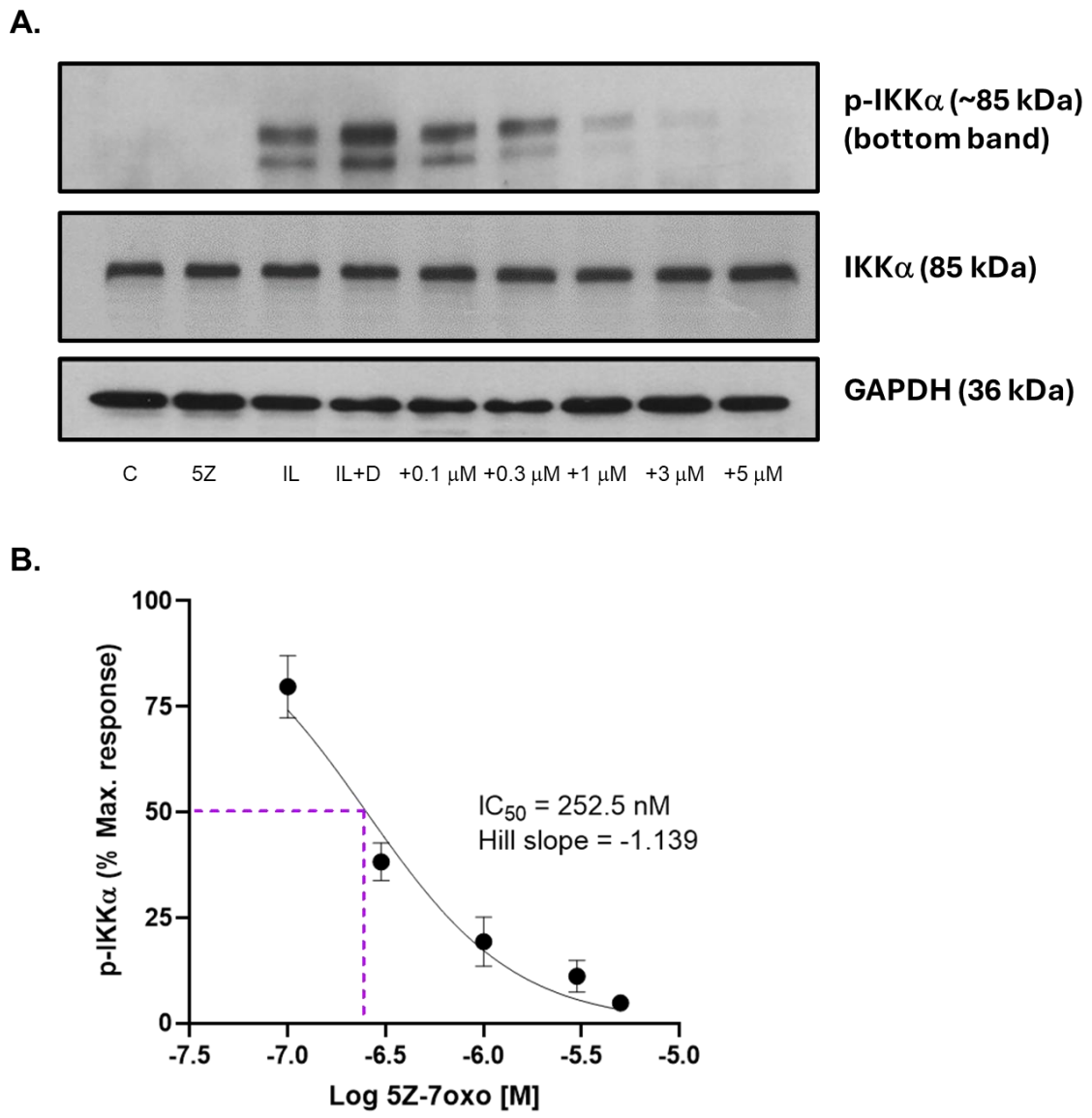

Figure 3.16. TAK1 inhibition downregulates phosphorylation of IKKα.
U2OS wildtype cells were pre-treated and incubated with increasing concentrations of 5Z-7-oxo (100 nM-5 μM) for 2 hours, and IL-1β for a further 1 hour. **A.** SDS-page and western blotting analysis techniques were carried out. **B.** A concentration-response curve displaying the IC_{50} value for the effect of 5Z-7-oxo on IKKα phosphorylation. Graph was fitted using the Hill equation. Semi-quantification was carried out to measure pixel density by application of ScionImage software. Pixel density was then converted into percentage of the maximal response (n=3).

3.9. The effects of TAK1 inhibition on canonical NF-κB signalling

After evaluating the effects of TAK1 inhibition on the IL-1β-induced non-canonical NF-κB signalling axis, 5Z-7-oxozeaenol was utilised to examine its effects on canonical NF-κB signalling. The IC_{50} for IκBα loss reversal was 1.56 μM, and the Hill slope was -1.562 (Figure 3.17). The IC_{50} for reversal of IκBα loss is much higher than that of non-canonical NF-κB signalling markers, phospho-IKKα and phospho-p100 shown previously. Therefore, this implies that TAK1 plays a more prominent or sensitive role in IL-1β-mediated non-canonical NF-κB signalling than canonical NF-κB signalling.

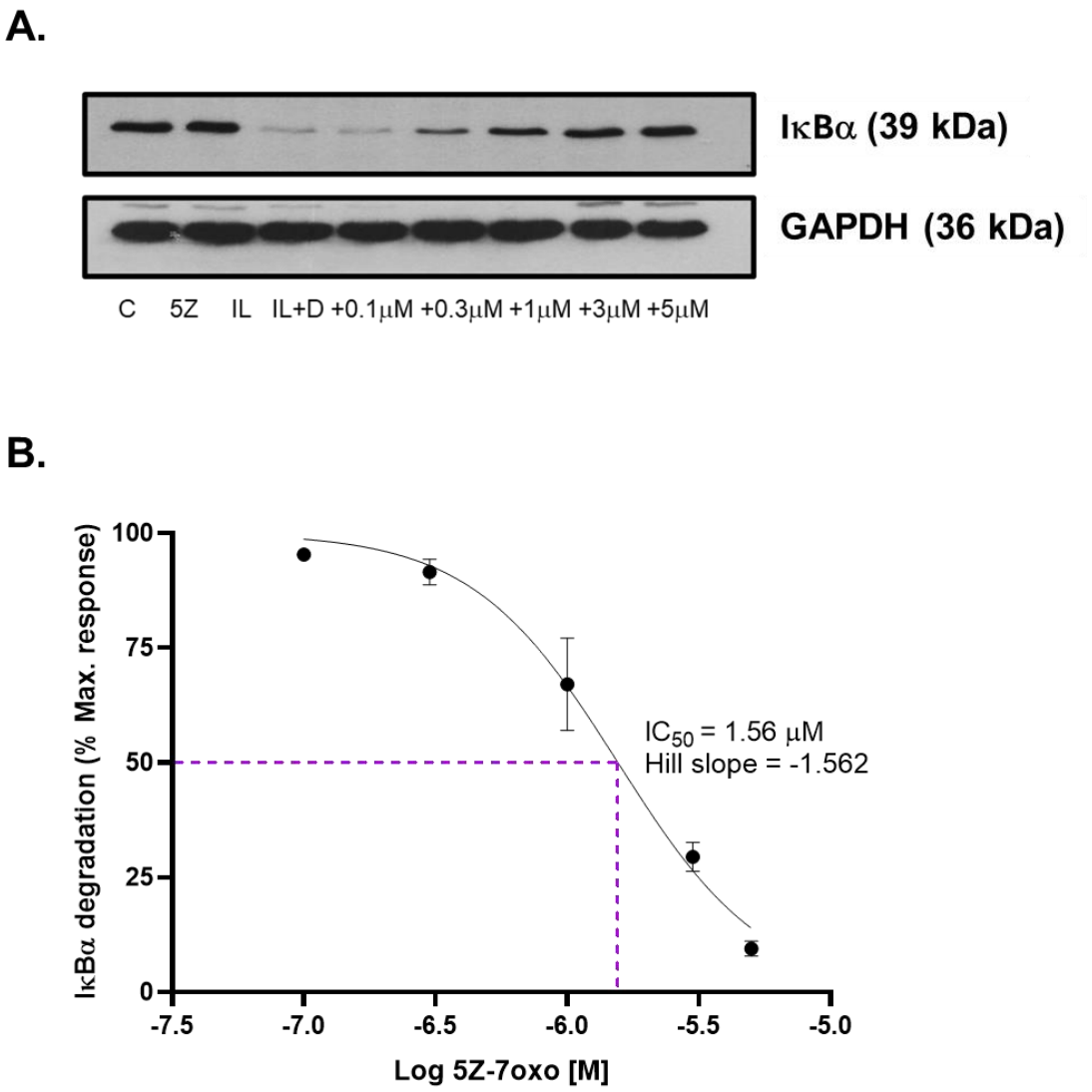

Figure 3.17. TAK1 inhibition causes reversal of IL-1β-mediated IκBα degradation in WT U2OS cells.

Cells were pre-treated and incubated with increasing concentrations of 5Z-7-oxo (100 nM-5 μM) for 2 hours, and IL-1β for a further 1 hour. **A.** SDS-page and western blotting analysis techniques were carried out. **B.** A concentration-response curve displaying the IC_{50} value for the effect of 5Z-7-oxo on IκBα expression. Semi-quantification was carried out to measure pixel density by application of ScionImage software. Graph was fitted using the Hill equation. Pixel density was then converted into percentage of the maximal response (n=3).

To further look at the effects of TAK1 inhibition and to validate the effects of TAK1 inhibition on IκBα degradation reversal further, the IC_{50} for 5Z-7-oxozeaenol on phosphor-IKKβ expression was evaluated (Figure 3.18). The IC_{50} for phospho-IKKβ was 1.01 μM and the Hill slope was -2.111, relatively consistent with IκBα loss reversal, and much higher than that seen for phospho-IKKα and phospho-p100. Therefore, these findings suggest that TAK1 inhibition is more effective at suppressing IL-1β-mediated non-canonical NF-κB signalling than canonical signalling, indicating a differential sensitivity or dependency on TAK1 activity between the two axes. This may reflect pathway-specific thresholds of TAK1 activity or the involvement of additional compensatory mechanisms in canonical NF-κB activation.

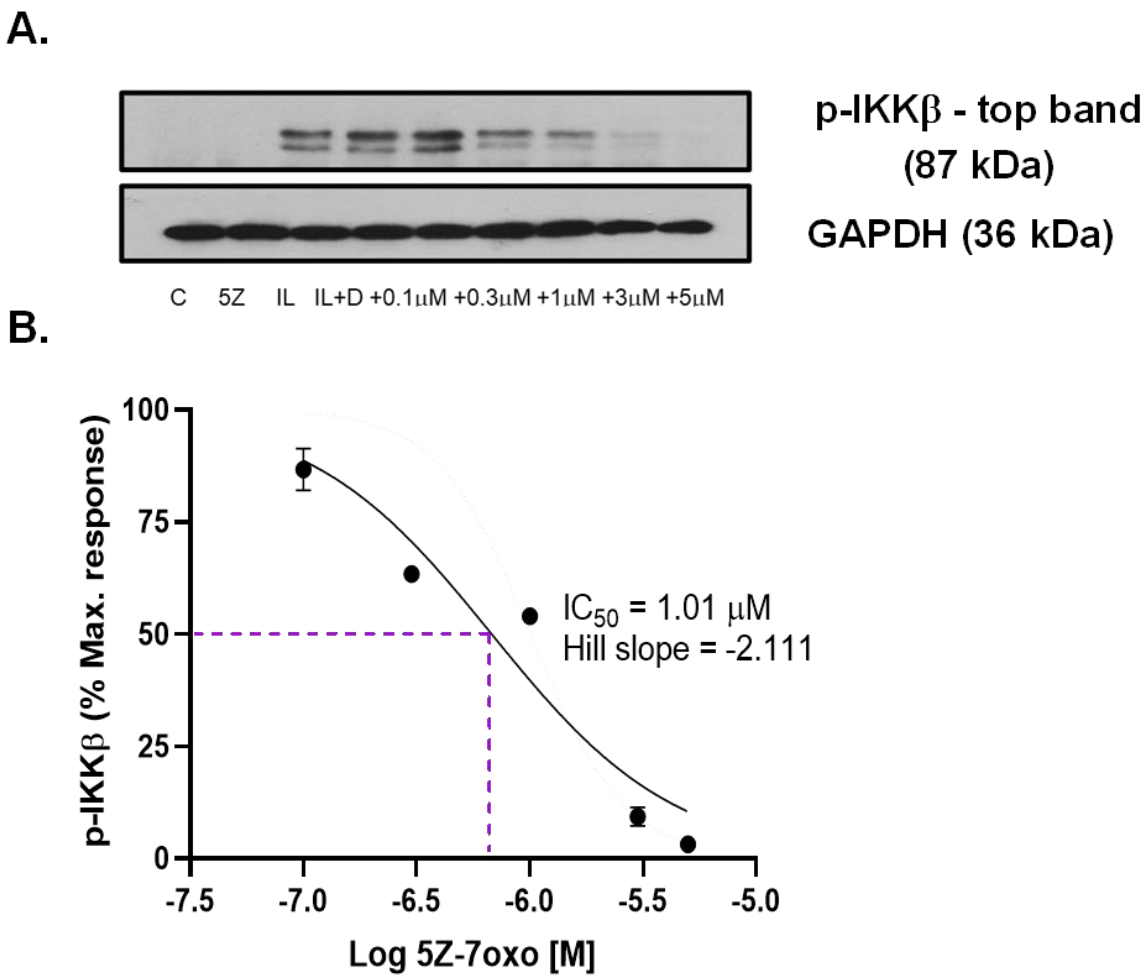

Figure 3.18. TAK1 inhibition decreases expression of phospho-IKKβ in WT U2OS cells.

Cells were pre-treated and incubated with increasing concentrations of 5Z-7-oxo (100 nM-5 μM) for 2 hours, and IL-1β for a further 1 hour. **A.** SDS-page and western blotting analysis techniques were carried out for phospho-IKKβ. **B.** A concentration-response curve displaying the IC_{50} value for the effect of 5Z-7-oxo on IKKβ phosphorylation. Graph was fitted using the Hill equation. Semi-quantification was carried out to measure pixel density by application of ScionImage software, (n=3).

3.10. The effects of TAK1 inhibition on IL-1β-mediated JNK signalling

Finally, to further test other known downstream mediators of TAK1, IL-1β-mediated phospho-JNK expression was semi-quantified across increasing concentrations of 5Z-7-oxozeaenol (0.1 μM-5 μM). Indeed, the IC_{50} for phospho-JNK was less than the lowest concentration of inhibitor tested, and was predicted at 50.3 nM, with a Hill slope of -1.37 (Figure 3.19). This demonstrates that the phospho-JNK signalling pathway is more sensitive for TAK1 inhibition than canonical or non-canonical NF-κB signalling pathways in response to IL-1β.

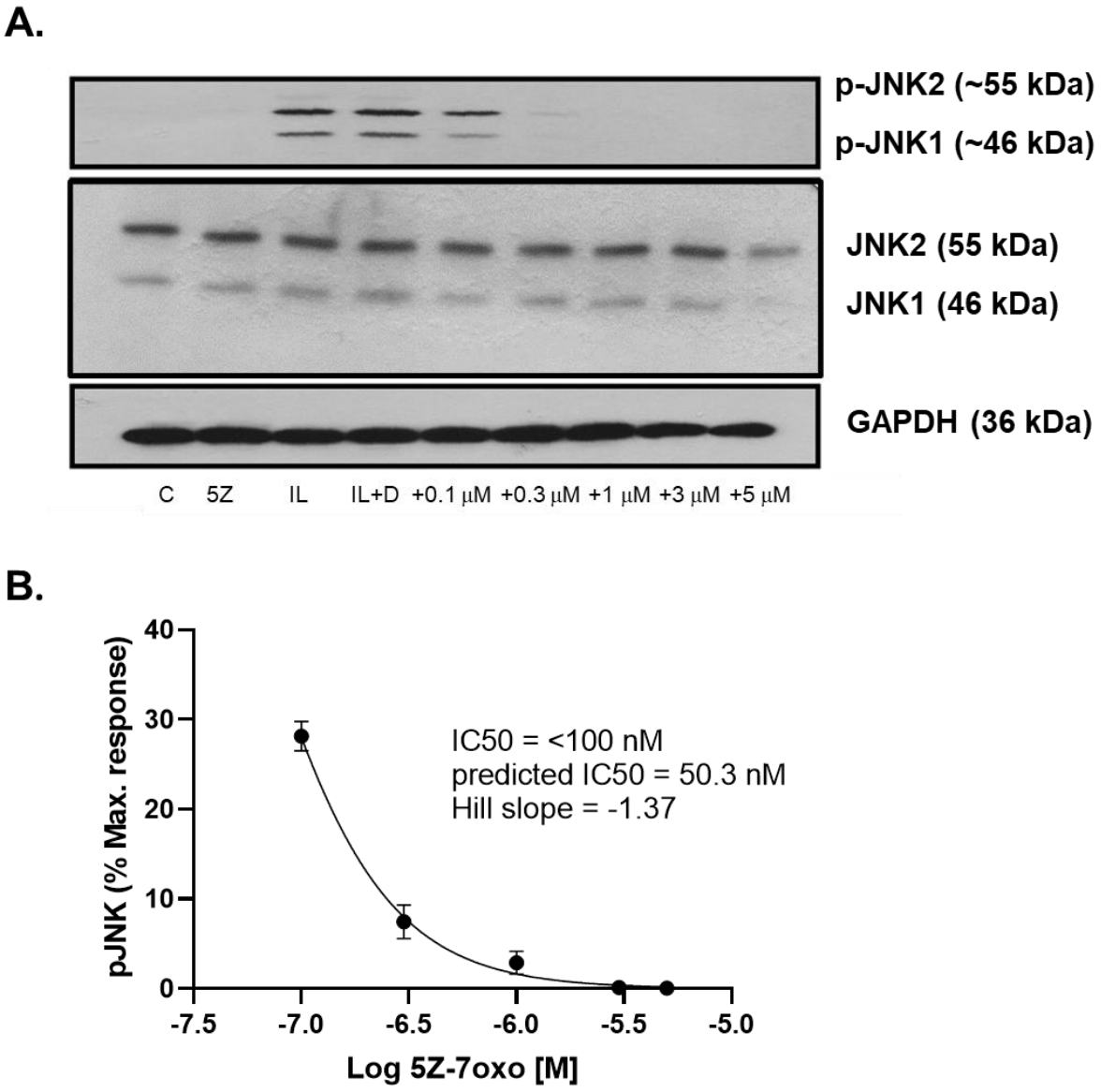

Figure 3.19. TAK1 inhibition downregulates phosphorylation of JNK.
U2OS wildtype cells were pre-treated and incubated with increasing concentrations of 5Z-7-oxo (100 nM-5 μM) for 2 hours, and IL-1β for a further 1 hour. **A.** SDS-page and western blotting analysis techniques were carried out. **B.** A concentration-response curve displaying the IC_{50} value for the effect of 5Z-7-oxo on JNK phosphorylation. Graph was fitted using the Hill equation. Semi-quantification was carried out to measure pixel density by application of ScionImage software. Pixel density was then converted into percentage of the maximal response (n=3).

3.11. Prediction of IKKα-binding partners with Colabfold

An additional approach to determine upstream regulation of IKKα-dependent signalling events would be to use ColabFold, which utilises AlphaFold2. This would provide an immediate more sophisticated into potential IKKα protein-binding partners. Figure 3.20 highlights five predicted representative structures of IKKα, all with relatively high confidence (81.7247≤pLDDT≤83.1461), as demonstrated in Table 3.1. The PAE graph demonstrates low PAE within the predicted structure, supporting the high pLDDT confidence measures. Notably, there are visual differences in the structural confirmation in relation to the folding where disordered amino acid residues are observed. Interestingly, this provides insight into a full model of IKKα structure, a protein which has not yet been fully solved by X-ray crystallography. This also demonstrates that the appearance protein structure is not fully consistent, as proteins can be flexible and have several different confirmations including open and closed confirmations. Additionally, the functional kinase domain within all five of the predicted IKKα structures located at the bottom right of the structures appears consistent with high levels of confidence. This is promising, as IKKα phosphorylation occurs within this domain.

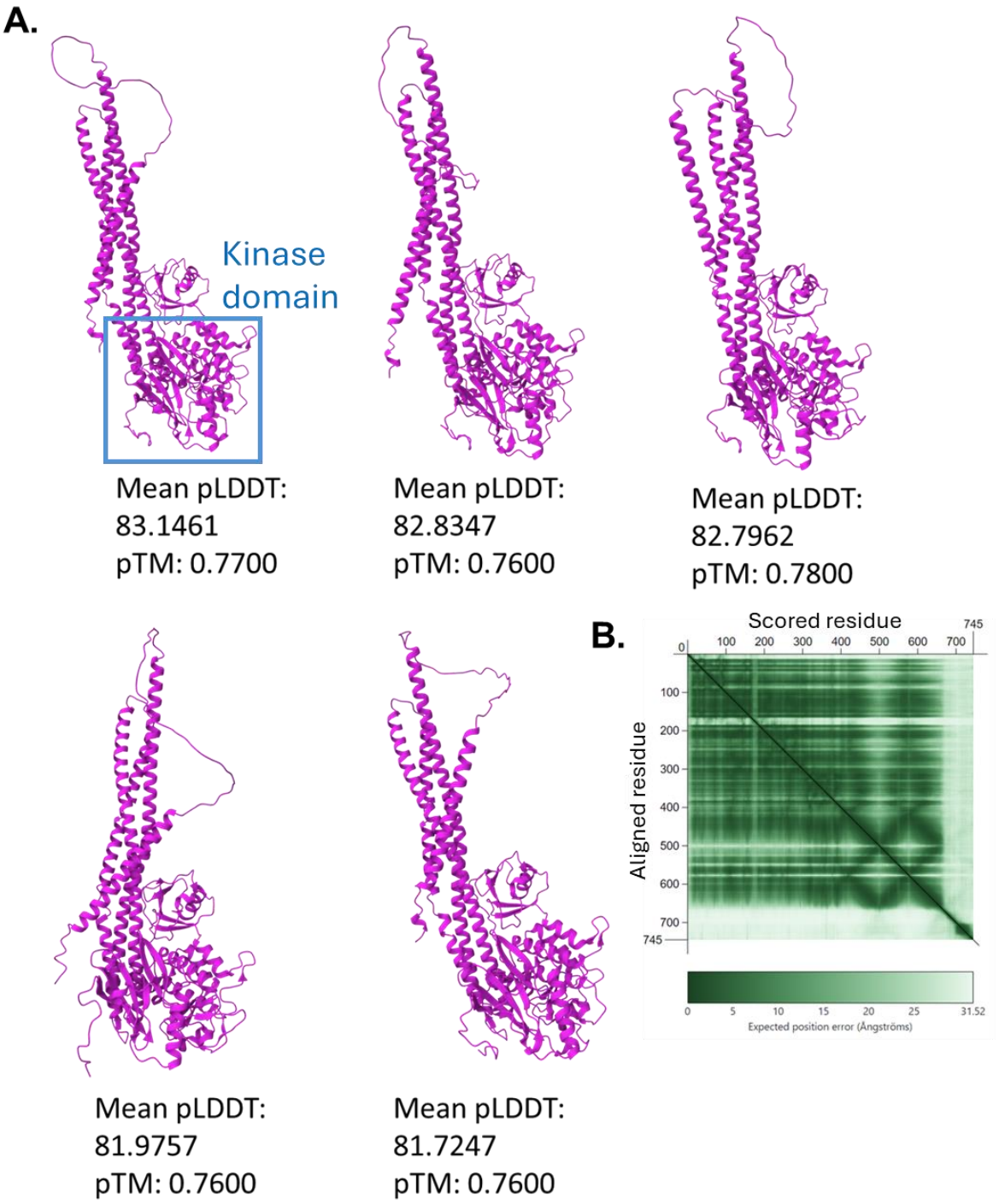

Figure 3.20. Prediction of IKKα structure by ColabFold.

A. ColabFold settings were utilised to obtain five structural predictions of IKKα were generated using ColabFold, employing 10 recycles and a pLDDT threshold set at 90. pLDDT and pTM scores are outlined within the figure. **B.** The predicted aligned error graph for the residues in the most highly ranked pLDDT structural model.

Table 3.1. An outline of the predicted confidence levels of IKKα structures as described in Figure 1.

Ranked IKKα structure	Mean Plddt	pTM
1	83.1461	0.77
2	82.8347	0.76
3	82.7962	0.78
4	81.9757	0.76
5	81.7247	0.76

Following the prediction of IKKα alone, ColabFold was utilised to predict a MEKK3-IKKα heterodimer, to determine whether MEKK3 could potentially be a MAP3K of interest in IKKα signalling, due to MEKK3 being previously shown to have homeostatic interactions with TAK1, which influences downstream NF-κB signalling. Interestingly, ColabFold predicted that MEKK3 Glu571 can bind IKKα Ser180, a phosphorylation site on IKKα (Figure 3.21), due to their close proximity (3.73 angstroms).

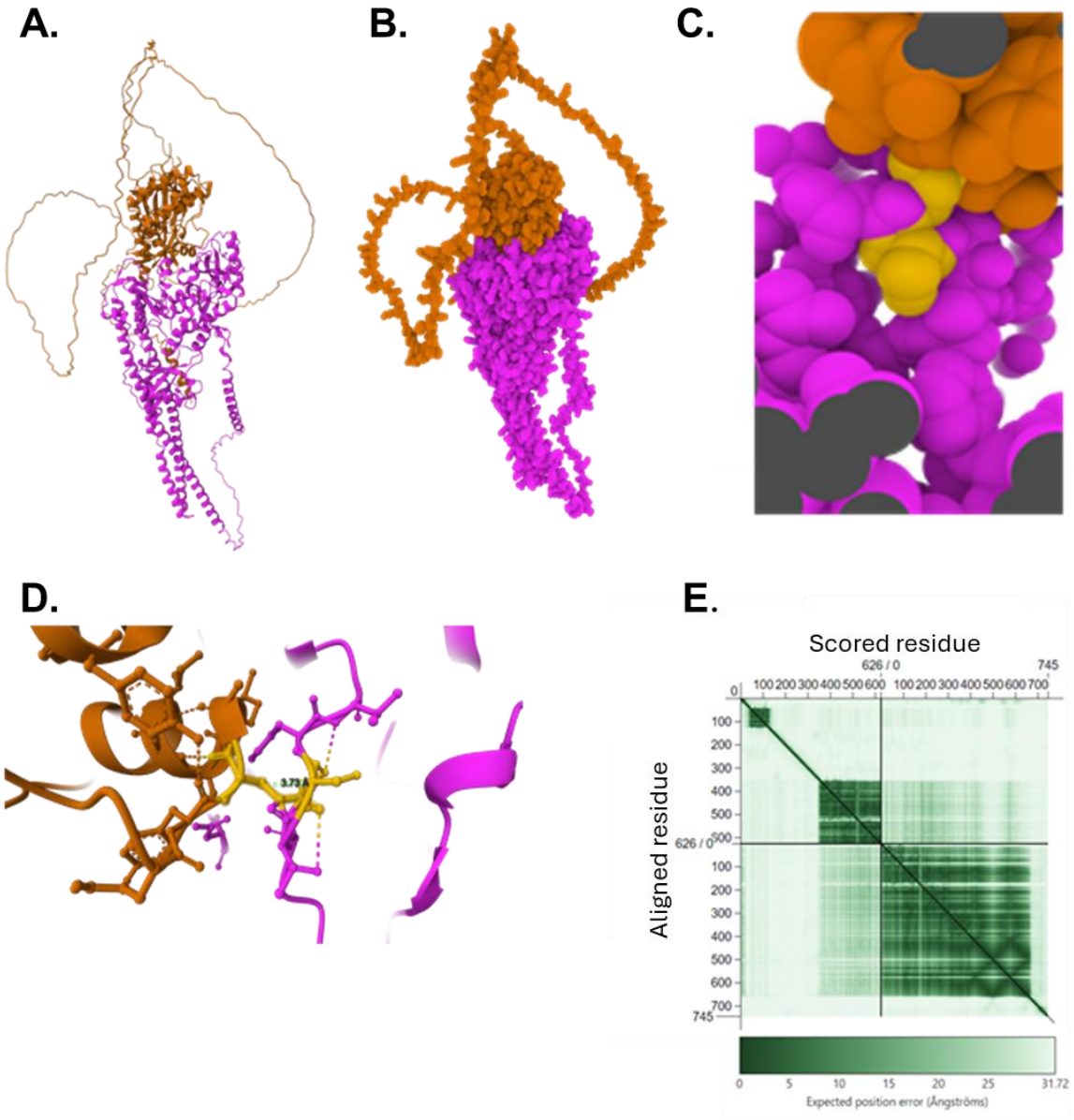

Figure 3.21. ColabFold prediction of a MEKK3-IKKα heterodimer.
A. A graphical representation of full MEKK3 and IKKα protein structures in a complex. **B.** A space fill model of MEKK3-IKKα heterodimer. **C.** A space fill model demonstrating IKKα Ser180 and MEKK3 Glu571 in proximity, with residues of interest in yellow. **D.** A representation of predicted direct binding between IKKα Ser180 and MEKK3 Glu571. **E.** PAE graph demonstrating confidence in amino acid residues within the complex. A-D were created by use of MolStar, E was adapted from PAE viewer.

However, given that IKKα has two prominent phosphorylation sites responsible for its activation, an IKKα-MEKK3-TAK1 trimeric complex was then predicted to establish whether MEKK3 and TAK1 could work in parallel or collectively to enable IKKα activation and phosphorylation. Indeed, MEKK3 was predicted to bind IKKα Ser180 again, even in the presence of TAK1, but this time by a different Glutamine reside, Glu207 (Figure 3.22). However, in this prediction, MEKK3 was also predicted to bind Ser176 on IKKα, the other phosphorylation residue on IKKα, by another Glutamine residue, Glu210. This provided interesting insights into the way that MEKK3 could potentially be a binding partner to IKKα, even in the presence of known canonical MAP3K, TAK1.

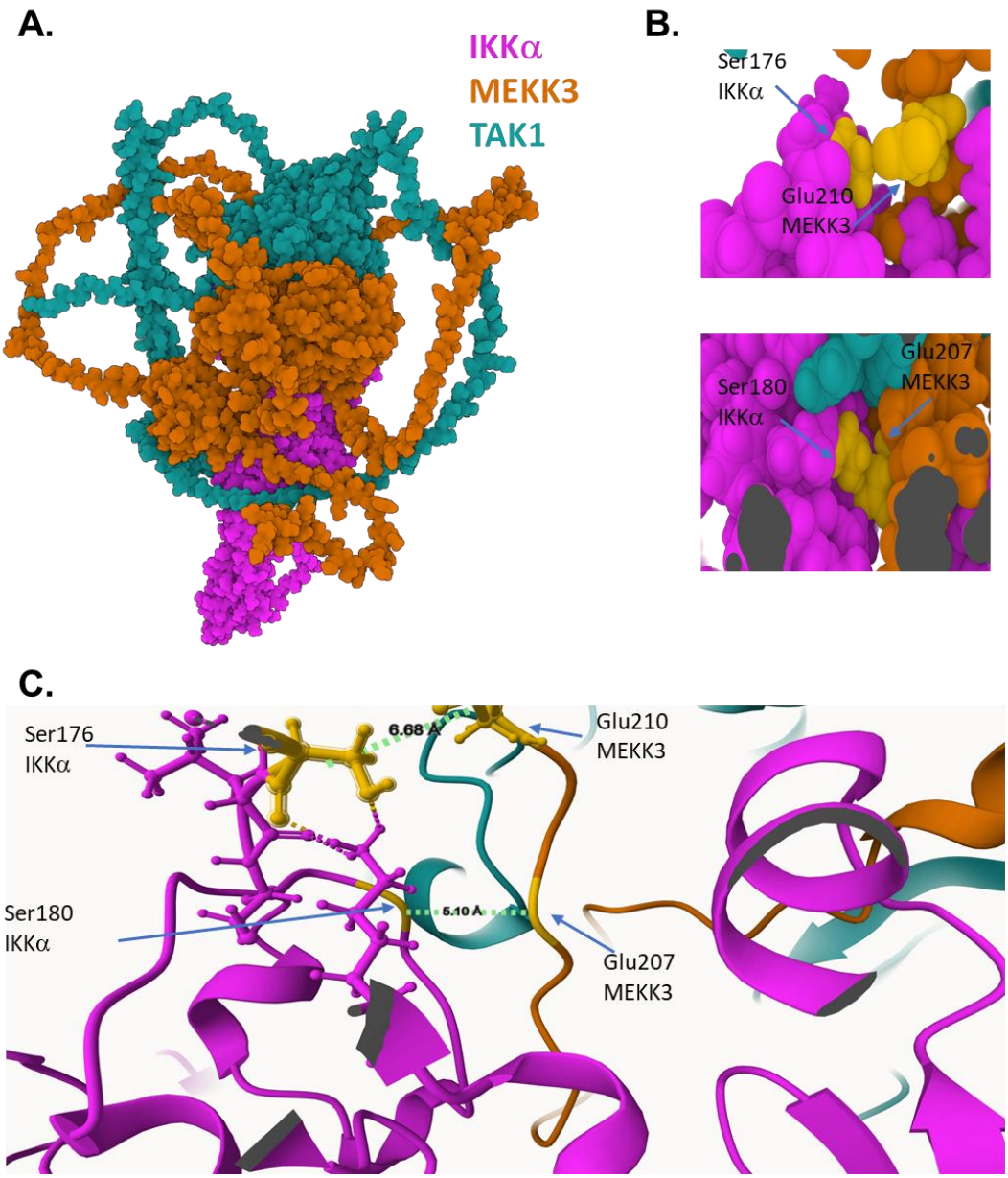

Figure 3.22. Prediction of a human MEKK3-TAK1-IKKα complex by ColabFold.
By application of ColabFold, five structural predictions of IKKα were produced, employing 10 recycles and a pLDDT threshold of 90. pLDDT and pTM scores are highlighted within the figure. **A.** The most highly ranked representation of MEKK3, TAK1 and IKKα 3D protein structures in a trimeric complex. **B.** Illustrative representations of protein-protein interactions at Ser176 within IKKα and Glu210 within MEKK3, and Ser180 within IKKα and Glu207 within MEKK3. **C.** A structural representation depicting the distance between interacting residues between IKKα and MEKK3. Interacting residues are displayed in yellow.

3.12. Immunoprecipitation of IKKα and MEKK3

To understand whether the ColabFold findings could be validated in the U2OS cell line, and whether this potential binding is relevant in IL-1β stimulated conditions, MEKK3 and IKKα immunoprecipitation experiments were conducted. While immunoprecipitation of IKKα resulted in the appearance of IKKα and an additional lower band (Figure 3.23 A), immunoprecipitation of MEKK3 resulted in the visualisation of only one molecular weight band (Figure 3.23 B). Therefore, this demonstrates IKKα is prebound to another protein in both unstimulated and stimulated conditions with IL-1β. However, this protein does not appear to be MEKK3.

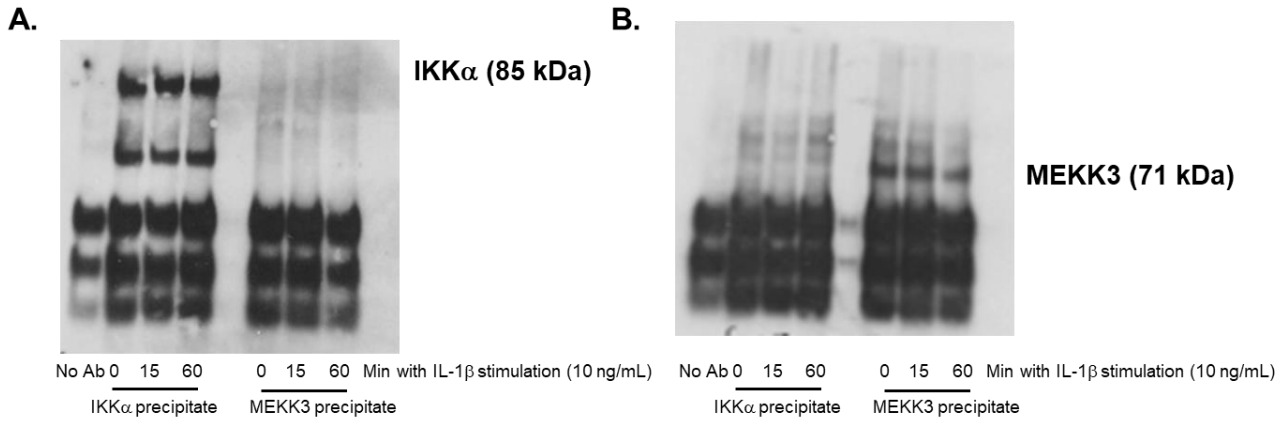

Figure 3.23. Immunoprecipitation of IKKα and MEKK3 in U2OS cells.

U2OS cells were subjected to immunoprecipitation (IP) using either (**A**) an anti-IKKα primary antibody or (**B**) an anti-MEKK3 primary antibody. Protein complexes were analysed by SDS-PAGE and Western blotting to assess the interaction and presence of IKKα and MEKK3 in the respective immunoprecipitates, n=2.

3.13. Assessing the effects of pharmacological inhibition of TAK1 and IKKα on potential downstream NF-κB family members

3.13.1. The effect of TAK1 inhibition on nuclear translocation of p52 and p65 NF-κB subfamily members

To determine whether p52 and p65 nuclear translocation in response to IL-1β is TAK1 dependent, U2OS wildtype cells were pre-treated with 5 μM or 10 μM 5Z-7-oxozaenol (5Z-7-oxo) or DMSO alone for one hour and treated the cells with IL-1β for a further 60 min where appropriate. Nuclear extraction was carried out from whole cell lysates, and p52 and p65 nuclear expression was measured by SDS-PAGE and western blotting analysis (Figure 3.24). Both p52 (Figure 3.24 B) and p65 (Figure 3.24 C) nuclear translocation were significantly increased following IL-1β & DMSO treatment (4.5-fold and 37.8-fold ± SEM, respectively). It is evident from these results that there is higher p52 nuclear expression in unstimulated U2OS cells compared to p65 expression, which may explain the smaller increase in p52 nuclear expression following IL-1β stimulation compared to p65 nuclear expression. Interestingly, pre-treatment with 5 μM and 10 μM 5Z-7-oxo significantly decreased IL-1β-mediated p52 and p65 nuclear translocation (**$p<0.01$).

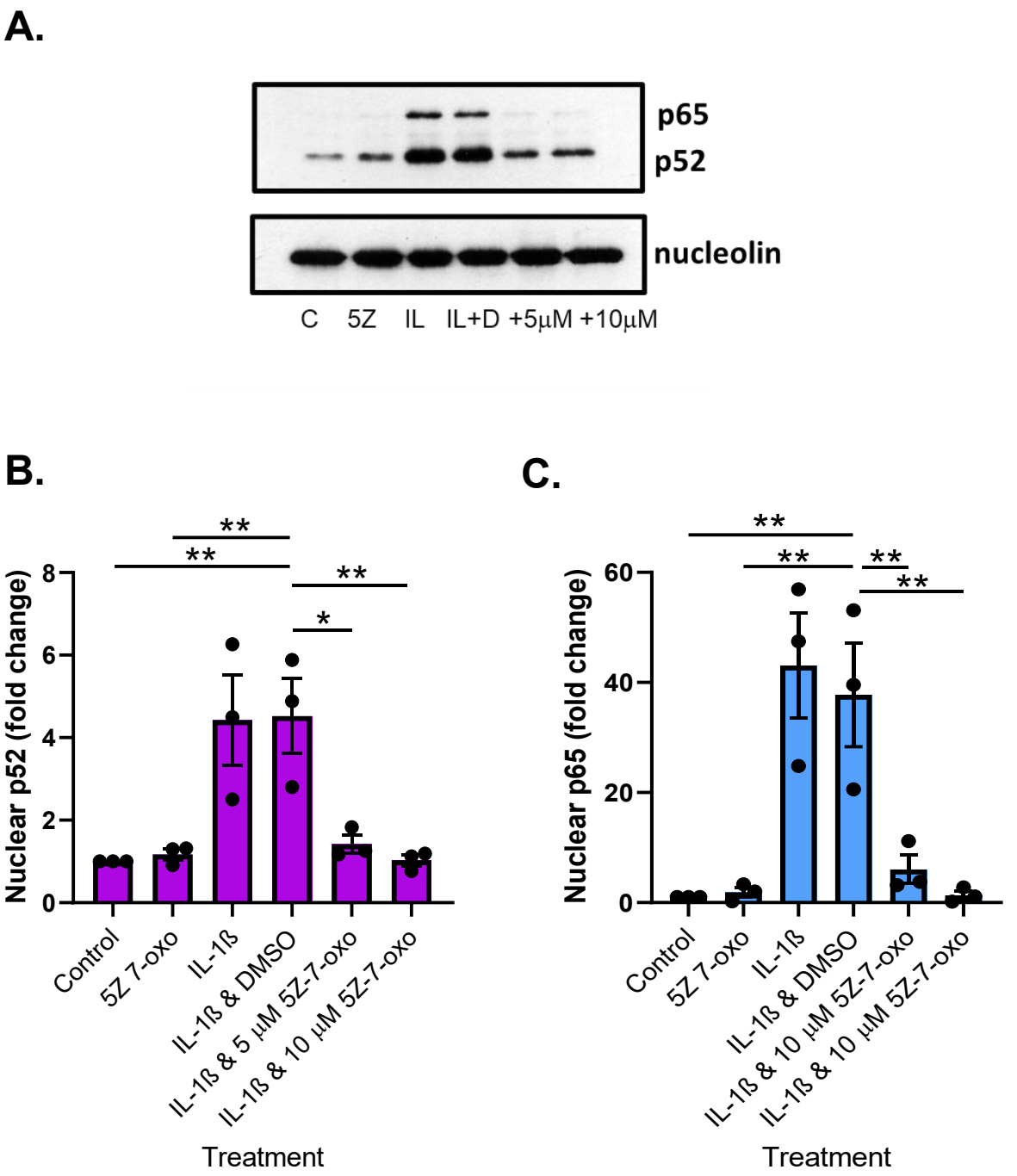

Figure 3.24. TAK1 inhibition decreases p52 and p65 nuclear translocation.
WT U2OS cells were pre-treated and incubated with 5Z-7-oxo (5 μM or 10 μM) for 1 hour, and IL-1β for a further 1 hour. Nuclear extraction techniques were applied to obtain nuclear lysates. **A.** SDS-page and western blotting analysis techniques were carried out. **B.** Pixel density measurement of p52 nuclear extract treatment groups. **C.** Pixel density measurement of p65 nuclear extract treatment groups. Semi-quantification was carried out to measure pixel density by application of ScionImage software. Pixel density fold change analysis was carried out by One-way ANOVA analysis using GraphPad prism 8, *p<0.05, **p<0.01 (n=3).

Following the 1-hour pre-incubation being effective with TAK1 inhibitor, 5Z-7-oxozeaenol, the pre-incubation time was increased to two hours to ensure maximal effect on inhibiting TAK1. Multiple concentrations of 5Z-7-oxozeaenol were utilised to determine if there is a concentration-dependent effect of TAK1 inhibition on p52 and p65 nuclear translocation (Figure 3.25). While lower concentrations of 5Z-7-oxozeaenol, including 100 nM, 300 nM and 1 μM did not result in a significant decrease in p52 or p65 nuclear translocation, IL-1β-induced p52 and p65 nuclear translocation was significantly reduced by 3 μM and 5 μM 5Z-7-oxozeaenol pretreatment.

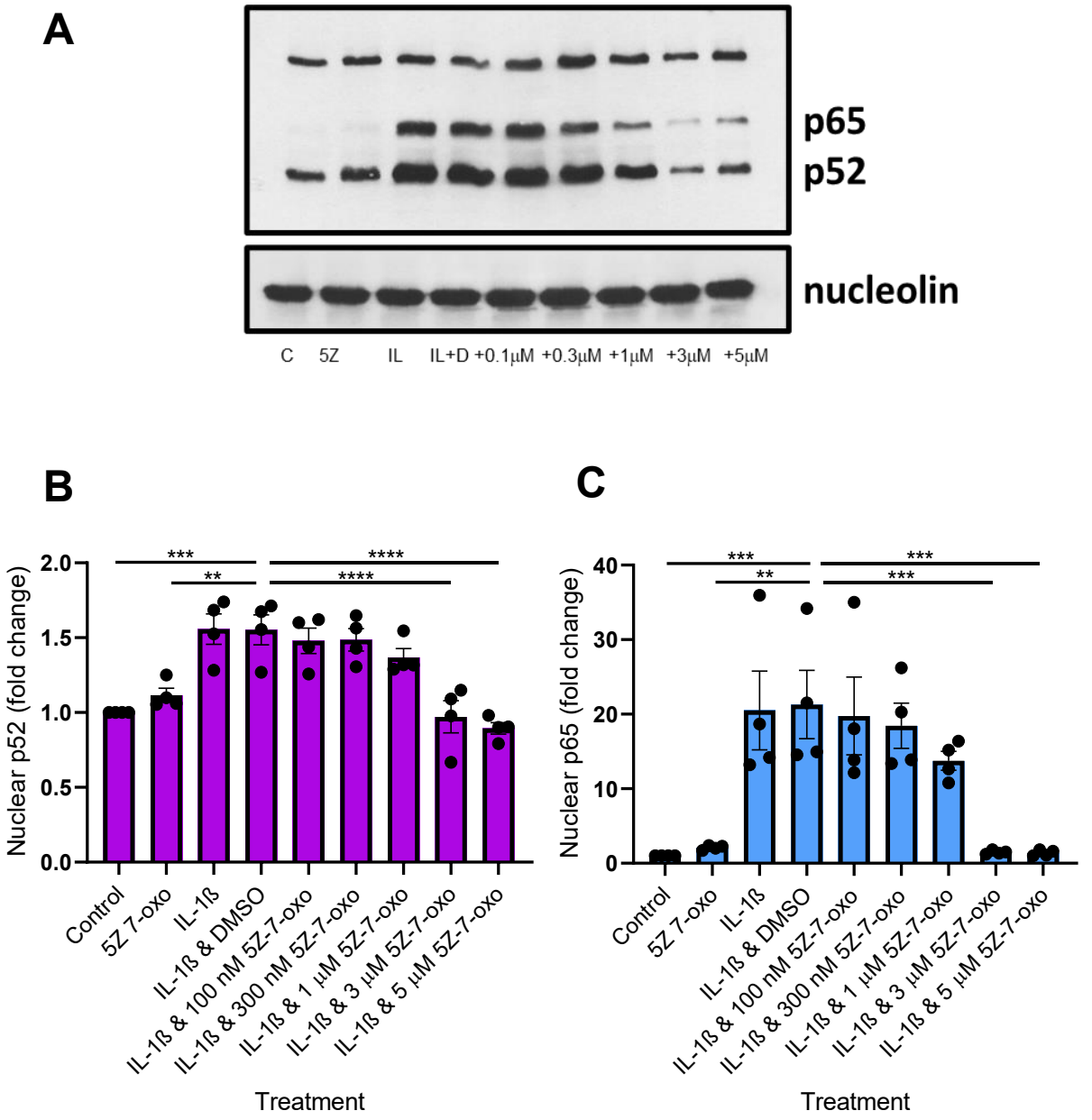

Figure 3.25. TAK1 inhibition decreases p52 and p65 nuclear translocation.
WT U2OS cells were pre-treated and incubated with 5Z-7-oxo (100 nM-5 μM) for 2 hours, and IL-1β for a further 1 hour. Nuclear extraction techniques were carried out. **A.** SDS-page and western blotting analysis techniques were applied. **B.** Bar graph displaying pixel density measurement of p52 nuclear extract treatment groups. **C.** Bar graph displaying pixel density measurement of p65 nuclear extract treatment groups. Semi-quantification was carried out to measure pixel density by application of ScionImage software. Pixel density fold change analysis was carried out using One-way ANOVA with GraphPad prism 8 software, **p<0.01, ***p<0.001 (n=4).

3.13.2. The effects of IKKα inhibition on p52 and p65 nuclear translocation

Given the concentration-dependent inhibition of p52 and p65 nuclear translocation by 5Z-7-oxozaenol, it was important to determine whether IKKα inhibition could similarly affect these processes, with the hope to understand whether inhibition of p100 phosphorylation would impact p52 nuclear translocation. Firstly, a novel IKKα inhibitor, SU1261 was applied. Indeed, SU1261 did not inhibit IL-1β-dependent p65 or p52 nuclear translocation (Figure 3.26). This exemplifies that p52 nuclear translocation is independent of IKKα inhibition, and therefore, independent of p100 phosphorylation and activation.

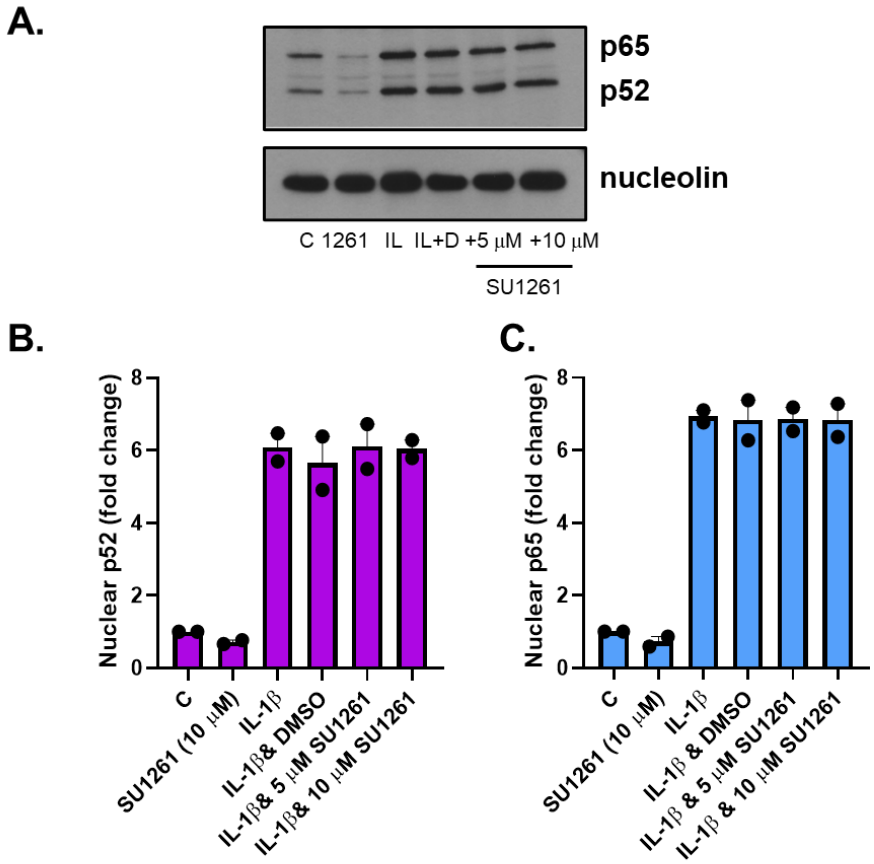

Figure 3.26. SU1261 does not inhibit the IL-1β-induced nuclear translocation of p52 and p65.

U2OS cells were pre-treated and incubated with SU1261 (5 μM or 10 μM) for 45 min, and IL-1β for a further 1 hour. Nuclear extraction techniques were carried out. **A.** SDS-page and western blotting analysis techniques were applied. **B.** Bar graph displaying pixel density measurement of p52 nuclear extract treatment groups. **C.** Bar graph displaying pixel density measurement of p65 nuclear extract treatment groups. Semi-

quantification was carried out to measure pixel density by application of ScionImage software, n=2.

SU1266 was also utilised to test its effect on IL-1β-mediated p52 and p65 nuclear translocation. SU1266 appears to reduce both IL-1β-induced p52 and p65 nuclear translocation (Figure 3.27). However, this is attributed to the effects of SU1266 on IKKβ at these concentrations.

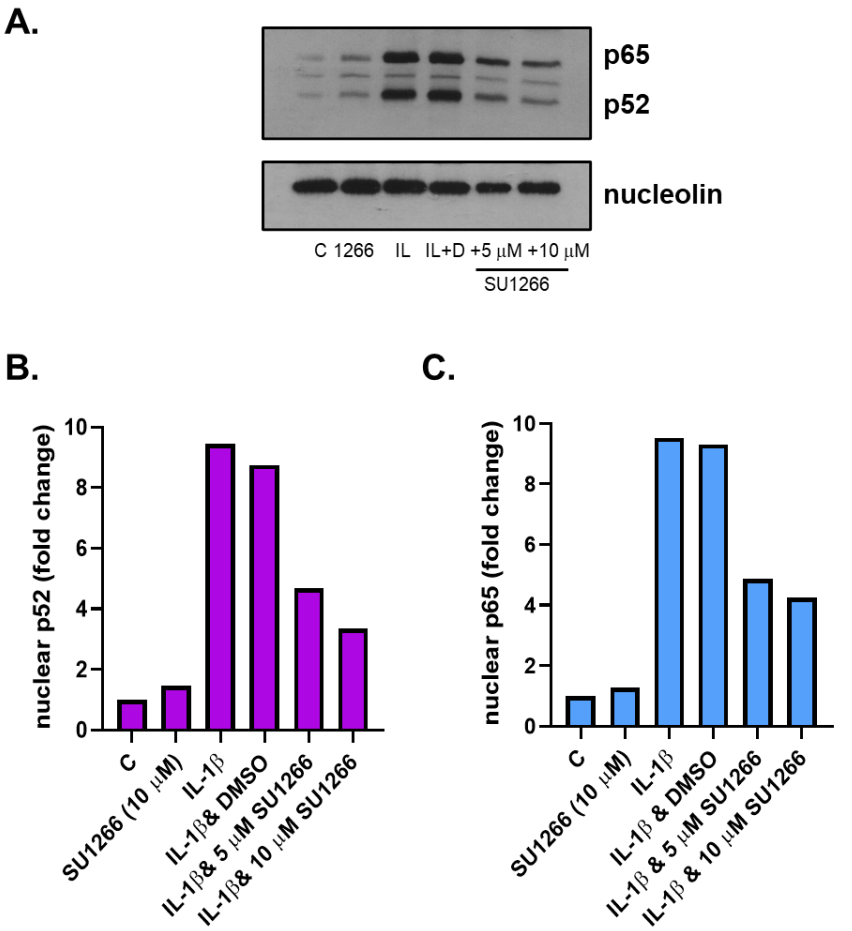

Figure 3.27. SU1266 inhibit the IL-1β-induced nuclear translocation of p52 and p65.

U2OS cells were pre-treated and incubated with SU1266 (5 μM or 10 μM) for 45 min, and IL-1β for a further 1 hour. Nuclear extraction techniques were carried out. **A.** SDS-page and western blotting analysis techniques were applied. **B.** Bar graph displaying pixel density measurement of p52 nuclear extract treatment groups. **C.** Bar graph displaying pixel density measurement of p65 nuclear extract treatment groups. Semi-quantification was carried out to measure pixel density by application of ScionImage software, n=1.

3.14. Investigation of IL-1β-mediated NF-κB DNA-binding activity by EMSA

To assess the effect of IL-1β on NF-κB nuclear activity, EMSA was performed using wildtype mouse embryonic fibroblasts (Figure 3.28). Two distinct DNA-binding complexes were observed: a higher molecular weight band likely representing p65-containing dimers and a lower band representing p50 or p52-containing dimers. IL-1β stimulation significantly increased NF-κB DNA-binding activity at 60 minutes (*$p<0.05$), indicating enhanced p65-dependent signalling, though this effect declined in subsequent time points (3 and 24 hours). No statistically significant difference was observed between 1 hour and 8 hour time points, suggesting a potential second wave of NF-κB activity. In $NIK^{-/-}$, an increase in NF-κB activity was observed following 3 hours following IL-1β stimulation, suggesting a lack of NIK accumulation potentially delays canonical NF-κB signalling (Figure 3.28 B). In $IKK\alpha^{-/-}$ fibroblasts, a smaller molecular weight complex increased after 8 hours of IL-1β treatment, likely corresponding to p50 or p52-containing dimers (Figure 3.28 C).

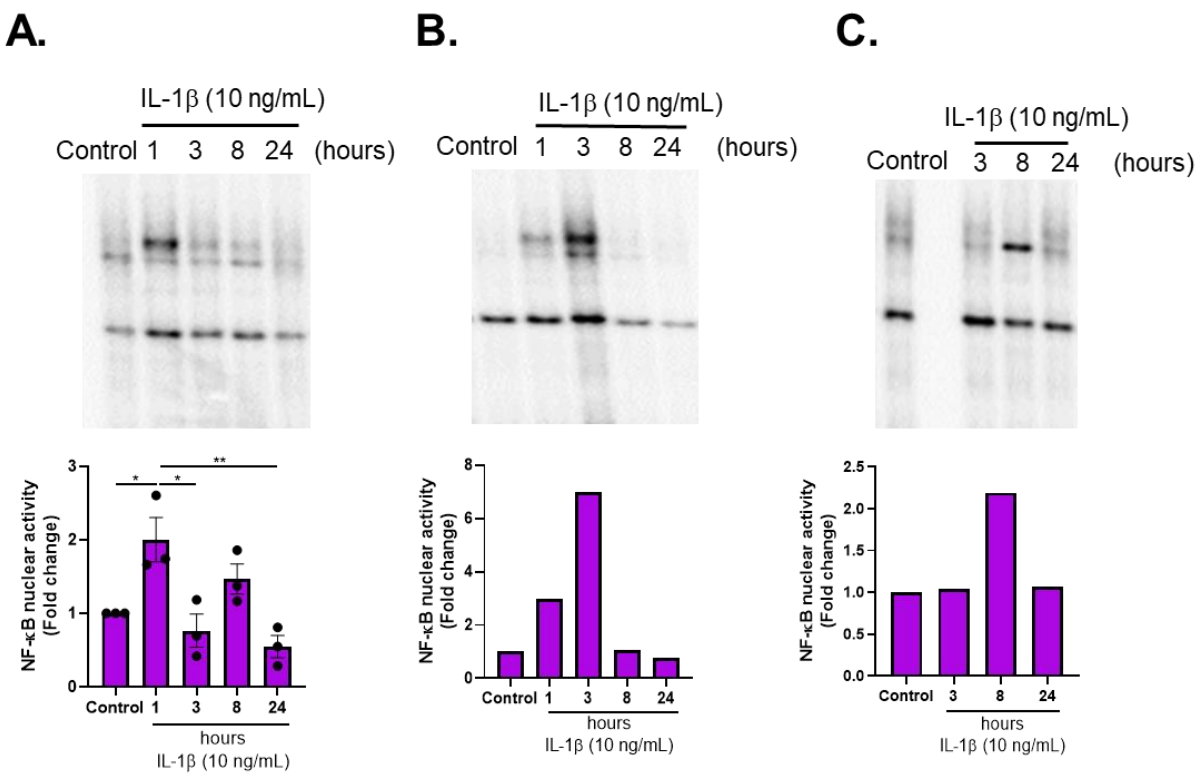

Figure 3.28. EMSA analysis of NF-κB DNA-binding activity using a tandem κB probe in wildtype, NIK$^{-/-}$ and IKKα$^{-/-}$ mouse embryonic fibroblasts.

Wildtype **(A)**, NIK$^{-/-}$ **(B)** and IKKα$^{-/-}$ **(C)** mouse embryonic fibroblasts were unstimulated or stimulated with IL-1β (10 ng/mL) for 1, 3, 8 or 24 hours followed by sample collection, nuclear extraction and protein normalisation. Double-stranded oligonucleotide probe containing two consensus NF-κB binding sites (Forward: 5′-GCTACAAGGGACTTTCCGCTGGGGACTTTCCAGGGAGG-3′; Reverse: 5′-CCTCCCTGGAAAGTCCCCAGCGGAAAGTCCCTTGTAGC-3′) was labelled with ^{32}P and incubated with nuclear extracts. Samples were resolved on a native polyacrylamide gel and visualised by autoradiography. Data represents n=3 (A), n=1 (B & C).

3.15. IκBα degradation in IL-1β stimulated wildtype and IKKα CRISPR/Cas9 knockout U2OS cells

Following the investigation of IKKα-dependent effects on non-canonical and canonical NF-κB components, it was of interest to examine the effects of IKKα CRISPR/Cas9 knockout on IL-1β-mediated IκBα loss. It is well established in the scientific literature that IκBα degradation is IKKβ-dependent rather than IKKα-dependent. Interestingly, disruption of the IKK complex via IKKα CRISPR/Cas9 knockout slowed the rate of IκBα proteasomal degradation, as evidenced by the higher levels of IκBα observed in IKKα knockout U2OS cells compared to wildtype U2OS cells after 15 minutes of IL-1β stimulation (****$p<0.0001$). Despite this delay, IκBα was ultimately degraded, and the patterns of IκBα loss and re-synthesis remain consistent between IKKα knockout and wildtype U2OS cells following 30, 60, 90 and 120 minutes of IL-1β stimulation. Therefore, while disruption of the IKK complex appears to delay the kinetics of canonical NF-κB signalling, it does not alter the overall downstream outcomes of the pathway.

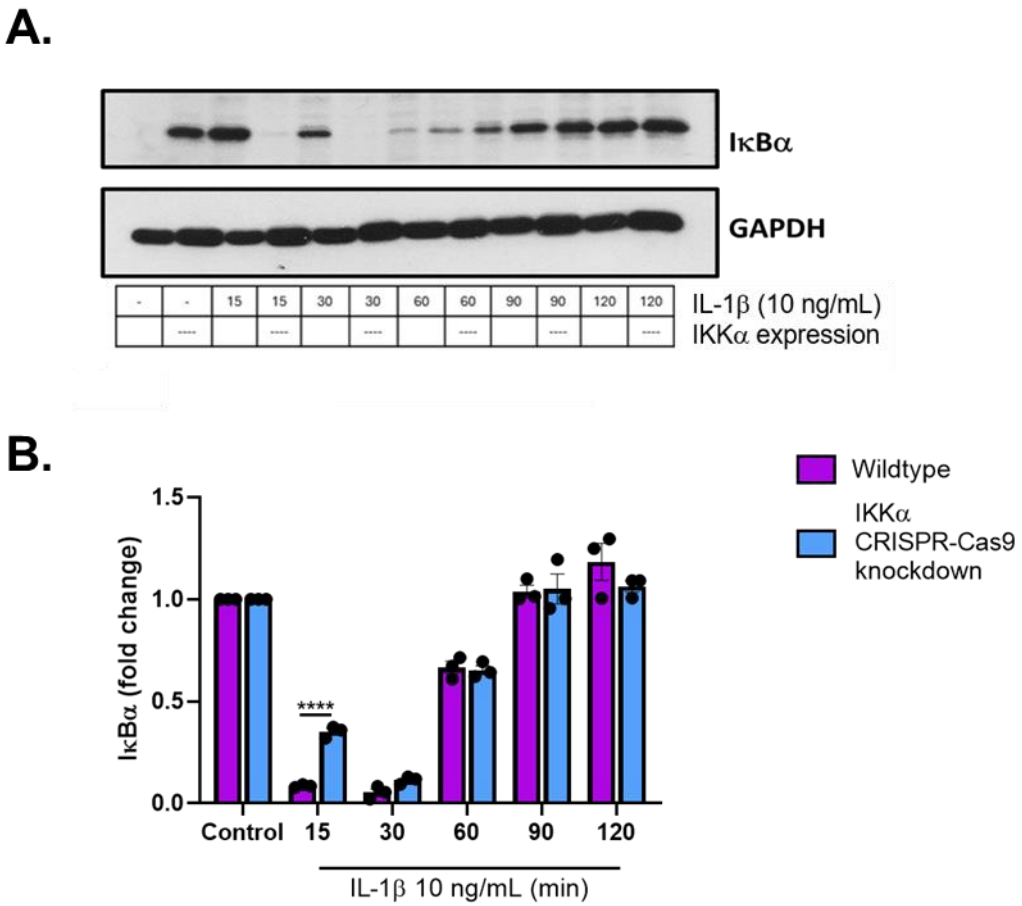

Figure 3.29. IL-1β-induced IκBα degradation is delayed but still occurs in IKKα knockout U2OS cells.

A. IκBα expression was measured in WT and IKKα CRISPR/Cas9 knockout U2OS cells by SDS-PAGE and western blot. **B.** Pixel density was quantified using ScionImage. An unpaired T-test was carried out at each time point to compare the wildtype and IKKα CRISPR/Cas9 knockout groups using GraphPad Prism 8, ****p<0.0001 (n=3).

3.16. Chapter Discussion

3.16.1. The subcellular localisation of IKKα

Initially, this chapter assessed whether IKKα protein expression could be detected in a healthy rat tibia. This allowed both hands-on tissue processing experience, as well as the ability to highlight IKKα expression in the bone by indirect immunofluorescence techniques, which appeared to be cytosolic. This was complimented by subsequently showing the cytosolic and nuclear localisation of IKKα in the U2OS cell line. This aligns closely with the known nuclear and cytosolic functions of IKKα (27, 345, 346).

3.16.2. Exploration of IKKα inhibitors on IL-1β-mediated signalling in U2OS cells

This chapter also explored the IKKα-dependent nature of IL-1β-mediated non-canonical NF-κB activation using IKKα CRISPR/Cas9 knockout U2OS cells and confirmed that IL-1β-mediated p100 phosphorylation is IKKα-dependent, at much earlier timepoints than traditional LIGHT-stimulated non-canonical NF-κB signalling. This highlights that IL-1β-mediated p100 phosphorylation is likely independent of NIK accumulation which complements published findings in HUVECs and U2OS cells (296, 347). This was further supported by the characterisation of IKKα inhibitors (348), SU1261 and SU1349 and a dual IKKα/IKKβ inhibitor SU1266, on the IL-1β-mediated p100 phosphorylation in U2OS cells. To ensure that the inhibitory effects of IKKα inhibition on p100 are not by mediating off-target effects on IKKβ, the effects of SU1261 and SU1266 on IL-1β-induced IKKβ-dependent IκBα loss were assessed. This highlighted that while selective IKKα inhibitor, SU1261 is unable to reverse IκBα degradation, SU1266 can reverse this. This highlights that IKKα selective inhibitors do not reverse IκBα loss, while a dual IKKα/IKKβ inhibitor can achieve this. Additionally, this further solidifies that the IL-1β-mediated p100 phosphorylation axis is IKKα dependent.

3.16.3. The effect of TAK1 inhibition on IL-1β-mediated signalling

Additionally, the novel IL-1β-mediated IKKα-dependent paradigm has been shown to be TAK1-mediated in human endothelial cells (340). Therefore, the role of TAK1 was validated by utilising a TAK1 inhibitor, with its effects on IL-1β-mediated responses

assessed through measurements of IKKα and p100 phosphorylation. Additionally, the effects of TAK1 inhibition on IKKβ phosphorylation and subsequent IκBα degradation was also explored, which exhibited higher IC_{50} values compared to those identified for IKKα and p100. This highlights that TAK1 potentially has higher selectivity for IKKα-mediated responses compared to IKKβ-dependent responses. Additionally, this suggests that 5Z-7-oxozaeanol could potentially be used as a pharmacological tool to differentiate between IKKα- and IKKβ-dependent processes in future studies. Furthermore, the effects of TAK1 inhibition were also assessed on JNK phosphorylation, to test the MAPK pathway as a comparator. This study identified that the IC_{50} for 5Z-7-oxozaeanol on JNK phosphorylation was less than the lowest concentration tested, 100 nM. Therefore, this further exemplifies that TAK1 plays a central and highly sensitive role in regulating MAPK signalling cascades in U2OS cells, with JNK activation being particularly susceptible to TAK1 inhibition.

3.16.4 Discrepancy Between Computational and Experimental Evidence for MEKK3-IKKα Interaction

Previous studies have demonstrated that phosphorylation of MEKK3 within its activation loop (Thr-516 and Ser-520) is crucial in Lysophosphatidic Acid-mediated, MEKK3-dependent phosphorylation of IKKβ (349). Therefore, this raised questions as to whether MEKK3 could also be involved in IKKα activation. One study which utilised in situ proximity ligation assay techniques indicated that IKKα and MEKK3 were direct protein-protein binding partners (350). This was investigated using ColabFold, an AlphaFold2-based computational tool. It was shown that MEKK3 and IKKα heterodimers were predicted to bind at Ser180 on IKKα and MEKK3 Glu571. Glutamine possesses an amide side chain, which can accept or transfer hydrogen bonds and therefore, this is chemically plausible. Indeed, Ser180 is one of the well-established phosphorylation sites within the IKKα activation loop, alongside Ser176 (27). To understand whether it could be a TAK1, MEKK3 and IKKα trimeric complex which is formed, a TAK1-MEKK3-IKKα trimer was predicted. Interestingly, this time, MEKK3 was found to bind both Ser176 and Ser180 in the presence of TAK1. Therefore, IKKα and MEKK3 immunoprecipitations were carried out in the presence and absence of IL-1β stimulation to try and understand whether this predicted binding was possible. IKKα immunoprecipitation revealed a lower band in unstimulated and

IL-1β-mediated conditions, while MEKK3 immunoprecipitation revealed MEKK3 only. Therefore, it may be that IKKα and MEKK3 can bind, but that this is not applicable in IL-1β-mediated conditions. Additionally, in some cell types, IKKα has different functions, for example, it can play a more dominant in canonical NF-κB signalling than IKKβ (276). Therefore, it may be that MEKK3 and IKKα are protein-protein binding partners, but only in specific cell types. Nevertheless, the second band which was revealed in IKKα immunoprecipitation is approximately the same molecular weight as seen in the MEKK3 immunoprecipitation. However, this band is potentially representative of TAK1 expression, as both MEKK3 and TAK1 are approximately 70 kDa (351, 352). However, further immunoprecipitation experiments would be required to definitively prove this. Additionally, given recent identification of a newly discovered MAP3K and IKKα-binding partner, MAP3K13-232aa, further studies would be required to assess whether this MAP3K could also potentially have any role in IL-1β-induced IKKα-dependent signalling (353).

3.16.5. HA-p100 expression levels in U2OS cells with IL-1β stimulation

However, despite the interesting upstream avenues explored, the IL-1β-mediated non-canonical NF-κB pathway remained the key focus throughout this chapter. U2OS cells were transfected with a HA-tagged p100 construct to evaluate whether the subcellular localisation changes following IL-1β stimulation, and whether there is apparent p100 processing as a result of IL-1β-induced p100 phosphorylation. It was observed that the fluorescence intensity of HA-p100 following IL-1β stimulation was unchanged, and therefore there was nothing to indicate that p100 is degraded when phosphorylated. However, given the nature of pcDNA transfections, there is also the possibility that there could be transfection efficiency variability across the samples.

Therefore, to gain an understanding of possible functional outcomes of IKKα-dependent p100 phosphorylation, the effects of IL-1β-dependent NF-κB DNA-binding activity was evaluated in nuclear extracts from MEFs by EMSA. These experiments highlighted a delay in IL-1β-induced NF-κB DNA-binding activity in $NIK^{-/-}$ MEFs observed at 3 hours compared to maximal activity being seen after 1 hour IL-1β stimulation in wildtype MEFs. While the 1 hour time point in $IKK\alpha^{-/-}$ MEFs was not evaluated, there was high levels of NF-κB DNA-binding activity post 8 hours IL-1β

stimulation observed under these conditions. This was an interesting find, and so it raised questions as to whether IL-1β-mediated IKKα-dependent signalling could potentially have a functional outcome by influencing the nuclear translocation of NF-κB family members. To gain a better understanding of potential downstream signalling events dependent on IKKα activity and p100 phosphorylation, it would be useful to knockout p100 expression to then look at the implications on NF-κB nuclear translocation expression. However, this is unfavourable, as p100 generally negatively regulates and stabilises other NF-κB subfamily members, and therefore, p100 knockout MEFs have demonstrated upregulated nuclear p52 and RelB expression (354). Therefore, knocking down p100 would disrupt the NF-κB system, subsequently creating artefactual effects on other NF-κB members. As an alternative, 5Z-7-oxozaeanol was utilised to understand whether p52 and p65 nuclear translocation is TAK1 dependent. P52 and p65 nuclear translocation were reduced in alignment with similar concentrations as observed to reduce IKKβ phosphorylation and reverse IκBα loss, and therefore these events align more closely with IKKβ signalling than IKKα signalling. Additionally, SU1261 was utilised to rule out that IL-1β-mediated p52 is IKKα-dependent, and this study highlights that SU1261 has no effect on IL-1β-induced p52 and p65 nuclear translocation. In contrast, SU1266, which inhibits both IKKα and IKKβ, was shown to reduce p52 and p65 nuclear translocation, supporting the theory that p52 and p65 nuclear translocation in the IL-1β-signalling arm is IKKα-independent.

3.16.6. Chapter Conclusion

In summary, this chapter establishes that IL-1β-mediated non-canonical NF-κB activation is an IKKα-dependent process, occurring at earlier timepoints and through distinct mechanisms from classical non-canonical NF-κB signalling. By demonstrating that p100 phosphorylation requires IKKα but does not lead to its degradation into p52, these findings challenge the prevailing assumption that IL-1β stimulation converges fully with non-canonical NF-κB processing events. The pharmacological data highlight that selective IKKα antagonists can effectively inhibit p100 phosphorylation, offering new tools to dissect IKKα-specific signalling and raising the possibility of targeting IKKα as a more refined therapeutic strategy compared with traditional, toxic IKKβ

inhibitors. Moreover, the differential sensitivity of IKKα and IKKβ signalling outputs to TAK1 inhibition uncovers an additional layer of complexity in IL-1β responses, suggesting that TAK1 may regulate these kinases with distinct thresholds or in cooperation with other MAP3Ks such as MEKK3. Collectively, these contributions expand our understanding of the molecular diversity of NF-κB signalling, provide mechanistic insights into IL-1β-driven inflammatory responses, and open new avenues for considering IKKα as both a signalling node and potential therapeutic target in contexts where canonical and non-canonical pathways intersect. Furthermore, IL-1β-dependent p100 phosphorylation does not appear to have any obvious functional outcome which reveals in nuclear translocation of NF-κB family members, and therefore, this remains unknown. Therefore, an alternative way to assess the downstream effects of p100 phosphorylation in this context would be to assess bulk gene expression by transcriptomics.

Chapter 4

IKKα-dependent genes in U2OS cells using RNA-sequencing

4.1. Chapter Introduction

The results in chapter 3 outlined that IKKα has clear activity in U2OS cells, however, it is not clear what the functions of IKKα are beyond promoting the phosphorylation of p100. Additionally, given the growing number of studies identifying various IKKα-dependent substrates, including TRAF4, CHK1, p300/CBP, and c-Myc, that promote diverse cellular responses, this highlights that IKKα can directly act on these targets to regulate processes beyond the NF-κB signalling pathways (311, 345, 355, 356). Given these diverse functions, it is likely that some IKKα-dependent genes operate independently of NF-κB and thus remain unidentified. To date, IKKα-dependent genes have remained rather undefined, and therefore, it would be beneficial to better understand the role of IKKα in regulating genes related to bone health, and in bone formation and bone degradation processes. Additionally, it would be overall advantageous to identify potential downstream roles of IKKα in the expression of IL-1β-mediated downstream genes to better understand the extent of the outcome of IKKα activation in this pathway. To identify such genes, RNA-sequencing provides a valuable approach.

Next-generation sequencing (NGS), including RNA sequencing, enables the simultaneous sequencing of millions of fragments in a single run. This technology offers a faster, high-throughput, more sensitive, and cost-effective alternative to Sanger sequencing for generating large-scale genomic data (357-360). NGS technologies include Illumina sequencing, Ion torrent sequencing, and Oxford Nanopore sequencing (361). This chapter utilises Illumina sequencing, which is a short-read sequencing technology (362). Illumina is the leading next generation technology making up 80% of the global DNA sequencing market, likely due to it producing the highest throughput per run while maintaining the lowest per base cost (363, 364).

Given the vast quantity of complete genomic structures which are now known, NGS sequencing is an exciting and cost-effective method to identify differential gene expression following induction of cellular signalling pathways. In the context of this study, Illumina RNA-sequencing is a useful tool to build on the information obtained in Chapter 3, and to gain a better understanding of IKKα more widely, by highlighting the clusters of genes which it regulates in the human genome.

4.2. Chapter Aim

The primary focuses of this chapter are to:

1. Identify IKKα-dependent genes in control conditions and following IL-1β cell stimulation by utilising Illumina RNA-sequencing techniques.
2. Determine whether IKKα is a key regulator in any genes associated with osteoclastogenesis or osteogenesis processes.
3. Utilise the findings of this study to examine the key effects induced by IKKα in U2OS cells by the generation of gene clusters from the output data of the study to understand the impact of IKKα activity on specific physiological and pathophysiological cellular processes.
4. Utilise the IKKα inhibitors which were characterised in chapter 3 and measure their ability to inhibit IL-1β-mediated IKKα-dependent downstream gene targets.

4.3. Results

4.3.1. Demonstration of sufficient IKKα CRISPR Cas/9 knockout in U2OS cells

Parallel to sample preparation for RNA-sequencing, SDS-PAGE was carried out to determine that IKKα CRISPR/Cas9 knockout was sufficient in knocking down the IKKα gene, and downstream IKKα-dependent p100 phosphorylation was measured to demonstrate IL-1β-mediated IKKα-dependent signalling events were adequately knocked down in IKKα CRISPR/Cas9 knockdown U2OS cells (Figure 4.1).

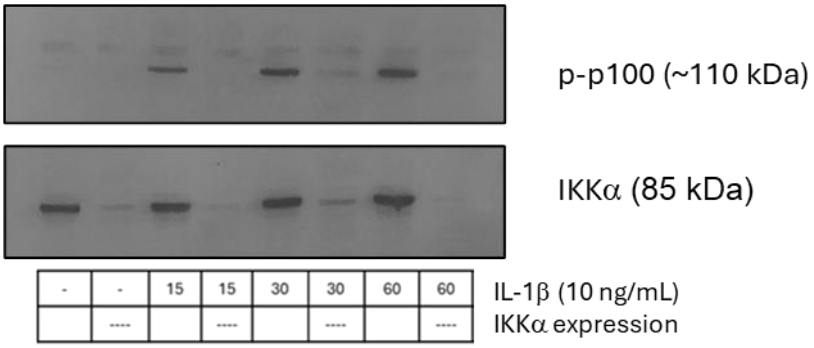

Figure 4.1. Demonstration of IKKα knockout in U2OS cells achieved with CRISPR/Cas9.
SDS-PAGE and western blot analyses were conducted on wildtype and IKKα CRISPR/Cas9 knockout cells, under basal conditions and after IL-1β (10 ng/mL) stimulation at various time intervals (15, 30, and 60 minutes). IKKα and phospho-p100 primary antibodies were applied. Data represents wildtype and IKKα CRISPR/Cas9 knockout cells beside one another for each condition. Membranes were exposed for 2 minutes, n=3.

4.3.2. RNA quality for RNA sequencing analysis

To determine whether RNA was of adequate quantity from total RNA extracted from cellular samples, RNA concentration was measured initially by utilisation of a ThermoFisher Scientific Nanodrop (data not shown). To rule out sample quantification overestimation which can commonly be influenced by contaminants when using the Nanodrop, Sample RNA was quantified again more sensitively by use of RNA Qubit assay techniques (Figure 4.2).

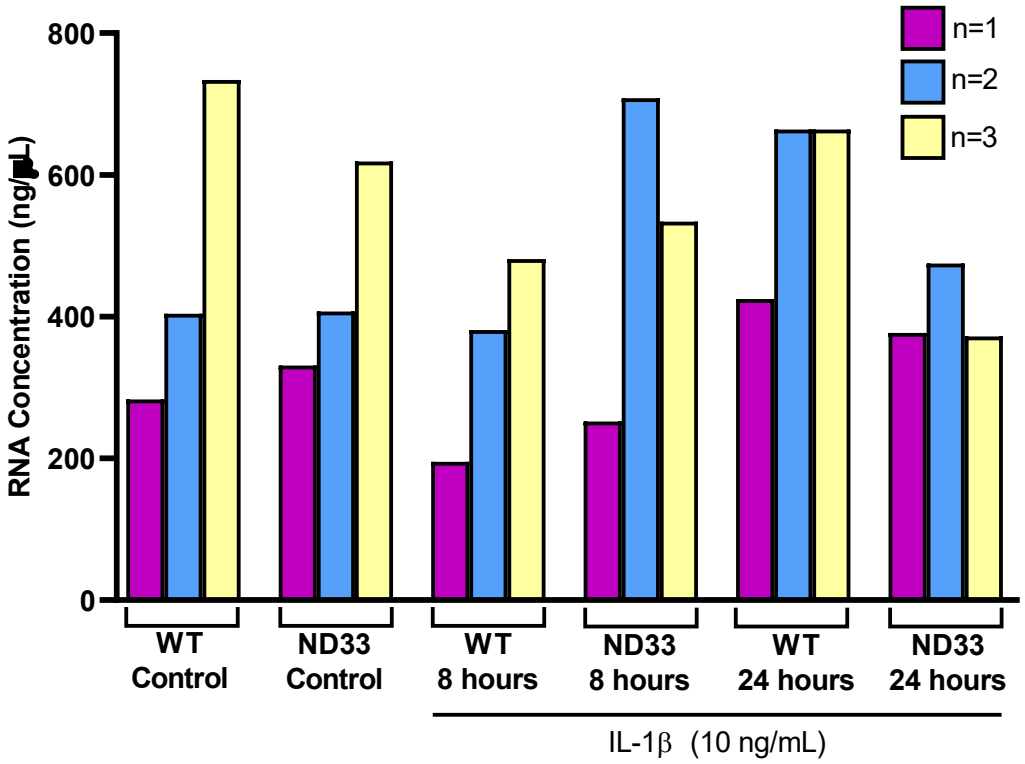

Figure 4.2. RNA concentration quantified by use of RNA Qubit assay techniques.
RNA concentration was quantified to determine adequate RNA following shipment of RNA samples. Figure created by GraphPad prism 8 software.

From Qubit assay techniques, it is evident that all samples had a sufficient abundance of total RNA for RNA-sequencing. To identify the quality of the RNA samples, quality control was then carried out by using a Fragment Analyzer (Figure 4.3).

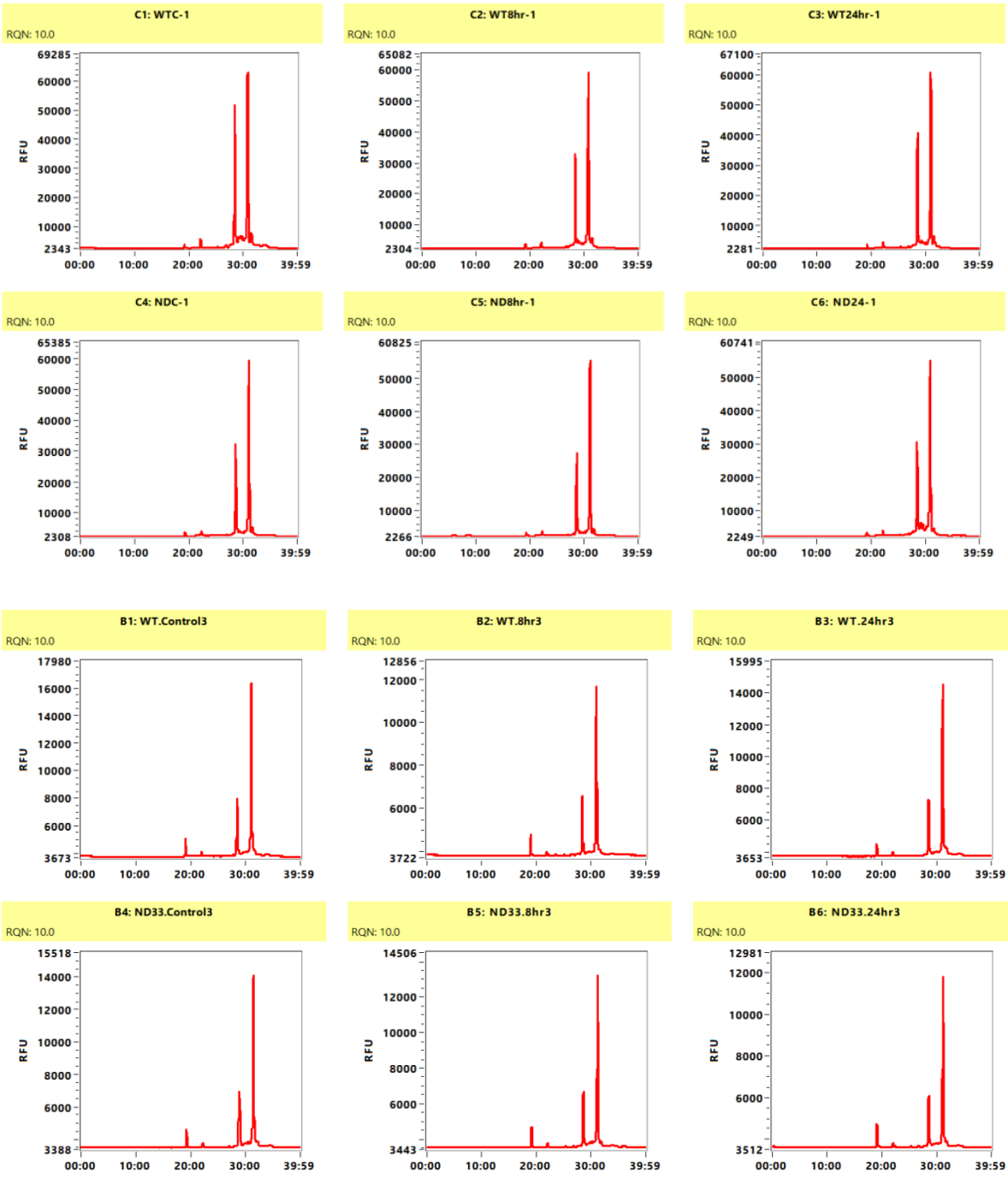
C1: WTC-1
RQN: 10.0
C2: WT8hr-1
RQN: 10.0
C3: WT24hr-1
RQN: 10.0
C4: NDC-1
RQN: 10.0
C5: ND8hr-1
RQN: 10.0
C6: ND24-1
RQN: 10.0
B1: WT.Control3
RQN: 10.0
B2: WT.8hr3
RQN: 10.0
B3: WT.24hr3
RQN: 10.0
B4: ND33.Control3
RQN: 10.0
B5: ND33.8hr3
RQN: 10.0
B6: ND33.24hr3
RQN: 10.0
RFU
00:00
10:00
20:00
30:00
39:59

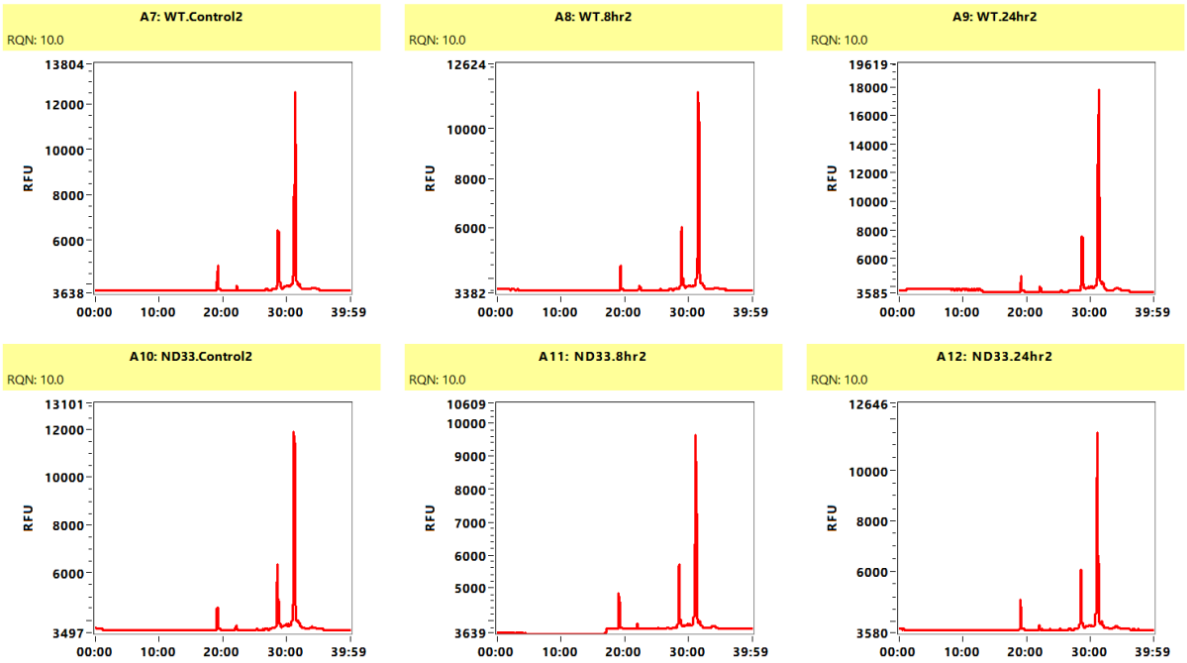

Figure 4.3. A summary of quality of samples by utilisation of a Fragment Analyzer instrument.

RNA Quality Number (RQN) was 10.0/10.0 for all 18 samples. Relative Fluorescence Units (RFU) differed between samples (y axis), but nucleotide sizes where peaks occurred remained similar (x axis).

4.3.3. Differentially expressed genes in unstimulated U2OS cells with and without IKKα CRISPR/Cas9 knockout

Following the 9 comparisons which were analysed, principal component analysis plots were constructed to evaluate similarity between samples in each sample group. The principal component analysis plots feature the first principal component (PC1) on the x-axis which highlights the largest difference between samples, and the second principal component (PC2) on the y-axis, which highlights the second greatest difference in samples. The first comparison made was unstimulated IKKα CRISPR/Cas9 knockout U2OS cells compared to wildtype U2OS cells (Figure 4.4).

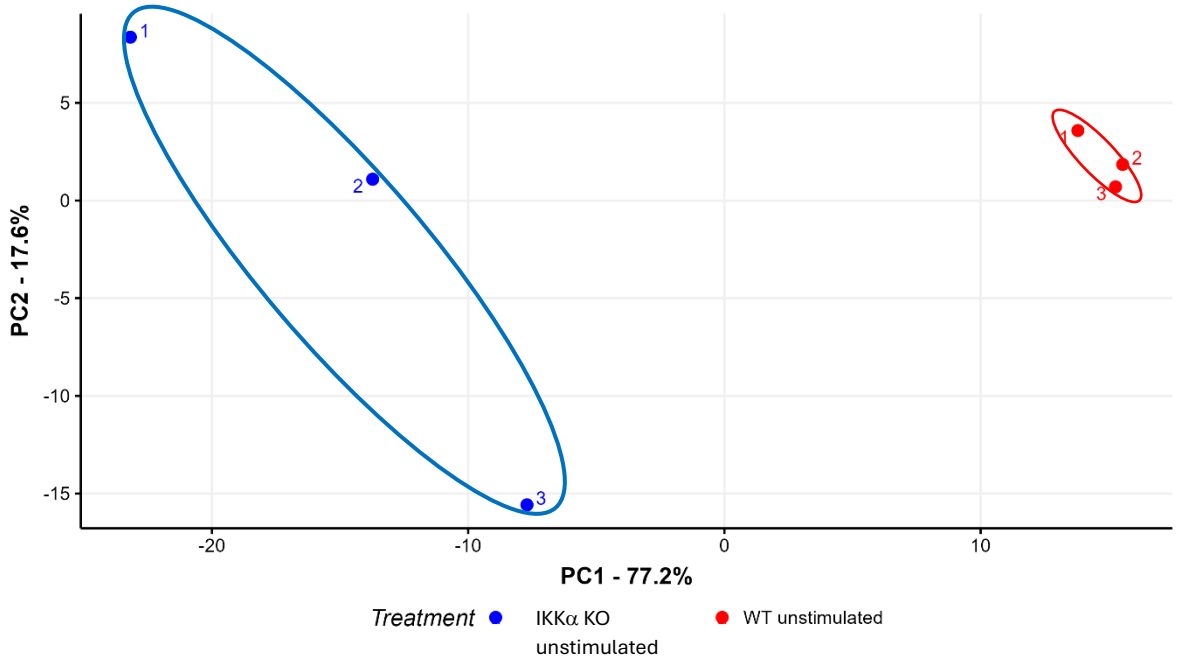

Figure 4.4. Principal Component Analysis plot for unstimulated WT U2OS cells compared to unstimulated IKKα CRISPR/Cas9 knockout U2OS cell comparisons.
Data set patterns between samples within sample groups which were utilised for RNA-sequencing analysis were assessed by construction of principal component analysis plot. The first principal component (PC1, x-axis) demonstrates the highest variability of differences in data, while the second principal component (PC2, y-axis) highlights the second highest variability in data sets.

The principal component analysis dot plot for the comparison between unstimulated IKKα CRISPR/Cas9 knockout and wildtype U2OS cells demonstrate distinct differences between the two sample groups. Following principal component analysis plot construction, the first sample group comparison was considered to assess IKKα-dependent genes in U2OS cells without stimulation. A volcano plot was constructed to demonstrate the top 20 differentially expressed genes between unstimulated IKKα CRISPR/Cas9 knockout U2OS cells and wildtype U2OS cells. Notably, the majority of top differentially expressed genes were significantly higher expressed in IKKα CRISPR/Cas9 knockout (blue) compared to wildtype (Figure 4.5).

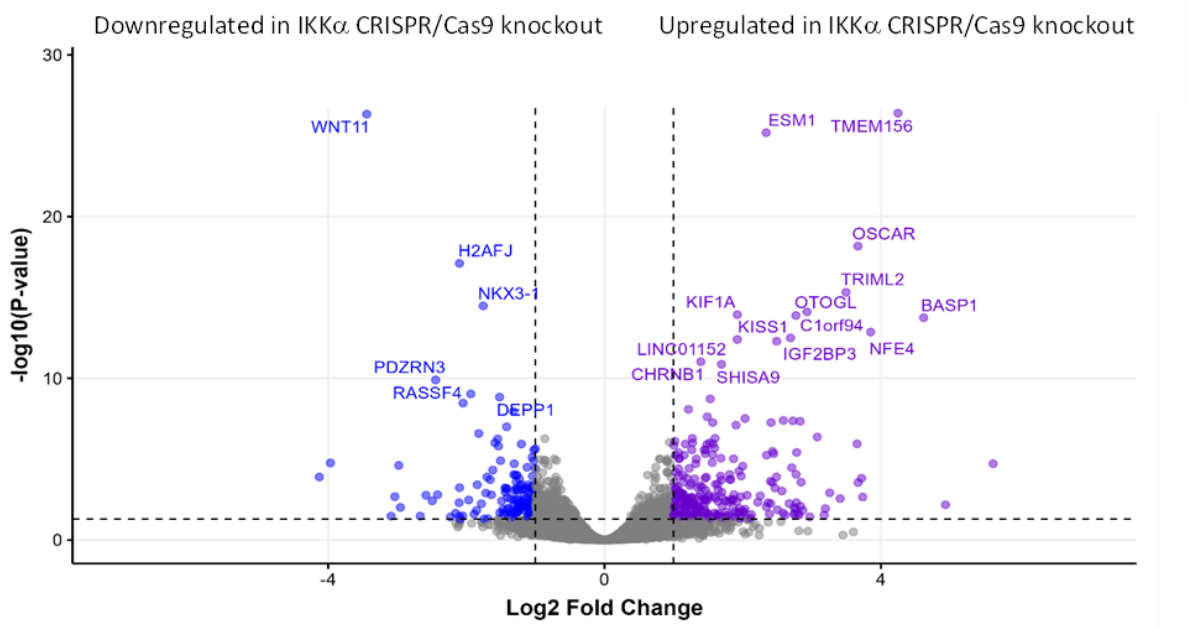

Figure 4.5. A volcano plot highlighting the top 20 differentially expressed genes between unstimulated IKKα CRISPR/Cas9 knockout and wildtype U2OS cells.

Genes which were upregulated (blue) and downregulated (purple) in the IKKα CRISPR/Cas9 knockout U2OS cells are displayed.

4.3.4. Upregulated genes in unstimulated IKKα CRISPR/Cas9 knockout U2OS cells compared to wildtype U2OS cells

A Heatmap was created to measure the top 20 upregulated genes in order of ascending p-value in IKKα CRISPR/Cas9 knockout compared to wildtype U2OS cells (Figure 4.6).

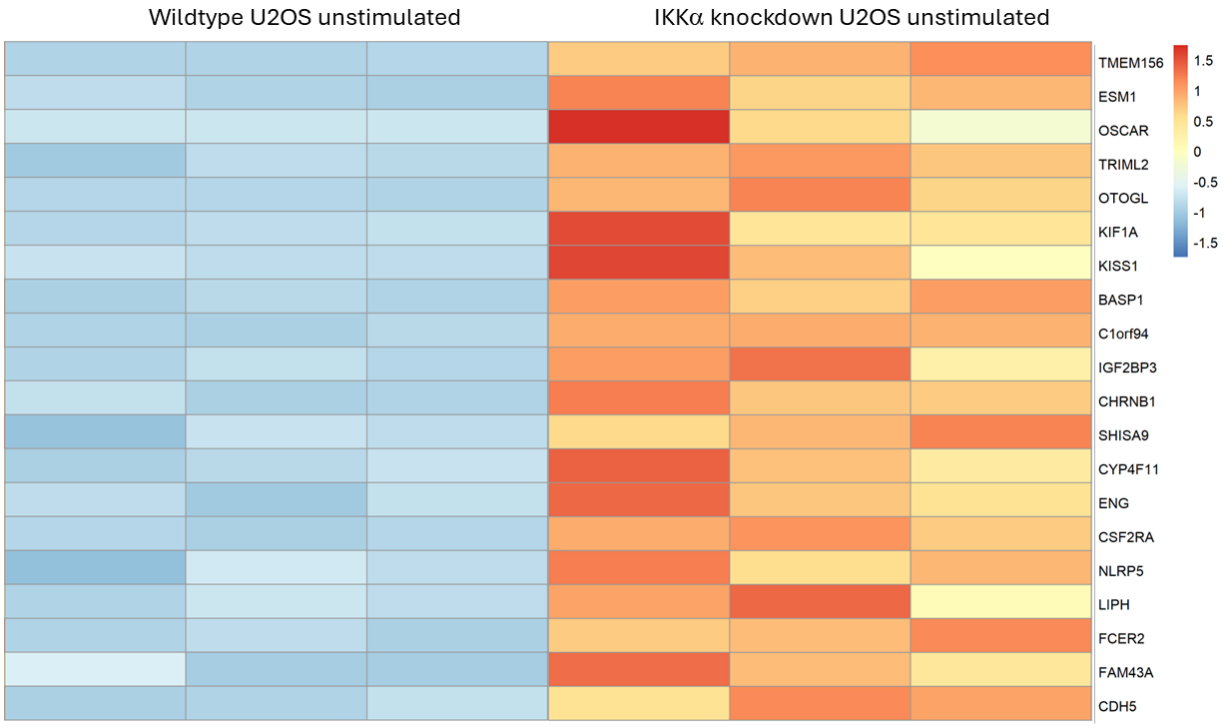

Figure 4.6. A heatmap depicting the top 20 differentially expressed genes which were significantly higher in unstimulated IKKα CRISPR/Cas9 knockout U2OS cells compared to wildtype.
The genes were filtered in order of ascending p-value, and the top 20 genes were selected. The smallest and largest p-value of the top 20 differentially genes are displayed by lowest to highest p-value, at the top to bottom of the heatmap, respectively. The colours shown in the heatmap are indicative of z score, where baseline expression = 0, positive integers = above baseline expression, and negative integers = below baseline expression. Heatmap was constructed by R, n=3.

As indicated in the heatmap (Figure 4.6), the relative expression of many genes was increased in IKKα CRISPR/Cas9 knockout U2OS cells compared to wildtype U2OS cells. The z score itself does not provide an absolute measure of gene expression and provides the relative deviation of that gene. However, only genes which were found to be differentially expressed by at least 2-fold, and $p<0.05$ were utilised in the heatmaps.

To further determine the function of the genes which were upregulated in IKKα CRISPR/Cas9 knockout U2OS cells, a table was constructed (Table 4.1).

Table 4.1. A table displaying the top 25 upregulated genes in IKKα CRISPR/Cas9 knockout U2OS cells.

Gene name	***Function***
Transmembrane protein 156 (TMEM156)	The role of TMEM156 is not fully characterised, but it has been shown to be upregulated in head and neck squamous cell carcinoma (365).
ESM1	Endothelial cell-specific molecule 1 (Esm1) is a secreted protein which is a target of and a regulator of VEGF signalling and thereby is a promoter of vascular permeability (366).
Osteoclast-associated receptor (OSCAR)	OSCAR is a receptor which promotes osteoclast differentiation and maturation (367).
Tripartite motif family-like 2 (TRIML2)	TRIML2 binds to p53 to promote p53-SUMOylation which subsequently enhances transactivation of proapoptotic genes (368).
Otogelin-like protein (OTOGL)	Lack of Otogelin-like protein or Otogelin have an association with hearing loss (369).
Kinesin-like protein (KIF1A)	The function of KIF1A is poorly understood.
KiSS-1 metastasis suppressor (KISS1)	KISS1 is a metastasis suppressor. A product of KISS1, kisspeptin, activates neurons which release gonadotropin-releasing hormone from the hypothalamus (370).
Membrane-attached signal protein 1 (BASP1)	BASP1 is involved in neuronal signalling which lead to neuronal elongation and plasticity (371).
Nuclear factor, erythroid 4 (NFE4)	The function of NFE4 is poorly understood.
Chromosome 1 open reading frame 94 (C1orf94)	The function of C1orf94 is poorly understood.

IGF2BP3	Oncogenic in colorectal cancer (372) and nasopharyngeal carcinoma (373).
Cholinergic receptor nicotinic beta 1 subunit (CHRNB1)	The CHRNB1 gene accounts for one out of five subunits of the nicotinic acetylcholine receptor, which is a pentameric ion channel generally found at neuromuscular junctions.
SHISA9	SHISA9 formerly known as CKAMP44, is a type 1 transmembrane protein which is an auxiliary subunit of the AMPA-type glutamate receptor. SHISA9 interacts with the C-terminus of the AMPA receptor (374).
CYP4F11	CYP4F11 is a cytochrome P450 family member and is involved in eicosanoid metabolism.
Endoglin (ENG)	ENG gene encodes endoglin, which is a type III accessory receptor for transforming growth factor-beta expressed on endothelial cells to enhance angiogenesis. Interestingly, ENG expression is regulated by bone morphogenetic protein 9 (BMP-9) (375). However, BMP9 is not expressed in U2OS cells in this study, suggesting these are IKKα-dependent effects on ENG expression.
Colony Stimulating Factor 2 Receptor Alpha Subunit (CSF2RA)	CSF2RA encodes the granulocyte-macrophage colony-stimulating factor (GM-CSF) alpha subunit. GM-CSF has an important role in osteoclastogenesis, and is particularly useful in osteoclast differentiation following short term GM-CSF exposure (376).
NLRP5	NLRP5 encodes for a maternal protein, where mutations in NLRP5 have been associated with multilocus imprinting disturbance (377), which can result in disruptions in foetal development.
Lipase H (LIPH)	LIPH can be upregulated by HIF-1a and has been associated with immunosuppressive effects in RNA-seq studies surrounding pancreatic cancer (378, 379).
FCER2	FCER2 single nucleotide polymorphisms (SNPs) have been associated with increased IgE expression in children with asthma and therefore appear to have a role in allergy responses (380).
family with sequence similarity 43 member A (FAM43A)	FAM43A expression has been used in a prediction model to determine recurrence of triple negative breast cancer in Taiwan (381).

Within the table outlined above (Table 4.1), there are genes with diverse functions which are upregulated by IKKα CRISPR/Cas9 knockout. ESM1, ENG and CYP4F11 are involved in endothelial cell behaviour, vascular permeability and angiogenesis, which are often influenced by inflammatory or hypoxic signalling. FCER2, CSF2RA, NLRP5 are linked to immune and inflammatory responses, where they participate in cytokine signalling, immunoglobulin regulation and inflammasome or immune signalling pathways. IGF2BP3, KISS1, LIPH, FAM43A and TMEM156 are a mixture of tumour-promoting genes and tumour-suppressing genes. TRIML2 promotes p53-mediated apoptosis. Two genes which are involved in osteoclastogenesis, OSCAR, the osteoclast-associated receptor, and CSF2RA, the GM-CSF alpha subunit gene were both within the top 25 significantly increased genes in IKKα CRISPR/Cas9 knockout U2OS cells. Due to its central role in bone degradation, OSCAR was of interest, as its expression was notably increased, from an average of 147.9 in wildtype U2OS cells to 1881.6 reads in IKKα knockout U2OS cells (p= 6.72E-19). However, CSF2RA, was also of interest which increased from a mean of 69.7 reads in wildtype U2OS cells to 195.8 reads in IKKα knockout U2OS cells (p=3.52E-11). However, given that the level of reads of CSF2RA were so low overall, OSCAR was a more viable target gene to pursue experimentally in the context of osteoclastogenesis.

Therefore, OSCAR was chosen as the main gene of interest for further validation within the laboratory, given its relevance to bone homeostasis and health, and the high statistically significant difference between its expression in wildtype compared to IKKα CRISPR/Cas9 knockout U2OS cells.

Initially Western blotting was applied to measure OSCAR protein expression in wildtype and IKKα CRISPR/Cas9 knockout U2OS whole cell lysates. However, this was repeatedly unsuccessful, due to relative low expression and so microscopy experiments were undertaken (Figure 4.7).

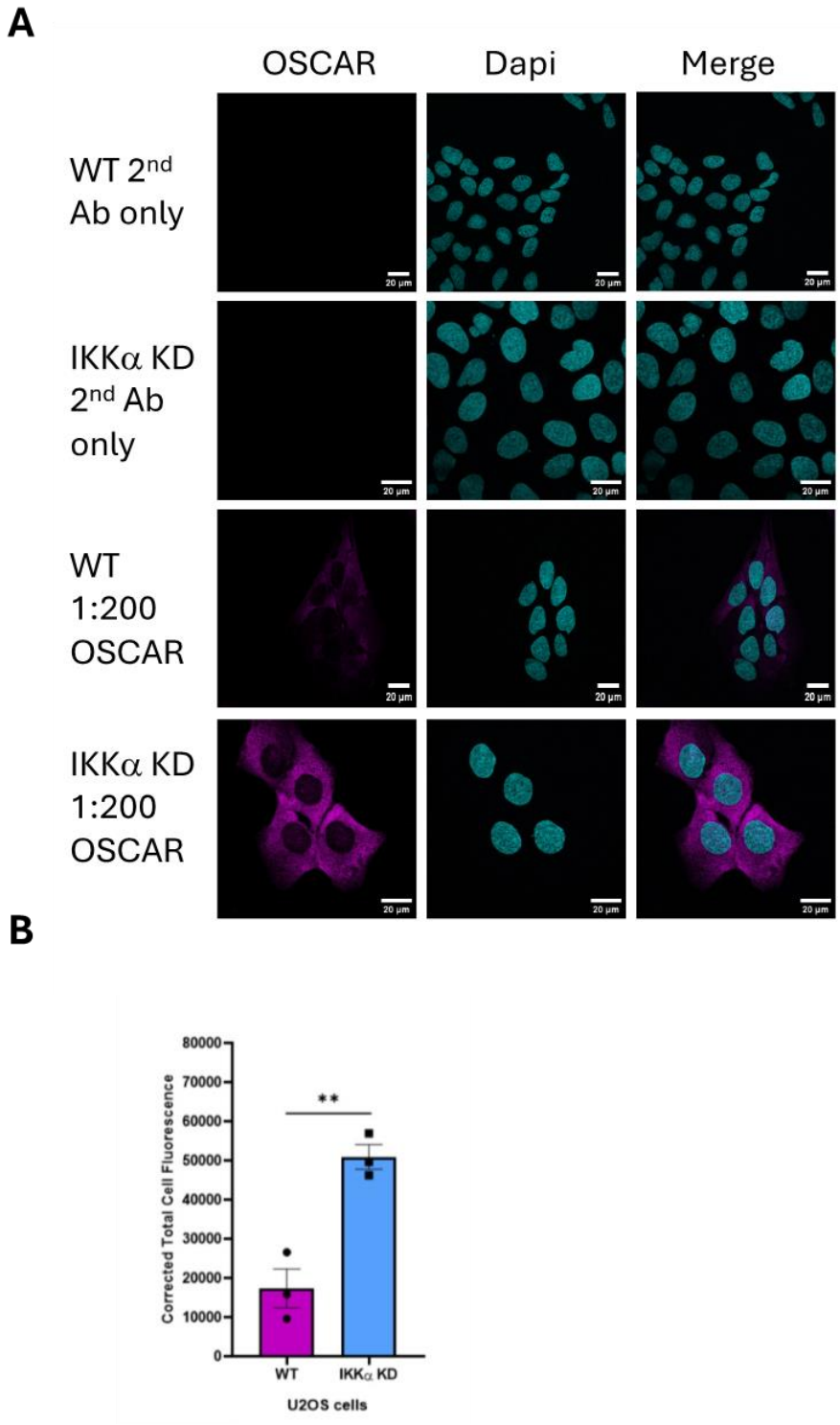

Figure 4.7. IKKα CRISPR/Cas9 knockout increases OSCAR protein expression in U2OS cells.

A. Immunofluorescence staining was utilised to highlight of protein expression of OSCAR in the presence and absence of IKKα CRISPR/Cas9 knockout. B. The corrected total cell fluorescence was measured in every cell in images taken, and each point represents the mean corrected total cell fluorescence of all cells across all images taken in one n number. Data analysis was conducted by using GraphPad prism 8 software, **$p<0.01$, n=3.

Notably, there was significantly higher OSCAR expression in unstimulated IKKα CRISPR/Cas9 knockout U2OS cells (**p<0.01) than wildtype U2OS cells. To further validate this, techniques beyond IKKα CRISPR/Cas9 were required to further validate these findings and eliminate any potential off-target CRISPR/Cas9 knockout effects. Therefore, to understand whether the IKKα siRNA could replicate the effects of IKKα CRISPR/Cas9 knockout and to determine if OSCAR expression was specifically reliant on IKKα expression, U2OS cells were untreated or treated with non-targeted siRNA, IKKα siRNA, or IKKβ siRNA (100 nM) and SDS-PAGE and western blotting was carried out (Figure 4.8).

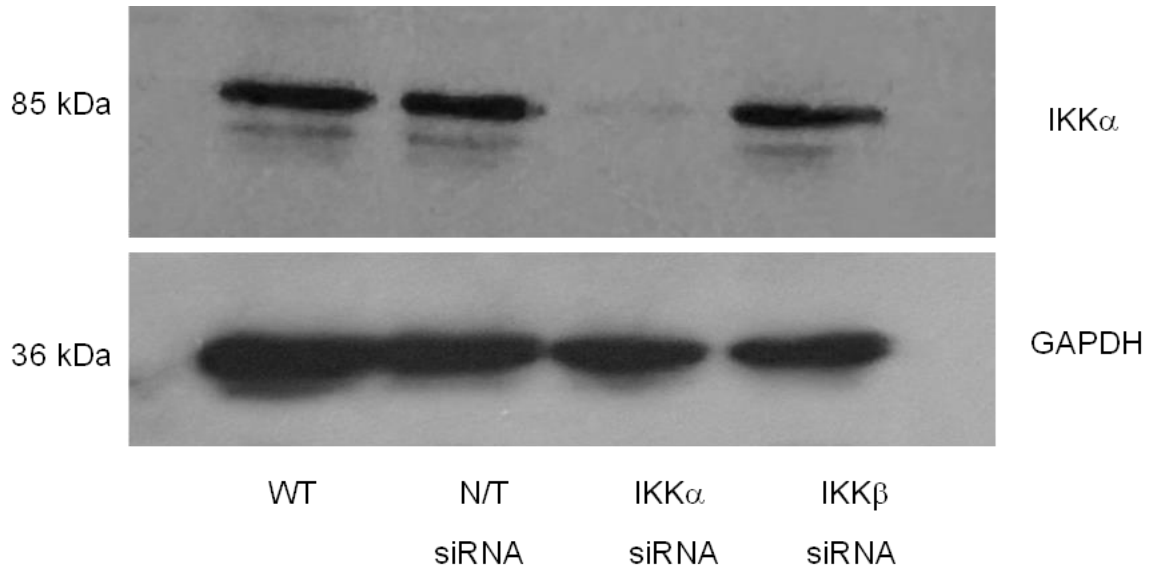

Figure 4.8. IKKα knockdown with siRNA in U2OS cells.
Cells were untreated or pre-treated with non-targeting siRNA, IKKα siRNA or IKKβ siRNA (100 nM) for 72 hours prior to cell lysis. Samples were prepared for SDS-PAGE and western blotting analysis, n=4.

Notably, IKKα knockdown was sufficient following IKKα siRNA treatment, and this did not appear to affect cell viability. Simultaneously to the siRNA treatment of samples utilised for western blotting, cells seeded on coverslips were also treated with siRNA to assess OSCAR mRNA expression. Interestingly, OSCAR mRNA expression was significantly decreased following both IKKα and IKKβ siRNA (Figure 4.9).

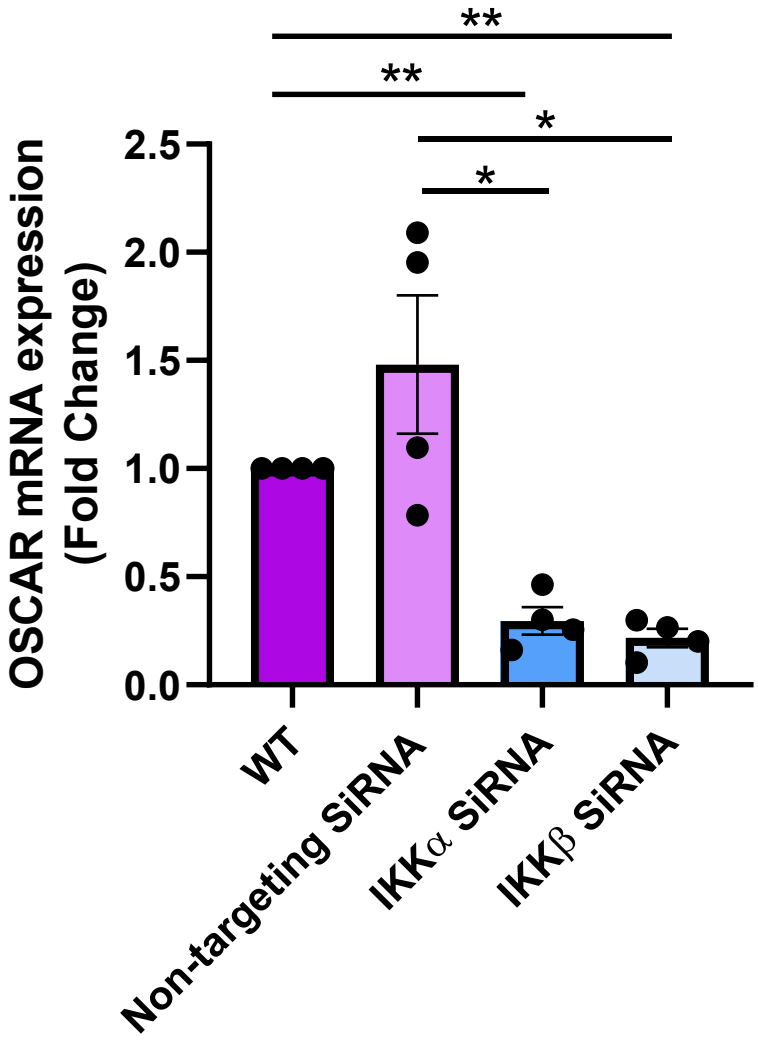

Figure 4.9. OSCAR mRNA expression is significantly reduced by IKKα or IKKβ siRNA knockdown.

U2OS cells were untransfected, or transfected with non-targeting siRNA, IKKα siRNA or IKKβ siRNA (100 nM) for 72 hours. Total RNA was extracted from cell samples, and reverse transcription and RT-qPCR. Comparative Ct analysis was performed to generate fold change values against untreated wildtype cells. ONE-WAY ANOVA was conducted by utilising GraphPadPrism 8 software, *p<0.05, **p<0.01, n=4.

In parallel to the cells being transfected with siRNA for RT-qPCR, U2OS cells were also transfected to measure OSCAR protein expression by immunofluorescence (Figure 4.10). It was highlighted that there was no statistical difference in OSCAR expression between WT, non-targeting siRNA (100 nM), IKKα siRNA (100 nM) and IKKβ siRNA (100 nM).

A.

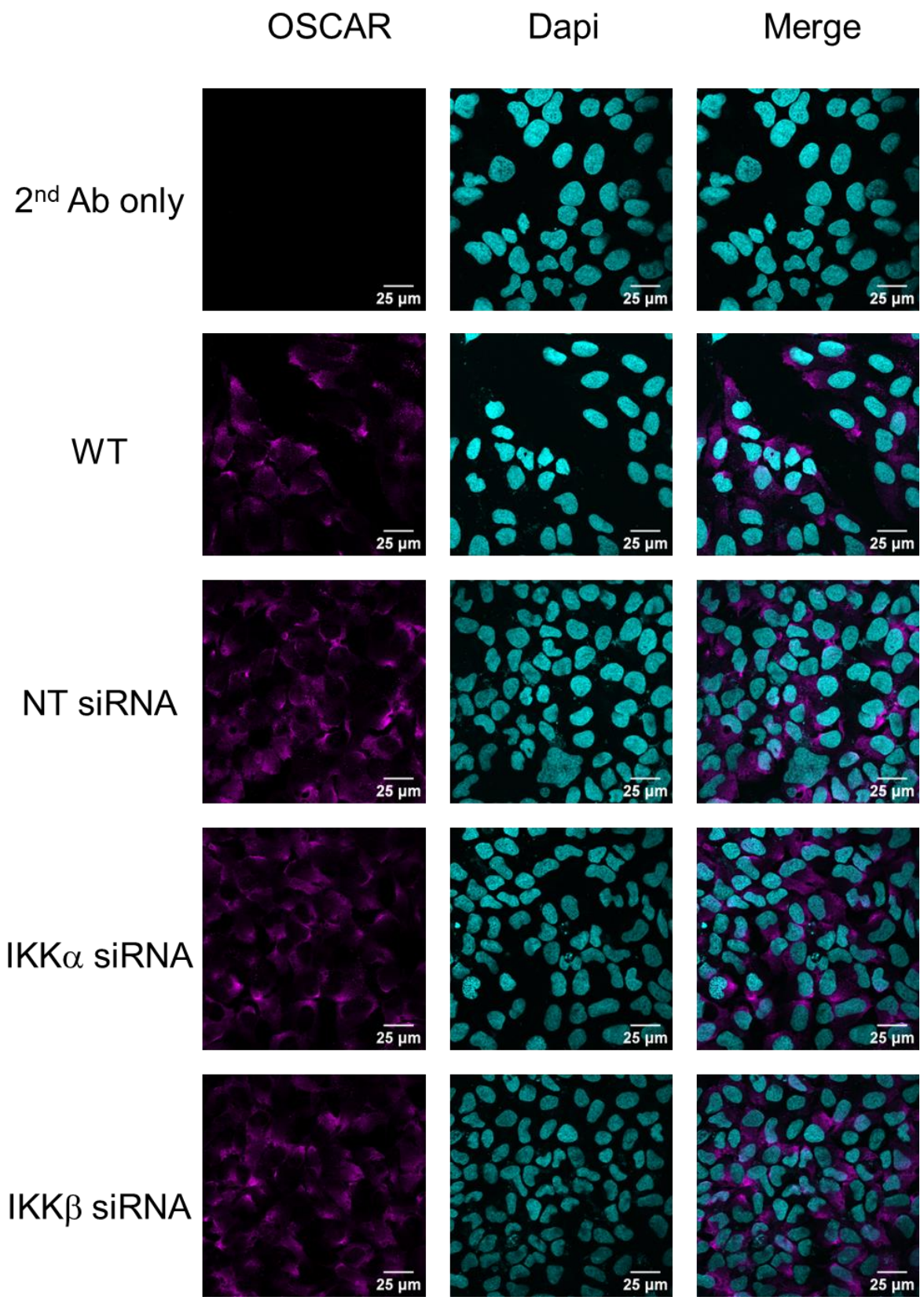
OSCAR
Dapi
Merge
2nd Ab only
WT
NT siRNA
IKKα siRNA
IKKβ siRNA
25 µm

B.

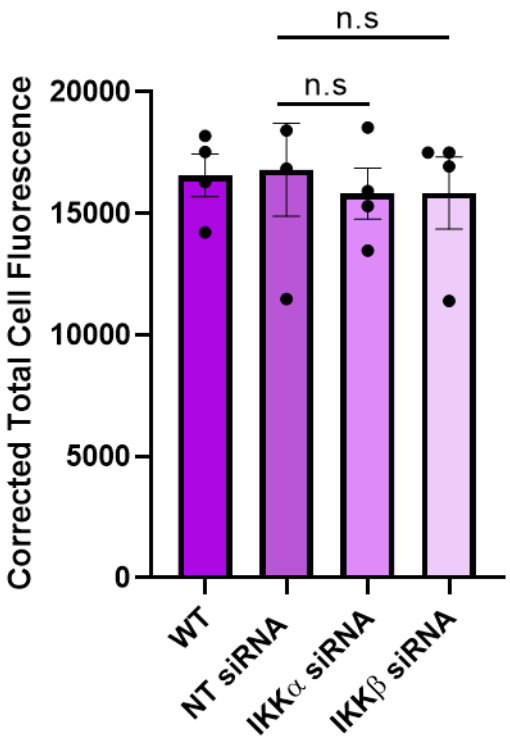

Figure 4.10. IKKα siRNA and IKKβ siRNA do not alter OSCAR protein expression in U2OS cells.

U2OS cells were untreated, or treated with non-targeting, IKKα, or IKKβ siRNA (100 nM) for 72 hours. Immunofluorescence staining was utilised to highlight of protein expression of OSCAR in the presence and absence of IKKα siRNA or IKKβ siRNA (100nM), n=4.

This highlights that IKKα siRNA cannot replicate the increase in OSCAR protein expression which is induced by IKKα CRISPR/Cas9 knockout. Next, to explore whether IKKα has a role in subcellular redistribution of OSCAR, subcellular fractionation was conducted by utilising a sucrose gradient method and several ultracentrifugation steps. Following this, SDS-PAGE and western blotting analysis was performed to assess OSCAR expression in various subcellular compartments in wildtype and IKKα CRISPR/Cas9 knockout U2OS cells (Figure 4.11).

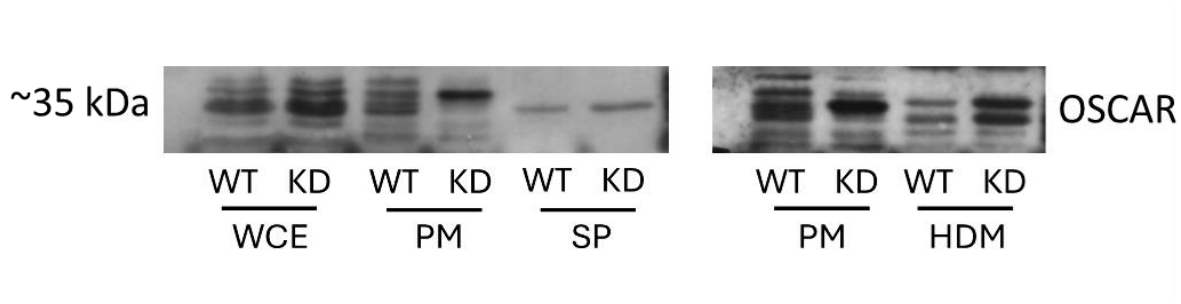

Figure 4.11. IKKα CRISPR/Cas9 knockout increases expression of OSCAR in plasma membrane and high-density subcellular fractions in U2OS cells.
Subcellular fractionation was performed as outlined in the methods section, and cell lysates were utilised for SDS-PAGE and western blotting using an OSCAR primary antibody. Data is indicative of whole cell extract (WCE), plasma membrane (PM), soluble proteins (SP) and high-density membrane fractions, consisting of the golgi and endoplasmic reticulum (HDM), n=2.

The results of from the subcellular fractionation experiment (Figure 3.11) demonstrate a shift in OSCAR expression in the plasma membrane and high-density cellular fractions which are composed of the Golgi apparatus and the ER. In the plasma membrane fractions, it appears that OSCAR has a higher molecular weight band present. Additionally, there are two protein bands which appear for OSCAR protein expression in high-density cellular fractions, and therefore, this suggests presence of OSCAR with post-translational modifications or alternatively, the two known isoforms of OSCAR may be expressed in this fraction. However, this is the first time where OSCAR subcellular localisation in high density membrane components of the cell has been identified. However, further replicates of the experiment and various markers of each subcellular fraction are required to validate this localisation.

Subcellular fractionation was also conducted for IKKα. IKKα was identified in the whole cell extract sample, the plasma membrane fraction, and the high-density subcellular fraction (Figure 4.12). Epithelial Cell Adhesion Molecule (EPCAM) was utilised as a transmembrane glycoprotein plasma membrane marker throughout these experiments. In this experiment, it was identified that there is low, but detectable protein levels of IKKα in the plasma membrane and high-density fractions, the Golgi and or the endoplasmic reticulum.

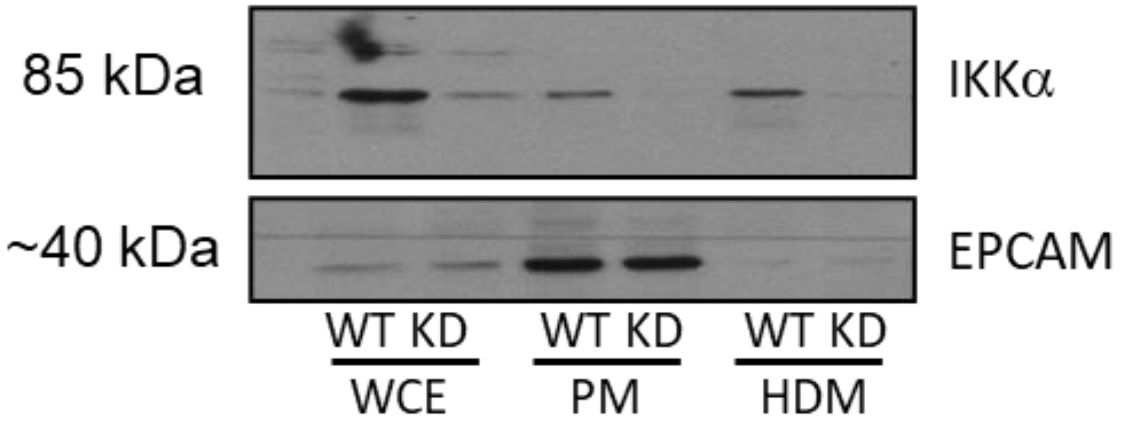

Figure 4.12. IKKα is expressed in plasma membrane and high-density subcellular fractions within U2OS cells.
Subcellular fractionation of U2OS cells was performed as outlined in the methods, followed by sample preparation, and SDS-PAGE and western blotting analysis using IKKα and EPCAM primary antibodies. EPCAM was used as a plasma membrane marker. Data is indicative of whole cell extract (WCE), plasma membrane (PM), soluble proteins (SP) and high-density membrane fractions, consisting of the golgi and endoplasmic reticulum (HDM), n=2.

4.3.5. OSCAR gene expression is upregulated in IKKα CRISPR/Cas9 knockout U2OS cells compared to wildtype U2OS cells stimulated with IL-1β for 8 hours

After validating an increase in OSCAR gene and protein expression in unstimulated IKKα CRISPR/Cas9 knockout U2OS cells, the effect of IKKα CRISPR/Cas-9 knockout on IL-1β stimulated genes was assessed. Notably, a significant increase in OSCAR expression in IKKα CRISPR/Cas9 knockout U2OS cells compared to wildtype U2OS cells stimulated cells with IL-1β (8 hours) was observed as one of the top 20 significantly differentiated genes between the two sample groups (Figure 4.13).

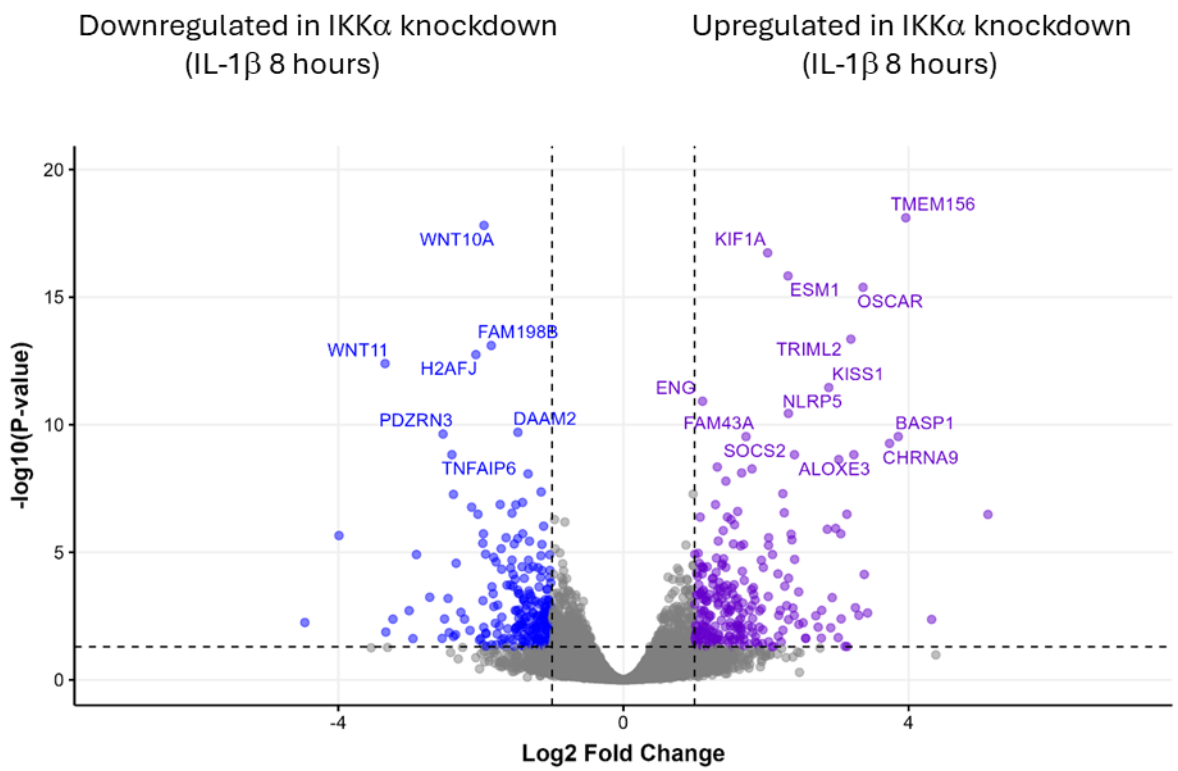

Figure 4.13. A volcano plot highlighting the top 20 differentially expressed genes between wildtype and IKKα CRISPR/Cas9 knockout U2OS cells stimulated with IL-1β for 8 hours.

Genes which were upregulated (blue) and downregulated (purple) in the IKKα CRISPR/Cas9 knockout U2OS cells are displayed.

To visualise differential gene expression, a heatmap was created showing the top 20 upregulated genes in IKKα CRISPR/Cas9 knockout samples following 8 hours of IL-1β stimulation, relative to identically treated wild-type controls (Figure 4.14).

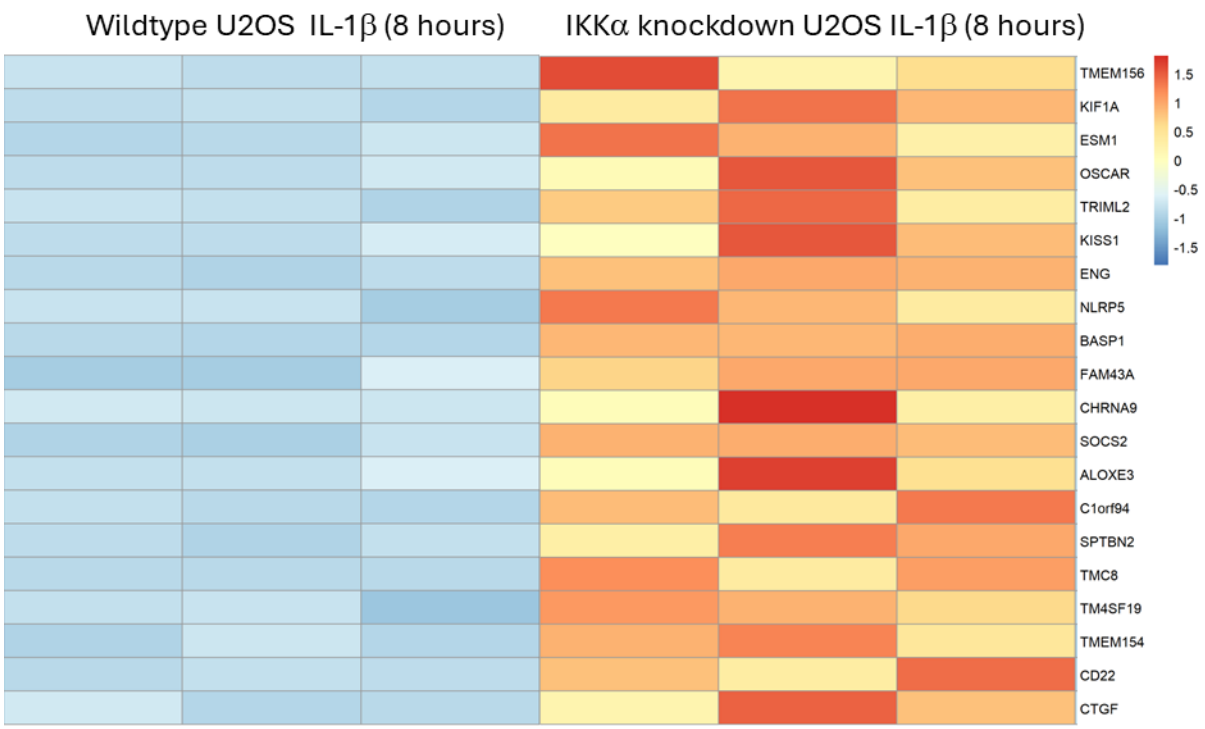

Figure 4.14. A heatmap depicting the top 20 differentially expressed genes which were significantly higher in IKKα CRISPR/Cas9 knockout U2OS cells compared to wildtype U2OS cells with IL-1β stimulation for 8 hours.
The genes were filtered in order of ascending p-value, and the top 20 genes were selected. The smallest and largest p-value of the top 20 differentially genes are displayed by lowest to highest p-value, at the top to bottom of the heatmap, respectively. The colours shown in the heatmap are indicative of z score, where baseline expression = 0, positive integers = above baseline expression, and negative integers = below baseline expression. Heatmap was constructed by R, n=3.

To assess whether there are any longer-term effects of IL-1β stimulation on increased OSCAR expression in IKKα CRISPR/Cas9 knockout U2OS cells, a volcano plot was created to depict the top 20 genes differentially expressed between wildtype and IKKα CRISPR/Cas9 knockout U2OS cells stimulated with IL-1β for 24 hours (Figure 4.15).

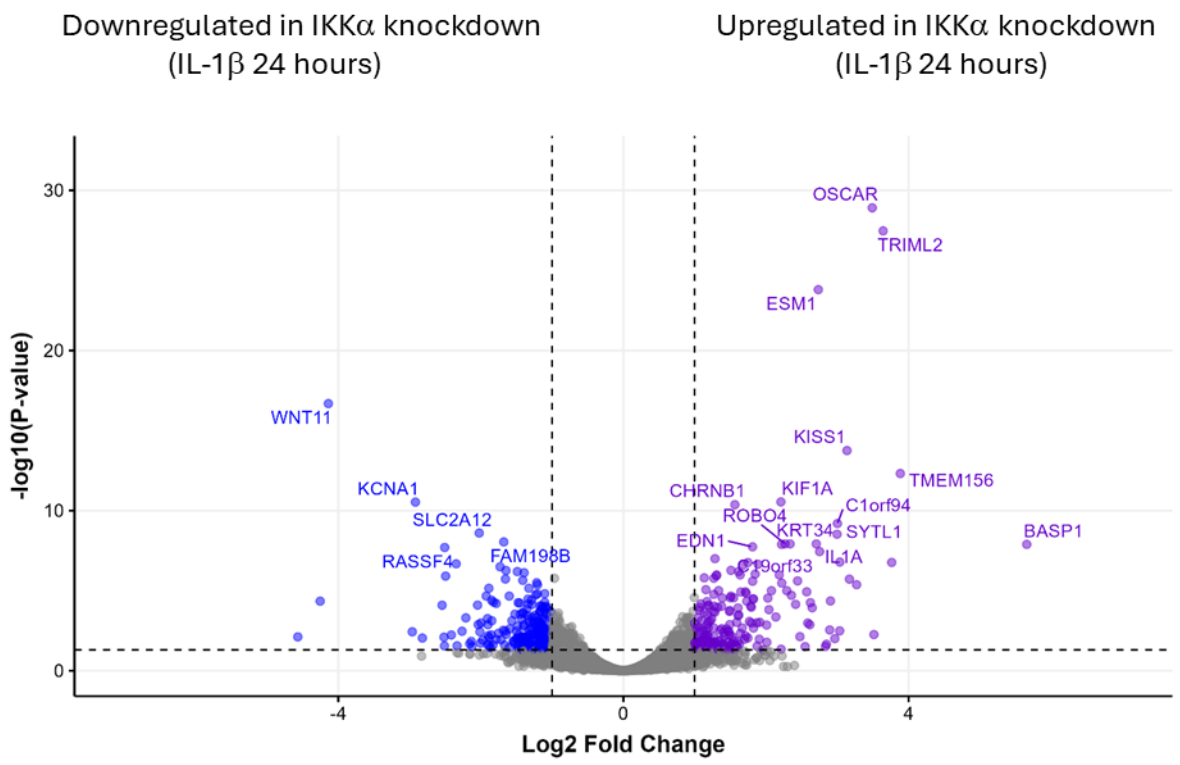

Figure 4.15. A volcano plot highlighting the top 20 differentially expressed genes between wildtype and IKKα CRISPR/Cas9 knockout U2OS cells stimulated with IL-1β for 24 hours.
Genes which were upregulated (blue) and downregulated (purple) in the IKKα CRISPR/Cas9 knockout U2OS cells are displayed.

The upregulation of OSCAR expression in IKKα CRISPR/Cas9 knockout U2OS cells was apparent compared to wildtype U2OS cells. The generation of this volcano plot was particularly useful as there was a total of 650 genes significantly differentially expressed between these groups. Indeed, OSCAR was the most significantly upregulated gene in IKKα CRISPR/Cas9 knockout cells compared to wildtype U2OS cells stimulated with IL-1β for 24 hours (Figure 4.16).

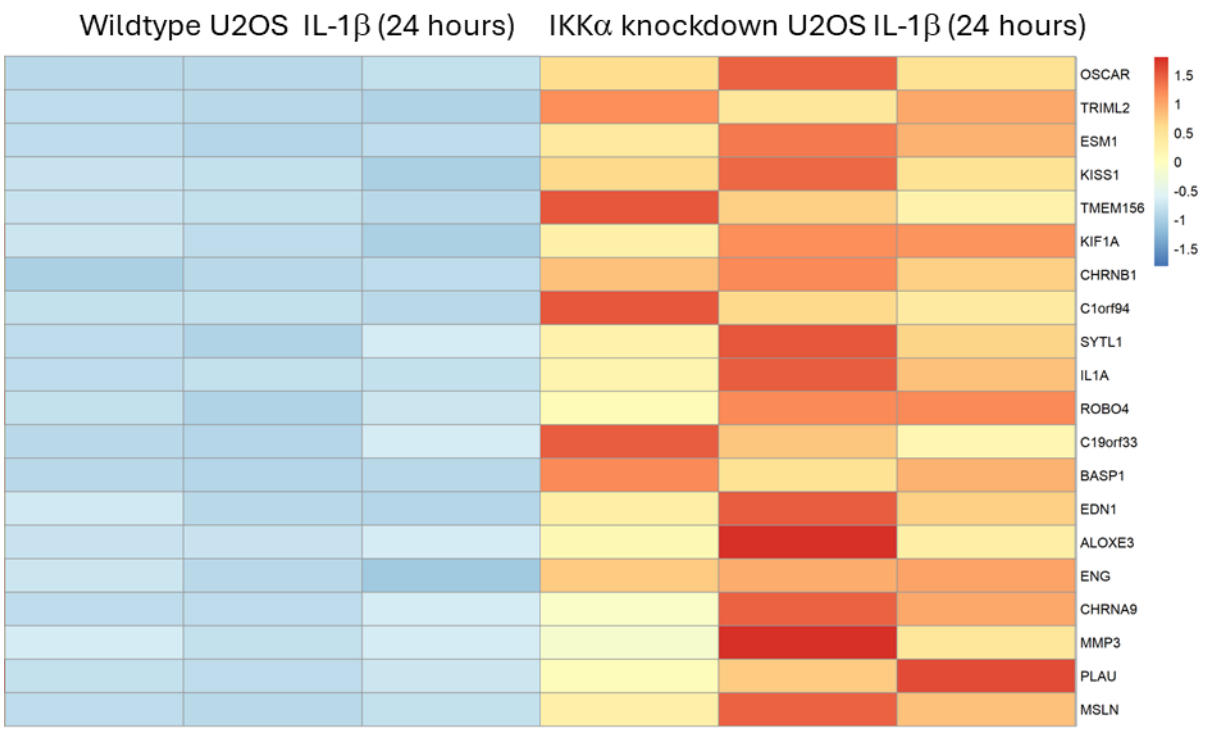

Figure 4.16. A heatmap depicting the top 20 differentially expressed genes which were significantly higher in IKKα CRISPR/Cas9 knockout U2OS cells compared to wildtype U2OS cells with IL-1β stimulation for 24 hours.
The genes were filtered in order of ascending p-value, and the top 20 genes were selected. The smallest and largest p-value of the top 20 differentially genes are displayed by lowest to highest p-value, at the top to bottom of the heatmap, respectively. The colours shown in the heatmap are indicative of z score, where baseline expression = 0, positive integers = above baseline expression, and negative integers = below baseline expression. Heatmap was constructed by R, n=3.

Collectively, these data demonstrate that terminal knockout of IKKα with CRISPR/Cas9 technology results in an upregulation of OSCAR mRNA expression and at a protein level independently of IL-1β stimulation as seen by corrected total cell fluorescence. However, transient knockdown methods, such as IKKα siRNA, do not replicate these findings.

4.3.6. Gene Expression Profiling in wildtype U2OS Cells: Effects of IL-1β stimulation over 8 hours

The next comparison which was made between sample sets was between unstimulated and stimulated (IL-1β 10 ng/mL for 8 hours) wildtype U2OS cells. The

upregulated genes as a consequence of IL-1β stimulation were assessed. A volcano plot was constructed to highlight the top 20 differentially expressed genes between unstimulated and stimulated (IL-1β 10 ng/mL for 8 hours) groups (Figure 4.17).

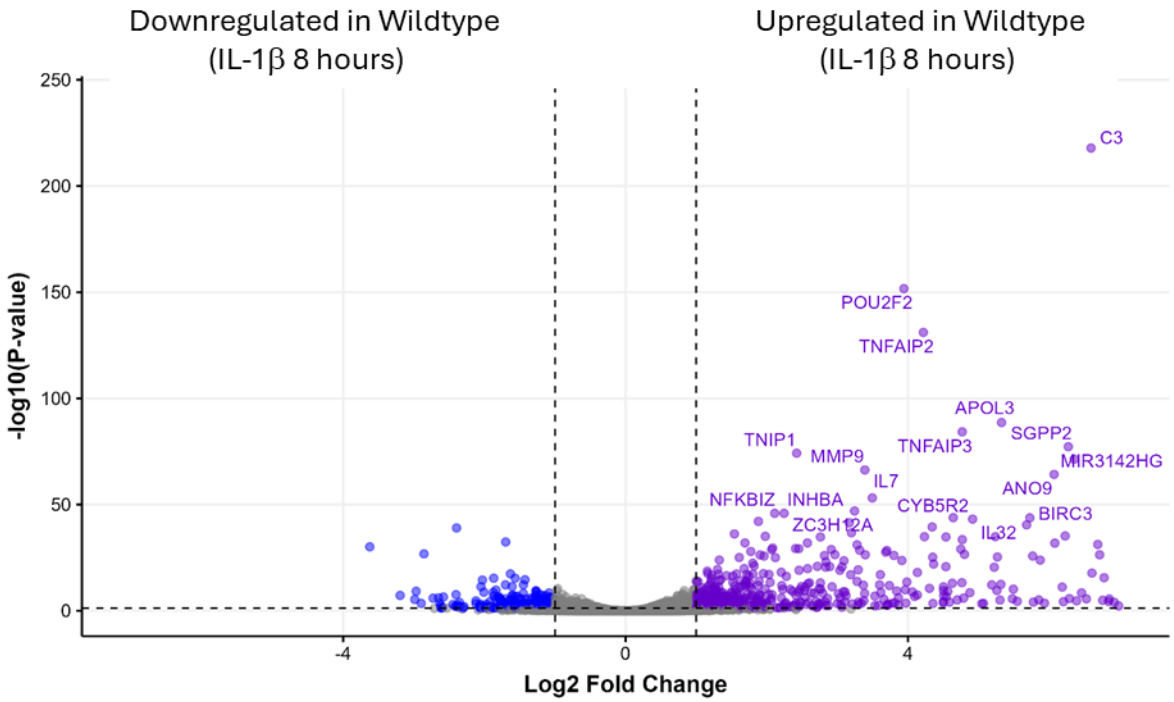

Figure 4.17. A volcano plot highlighting the top 20 differentially expressed genes as a result of IL-1β stimulation for 8 hours in wildtype U2OS cells.
Genes which were significantly higher (purple) following IL-1β stimulation for 8 hours, and significantly higher in unstimulated cells (blue).

A heatmap was then constructed to demonstrate the top 20 genes which were expressed significantly higher in wildtype U2OS cells following IL-1β stimulation for 8 hours (Figure 4.18).

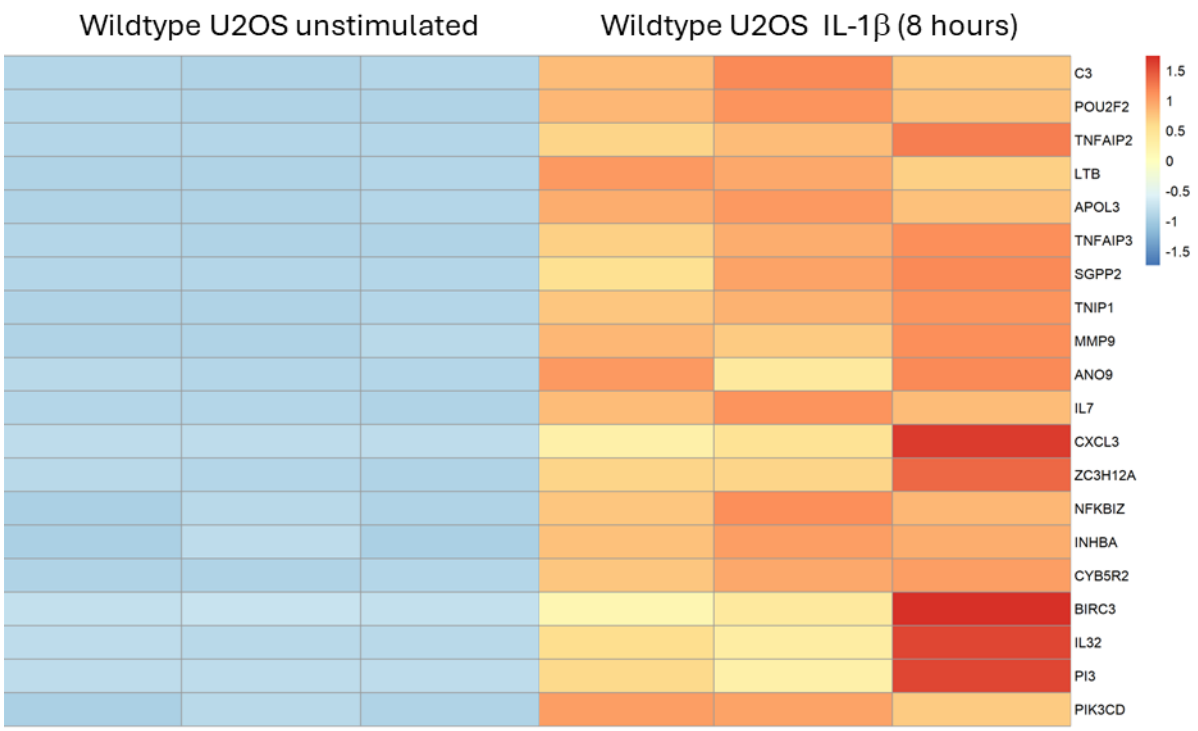

Figure 4.18. A heatmap depicting the top 20 upregulated genes in wildtype U2OS cells following IL-1β stimulation for 8 hours.

Genes were filtered in order of ascending p-value, and the top 20 genes were selected. The smallest and largest p-value of the top 20 differentially genes are displayed by lowest to highest p-value, at the top to bottom of the heatmap, respectively. The colours shown in the heatmap are indicative of z score, where baseline expression = 0, positive integers = above baseline expression, and negative integers = below baseline expression. Heatmap was constructed by R, n=3.

Figure 4.18 revealed several interesting genes which were upregulated as a result of IL-1β stimulation for 8 hours. Some of these genes included C3, which initiates the complement system in immune responses and LTB, which encodes for lymphotoxin β, which is an activator of non-canonical IKKα-dependent NF-κB signalling. Interestingly, CXCL3 appeared as one of the top 20 upregulated genes following IL-1β stimulation for 8 hours. Given that CXCL3 is a CXCR2 ligand, this indicates that IL-1β stimulation can result in an increase in expression of genes involved in the CXCR2 axis which ultimately initiates osteogenesis.

After assessing genes which were IKKα-dependent and IL-1β-independent, IKKα-dependent and IL-1β dependent genes were assessed. Gene ontology was performed for molecular functions to gain an understanding of the clusters of genes which were affected by IKKα CRISPR/Cas9 knockout in U2OS cells stimulated with IL-1β for 8 hours. The top 20 molecular functions revealed links to receptor ligand activity, cytokine activity and chemoattractant activity, among others (Figure 4.19).

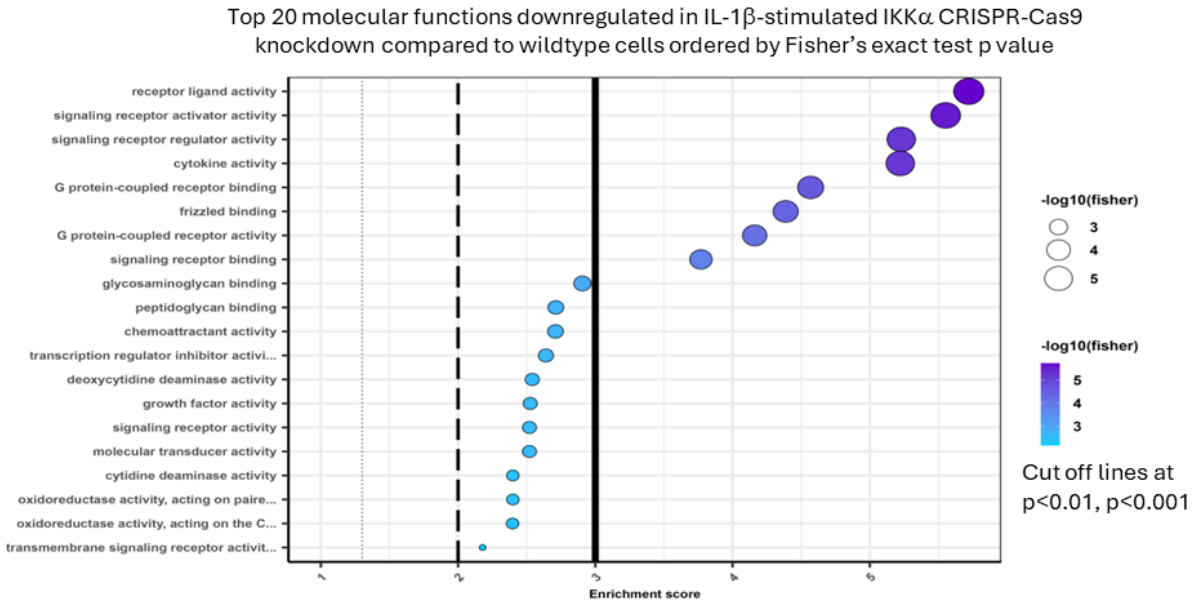

Figure 4.19. Gene ontology plot showing the top 20 molecular function terms significantly altered between IKKα CRISPR/Cas9 knockout and wild-type U2OS cells following IL-1β stimulation for 8 hours.
Terms are based on differentially expressed genes identified by short-read RNA sequencing and evaluated by Fisher's exact test. Vertical cut off lines represent **p<0.01 and ***p<0.001, n=3.

The association with cytokines and chemoattractant activity was compelling, and the data was manually sifted through to identify potential targets. One target which was particularly interesting but was statistically insignificant as it was only reduced in two out of three IKKα CRISPR/Cas9 knockout experiments was CXCL5. Given the role of CXCL5 in OS progression and metastasis, this was chosen as a target to explore in the laboratory.

Therefore, RT-qPCR was utilised to measure CXCL5 mRNA expression, where IL-1β stimulation for 8 h significantly increased CXCL5 mRNA from 0.17% in control to 100% maximal in the IL-1β 8 h stimulation (****p<0.0001). However, this maximal IL-1β-induced CXCL5 mRNA was significantly reduced to 23.3% maximal mRNA (****p<0.0001) in IKKα CRISPR/Cas9 knockout cells (Figure 4.20).

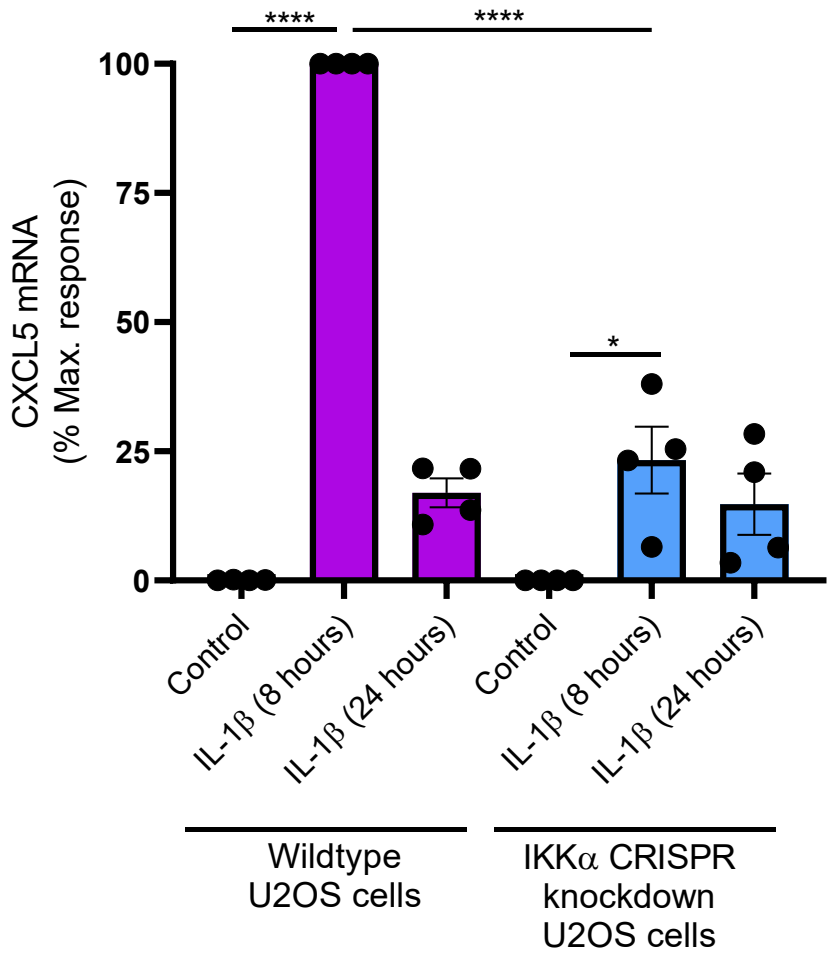

Figure 4.20. Increased CXCL5 mRNA expression following IL-1β stimulation is IKKα-dependent.

U2OS wildtype and IKKα CRISPR/Cas9 knockout cells were stimulated with 10 ng/mL IL-1β for 8 hours, or left unstimulated, prior to RNA extraction. RT-qPCR was performed to measure relative expression of CXCL5 mRNA. HRPT1 was used as an internal control. GraphPad Prism 8 software was utilised to carry out Gaussian distribution with Shapiro-Wilk test to ensure normality of samples. Unpaired T-test with Welch correction was used to compare wildtype to IKKα CRISPR/Cas9 knockout samples with identical stimulation methods. Paired T-tests were utilised to compare wildtype samples or IKKαCRISPR/Cas9 knockout samples to their own cell type with different stimulation methods. Data represents n=4, *p<0.05, ****p<0.0001.

Prior to assessing the reproducibility of IKKα-dependent effects on CXCL5 mRNA expression using an alternative knockdown approach, U2OS cells were transfected with IKKα siRNA. RT-qPCR was performed to confirm knockdown efficiency by measuring IKKα mRNA levels in wild-type U2OS cells and those pre-treated with non-targeting siRNA (100 nM), IKKα siRNA (100 nM), or IKKβ siRNA (100 nM) for 72 hours. IKKα siRNA significantly reduced IKKα mRNA levels, while non-targeting siRNA had no effect, confirming the specificity of the knockdown. Notably, IKKβ siRNA treatment led to increased IKKα mRNA expression, suggesting a compensatory upregulation upon IKK complex disruption (Figure 4.21).

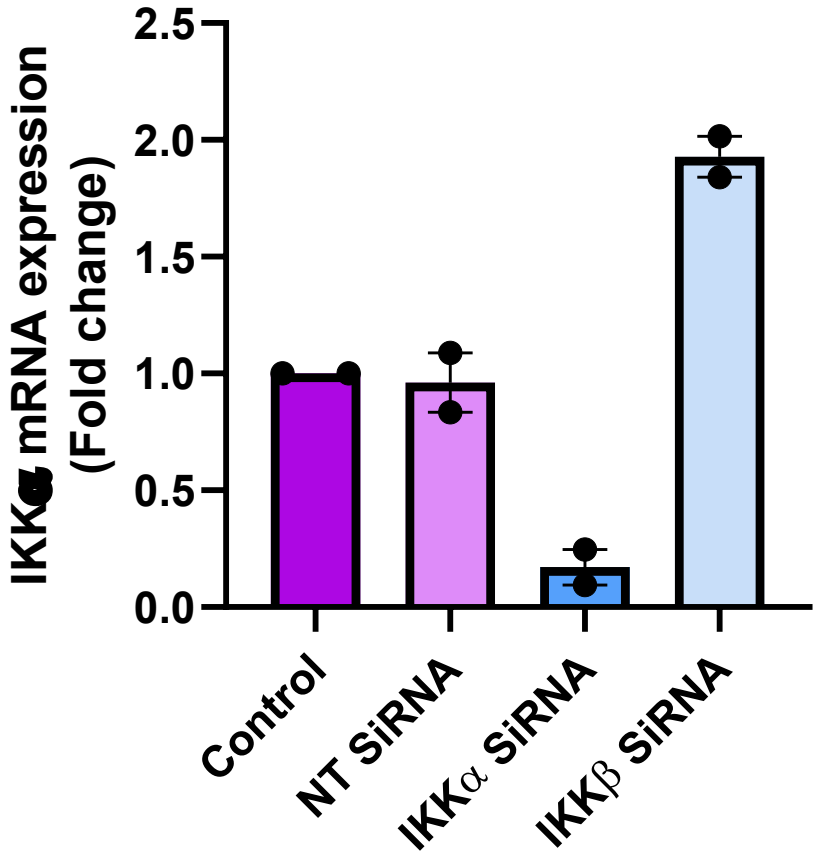

Figure 4.21. IKKα mRNA is decreased by IKKα siRNA knockdown.
U2OS cells were grown to 50% confluency and then left untransfected, or transfected with non-targeting siRNA (NT siRNA), IKKα siRNA or IKKβ siRNA for 72 hours. Cells were quiesced in serum-free media after 48 hours of transfection for 24 hours. Cells were scraped and collected; RNA extraction was carried out followed by reverse transcription. RT-qPCR was carried out using the comparative Ct method for IKKα mRNA expression (fold change) ± SEM, n=2.

Following results demonstrating successful IKKα knockdown with siRNA, CXCL5 mRNA expression was measured in wildtype U2OS cells, and U2OS cells transfected with non-targeting siRNA, IKKα siRNA and IKKβ siRNA, all of which were prepared in unstimulated conditions and with IL-1β stimulation for 8 hours (Figure 4.22). In wildtype U2OS cells, CXCL5 mRNA was significantly increased from 6.9% to 100% of the maximal response (****p<0.0001). Similarly, U2OS cells transfected with non-targeting siRNA demonstrated an increase in CXCL5 mRNA expression with IL-1β stimulation, from 5.4% to 81.9% of the maximal response (****p<0.0001). However, in U2OS cells transfected with IKKα siRNA, IL-1β stimulation did not significantly increase CXCL5 mRNA expression, rising from 6.3% to 38.7% (p = 0.0651). Additionally, CXCL5 mRNA levels were significantly reduced from 81.9% to 38.7% (**p<0.01) in U2OS cells transfected with IKKα siRNA and stimulated with IL-1β, compared to those transfected with non-targeting siRNA and stimulated with IL-1β. However, CXCL5 mRNA was not significantly reduced in U2OS cells transfected with IKKβ siRNA and stimulated with IL-1β (63.6% maximal response) compared to non-targeting siRNA and IL-1β (81.9%, p=0.59). These data indicate that CXCL5 mRNA expression is dependent on IKKα rather than IKKβ in the IKK complex.

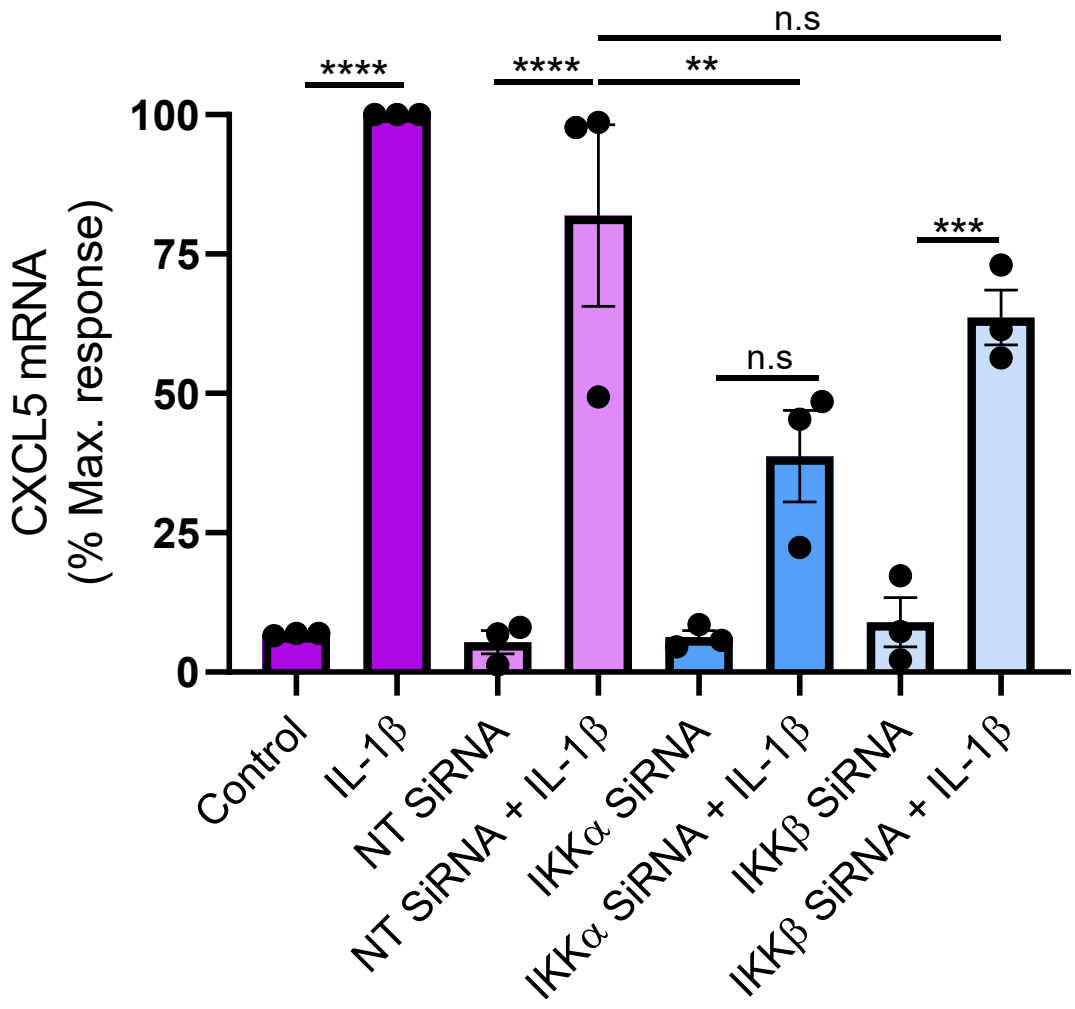

Figure 4.22. IL-1β-induced CXCL5 mRNA is IKKα-dependent.
U2OS wildtype cells were grown until approximately 50% confluence, and then either maintained untreated, or incubated with non-targeting (100 nM), IKKα (100 nM), or IKKβ siRNA (100 nM) for 72 hours. Cells were stimulated with IL-1β (10 ng/mL) for 8 hours, or left unstimulated, prior to RNA extraction. RT-qPCR was performed to measure relative expression of CXCL5 mRNA. HRPT1 was used as an internal control. GraphPad Prism 8 software was utilised to carry out Gaussian distribution with Shapiro-Wilk test to ensure normality of samples. One-way ANOVA was used to compare relevant controls with appropriate stimulated samples, and stimulated samples to one another. Data represents mean CXCL5 (% maximum response) ± SEM, n=3, **p<0.01, ***p<0.001, ****p<0.0001.

To further investigate and confirm the role of IKKα with respect to promoting CXCL5 expression, the selective ATP-competitive IKKα inhibitors utilised in Chapter 3, SU1261 and SU1349, were applied. RT-qPCR findings revealed that CXCL5 expression was significantly reduced to 29.5%, 12.5%, and 9.4% of maximal CXCL5 expression measured in U2OS cells transfected with IKKα siRNA and pre-treated with 10 μM SU1261 or 10 μM SU1349, respectively (Figure 4.23). Similarly, the concentrations of SU1261 and SU1349 used exhibited complete inhibition of p100 phosphorylation (see Chapter 3). This demonstrates that not only do the IKKα inhibitors also reduce CXCL5 mRNA expression, but also that they can reduce CXCL5 to a greater extent than IKKα siRNA, demonstrating their effectiveness in regulating CXCL5.

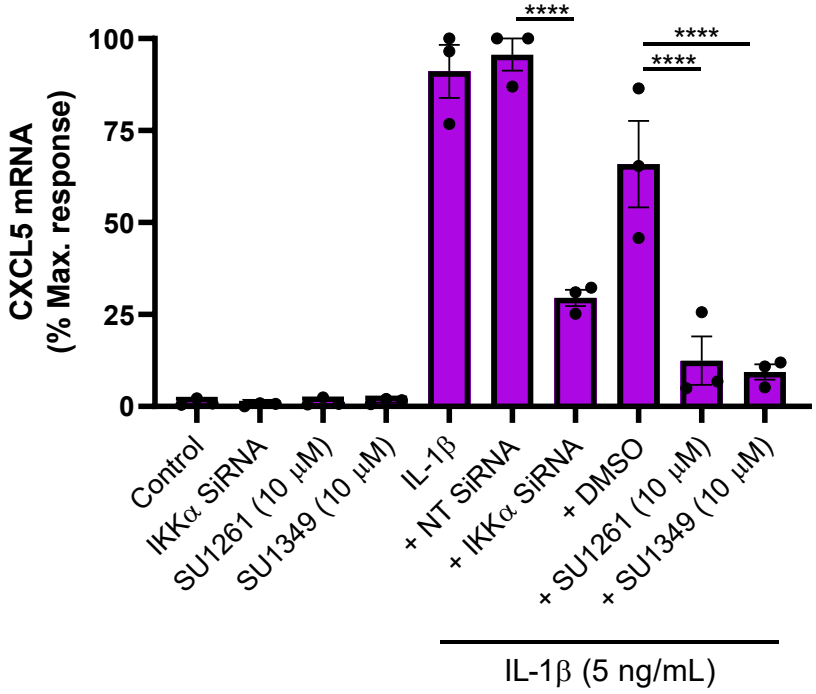

Figure 4.23. IL-1β-induced CXCL5 mRNA expression is reduced by IKKα siRNA, SU1261 and SU1349.
Cells were either not treated or treated with DMSO or SU1261 or SU1349 45 min pre-stimulation. Cells were then unstimulated or stimulated with with IL-1β (5 ng/mL) for 8 hours, or left unstimulated, prior to RNA extraction. RT-qPCR was performed to measure relative expression of CXCL5 mRNA. HRPT1 was used as an internal control. GraphPad Prism 8 software was utilised to carry out Gaussian distribution with Shapiro-Wilk test to ensure normality of samples. One-way ANOVA was used to compare IL-1β + DMSO or IL-1β + non-targeting siRNA compared to appropriate samples. Data represents mean CXCL5 (% maximum response) ± SEM n=3, ****p<0.0001.

Following the observation that IKKα inhibitors at relatively high concentrations regulate CXCL5 mRNA expression, the concentration-dependent effects of SU1261 on CXCL5 mRNA were investigated (Figure 4.24). U2OS cells stimulated with IL-1β and treated with DMSO were used as positive controls for comparisons in data analysis, as the tested compounds were dissolved in DMSO. There was no significant difference in CXCL5 mRNA expression between cells treated with IL-1β alone and those treated with IL-1β plus DMSO. Treatment with SU1261, however, significantly reduced IL-1β induced CXCL5 mRNA expression from 81.5 % (IL-1β plus DMSO) to 11.5 % (IL-1β plus SU1261) ($p<0.0001$). This effect displayed a clear concentration response relationship, confirming that SU1261 effectively decreases CXCL5 mRNA expression in a dose dependent manner.

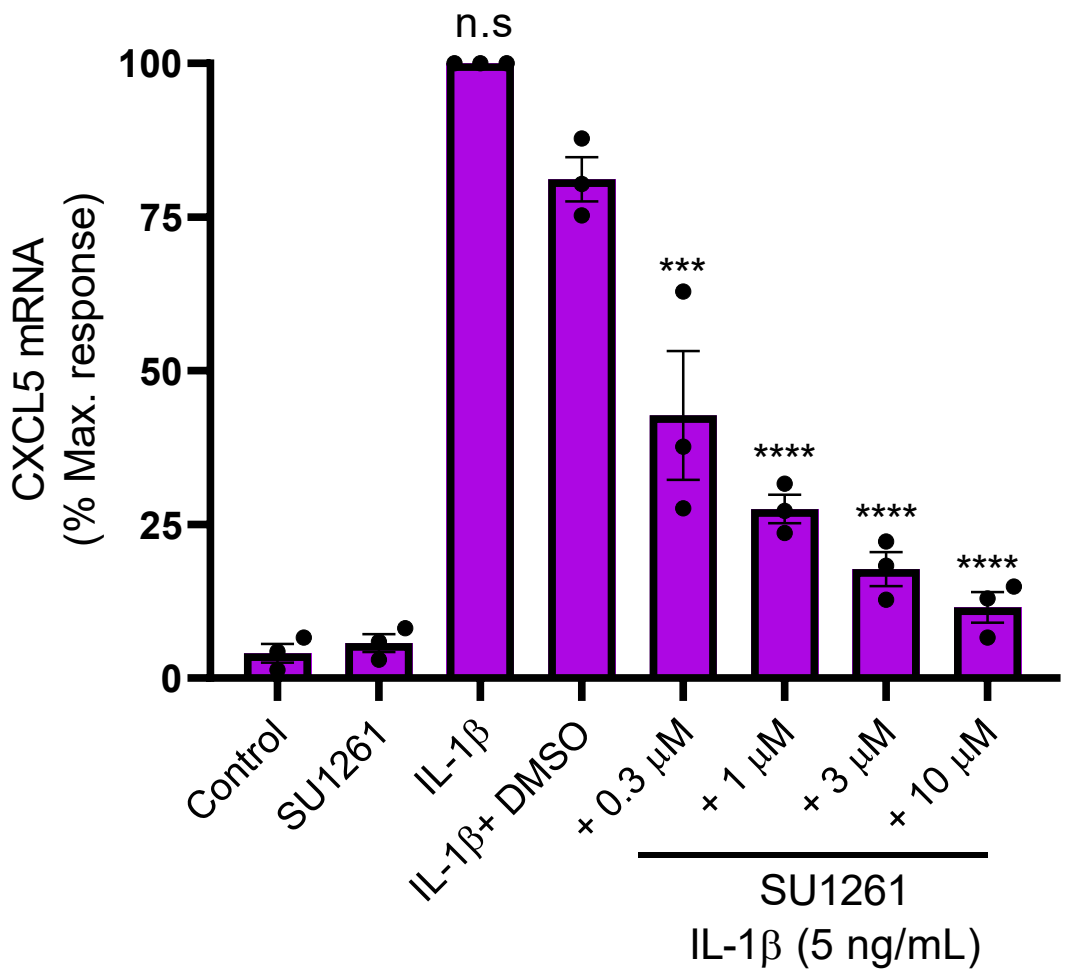

Figure 4.24. IL-1β-induced CXCL5 mRNA is decreased in a concentration-dependent manner when treated with SU1261.

Cells were either not treated or treated with DMSO or SU1261 45 min pre-stimulation. Cells were then unstimulated or stimulated with with IL-1β (5 ng/mL) for 8 hours, or left unstimulated, prior to RNA extraction. RT-qPCR was performed to measure relative expression of CXCL5 mRNA. HRPT1 was used as an internal control. GraphPad Prism 8 software was utilised to carry out Gaussian distribution with Shapiro-Wilk test to ensure normality of samples. One-way ANOVA was used to compare IL-1β + DMSO to appropriate samples. Data represents mean CXCL5 (% maximum response) ± SEM n=3, ***p<0.001, ****p<0.0001.

Although previous studies have reported that SU1261 selectively targets IKKα rather than IKKβ, this was further examined by assessing its effect on CXCL8, a well-established IKKβ- and p65-dependent gene (382, 383). RT-qPCR analysis showed that at a low concentration of 0.3 μM, SU1261 produced a strong increase in CXCL8 mRNA expression, reaching 93.3 percent of the maximal response. This was significantly higher than levels observed with IL-1β alone (19.6%), IL-1β plus DMSO (6.3 %), or IL-1β with higher concentrations of SU1261 at 3 μM (32.7 %) and 10 μM (16.5 %) (Figure 4.25). Thus, low concentrations of SU1261 enhance IL-1β-induced CXCL8 expression, likely due to disruption of the IKK complex. At 10 μM SU1261, CXCL8 expression were reduced to levels similar to those seen with IL-1β stimulation alone. These findings suggest that SU1261 has a complex, concentration-dependent effect on CXCL8 regulation and may exert off-target effects on IKKβ at higher concentrations.

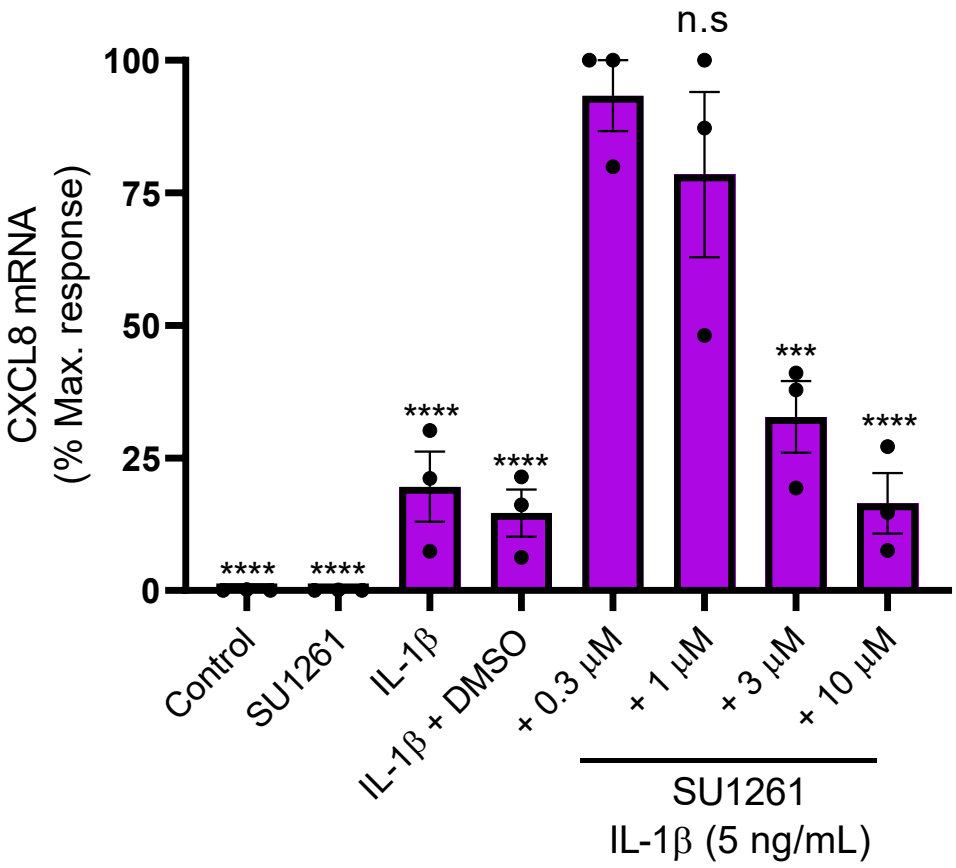

Figure 4.25. SU1261 causes a concentration potentiation of IL-1β-induced CXCL8 mRNA in U2OS cells.

Cells were either not treated or treated with DMSO or SU1261 45 min pre-stimulation. Cells were then unstimulated or stimulated with with IL-1β (5 ng/mL) for 8 hours, or left unstimulated, prior to RNA extraction. RT-qPCR was performed to measure relative expression of CXCL8 mRNA. HRPT1 was used as an internal control. GraphPad Prism 8 software was utilised to carry out Gaussian distribution with Shapiro-Wilk test to ensure normality of samples. One-way ANOVA was used to compare IL-1β + 0.3 μM compared to appropriate samples. Data represents mean CXCL8 (% maximum response) ± SEM n=3, **p<0.01, ***p<0.001, ****p<0.0001.

In order to confirm the effects of SU1261 a second IKKα inhibitor, SU1349 was utilised to assess effects on CXCL5 mRNA expression. Indeed, RT-qPCR findings demonstrated that CXCL5 mRNA was reduced to of maximal IL-1β-induced CXCL5 mRNA expression to 18.9% with application of 10 μM SU1349 (Figure 4.26). This highlights a clear concentration-dependent effect, closely resembling that observed with SU1261, and further supports the role of selective IKKα inhibition in regulating CXCL5 expression.

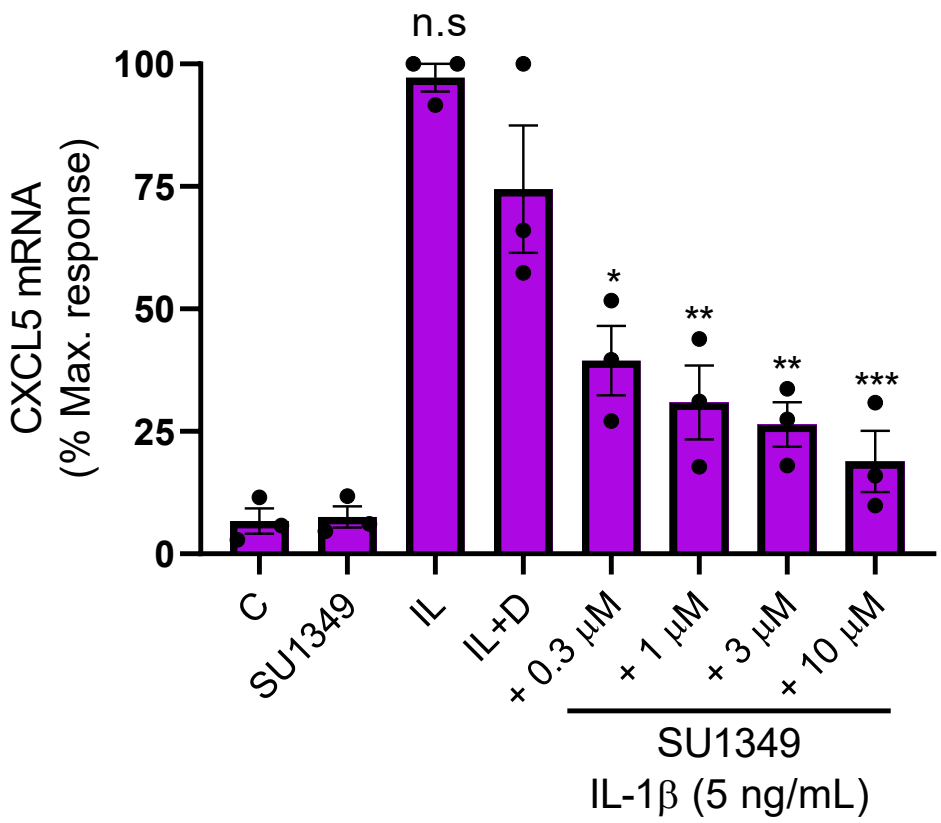

Figure 4.26. IL-1β-induced CXCL5 mRNA is decreased with SU1349 in a concentration-dependent manner.

Cells were either not treated or treated with DMSO or SU1349 45 min pre-stimulation. Cells were then unstimulated or stimulated with with IL-1β (5 ng/mL) for 8 hours, or left unstimulated, prior to RNA extraction. RT-qPCR was performed to measure relative expression of CXCL5 mRNA. HRPT1 was used as an internal control. GraphPad Prism 8 software was utilised to carry out Gaussian distribution with Shapiro-Wilk test to ensure normality of samples. One-way ANOVA was used to compare IL-1β + DMSO compared to appropriate samples. Data represents mean CXCL5 (% maximum response) ± SEM n=3, *p<0.05, **p<0.01, ***p<0.001.

Further, the effects of SU1349 on CXCL8 expression were investigated. In this instance, CXCL8 mRNA expression was significantly increased by pre-treating the U2OS cells with 10 μM SU1349 prior to IL-1β stimulation compared to cells pre-treated with 0.3 μM SU1349 or IL-1β or IL-1β and DMSO (Figure 4.27). The expression of CXCL8 was not statistically significant in U2OS pre-treated with 1 μM or 3 μM SU1349 prior to IL-1β stimulation compared to pre-treated samples with 10 mM SU1349. This demonstrates that SU1349 induces a different concentration-dependent effect on CXCL8 mRNA expression to that observed for SU1261.

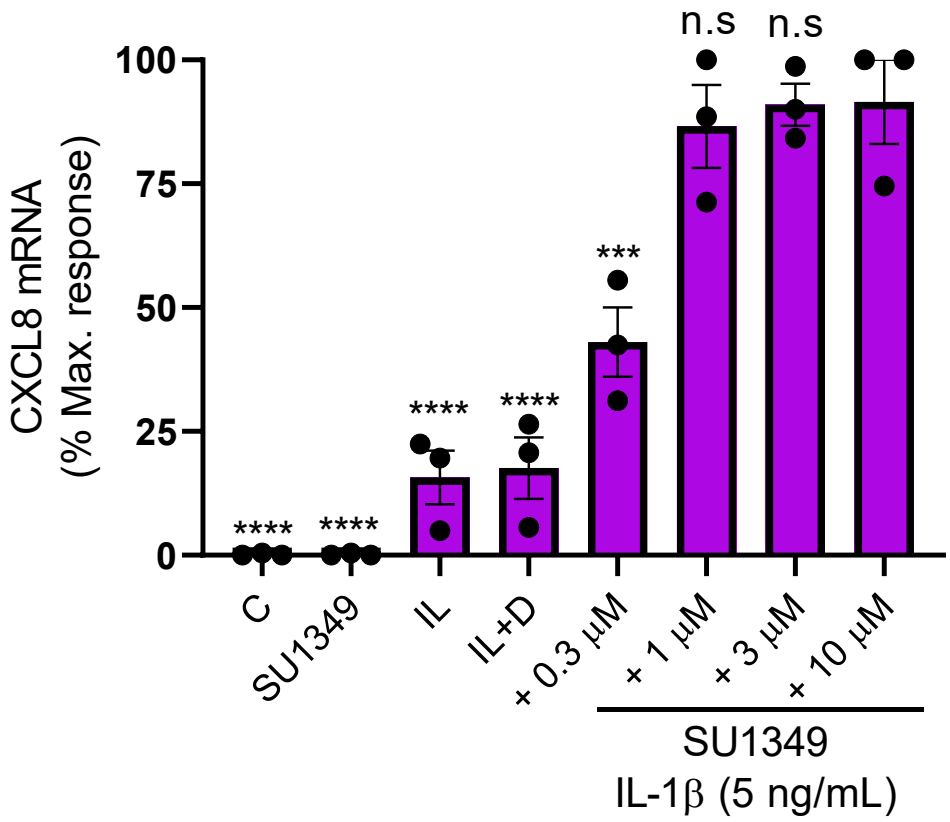

Figure 4.27. IL-1β-induced CXCL8 mRNA is increased with SU1349.
Cells were either not treated or treated with DMSO or SU1349 45 min pre-stimulation. Cells were then unstimulated or stimulated with IL-1β (5 ng/mL) for 8 hours, or left unstimulated, prior to RNA extraction. RT-qPCR was performed to measure relative expression of CXCL8 mRNA. HRPT1 was used as an internal control. GraphPad Prism 8 software was utilised to carry out Gaussian distribution with Shapiro-Wilk test to ensure normality of samples. One-way ANOVA was used to compare IL-1β + 10 μM compared to appropriate samples. Data represents mean CXCL8 (% maximum response) ± SEM n=3, **p<0.01, ***p<0.001, ****p<0.0001.

After confirming that CXCL5 mRNA is reduced by interventions that inhibit IKKα expression or activity, ELISA was used to measure CXCL5 protein secretion. CXCL5 levels were assessed following IL-1β stimulation for 12 and 24 hours. In a preliminary experiment, both IKKα siRNA and IKKα CRISPR-Cas9 knockout reduced CXCL5 protein secretion (Figure 4.28). IKKβ did not appear to have any effect on CXCL5 production. This indicates that IKKα plays a critical role in regulating IL-1β-induced CXCL5 expression at the protein level.

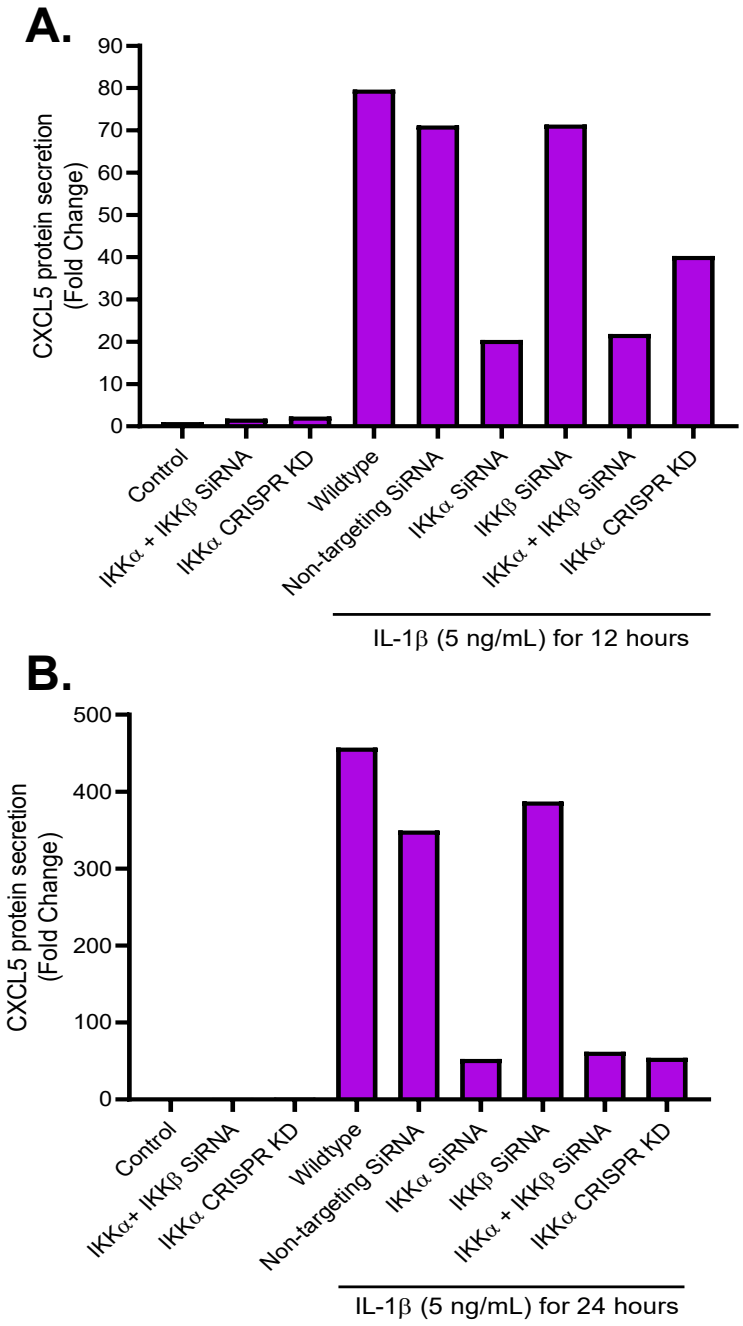

Figure 4.28. IL-1β-mediated CXCL5 protein secretion is IKKα-dependent.
U2OS cells were untransfected or transfected with IKKα siRNA, IKKβ siRNA or at 50% confluency for 72 hours. Cells were quiesced in serum-free media 24 hours prior to treatment. Cells were untreated or treated with SU1261 or SU1349 and stimulated with IL-1β for 12 hours **(A)** or 24 hours **(B)** where appropriate. Serum-free media was collected and utilised for Sandwich ELISA to quantify CXCL5 secretion. Data represents n=1.

After determining that CXCL5 protein secretion is increased by IL-1β stimulation at 12 and 24 hours, 12 hours was chosen as the stimulation time for further ELISA experiments including the IKKα inhibitors. This time was chosen to provide a balance to both enhance CXCL5 production following IL-1β stimulation, but to prevent the potential of deleterious effects on cell viability in the U2OS cells. Therefore, the effects of IKKα siRNA, SU1261 and SU1349 on CXCL5 production were explored (Figure 4.29). The results showed that secreted CXCL5 was markedly reduced from 1023.5 pg/mL in IL-1β plus non-targeting siRNA samples to 142.7 pg/mL in IL-1β plus IKKα siRNA samples (****p<0.0001), confirming IKKα dependency. Additionally, secreted CXCL5, which measured 772.4 pg/mL in IL-1β plus DMSO samples, was reduced to 50.8 pg/mL (***p<0.001) and 21.1 pg/mL (****p<0.0001) in cells pre-treated with 1 μM and 10 μM SU1261, respectively. Similarly, secreted CXCL5 levels were reduced to 55.0 pg/mL (***p<0.001) and 56.1 pg/mL (****p<0.0001) in cells pre-treated with 1 μM and 10 μM SU1349 respectively.

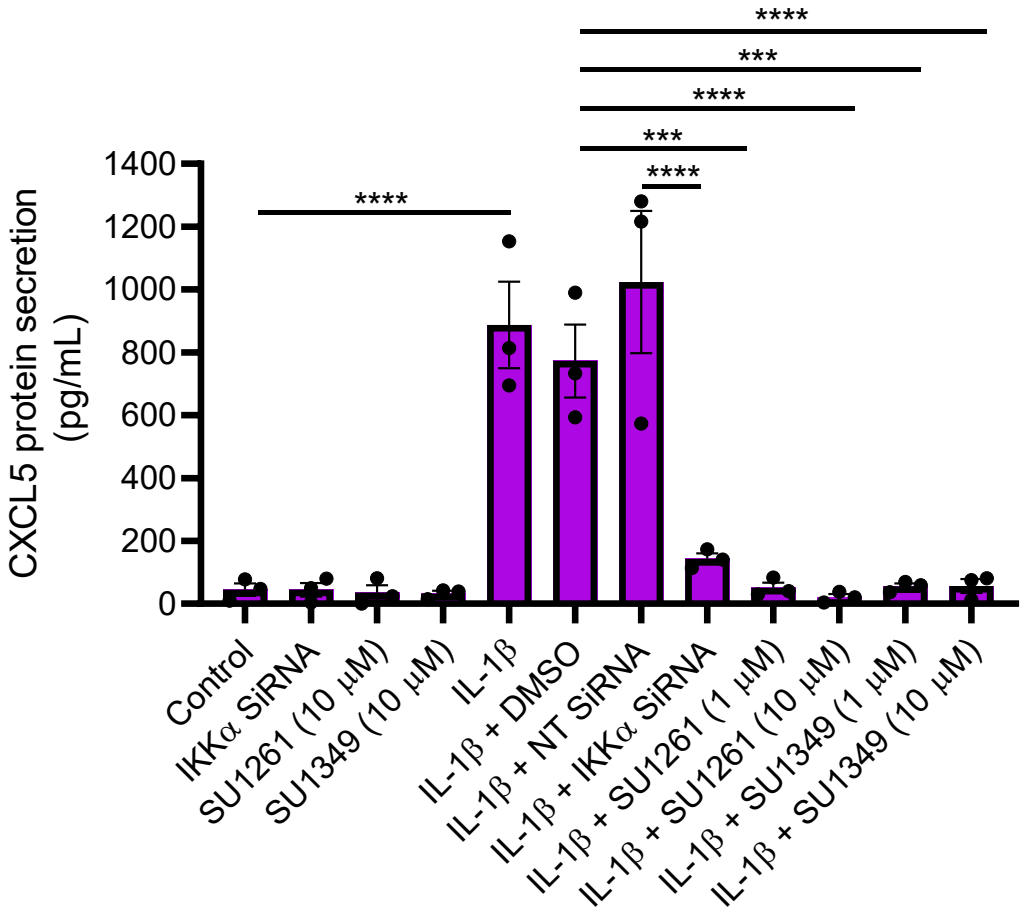

Figure 4.29. CXCL5 protein secretion from U2OS cells is IKKα-dependent.
U2OS cells were grown to 50% confluency then transfected with non-targeting or IKKα siRNA for 72 hours. Cells were quiesced in serum-free media 24 hours prior to treatment. Cells were untreated or treated with SU1261 or SU1349 45 min prior to stimulation. Cells were unstimulated or stimulated with IL-1β for 12 hours where appropriate. Serum-free media was collected 12 hours post IL-1β stimulation and stored on ice until used. Sandwich ELISA was conducted to measure CXCL5 secretion into cell medium. One-way ANOVA was utilised to compare control, IL-1β + non-targeting siRNA or IL-1β + DMSO to relevant samples. Data represents n=3 ± SEM, ***p<0.001, ****p<0.0001.

Since selective IKKα inhibitors reduced CXCL5 mRNA and protein secretion but increased CXCL8 mRNA, the effects of SU1266 were examined given its ability to inhibit IKKα at low concentrations and IKKβ at higher concentrations. Pretreatment with 0.01 μM SU1266 significantly reduced IL-1β-mediated CXCL5 mRNA from 94 % to 54.1 % maximal response (***p<0.001) (Figure 4.30). The IC_{50} for SU1266 was ~130 nM, demonstrating activity at lower concentrations compared with SU1261 and SU1349, which were tested at a minimum of 300 nM.

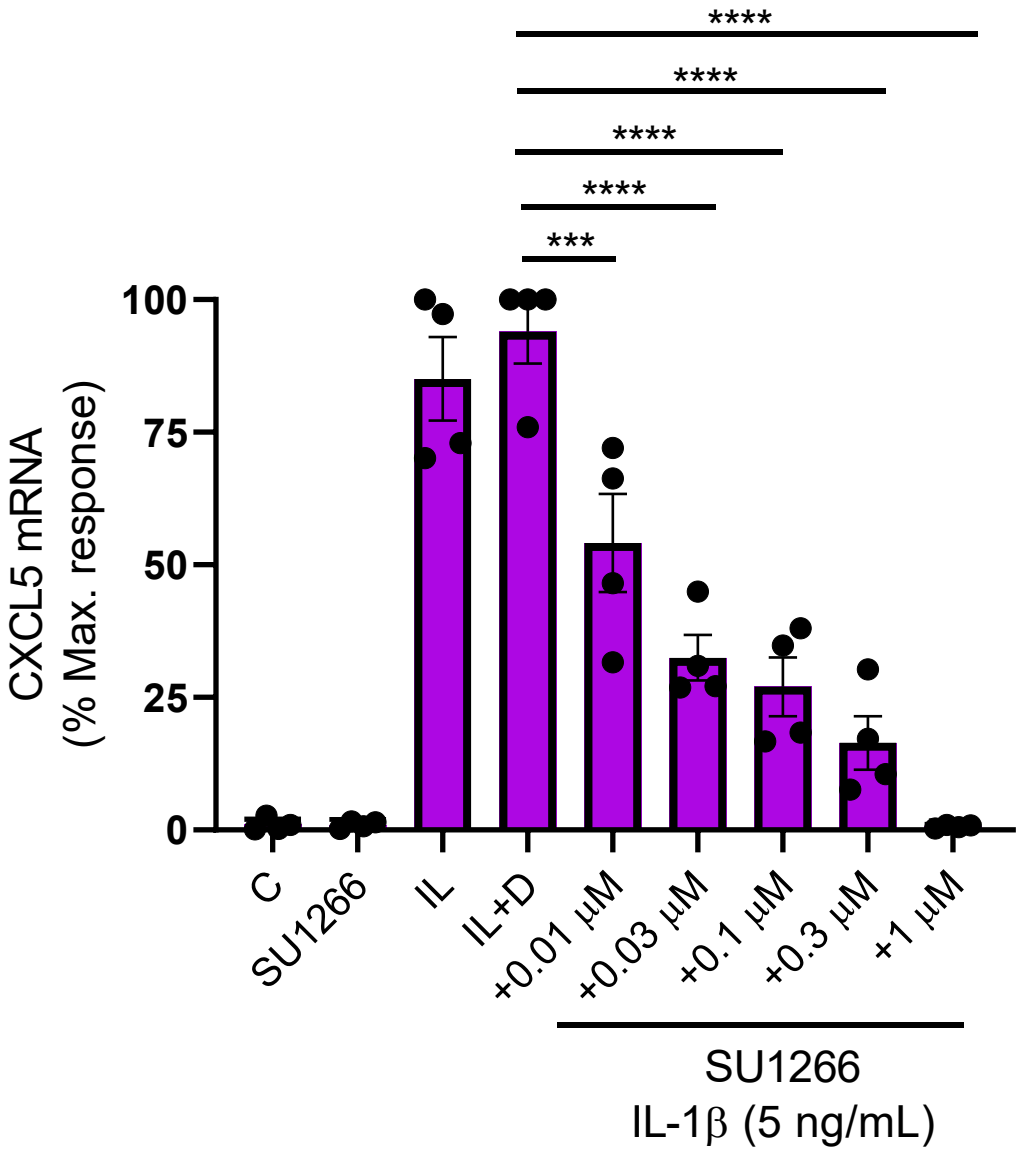

Figure 4.30. The effect of SU1266 on IL-1β-induced CXCL5 mRNA in U2OS cells.

Cells were either not treated or treated with DMSO or SU1261 45 min pre-stimulation. Following pretreatment, cells were unstimulated or stimulated with with IL-1β (5 ng/mL) for 8 hours, or left unstimulated, prior to RNA extraction. RT-qPCR was performed to measure relative expression of CXCL5 mRNA. RT-qPCR was performed to measure relative expression of CXCL5 mRNA. HRPT1 was used as an internal control. GraphPad Prism 8 software was utilised to carry out Gaussian distribution with Shapiro-Wilk test to ensure normality of samples. One-way ANOVA was used to compare IL-1β + DMSO compared to appropriate samples. Data represents mean CXCL5 (% maximum response) ± SEM n=4, ***p<0.001, ****p<0.0001.

Intriguingly, IL-1β-mediated CXCL8 mRNA expression was also decreased by utilising SU1266 to 18.6% of maximal response in U2OS cells pre-treated with 0.3 μM SU1266 prior to IL-1β stimulation (****p<0.0001) (Figure 4.31). However, it is apparent that while CXCL5 is significantly reduced by SU1266 at 0.01 μM, CXCL8 is unaffected. This demonstrates that CXCL5 is an IKKα target gene, which supports the previous results, while IL-1β-induced CXCL8 mRNA induction is inhibited with higher concentrations of SU1266 consistent with its effects on IKKβ. Furthermore, this highlights that potentially an IKKα inhibitor which has some non-selective properties to also target IKKβ may be more favourable for reducing downstream chemokine activity in OS.

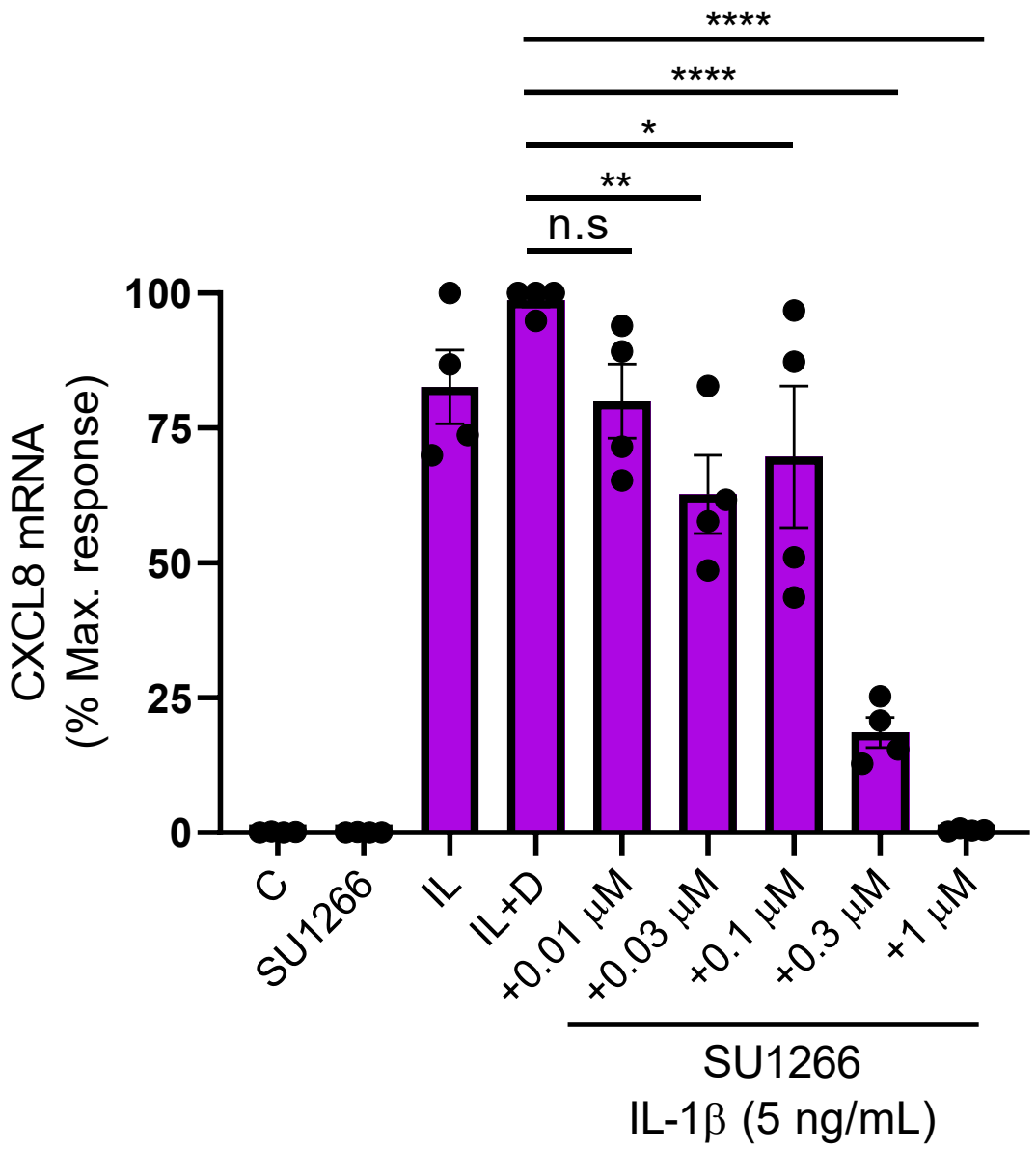

Figure 4.31. The effect of SU1266 on IL-1β-mediated CXCL8 mRNA.
Cells were either not treated or treated with DMSO or SU1261 45 min pre-stimulation. Following pretreatment, cells were unstimulated or stimulated with with IL-1β (5 ng/mL) for 8 hours, or left unstimulated, prior to RNA extraction. RT-qPCR was performed to measure relative expression of CXCL8 mRNA. HRPT1 was used as an internal control. GraphPad Prism 8 software was utilised to carry out Gaussian distribution with Shapiro-Wilk test to ensure normality of samples. One-way ANOVA was used to compare IL-1β + DMSO compared to appropriate samples. Data represents mean CXCL8 (% maximum response) ± SEM n=3, *p<0.05, **p<0.01, ****p<0.0001.

To explore the novel mechanisms by which IKKα regulates CXCL5 gene and protein expression, it is essential to understand the pathways it employs. To this end, the CXCL5 promoter was analysed for predicted transcription factor binding sites. Using the UCSC Genome Browser for Human (GRCh38/hg38), the transcription start site (TSS) for CXCL5 was identified as chr4:73998677 on the – strand. Interestingly, upstream of the TSS, potential binding sites for NF-κB2, Rel, and RelA were identified. Notably, the predicted presence of NF-κB2 and Rel binding sites was assigned a higher confidence than that of RelA at one position, while Rel and RelA were predicted at another position with similar confidence levels to one another. This is summarised in Table 4.2.

Table 4.2. A summary of NF-κB predicted transcription factor binding sites on the CXCL5 gene promoter using the UCSC Genome Browser for Human (GRCh38/hg38).

Predicted transcription factor	Upstream or Downstream of transcription start site	Base pair position (on chromosome 4)	Score	P-value
NFkB2	Upstream	chr4:73998758-73998768	520	P<0.00001
Rel	Upstream	chr4:73998759-73998768	541	P<0.00001
RelA	Upstream	chr4:73998759-73998768	343	P<0.001
Rel	Upstream	chr4:73998758-73998767	469	P<0.0001
RelA	Upstream	chr4:73998758-73998767	487	P<0.0001

Overall, a key role of IKKα is the phosphorylation of NF-κB2/p100. The findings in Table 4.2. suggest a potential mechanism by which IKKα may regulate CXCL5 expression. This is noteworthy, as no IL-1β-mediated, p100-dependent genes have yet been identified. Therefore, this study is the first to propose a mechanism through which p100 could regulate an IL-1β-mediated, IKKα-dependent gene.

This provides interesting insights into a mechanism by which IKKα can promote CXCL5 to enable downstream osteogenesis signalling (Figure 4.32). Notably, IKKβ-mediated CXCL8 is also highlighted in this figure, demonstrating the central role for both CXCL5 and CXCL8 on CXCR2-mediated signalling.

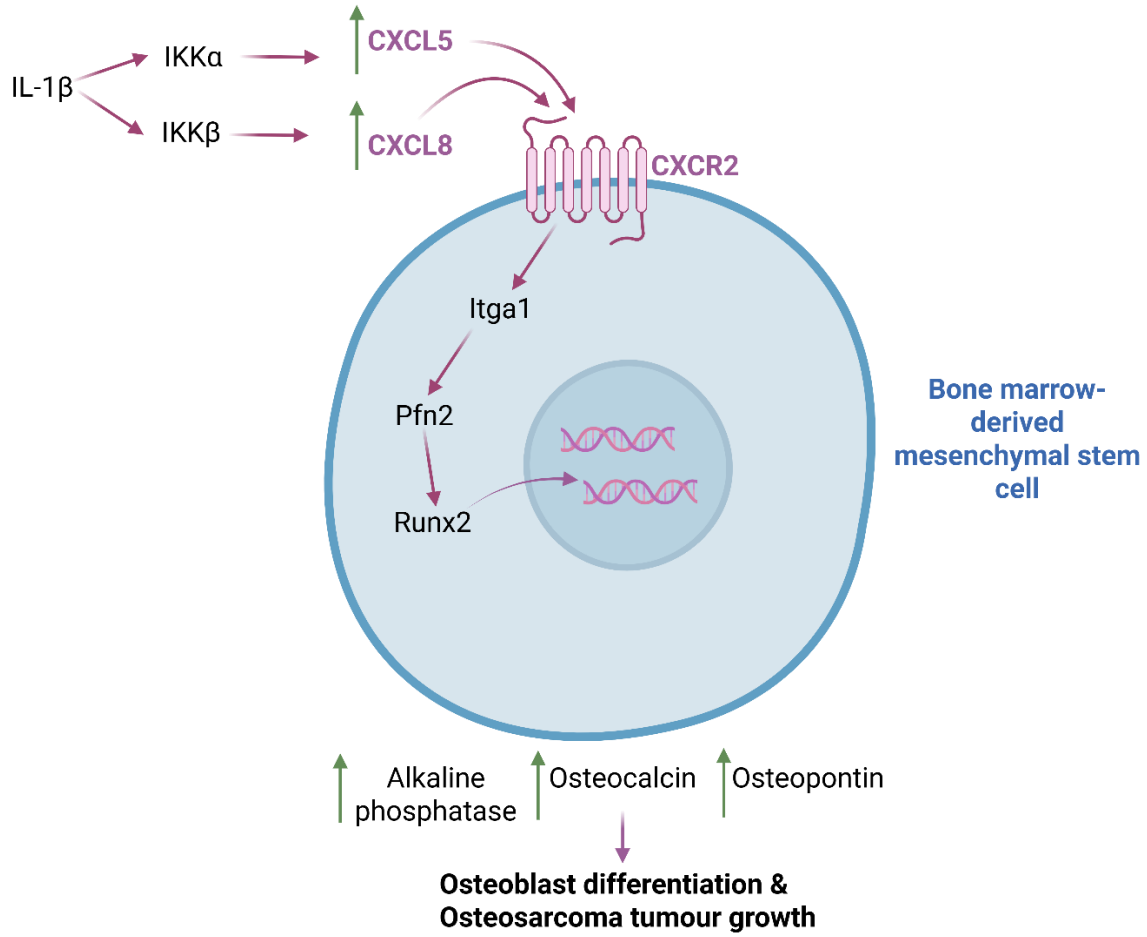

Figure 4.32. A schematic demonstrating the role of IKKα in regulation of CXCL5 in osteogenesis signalling.
Original figure was created on BioRender.com.

4.3.9 A role for IKKα in regulating cholesterol biosynthetic enzymes

Another comparison which was broadly looked at in this study was the genes which were significantly reduced in unstimulated IKKα CRISPR/Cas9 knockout U2OS cells compared to wildtype unstimulated U2OS cells. The top 20 downregulated genes in IKKα CRISPR/Cas9 knockout U2OS cells was plotted as a heatmap (Figure 4.33).

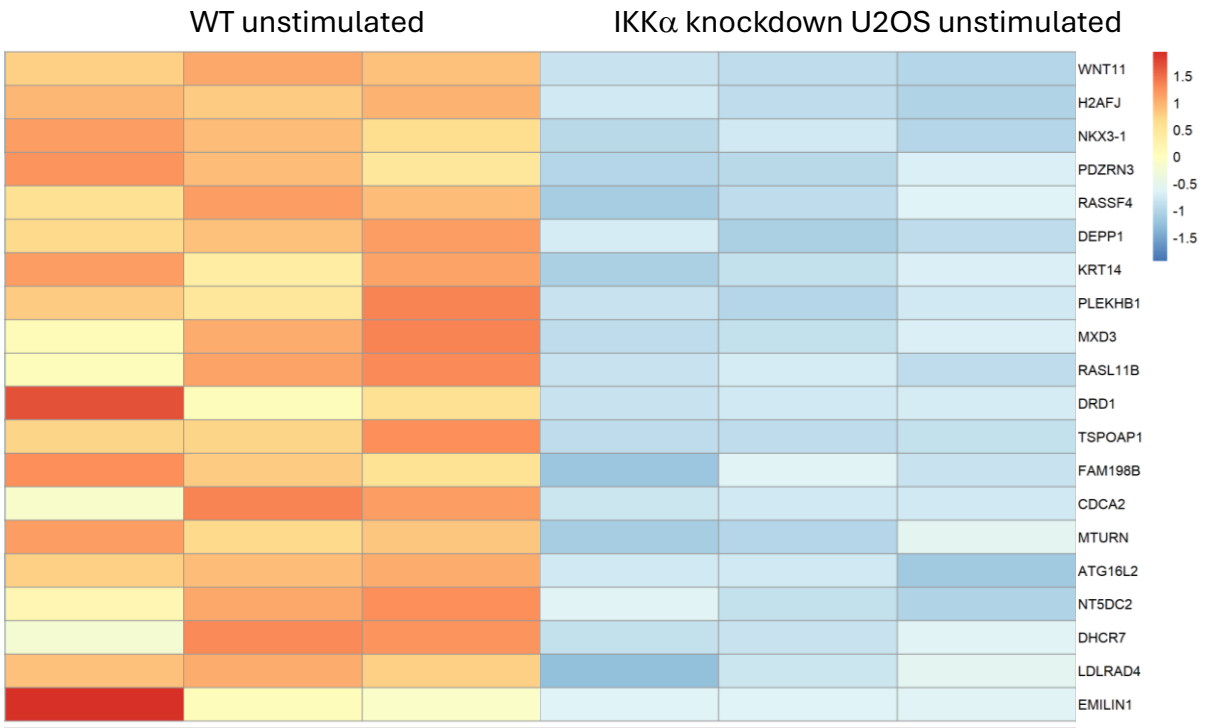

Figure 4.33. A heatmap depicting the top 20 differentially expressed genes which were significantly downregulated in unstimulated IKKα CRISPR/Cas9 knockout U2OS cells compared to wildtype.

The genes were filtered in order of ascending p-value, and the top 20 genes were selected. The smallest and largest p-value of the top 20 differentially genes are displayed by lowest to highest p-value, at the top to bottom of the heatmap, respectively. The colours shown in the heatmap are indicative of z score, where baseline expression = 0, positive integers = above baseline expression, and negative integers = below baseline expression. Heatmap was constructed by R, n=3.

Interestingly, in the top 20 downregulated genes, Wnt11 and DHCR7 presented as potentially interesting targets. However, when referring to the literature, Wnt11 is undetectable by RT-qPCR in U2OS cells and so, validation for this target was not pursued. DHCR7, on the other hand, presented an exciting opportunity to look at IKKα in the context of cholesterol biosynthesis, given the prominent role of DHCR7 as an enzyme at the final stages of this process. Therefore, this prompted a manual data mining investigation, to better understand what role IKKα has on cholesterol biosynthetic genes. Indeed, in the RNA-sequencing study, several of the genes encoding cholesterol biosynthetic enzymes were significantly reduced in IKKα CRISPR/Cas9 knockout U2OS cells (Figure 4.34).

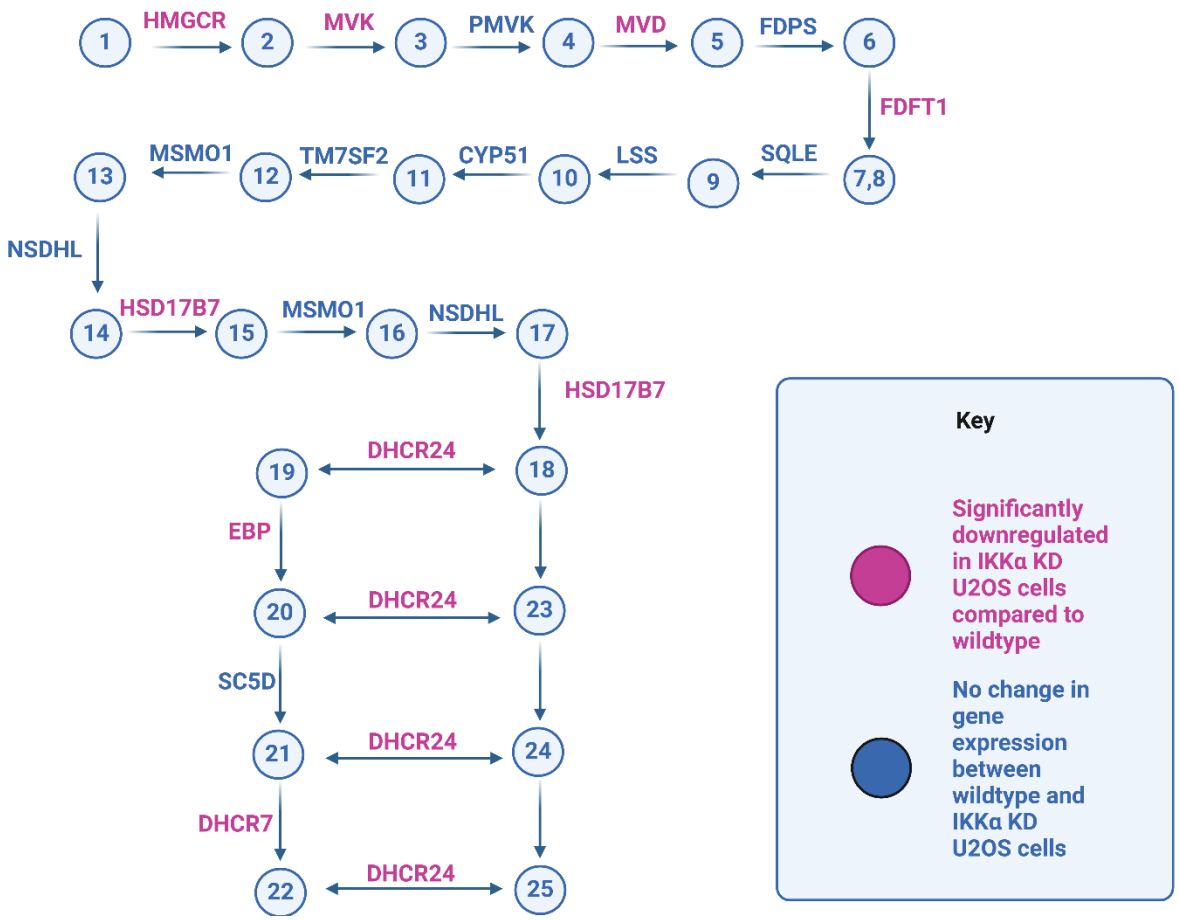

Figure 4.34. A diagrammatical representation of the effects of IKKα CRISPR/Cas9 knockout on genes encoding cholesterol biosynthetic enzymes. Original figure created on BioRender.com.

As DHCR7 was the most downregulated gene in this pathway as a result of IKKα knockout (Figure 4.33), this was investigated with RT-qPCR experiments. Indeed, a significant decrease was observed in unstimulated IKKα CRISPR/Cas9 knockout U2OS cells compared to wildtype (Figure 4.35). This effect was replicated in cells stimulated with IL-1β (10 ng/mL) for 8 hours.

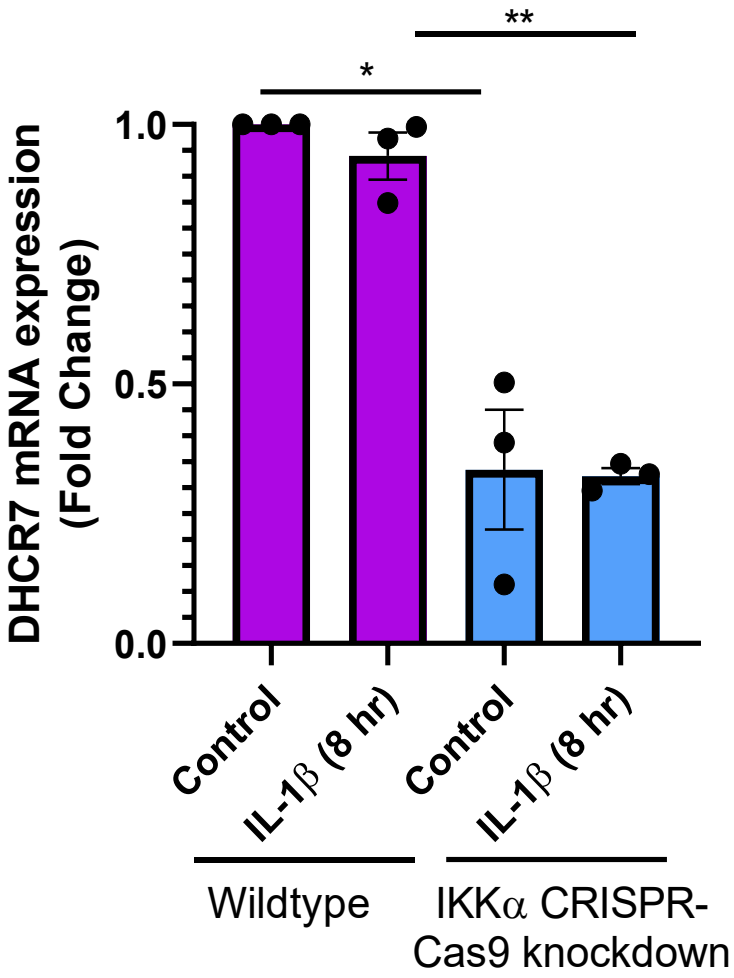

Figure 4.35. DHCR7 mRNA expression is reduced in IKKα CRISPR/Cas9 knockout U2OS cells.

Cells were unstimulated or stimulated with IL-1β for 8 or 24 hours (10 ng/mL). Total RNA was extracted from cell samples, followed by reverse transcription and RT-qPCR. Comparative Ct analysis was performed to generate fold change values against untreated wildtype cells. ONE-WAY ANOVA was conducted by utilising GraphPadPrism 8 software, *p<0.05, **p<0.01, n=3.

Figure 4.35 demonstrates that IL-1β-mediated signalling is evidently not involved in IKKα regulation of DHCR7, and therefore IKKα phosphorylation and activation do not appear to be instrumental in promotion of DHCR7 gene expression. Therefore, further experiments focused on IKKα-dependent cholesterol biosynthetic gene regulation without stimulation.

In the next experiment, IKKα siRNA was utilised to induce a transient IKKα knockdown approach, to counteract the possibility that permanent gene editing through CRISPR/Cas9 could potentially disrupt mechanisms which could influence expression of cholesterol biosynthetic genes. Further, utilisation of IKKα siRNA enabled the cell passage used to be truly comparable compared to wildtype U2OS cells. Interestingly, in U2OS cells treated with IKKα siRNA, DHCR7 gene expression was significantly reduced (Figure 4.36).

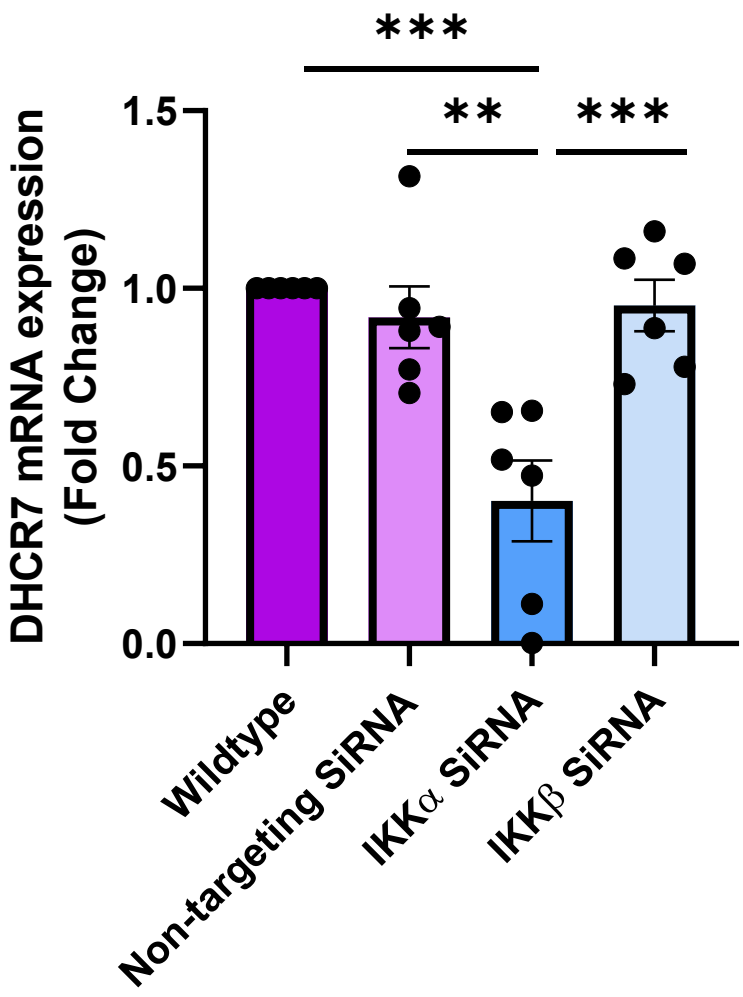

Figure 4.36. DHCR7 gene expression is IKKα-dependent but and IKKβ-independent.

Wildtype U2OS cells were untreated or pre-treated with non-targeting, IKKα or IKKβ siRNA for 72 hours. Total RNA was extracted from cell samples, followed by reverse transcription and RT-qPCR. Comparative Ct analysis was performed to generate fold change values against untreated wildtype cells. ONE-WAY ANOVA was conducted by utilising GraphPadPrism 8 software, **p<0.01, ***p<0.001, n=6.

As DHCR7 mRNA expression is reduced in both IKKα CRISPR/Cas9 knockout U2OS cells and U2OS cells pre-treated with IKKα siRNA, this suggests a role for IKKα in promoting DHCR7 gene expression. Notably, DHCR7 has not been linked to IKKα before directly. Therefore, JASPAR Core, which is a tool which predicts transcription factor binding sites on genes was utilised on the University of California Santa Cruz (UCSC) Genome Browser to depict potential transcription factor binding sites for IKKα target genes on the DHCR7 gene promoter and base pairs surrounding the promoter region. To carry this out, 2,000 base pairs upstream and downstream of the transcription start site were evaluated for transcription factor binding. Relevant predicted transcription factor binding sites which were discovered on UCSC by utilising hg38 Human: JASPAR CORE 2024 and are outlined in Table 4.3. FOS, a gene encoding c-fos, an IKKα-dependent gene was identified.

Table 4.3. Predicted transcription factor binding sites on the DHCR7 gene promoter.

Predicted Transcription factor	Upstream or Downstream of transcription start site	Base pair position (on chromosome 11)
FOS	Downstream	chr11:71447488-71447495
RelA	Downstream	chr11:71446446-71446455
FOS	Upstream	chr11:71448415-71448427
FOS	Upstream	chr11:71448416-71448428
JUND	Upstream	chr11:71448416-71448426
JUN	Upstream	chr11:71448417-71448426

Given that there were two predicted binding sites which FOS (c-fos) could bind, this has the potential to be a true binding site. Therefore, the regulatory effects which IKKα has on DHCR7 gene expression, which are significant, but knockdown of IKKα with siRNA does not complete deplete DHCR7 expression, may be due to indirect effects of IKKα via c-fos. However, this is highly speculative and would require experimental validation.

One laboratory technique which was applied to look at the effects of IKKα on cholesterol was immunofluorescent staining. To achieve this, filipin complex staining was carried out. Wildtype and IKKα CRISPR/Cas9 knockout U2OS cells were stained with filipin complex, which resulted in a significant decrease in IKKα knockout U2OS cells (Figure 4.37). This indicates that IKKα CRISPR/Cas9 knockout U2OS cells express lower levels of intracellular lipids generally. However, the majority of filipin complex is made up of filipin III, which binds specifically to free cholesterol. Therefore, this is a good indicator, and broadly accepted way to measure cholesterol in cells.

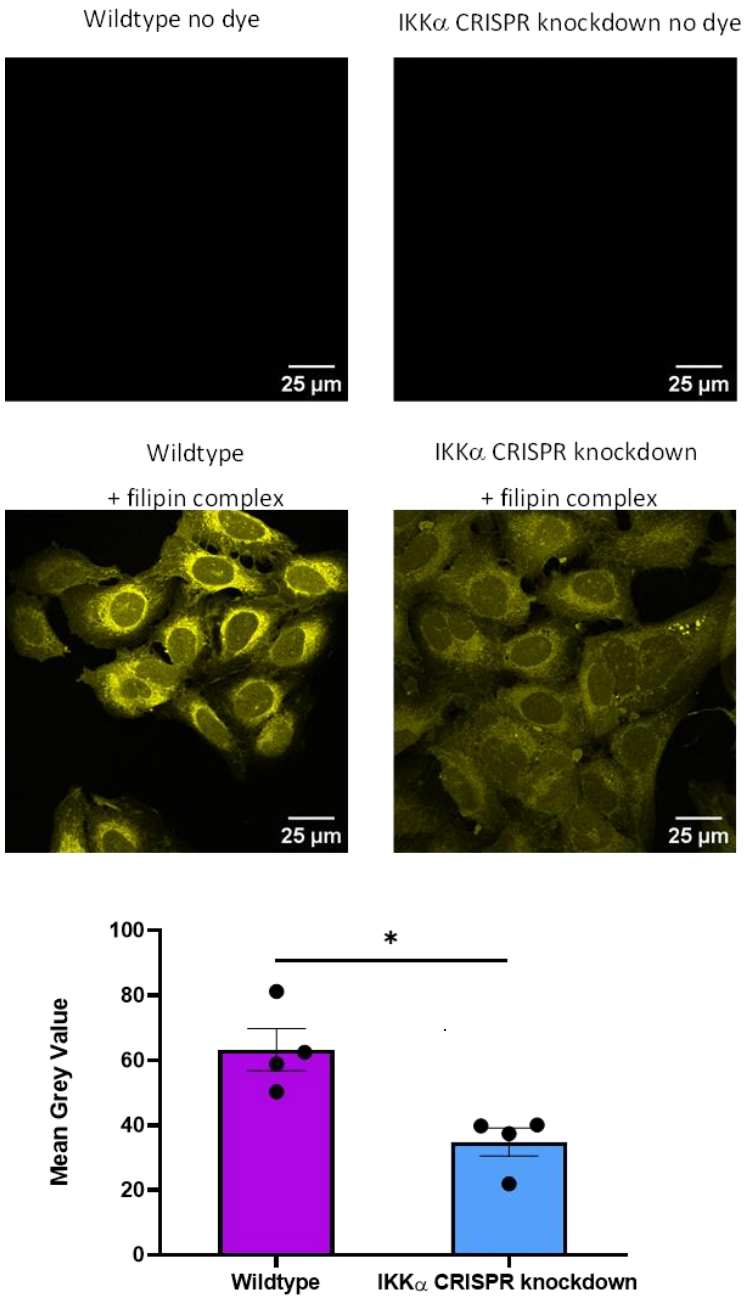

Figure 4.37. IKKα CRISPR/Cas9 knockout reduces lipid expression in U2OS cells.

Wildtype and IKKα CRISPR/Cas9 knockout U2OS cells were washed with PBS, fixed with 3.6% paraformaldehyde solution for 15 minutes, washed with PBS again and then either left in PBS and utilised as a no dye control or stained with filipin complex (0.5 mg/mL) for 30 minutes. Coverslips containing cells were mounted onto microscope slides and stored in the dark until imaged. Images were captured on a Leica SP8 confocal microscope. Images were processed and grey value was quantified by use of ImageJ software. An unpaired T-test was conducted to perform data analysis, *$p<0.05$, $n=4$.

Simultaneously Gene ontology was performed and the top 20 terms for gene clusters which were downregulated as a result of IKKα CRISPR/Cas9 in unstimulated U2OS cells were sorted by biological process (Figure 4.38).

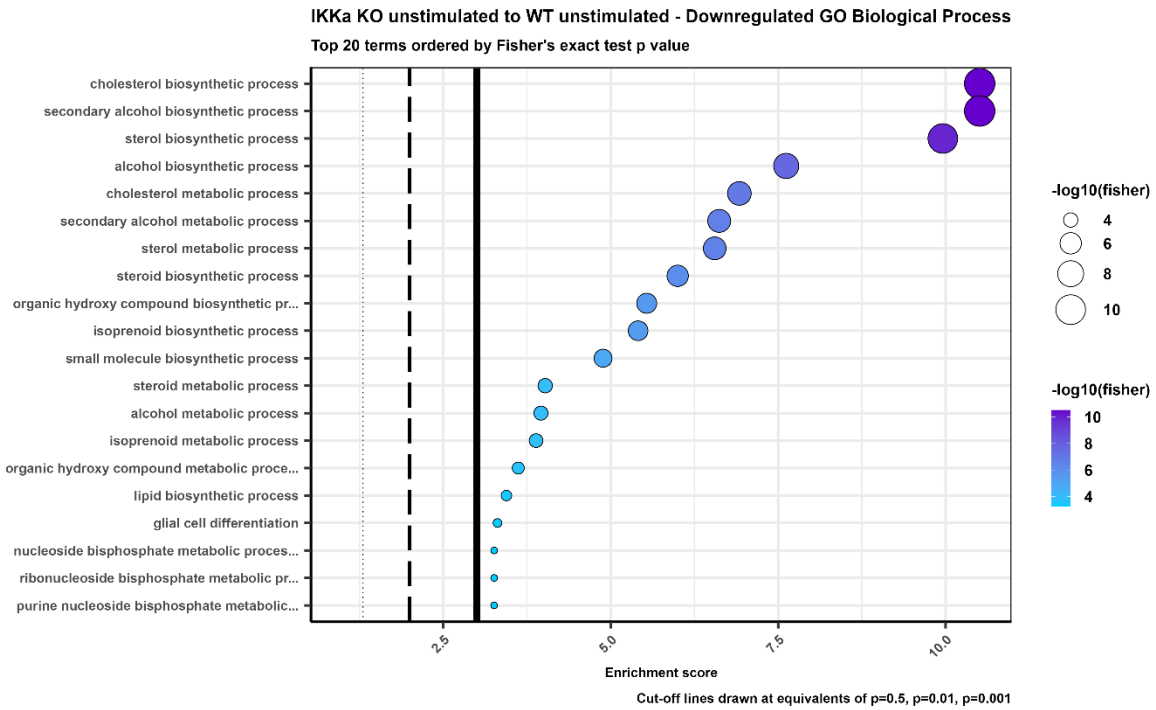

Figure 4.38. Gene ontology enrichment dot plot depicting downregulated biological process gene terms in unstimulated IKKα CRISPR/Cas9 knockout U2OS cells compared to unstimulated WT U2OS cells.
The top 20 enriched gene terms are displayed and ranked by statistical significance (Fisher's exact test).

Gene ontology revealed an important correlation between IKKα CRISPR/Cas9 knockout and downregulation of cholesterol biosynthetic processes in unstimulated U2OS cells. This was similarly seen in IKKα CRISPR/Cas9 knockout cells stimulated with IL-1β for 8 hours and 24 hours compared to wildtype equivalent samples (Figure 4.39 and Figure 4.40).

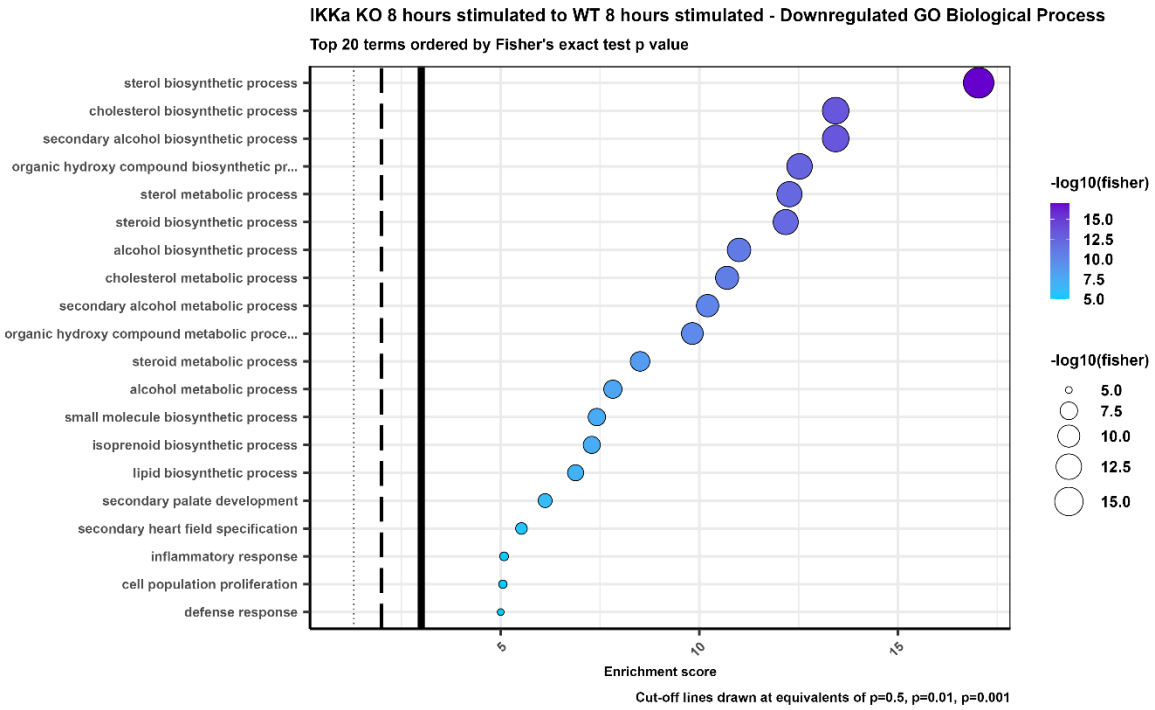

Figure 4.39. Gene ontology enrichment dot plot depicting downregulated biological process gene terms in IKKα CRISPR/Cas9 knockout U2OS cells compared to WT U2OS cells stimulated with IL-1β for 8 hours.
The top 20 enriched gene terms are displayed and ranked by statistical significance (Fisher's exact test).

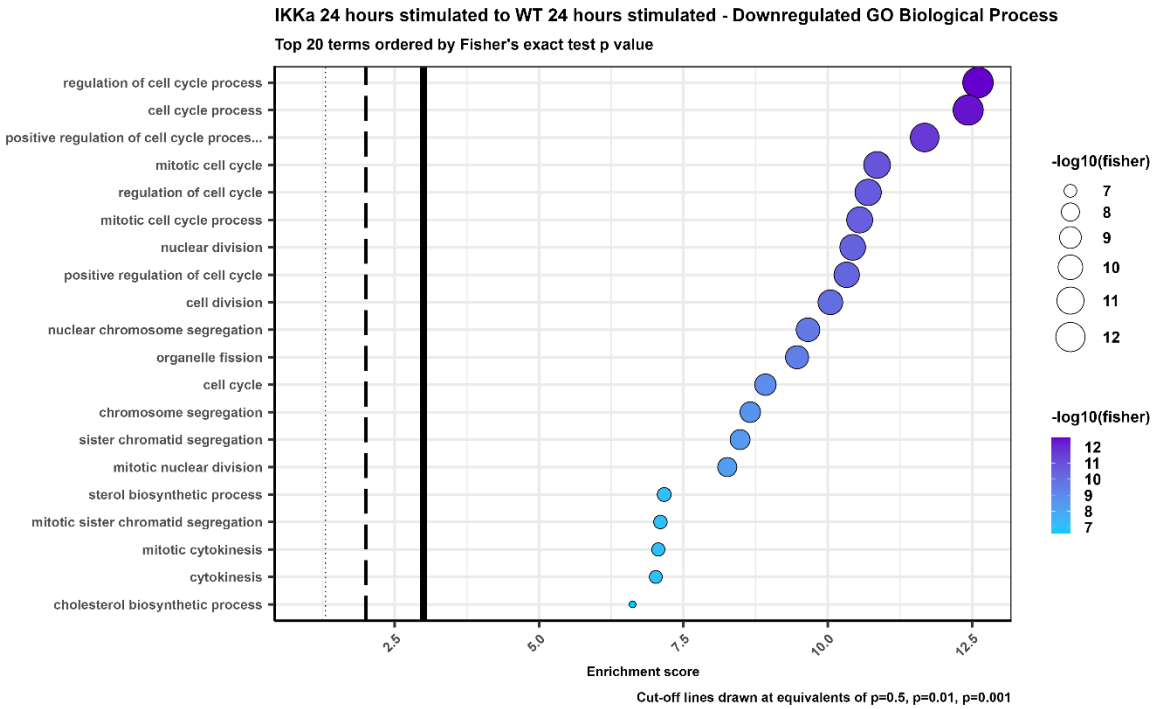

Figure 4.40. Gene ontology enrichment dot plot depicting downregulated biological process gene terms in IKKα CRISPR/Cas9 knockout U2OS cells compared to WT U2OS cells stimulated with IL-1β for 24 hours.
The top 20 enriched gene terms are displayed and ranked by statistical significance (Fisher's exact test).

To build on these findings from the RNA-sequencing study, RT-qPCR and immunofluorescent staining, it was important to measure cholesterol itself to truly understand the extent of the influence which IKKα has on cholesterol within U2OS cells. Therefore, Red Amplex cholesterol assays were applied. These experiments highlighted that IKKα siRNA induces a small, but significant reduction in intracellular concentration, while IKKα CRISPR/Cas9 knockout results in a much greater reduction (Figure 4.41). Additionally, IKKβ siRNA results in no significant decrease in cholesterol production. This indicates that while transient knockdown of IKKα with siRNA result in minor suppression of cholesterol levels in U2OS cells, the effects by terminal knockout with IKKα CRISPR/Cas9 are much more prominent.

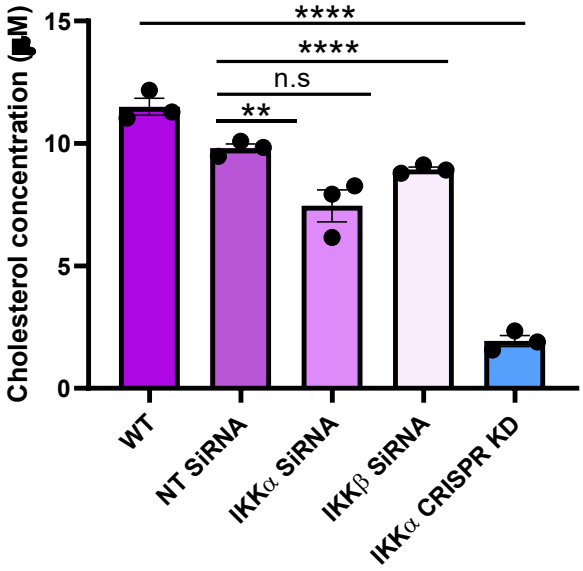

Figure 4.41. Intracellular cholesterol is decreased in IKKα CRISPR/Cas9 knockout U2OS cells and U2OS cells transfected with IKKα siRNA.
Wildtype U2OS cells were untreated or pre-treated with non-targeting, IKKα or IKKβ siRNA for 72 hours. IKKα CRISPR/Cas9 knockout U2OS cells were grown in parallel. Cells were quiesced for 24 hours prior to cell collection. Total RNA was extracted from cell samples, followed by reverse transcription and RT-qPCR. Comparative Ct analysis was performed to generate fold change values against untreated wildtype cells. One-Way ANOVA was conducted between non-targeting siRNA, IKKα siRNA and IKKβ siRNA. Two-way ANOVA was conducted between wildtype and IKKα CRISPR/Cas9 knockout samples. Data analysis was carried out by utilising GraphPad Prism 8 software, **p<0.01, ****p<0.0001, n=3.

This understanding is extended by further studies, although as cholesterol biosynthesis is overlooked in the context of OS, this is often not the focus of studies. One study which conducted microarray technologies by utilising fluorescent probes identified gene profiles across 19 OS cell lines compared to 2 healthy osteoblast cells and 4 bone tissues (Figure 4.42). Taken directly from Gene Expression Omnibus (study GSE36001), there are trends in increased DHCR7 expression in adolescent male-derived OS cell lines (blue) compared to healthy osteoblast 2 (20 years old) and healthy bone (26 years old).

This suggests a potential increase in cholesterol synthesis in males within this age group with OS compared to healthy individuals (Figure 4.44). Similarly, in females, there was a notable trend demonstrating an increase in DHCR7 expression compared to a healthy control. However, this is not reliable as the healthy control for female representation was much older than any of the patients who had an OS cell line derived from their tumours.

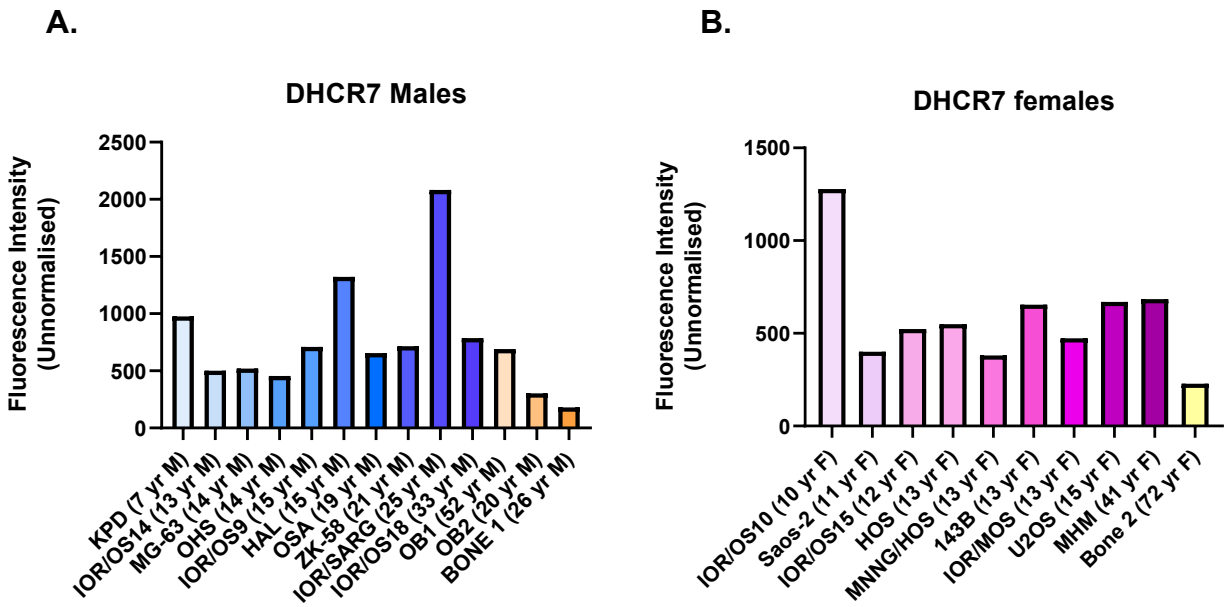

Figure 4.42. DHCR7 is increased in OS compared to healthy controls.
A. DHCR7 gene expression is higher in male-derived OS cells (blue), compared to healthy bone or osteoblast cells (orange). B. DHCR7 gene expression is higher in female-derived OS cells (pink) compared to healthy bone (yellow). Data was found readily in a microarray dataset (study GSE36001) on Gene Expression Omnibus. Mean fluorescence intensity corresponding to DHCR7 was plotted on GraphPad prism 8.

4.4. Chapter Discussion

4.4.1. Addressing research gap in IKKα-related research

Despite a broad focus on targeting the NF-κB pathway over the past few decades, there have yet to be any drugs which have been approved as medicines which specifically target any of the kinases involved in the NF-κB pathway. This is despite several attempts to target IKKβ for several diseases, where IKKβ inhibitors were found to be intrinsically toxic resulting in repeated failure in clinical trials (384). The significant research effort invested into the development of IKKβ antagonists has led to a gap in IKKα-focused research, and therefore many of its roles have remained unexplored. Moreover, given the additional nuclear IKKα active isoform, undoubtedly IKKα appears to have some distinct functional differences from its highly homologous protein partner, IKKβ.

Due to the saturation in IKKβ-related research, there have been several IKKβ-dependent genes previously identified (384-388). However, as a result of the lack of research into the role of IKKα, particularly following canonical ligand stimulation such as IL-1β, IKKα-dependent genes have been unexplored in this context. Therefore, this aim of this chapter was to uncover the role of IKKα activity on genes at basal level, and with IL-1β stimulation. This study was designed to identify expression of IKKα-dependent early genes (8-hour stimulation), and genes which are induced later, following 24 hours of IL-1β stimulation. Due to the nature of the study, all differentially expressed genes which were identified between comparisons could not be experimentally validated. Therefore, selected genes which were upregulated or downregulated by IKKα CRISPR/Cas9 knockout were validated in the laboratory.

4.4.2 Contradictory evidence for the role of IKKα in osteoclastogenesis using different knockout and knockdown methods

Surprisingly, RNA sequencing revealed that without agonist activation of the canonical NF-κB pathway, IKKα knockout using CRISPR/Cas9 increased the expression of OSCAR in basal U2OS cells. OSCAR (osteoclast-associated receptor) functions as a co-stimulatory receptor on osteoclast precursors, promoting bone resorption (389). This was further supported by assessing cellular protein levels using immunofluorescence, which revealed OSCAR is not only localised at the plasma

membrane, but also in the cytosol. Further, subcellular fractionation and Western blotting experiments revealed that there are two OSCAR isoforms in high density organelles, the Golgi and Endoplasmic Reticulum within U2OS cells, which may be attributed to being splice variants. This is interesting as at least 6 OSCAR isoforms have been previously described (389). This may suggest that OSCAR observed in the Endoplasmic Reticulum may be an immature form, or incompletely processed forms which are still undergoing folding before being processed and trafficked to the plasma membrane (390). The subcellular fractionation is interesting generally, where OSCAR appears to be in the Endoplasmic Reticulum and/or the Golgi, and therefore, this study uncovers more about its localisation, beyond the plasma membrane and being secreted.

The findings using CRISPR/Cas9 were not replicated by IKKα siRNA at a mRNA level, where OSCAR was significantly reduced, or at a protein level by using immunofluorescence. Therefore, different knockdown strategies in this instance have produced contradictory results, which highlights the differences observed between terminal knockdown with CRISPR/Cas9 compared to short-term transient knockdown strategies such as siRNA. Additionally, U2OS cells do not express RANK, which has a central role in co-stimulatory effects alongside OSCAR to promote osteoclastogenesis. Therefore, U2OS cells do not possess characteristics of a typical osteoclast and are a difficult model to utilise to increase understanding of osteoclastogenesis processes. However, it is possible that IKKα CRISPR/Cas9 knockout results in an increase in OSCAR expression to promote OSCAR-mediated cellular signalling to compensate for the incapability of cells to enhance osteoclast differentiation via RANK-mediated IKKα-dependent signalling. Therefore, this may be a negative feedback loop to promote an alternative route to osteoclastogenesis when IKKα is expressed at lower levels over a sustained period. However, different knockdown technologies, can result in fundamental gene differences, as shown by comparing short hairpin RNA and CRISPR/Cas9 human chronic myelogenous leukaemia cell line (391).

Another noteworthy observation observed in this study include that for the first time, U2OS cells have been shown to have some aspects of osteoclast-like characteristics as shown by the ability to express OSCAR, and the subcellular localisation of OSCAR shown by confocal microscopy which would likely directly target the bone interface to

promote bone resorption. This shows a significant limitation in the utilisation of U2OS cells for primary OS observations, as primary OS is driven by osteoblastogenesis. Notably, this also demonstrates that U2OS cells do not have all the osteoblast-related characteristics, and therefore it would be favourable to utilise other OS cell lines, or primary human OS cells in future studies. Further research could also incorporate OS tissue to evaluate the relationship between IKKα and OSCAR, and how this expression relates to osteoclastogenesis-associated transcription factors. However, there will be additional limitations when utilising tissue samples, despite tissue being more physiologically relevant and translatable. These include variations in gene expression across each tissue, and that OSCAR expression should be low in tissue obtained from primary OS samples, and therefore OSCAR expression may be undetectable. Additional research may also be carried out on healthy bone tissue to highlight whether the relationship between IKKα and OSCAR at a fundamental level where bone homeostasis would be normal. This may in turn lead to future observations which correspond to other bone conditions, including inflammatory arthritis and osteoporosis where bone is degraded, as it may be counterintuitive to utilise IKKα as a drug target for these conditions.

4.4.3. IKKα-dependent CXCL5 mRNA expression and protein production

A second significant focus within this chapter was the exploration of the role of IKKα on regulating inflammatory gene expression. Given the established pro-inflammatory role of IKKα, this was of particular interest in an OS setting (345, 392). Indeed, it was found that IL-1β stimulation for 8 hours promoted a substantial increase in expression of CXCL5, consistent with IL-1β-mediated CXCL5 mRNA expression previously demonstrated in fibroblasts, endothelial cells, cholangiocarcinoma cells (393-395). RT-qPCR demonstrated that IL-1β-dependent CXCL5 gene mRNA expression was decreased to basal levels in the absence of IKKα. Therefore, this implies that CXCL5 mRNA expression is IKKα-dependent. CXCL5 expression is particularly relevant to OS, given its ability to be induced by TNF-α in a NF-κB-dependent manner, as demonstrated in Alveolar Type II cells (396). Further research could therefore focus on utilising TNFα as a comparison to IL-1β-mediated CXCL5 in an OS context. Additionally, CXCL5 contains a NF-κB element within its proximal component, which has been attributed to being a p65 binding site (397). However, it has not been

previously shown whether CXCL5 is IKKα- or IKKβ-dependent. This study eloquently highlights CXCL5 as an IL-1β-mediated IKKα-dependent gene in U2OS cells, as demonstrated by the multiple interventions utilised throughout chapter 4. This was further investigated by measuring secreted CXCL5 protein concentration from U2OS cells by ELISA. After 12 hours with IL-1β stimulation, it was shown that CXCL5 secretion was significantly upregulated, and transfection with IKKα siRNA or treatment of IKKα inhibitors, SU1261, SU1349 and SU1266, were sufficient in significantly reducing IL-1β-induced CXCL5 production. Taken together, the findings establish CXCL5 as a bona fide transcriptional target of IKKα, representing the first evidence of this regulatory relationship. Future studies are required to validate whether this is through p65-dependent mechanisms, like implied in previous studies. However, a potential NF-κB2-binding site at chr4:73998758-73998768 was identified on UCSC Genome Browser, upstream of the TSS (chr4:73998677) on the - strand. This would be an exciting avenue to explore, as there are currently no known outcomes for IL-1β-mediated p100 signalling, and this could potentially provide a functional outcome for IKKα-dependent p100 phosphorylation in this context.

This study for the first time identified an intricate potential role for IKKα in mediating osteogenesis. By positively regulating CXCL5 gene expression and secretion which subsequently target CXCR2 to aid osteogenesis, this places IKKα as an interesting regulator of CXCR2 ligands. However, the effects of these drugs on global gene expression should also be considered. Alongside the research efforts outlined in this study, transcriptomics has been performed to try and negate the limitations of potential changes inflicted on the cells by IKKα CRISPR/Cas9, by measuring global gene expression in cells transfected with IKKα siRNA and treated with SU1261 or SU1349. This will provide insights into the real effects of these novel compounds on global gene expression, as opposed to measuring single genes which may be affected by disruption of the IKK complex, or alternatively, off-target effects. Understanding this will be vital in the further characterisation of these compounds, and in the development of potentially more selective derivatives of these compounds in the future. As U2OS cells have some osteoblastic characteristics, but do not display the characteristics of mesenchymal cells which would undergo differentiation into osteoblasts, this has implemented challenges in measuring the effects of IKKα expression on downstream

transcription factors involved in osteogenesis such as Runx2 and downstream genes which would be upregulated including osteopontin and osteocalcin (398-400). However, subsequent research following this study could utilise human OS tissue, or alternatively, canine OS tissue due to the similarities in the way in which OS presents in humans and dogs (401). This of course would be challenging to retrieve, given the rarity of OS, which is a likely factor that halts OS research generally. However, tissue could be utilised to carry out correlation studies to measure the gene and protein expression of IKKα and whether this can be correlated to the expression of CXCL5. These experiments will be crucial to provide the fundamental understanding of the role of IKKα in downstream transcription factors involved in OS development.

4.4.4. The effects of IKKα inhibition on IL-1β-mediated IKKβ-dependent CXCL8 mRNA expression

This study also takes this investigation further, by measuring expression of a known IL-1β-mediated IKKβ-dependent gene, CXCL8. Not only is CXCL8 also a CXCR2 ligand (402), but measuring this gene presented the opportunity to test if the IKKα inhibitors disrupt the IKK complex and therefore, assesses any effect on the expression of IKKβ-dependent genes. Interestingly, SU1261 pre-treatment with lower concentrations used (0.3 μM and 1 μM) resulted in increased CXCL8 gene expression compared to that observed in controls, and IL-1β stimulation. This highlights a key concern with IKKα inhibition going forward, as while it is useful to inhibit CXCL5 gene expression, with the key role of CXCL8 in cancer processes, it is unfavourable to simultaneously induce CXCL8 in this way. However, pre-treatment with higher concentrations of SU1261, 3 μM and 10 μM, CXCL8 gene expression returned to IL-1β-induced CXCL8 gene expression levels. Therefore, this demonstrates a biphasic concentration-dependent cross-regulation between IKKα and IKKβ, where 0.3 μM SU1261 treatment results in a loss of 53% of IL-1β -induced CXCL5 gene expression, but results in increased CXCL8 gene expression. This highlights that partial inhibition of IKKα responses enhance IKKβ-dependent transcription of CXCL8, but stronger inhibition of IKKα alleviates this effect and restores CXCL8 gene expression to baseline IL-1β-induced levels. Furthermore, it is important that going forward, selected concentrations of SU1261 being used in studies should be utilised with care and consideration, to avoid induction of IKKβ-dependent responses. Interestingly, SU1349

resulted in a distinct trend, where CXCL5 was reduced in a concentration-dependent manner, but IL-1β-induced CXCL8 expression was increased in a concentration-dependent manner, expressed maximally with 10 μM of SU1349. Mechanistic insight from these data suggests that SU1261 exerts off-target inhibition on IKKβ at higher concentrations, thereby reducing IKKβ-dependent transcription, whereas SU1349 remains selective for IKKα, even at 10 μM. This compliments findings from the chemistry team involved in producing these compounds, who have found similar off-target effects of SU1261 on IKKβ (348). This highlights key differences in selectivity and off-target effects between the two compounds.

4.4.5. The effects of a dual IKKα/IKKβ inhibitor on CXCL5 and CXCL8 mRNA expression

These findings prompted a new scientific question: what happens when you inhibit IL-1β-induced gene expression with SU1266, a compound that is more selective for IKKα than IKKβ but can inhibit IKKβ at higher concentrations? SU1266 presents a unique opportunity because previous inhibitors were developed primarily for IKKβ selectivity, with demonstrated IKKβ-mediated toxicity. Therefore, utilising this compound potentially offers the ability to inhibit IKKα-dependent responses, without potentially inducing IKKβ inhibition-mediated toxicity. Previous studies have not explored this concept, and so, U2OS cells were pre-treated with SU1266 to explore whether this compound could provide a balance between inhibiting IKKα-dependent genes and with higher concentrations, could also inhibit IKKβ-dependent genes. Indeed, at lower concentrations, CXCL5 was significantly reduced, reinforcing that CXCL5 is IKKα-dependent, meanwhile at higher concentrations, IKKβ-dependent CXCL8 was significantly reduced. Not only did SU1266 appear more potent for IKKα-dependent transcriptional activity, but its ability to reduce IKKβ-dependent genes at higher concentrations may be a potential way to strike a balance between inhibiting IKKα-dependent gene expression, avoiding enhanced IKKβ-dependent gene expression as a result, and at higher concentrations, reduce IKKβ-dependent genes including CXCL8. Overall, this approach offers a novel perspective on targeting the IKK complex.

4.5.6. The relationship between IKKα and cholesterol production

The final part of the study investigated the relationship between IKKα and the regulation of cholesterol production. This was achieved by visualising the findings from the transcriptomics study, showing a significant decrease in cholesterol biosynthetic enzyme genes, particularly DHCR7 in IKKα CRISPR/Cas9 knockout U2OS cells. This was validated in the laboratory, where DHCR7 mRNA was significantly decreased by IKKα CRISPR/Cas9 knockout and IKKα siRNA knockdown methods. These experiments were complimented by the subsequent Red Amplex cholesterol assays which demonstrated a significant reduction in intracellular cholesterol concentration in IKKα CRISPR/Cas9 knockout U2OS cells compared to wildtype U2OS cells. However, a significant reduction was also highlighted in U2OS cells treated with IKKα siRNA, but this reduction was minor. This demonstrates that although IKKα may have a role in regulating DHCR7 gene expression, it may not possess prominent or direct regulatory roles. This highlights key differences in findings between different knockdown methods, which may be attributed to metabolic cellular changes which can arise as a result of long-term terminal gene knockout with technologies including CRISPR/Cas9. However, it is also a possibility that siRNA does not result in gene knockdown to the same extent as CRISPR/Cas9 methods. In the context of bone physiology and health, several studies have investigated the role of cholesterol. Notably, expression of endoplasmic reticulum localised genes which mediate cholesterol biosynthesis, SREBP cleavage-activating protein (SCAP), and HMGCR, are significantly downregulated in the hypertrophic zone (HZ) compared to proliferative zone (PZ) in E16.5 embryo distal femur chondrocytes (325). Additionally, hedgehog signalling promotes genes involved in the cholesterol biosynthetic pathway, and mutually, intracellular cholesterol also regulates hedgehog signalling (325, 326). In a cancer setting, hedgehog signalling has been linked to osteoblast regulation in OS by overexpression of the YAP-1 gene and long-coding RNA, H19 (327). Several antagonists including ATO, vismodegib and GANT61 which target the hedgehog/GLI2 signalling pathway have shown promising therapeutic potential in OS, by downregulating invasion and metastasis of OS cells (328). Therefore, this implicates a role for genes which enhance cholesterol biosynthesis in OS development and migration. In support of this, a recent study utilised open access datasets to identify four distinct groups of OS patients based on their median gene expression into a

glycolysis, cholesterol, quiescent and mixed subgroup. This study identified that the cholesterol and mixed OS patient subtypes displayed the worst prognosis in relation to patient survival (329). In addition, other studies have highlighted some cholesterol biosynthetic enzymatic genes including SQLE and TM7SF2 in a prognostic OS gene model (330). Notably, both genes were not IKKα-dependent in this study. However, the several IKKα-dependent cholesterol biosynthetic genes highlighted within this study could potentially significantly influence cholesterol production, and therefore, prognosis in OS patients in the future. Furthermore, our study reveals for the first time, a potential link between IKKα and cholesterol biosynthesis. However, this association remains tenuous, as the reduction in intracellular cholesterol production observed in siRNA-treated cells was considerably smaller than that seen in IKKα CRISPR/Cas9 knockout U2OS cells. However, given that DHCR7 mRNA and intracellular cholesterol production are not reduced by knockdown of IKKβ by siRNA, this excludes the possibility that cholesterol biosynthesis is downregulated by simply disruption of the IKK complex and is a potentially highly specific role for IKKα in promoting expression of cholesterol biosynthetic genes and therefore mediating cholesterol production.

Furthermore, there is the potential that selective IKKα inhibitors could be used in the future to reduce cholesterol levels, which would be highly useful for patients with OS, but also a variety of other diseases. However, it is yet to be assessed to what extent IKKα inhibitors can reduce cholesterol synthesis.

4.5.7. Chapter Conclusion

Overall, this study demonstrates a plethora of genes which are differentially expressed by IKKα CRISPR/Cas9 knockout U2OS cells. However, the follow-up experimental validation conducted also demonstrates the challenges with CRISPR/Cas9 technology. Additionally, studies which produce such large datasets in a sensitive manner like RNA-sequencing are extremely useful, but it is essential to be able to detect these changes with assays which are accessible in the laboratory to ensure further validation can be carried out at a gene and protein level with respect to the differentially expressed genes highlighted in this study. This study presents CXCL5 as a Bonafide downstream target of IKKα, as well as a regulatory relationship with DHCR7, and a potentially complex relationship with OSCAR. Future studies would benefit from conducting RNA-sequencing in cells treated with IKKα siRNA as a short-

term knockdown approach, or potentially, with the novel and selective IKKα inhibitors outlined. Additionally, IKKα being a novel regulator of CXCL5 is interesting from a molecular perspective, understanding how this knowledge could potentially be translated into the context of OS is also important. One study revealed that CXCL5 promotes invasion and metastasis of OS, and that CXCL5 protein expression is increased in OS tissue samples compared to nontumorigenic tissues (94). High CXCL5 expression is also associated with a worsened prognosis (403). In summary, CXCL5 appears to be an IKKα-dependent chemokine, and an important contributor to OS prognosis, migration, and metastasis, but the relevant NF-κB pathways involved in its regulation are not yet fully understood.

Chapter 5

General Discussion

5.1. A collective summary of research conducted

There have been many attempts to develop inhibitors which target canonical NF-κB signalling. However, due to the general emphasis on the role of IKKβ across scientific literature, there has been little research into inhibiting IKKα in this context. Additionally, due to the small number of selective IKKα inhibitors available, considering currently the structures of only selective IKKα small molecule inhibitors has been published, this has been a truly neglected research area (348). IKKα-dependent genes in canonical NF-κB signalling have also been broadly neglected, as traditionally, IKKα has been considered to have a limited role in this pathway (290, 404). However, due to the recent discovery of the IL-1β-mediated, IKKα-dependent pathway which results in p100 phosphorylation, suggests a functional convergence of canonical and non-canonical NF-κB signalling (296, 347). this merges the canonical and non-canonical NF-κB pathway together. Within this study, the focus of IL-1β-mediated IKKα-dependent signalling (as outlined in Chapter 3) demonstrated that while IKKα mediates p100 phosphorylation, there are no obvious NF-κB related functional downstream functions for this phosphorylation events. Therefore, RNA-sequencing analysis conducted as part of this study provided valuable insights into IKKα-dependent genes and offered a broad transcriptome-wide overview of human gene activity in U2OS cell lines.

5.2. The role of IKKα in cancer hallmarks

The role of IKKα in OS has also not been well-defined, although IKKα is known to play a role in several of the cancer hallmarks (As discussed in chapter 1). To look widely at the identified IKKα-related cancer hallmarks, to determine the mechanisms which IKKα utilises to have its most prominent roles in cancer, CancerHallmarks.com was used. This is a tool which utilises available human datasets to visualise the role which one or multiple genes have on cancer hallmarks. The most significant hallmarks associated with IKKα gene expression were identified as reprogramming energy metabolism, evading immune destruction and tumour-promoting inflammation (Figure 5.1). This in many aspects relates closely to the findings in this study. By identifying that the IL-1β IKKα-dependent clusters of genes by biological process included cytokine and chemoattractant activity, this effectively fits in with tumour-promoting inflammation, aligning with available datasets.

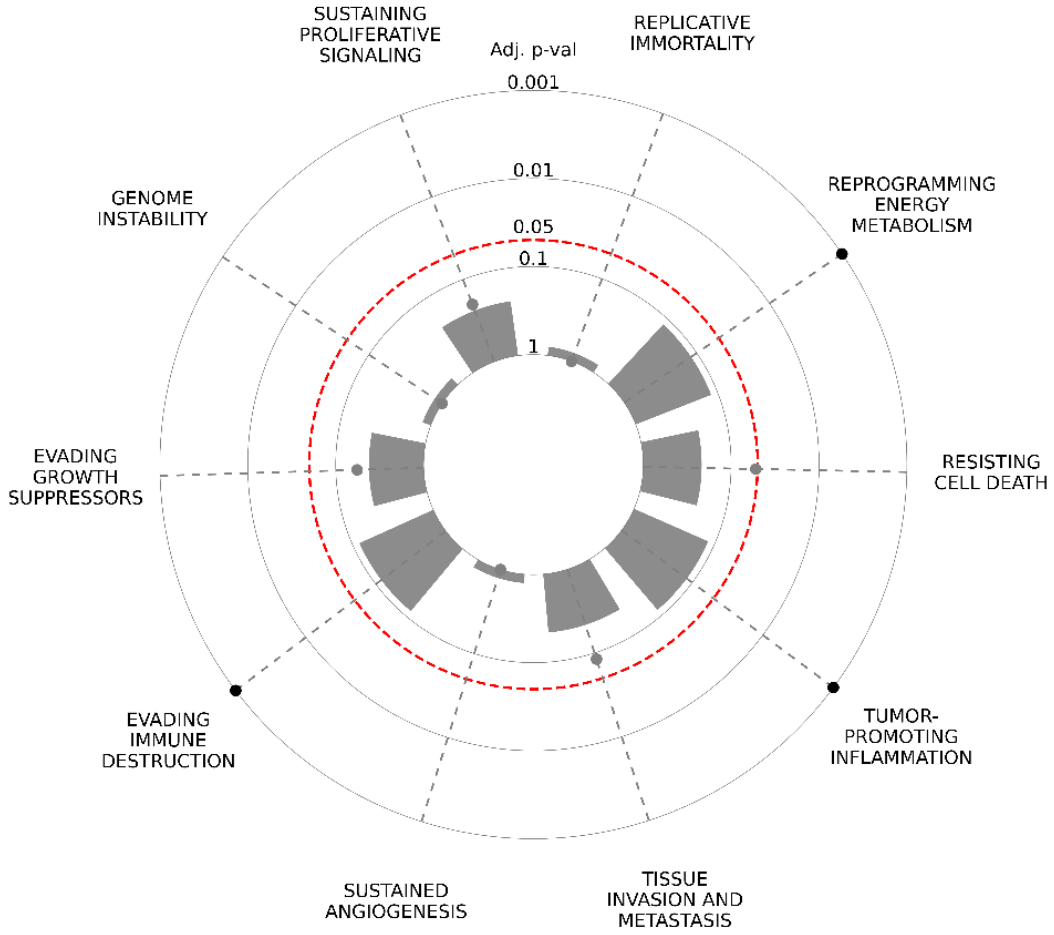

Figure 5.1. The role of IKKα in the eight hallmarks of cancer and two enabling characteristics.

The grey dots represent hallmarks where IKKα has a smaller and insignificant role, and the black dots represent hallmarks where IKKα has a significant role according to available human datasets. Figure was obtained from CancerHallmarks.com, after inputing CHUK, the gene encoding IKKα.

5.3. The use of IKKα inhibitors

This study not only identifies a plethora of IKKα-dependent genes but also investigates how IKKα inhibitors can be utilised effectively. Indeed, applying selective IKKα inhibitors such as SU1261 and SU1349 is an exciting way to inhibit IKKα-dependent genes, including CXCL5 which was highlighted in this study. However, given that these inhibitors induce upregulation of CXCL8, an IKKβ-dependent gene, which also has an important role in cancer and binds to the same receptor as CXCL5, CXCR2, it would be somewhat unfavourable to inhibit IKKα selectively in this way. However, the real

novel approach of this study was utilising a less selective IKKα inhibitor compared to the others previously mentioned, SU1266, which also has off-target effects on IKKβ at higher concentrations. The exciting prospect of applying this inhibitor is that most of the focus on inhibiting NF-κB signalling aims to selectively inhibiting IKKβ, which has demonstrated to illicit several toxicities, and therefore there has been repeated failure of IKKβ inhibitors. However, this study potentially offers a way to inhibit IKKα-dependent genes, and therefore its role in promoting CXCL5 in OS, but also if at high enough concentrations, there could be the potential for partial inhibition of IKKβ, to elicit therapeutic effects, without necessarily fully inhibiting the essential roles of IKKβ. This could offer a multi-target strategy with one compound. The main findings throughout this thesis are highlighted in Figure 5.2.

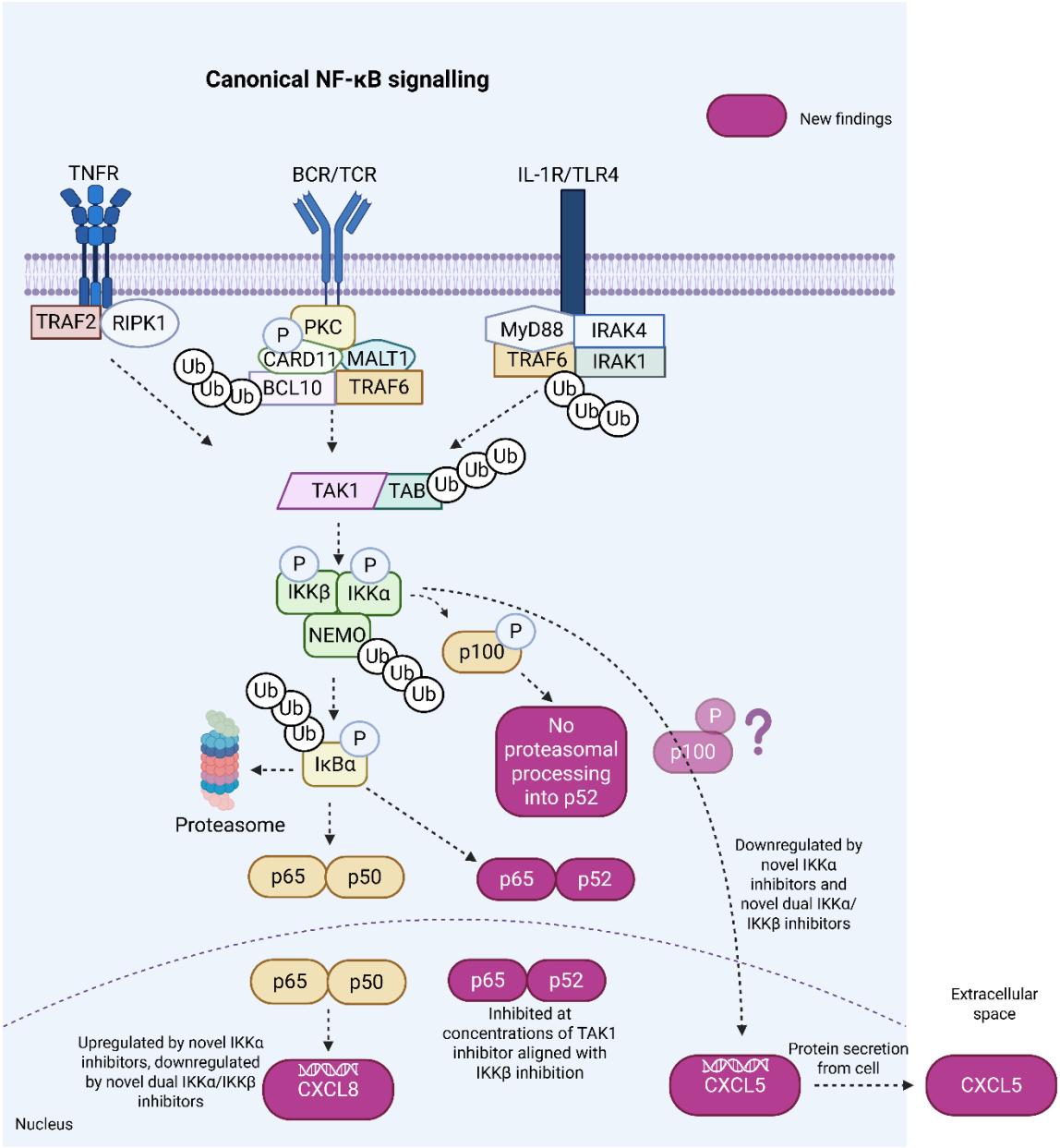

Figure 5.2. A diagrammatical summary of novel findings. The figure highlights p52 and p65 as IKKβ-mediated NF-κB dimers which translocate to the nucleus. CXCL5 is highlighted as an IKKα-dependent gene, inhibited by selective IKKα and dual IKKα/IKKβ inhibition. CXCL5 is secreted from U2OS cells in an IKKα-dependent manner. CXCL8 expression is upregulated by selective IKKα inhibition but downregulated by dual IKKα/IKKβ inhibition. Figure was created on BioRender.com.

More broadly, there have been several clinical examples of where off-target or multi-target drugs have been therapeutically viable. A very famous example of this is a small-molecule inhibitor, Sunitinib, which targets several antiangiogenic receptor tyrosine kinases including vascular endothelial growth factor receptor (VEGFR) and platelet-derived growth factor receptor (PDGFR), and additional tyrosine kinases to effectively advanced renal cell carcinoma and in imatinib-resistant GI stromal tumours (405). Therefore, it may be beneficial in OS to utilise multi-target drugs, or alternatively, to utilise combination therapies. Notably, the research conducted in this study has contributed to obtaining funding from the Bone Cancer Research Trust, the Children and Young People's Cancer Association which will entail further testing of IKKα inhibitors in various OS cell lines. However, given the complexity of OS, it is likely that combination therapies will be required to effectively treat or slow the progression of OS in patients.

5.4. Potential future studies

There are several future studies which could be conducted to strengthen the RNA-sequencing findings within this study. First and foremost, it would be useful to determine whether IKKα binds directly to the promoter of the genes it has been shown to regulate in this study, given its nuclear role. ChIP could be utilised to determine whether there is enrichment of the CXCL5 promoter or DHCR7 promoter bound to IKKα. Additionally, RNA-sequencing from 3D cell cultures, such as spheroids, would be beneficial to better represent the structure of a tumour compared to the 2D human cell line utilised within this study, as in some cases 3D cell cultures have shown increased resistance to anticancer drugs compared to 2D cell lines (406, 407).

Co cultures could be used, for example to overexpress CXCL5 and knockdown CXCL5 expression and measure differences in tumour-associated neutrophil or tumour-associated macrophage recruitment. Molecular insights into the role of IKKα in OS can be achieved by the potential future studies outlined previously to some extent. However, there remains key challenges into obtaining human tumour tissue from OS patients given the rarity of the cancer, and the amplified ethics required as some OS patients are paediatrics. In the interim, there has been several mouse models developed with the aim to mimic OS features, including mice which do not express tumour suppressors p53 and Rb genes in Sca-1-positive mesenchymal

stem/progenitor cells (408). These translational scientific advancements will be crucial in future OS research.

Further studies may also include looking at the IL-1β-IKKα-p100 axis further, to fundamentally identify the downstream functions of this signalling axis. Due to the range of roles which IKKα has within the cell, it would be more beneficial to look at p100 function directly, as we know this is IKKα dependent. While it is unfavourable to knockout p100 as its expression inhibits and regulates other NF-κB family members, it would be beneficial to identify the role of p100 following its IKKα-dependent phosphorylation in this context and identify why it does not appear to be degraded at the proteasome. One way to uncover the downstream effects of this would be to overexpress a tagged-p100, like the HA-p100 utilised within this study, and conduct proteomic analysis to identify p100-protein binding partners. Proteomics is characterised as a study of a large number of proteins in a biological system (409). In comparison to RNA-sequencing, it has several advantages, including that it accounts for protein expression, whereas a limitation of RNA-sequencing is that there is no ability to predict the quantity of genes expressed will undergo translation into protein, or post-translational modifications (409-411). Proteomics can be performed in by a variety of experimental approaches, depending on the scientific question of a project, whether quantitative or qualitative data is desirable and the cost (412). For this study, it would be beneficial to compare unstimulated cells, and cells with IL-1β stimulation where p100 phosphorylation is maximal (30-60 mins) and in IKKα CRISPR-Cas9 knockout cells or WT cells transfected with IKKα siRNA knockdown with and without IL-1β stimulation. One way which this could be achieved is by using Isotopomer labels such as Tandem Mass Tags (TMT), which are chemical labels utilised to label peptides, which are then analysed by Tandem Mass Spectrometry (413). Tandem Mass Tagging has become a widely used and cost-effective proteomics approach, including for deep-scale quantitative (phospho)proteome studies (414-418). Therefore, this approach can be an excellent tool to identify both interacting proteins and phosphorylation sites responsible for p100-protein interactions, which provides opportunity for multiplexed, quantitative analysis. This experimental approach could be particularly powerful with respect to understanding phosphorylation dynamics of kinases and transcription factors, such as p100, in cellular signalling pathways involved in OS, and in general cellular signalling events. Additionally, TMT-based proteomics could be applied to

identify and quantify proteins enriched in the IKKα-dependent secretome. This would provide a deeper understanding of the proteins produced and secreted by U2OS cells in an IKKα mediated manner, thereby enhancing knowledge of the role of IKKα in OS. and therefore, increase the level of understanding of the role of IKKα in OS.

Additionally, the prognostic factors in OS have recently been analysed in a systematic review, which include increased adverse outcomes in correlation with increased age, and increased sites of metastasis correlated with worse prognosis (129). Therefore, it would be beneficial to identify the role of IKKα in aging, as aging is known to have closely related links with inflammatory processes, known as "inflammaging" and therefore it is very likely that IKKα plays a contributory role in this OS prognostic factor (419).

5.5. An integrative summary of how this thesis advances current understanding

Overall, this study offers much needed molecular investigation into the IL-1β-induced IKKα-dependent signalling axis, as well as potential drug targets in OS and offers a new basis by which IKKα could promote cancer progression and metastasis, particularly by CXCL5 expression. From a translational perspective, this study offers the characterisation of novel small molecule inhibitors and utilises these to identify the selective downstream IKKα-dependent gene, CXCL5. This undoubtedly offers promising preliminary data for a field which has lacked progression in treatment for many years. Despite this being a small-scale study in an OS cell line, this study makes small steps forward to the much-needed novel treatments required for OS patients.

References

1. Brown JS, Amend SR, Austin RH, Gatenby RA, Hammarlund EU, Pienta KJ. Updating the Definition of Cancer. Mol Cancer Res. 2023;21(11):1142-7.
2. Lewandowska AM, Rudzki M, Rudzki S, Lewandowski T, Laskowska B. Environmental risk factors for cancer – review paper. Annals of Agricultural and Environmental Medicine. 2019;26(1):1-7.
3. Machlowska J, Baj J, Sitarz M, Maciejewski R, Sitarz R. Gastric Cancer: Epidemiology, Risk Factors, Classification, Genomic Characteristics and Treatment Strategies. Int J Mol Sci. 2020;21(11).
4. Buder T, Deutsch A, Klink B, Voss-Böhme A. Patterns of Tumor Progression Predict Small and Tissue-Specific Tumor-Originating Niches. Front Oncol. 2018;8:668.
5. Ryan BM, Faupel-Badger JM. The hallmarks of premalignant conditions: a molecular basis for cancer prevention. Semin Oncol. 2016;43(1):22-35.
6. Sarkar S, Horn G, Moulton K, Oza A, Byler S, Kokolus S, et al. Cancer development, progression, and therapy: an epigenetic overview. Int J Mol Sci. 2013;14(10):21087-113.
7. Ant A. Chapter 6 - Oxidative stress and oral cavity cancer. In: Preedy VR, Patel VB, editors. Cancer (Second Edition). San Diego: Academic Press; 2021. p. 55-65.
8. Afridi WA, Picos SH, Bark JM, Stamoudis DAF, Vasani S, Irwin D, et al. Minimally invasive biomarkers for triaging lung nodules-challenges and future perspectives. Cancer Metastasis Rev. 2025;44(1):29.
9. Li F, Liang H, You H, Xiao J, Xia H, Chen X, et al. Targeting HECTD3-IKKα axis inhibits inflammation-related metastasis. Signal Transduct Target Ther. 2022;7(1):264.
10. Sung H, Ferlay J, Siegel RL, Laversanne M, Soerjomataram I, Jemal A, et al. Global Cancer Statistics 2020: GLOBOCAN Estimates of Incidence and Mortality Worldwide for 36 Cancers in 185 Countries. CA Cancer J Clin. 2021;71(3):209-49.
11. Shelton J, Zotow E, Smith L, Johnson SA, Thomson CS, Ahmad A, et al. 25 year trends in cancer incidence and mortality among adults aged 35-69 years in the UK, 1993-2018: retrospective secondary analysis. Bmj. 2024;384:e076962.
12. Berben L, Floris G, Wildiers H, Hatse S. Cancer and Aging: Two Tightly Interconnected Biological Processes. Cancers (Basel). 2021;13(6).
13. Lortet-Tieulent J, Georges D, Bray F, Vaccarella S. Profiling global cancer incidence and mortality by socioeconomic development. Int J Cancer. 2020;147(11):3029-36.
14. Upadhyay A. Cancer: An unknown territory; rethinking before going ahead. Genes Dis. 2021;8(5):655-61.
15. Bray F, Laversanne M, Weiderpass E, Soerjomataram I. The ever-increasing importance of cancer as a leading cause of premature death worldwide. Cancer. 2021;127(16):3029-30.
16. Bona LG, Geleta D, Dulla D, Deribe B, Ayalew M, Ababi G, et al. Economic Burden of Cancer on Cancer Patients Treated at Hawassa University Comprehensive Specialized Hospital. Cancer Control. 2021;28:10732748211009252.
17. Ciro M, Bracken AP, Helin K. Profiling cancer. Current Opinion in Cell Biology. 2003;15(2):213-20.
18. Rashid S. Classification of Cancer. In: Rashid S, editor. Cancer and Chemoprevention: An Overview. Singapore: Springer Singapore; 2017. p. 15-6.
19. Méndez-López LF. Revisiting Epithelial Carcinogenesis. Int J Mol Sci. 2022;23(13).
20. Bleloch JS, Ballim RD, Kimani S, Parkes J, Panieri E, Willmer T, et al. Managing sarcoma: where have we come from and where are we going? Ther Adv Med Oncol. 2017;9(10):637-59.
21. King RL, Goodlad JR, Calaminici M, Dotlic S, Montes-Moreno S, Oschlies I, et al. Lymphomas arising in immune-privileged sites: insights into biology, diagnosis, and pathogenesis. Virchows Arch. 2020;476(5):647-65.
22. Brown G. Introduction and Classification of Leukemias. In: Cobaleda C, Sánchez-García I, editors. Leukemia Stem Cells: Methods and Protocols. New York, NY: Springer US; 2021. p. 3-23.

23. Abduh MS. An overview of multiple myeloma: A monoclonal plasma cell malignancy's diagnosis, management, and treatment modalities. Saudi J Biol Sci. 2024;31(2):103920.
24. Gheorghișan-Gălățeanu AA, Ilieșiu A, Lambrescu IM, Țăpoi DA. The Complex Histopathological and Immunohistochemical Spectrum of Neuroendocrine Tumors-An Overview of the Latest Classifications. Int J Mol Sci. 2023;24(2).
25. Hanahan D, Weinberg RA. The hallmarks of cancer. Cell. 2000;100(1):57-70.
26. Hanahan D. Hallmarks of Cancer: New Dimensions. Cancer Discovery. 2022;12(1):31-46.
27. Tinto K, Cunningham M, Plevin R. Double trouble: cytosolic and nuclear IKKα in cancer. Open Biology. 2025;15(8):240375.
28. Turlej E, Domaradzka A, Radzka J, Drulis-Fajdasz D, Kulbacka J, Gizak A. Cross-Talk Between Cancer and Its Cellular Environment-A Role in Cancer Progression. Cells. 2025;14(6).
29. Anderson NM, Simon MC. The tumor microenvironment. Curr Biol. 2020;30(16):R921-r5.
30. De Palma M, Biziato D, Petrova TV. Microenvironmental regulation of tumour angiogenesis. Nature Reviews Cancer. 2017;17(8):457-74.
31. Otrock ZK, Mahfouz RAR, Makarem JA, Shamseddine AI. Understanding the biology of angiogenesis: Review of the most important molecular mechanisms. Blood Cells, Molecules, and Diseases. 2007;39(2):212-20.
32. Teleanu RI, Chircov C, Grumezescu AM, Teleanu DM. Tumor Angiogenesis and Anti-Angiogenic Strategies for Cancer Treatment. J Clin Med. 2019;9(1).
33. Lan H, Liu H, Hou H, Zhang C, Zhu J, Zhou N, et al. Combination of anlotinib with immunotherapy enhanced both anti-angiogenesis and immune response in high-grade serous ovarian cancer. Front Immunol. 2025;16:1539616.
34. Sleeboom JJF, van Tienderen GS, Schenke-Layland K, van der Laan LJW, Khalil AA, Verstegen MMA. The extracellular matrix as hallmark of cancer and metastasis: From biomechanics to therapeutic targets. Sci Transl Med. 2024;16(728):eadg3840.
35. Yang Q, Guo N, Zhou Y, Chen J, Wei Q, Han M. The role of tumor-associated macrophages (TAMs) in tumor progression and relevant advance in targeted therapy. Acta Pharm Sin B. 2020;10(11):2156-70.
36. Kazakova A, Sudarskikh T, Kovalev O, Kzhyshkowska J, Larionova I. Interaction of tumor-associated macrophages with stromal and immune components in solid tumors: Research progress (Review). Int J Oncol. 2023;62(2).
37. Fellhofer-Hofer J, Franz C, Vey JA, Kahlert C, Kalkum E, Mehrabi A, et al. Chemokines as Prognostic Factor in Colorectal Cancer Patients: A Systematic Review and Meta-Analysis. Int J Mol Sci. 2024;25(10).
38. Xavier H, Gireesh AGM, Thomas JA, Suboj P, Suresh A, Biju E, et al. Chemokines: humble yet mighty players in the tumour microenvironment. Front Immunol. 2025;16:1601756.
39. Griffith JW, Sokol CL, Luster AD. Chemokines and chemokine receptors: positioning cells for host defense and immunity. Annu Rev Immunol. 2014;32:659-702.
40. Li H, Wu M, Zhao X. Role of chemokine systems in cancer and inflammatory diseases. MedComm (2020). 2022;3(2):e147.
41. Torphy RJ, Yee EJ, Schulick RD, Zhu Y. Atypical chemokine receptors: emerging therapeutic targets in cancer. Trends Pharmacol Sci. 2022;43(12):1085-97.
42. Miller MC, Mayo KH. Chemokines from a Structural Perspective. Int J Mol Sci. 2017;18(10).
43. Andre F, Cabioglu N, Assi H, Sabourin JC, Delaloge S, Sahin A, et al. Expression of chemokine receptors predicts the site of metastatic relapse in patients with axillary node positive primary breast cancer. Annals of Oncology. 2006;17(6):945-51.
44. Wu T, Yang W, Sun A, Wei Z, Lin Q. The Role of CXC Chemokines in Cancer Progression. Cancers (Basel). 2022;15(1).
45. Rajagopalan L, Rajarathnam K. Ligand selectivity and affinity of chemokine receptor CXCR1. Role of N-terminal domain. J Biol Chem. 2004;279(29):30000-8.

46. Korbecki J, Kupnicka P, Chlubek M, Gorący J, Gutowska I, Baranowska-Bosiacka I. CXCR2 Receptor: Regulation of Expression, Signal Transduction, and Involvement in Cancer. Int J Mol Sci. 2022;23(4).
47. Shen Y, Zhou C, Cao Y, Li Q, Deng H, Gu S, et al. Expression profile and prognostic value of CXCR family members in head and neck squamous cell carcinoma. World J Surg Oncol. 2022;20(1):259.
48. Loetscher M, Gerber B, Loetscher P, Jones SA, Piali L, Clark-Lewis I, et al. Chemokine receptor specific for IP10 and mig: structure, function, and expression in activated T-lymphocytes. J Exp Med. 1996;184(3):963-9.
49. Gao Q, Zhang Y. CXCL11 Signaling in the Tumor Microenvironment. Adv Exp Med Biol. 2021;1302:41-50.
50. Butler KL, Clancy-Thompson E, Mullins DW. CXCR3+ monocytes/macrophages are required for establishment of pulmonary metastases. Scientific Reports. 2017;7(1):45593.
51. Groom JR, Luster AD. CXCR3 in T cell function. Exp Cell Res. 2011;317(5):620-31.
52. Moreno Ayala MA, Campbell TF, Zhang C, Dahan N, Bockman A, Prakash V, et al. CXCR3 expression in regulatory T cells drives interactions with type I dendritic cells in tumors to restrict CD8(+) T cell antitumor immunity. Immunity. 2023;56(7):1613-30.e5.
53. Wang X, Zhang Y, Wang S, Ni H, Zhao P, Chen G, et al. The role of CXCR3 and its ligands in cancer. Front Oncol. 2022;12:1022688.
54. Guo F, Wang Y, Liu J, Mok SC, Xue F, Zhang W. CXCL12/CXCR4: a symbiotic bridge linking cancer cells and their stromal neighbors in oncogenic communication networks. Oncogene. 2016;35(7):816-26.
55. Santagata S, Ieranò C, Trotta AM, Capiluongo A, Auletta F, Guardascione G, et al. CXCR4 and CXCR7 Signaling Pathways: A Focus on the Cross-Talk Between Cancer Cells and Tumor Microenvironment. Front Oncol. 2021;11:591386.
56. Nie Y, Waite J, Brewer F, Sunshine MJ, Littman DR, Zou YR. The role of CXCR4 in maintaining peripheral B cell compartments and humoral immunity. J Exp Med. 2004;200(9):1145-56.
57. Caulfield J, Fernandez M, Snetkov V, Lee T, Hawrylowicz C. CXCR4 expression on monocytes is up-regulated by dexamethasone and is modulated by autologous CD3+ T cells. Immunology. 2002;105(2):155-62.
58. Weng AP, Shahsafaei A, Dorfman DM. CXCR4/CD184 immunoreactivity in T-cell non-Hodgkin lymphomas with an overall Th1- Th2+ immunophenotype. Am J Clin Pathol. 2003;119(3):424-30.
59. Ogawa T, Maki Y, Takahashi S, Ono T, Sato K, Kawana A, et al. Airway Epithelium-derived CXCL14 Promotes Eosinophil Accumulation in Allergic Airway Inflammation. Am J Respir Cell Mol Biol. 2024.
60. Kazanietz MG, Durando M, Cooke M. CXCL13 and Its Receptor CXCR5 in Cancer: Inflammation, Immune Response, and Beyond. Front Endocrinol (Lausanne). 2019;10:471.
61. Pabst O, Herbrand H, Bernhardt G, Förster R. Elucidating the functional anatomy of secondary lymphoid organs. Current Opinion in Immunology. 2004;16(4):394-9.
62. Schmutz C, Hulme A, Burman A, Salmon M, Ashton B, Buckley C, et al. Chemokine receptors in the rheumatoid synovium: upregulation of CXCR5. Arthritis Res Ther. 2004;7(2):R217.
63. Matloubian M, David A, Engel S, Ryan JE, Cyster JG. A transmembrane CXC chemokine is a ligand for HIV-coreceptor Bonzo. Nature Immunology. 2000;1(4):298-304.
64. Mabrouk N, Tran T, Sam I, Pourmir I, Gruel N, Granier C, et al. CXCR6 expressing T cells: Functions and role in the control of tumors. Front Immunol. 2022;13:1022136.
65. Paust S, Gill HS, Wang BZ, Flynn MP, Moseman EA, Senman B, et al. Critical role for the chemokine receptor CXCR6 in NK cell-mediated antigen-specific memory of haptens and viruses. Nat Immunol. 2010;11(12):1127-35.
66. Bachelerie F, Ben-Baruch A, Burkhardt AM, Combadiere C, Farber JM, Graham GJ, et al. International Union of Basic and Clinical Pharmacology. [corrected]. LXXXIX. Update on the extended

family of chemokine receptors and introducing a new nomenclature for atypical chemokine receptors. Pharmacol Rev. 2014;66(1):1-79.
67. Naumann U, Cameroni E, Pruenster M, Mahabaleshwar H, Raz E, Zerwes HG, et al. CXCR7 functions as a scavenger for CXCL12 and CXCL11. PLoS One. 2010;5(2):e9175.
68. Chatterjee M, von Ungern-Sternberg SN, Seizer P, Schlegel F, Büttcher M, Sindhu NA, et al. Platelet-derived CXCL12 regulates monocyte function, survival, differentiation into macrophages and foam cells through differential involvement of CXCR4-CXCR7. Cell Death Dis. 2015;6(11):e1989.
69. Maravillas-Montero JL, Burkhardt AM, Hevezi PA, Carnevale CD, Smit MJ, Zlotnik A. Cutting edge: GPR35/CXCR8 is the receptor of the mucosal chemokine CXCL17. J Immunol. 2015;194(1):29-33.
70. Ponzetti M, Rucci N. Osteoblast Differentiation and Signaling: Established Concepts and Emerging Topics. Int J Mol Sci. 2021;22(13).
71. Kansara M, Teng MW, Smyth MJ, Thomas DM. Translational biology of osteosarcoma. Nat Rev Cancer. 2014;14(11):722-35.
72. Hasegawa T, Ishii M. Pathological Osteoclasts and Precursor Macrophages in Inflammatory Arthritis. Front Immunol. 2022;13:867368.
73. Kim JM, Lin C, Stavre Z, Greenblatt MB, Shim JH. Osteoblast-Osteoclast Communication and Bone Homeostasis. Cells. 2020;9(9).
74. Yang D, Wan Y. Molecular determinants for the polarization of macrophage and osteoclast. Semin Immunopathol. 2019;41(5):551-63.
75. Huang X, Wang L, Guo H, Zhang W. Single-cell RNA sequencing reveals SERPINE1-expressing CAFs remodelling tumour microenvironment in recurrent osteosarcoma. Clin Transl Med. 2024;14(1):e1527.
76. Beird HC, Bielack SS, Flanagan AM, Gill J, Heymann D, Janeway KA, et al. Osteosarcoma. Nature Reviews Disease Primers. 2022;8(1):77.
77. Endo-Munoz L, Cumming A, Sommerville S, Dickinson I, Saunders NA. Osteosarcoma is characterised by reduced expression of markers of osteoclastogenesis and antigen presentation compared with normal bone. Br J Cancer. 2010;103(1):73-81.
78. Jones KB. Osteosarcomagenesis: modeling cancer initiation in the mouse. Sarcoma. 2011;2011:694136.
79. Ottaviani G, Jaffe N. The epidemiology of osteosarcoma. Cancer Treat Res. 2009;152:3-13.
80. Luetke A, Meyers PA, Lewis I, Juergens H. Osteosarcoma treatment - where do we stand? A state of the art review. Cancer Treat Rev. 2014;40(4):523-32.
81. Ottaviani G, Jaffe N. The Epidemiology of Osteosarcoma. In: Jaffe N, Bruland OS, Bielack S, editors. Pediatric and Adolescent Osteosarcoma. Boston, MA: Springer US; 2010. p. 3-13.
82. Mirabello L, Troisi RJ, Savage SA. Osteosarcoma incidence and survival rates from 1973 to 2004: data from the Surveillance, Epidemiology, and End Results Program. Cancer. 2009;115(7):1531-43.
83. Xin S, Wei G. Prognostic factors in osteosarcoma: A study level meta-analysis and systematic review of current practice. J Bone Oncol. 2020;21:100281.
84. Fu P, Shi Y, Chen G, Fan Y, Gu Y, Gao Z. Prognostic Factors in Patients With Osteosarcoma With the Surveillance, Epidemiology, and End Results Database. Technol Cancer Res Treat. 2020;19:1533033820947701.
85. Yao Z, Tan Z, Yang J, Yang Y, Wang C, Chen J, et al. Prognostic nomogram for predicting 5-year overall survival in Chinese patients with high-grade osteosarcoma. Scientific Reports. 2021;11(1):17728.
86. Jafari F, Javdansirat S, Sanaie S, Naseri A, Shamekh A, Rostamzadeh D, et al. Osteosarcoma: A comprehensive review of management and treatment strategies. Ann Diagn Pathol. 2020;49:151654.
87. Xiang Y, Yang Y, Liu J, Yang X. Functional role of MicroRNA/PI3K/AKT axis in osteosarcoma. Front Oncol. 2023;13:1219211.

88. Bodmer N, Hecker-Nolting S, Friedel G, Blattmann C, Kager L, Kessler T, et al. Primary osteosarcoma of the ribs: A report from the Cooperative Osteosarcoma Study Group. Cancer. 2023;129(12):1895-903.
89. Gianferante DM, Mirabello L, Savage SA. Germline and somatic genetics of osteosarcoma — connecting aetiology, biology and therapy. Nature Reviews Endocrinology. 2017;13(8):480-91.
90. Kovar H, Bierbaumer L, Radic-Sarikas B. The YAP/TAZ Pathway in Osteogenesis and Bone Sarcoma Pathogenesis. Cells. 2020;9(4).
91. Bjørnland K, Flatmark K, Pettersen S, Aaasen AO, Fodstad Ø, Mælandsmo GM. Matrix Metalloproteinases Participate in Osteosarcoma Invasion. Journal of Surgical Research. 2005;127(2):151-6.
92. Garcia-Ortega DY, Cabrera-Nieto SA, Caro-Sánchez HS, Cruz-Ramos M. An overview of resistance to chemotherapy in osteosarcoma and future perspectives. Cancer Drug Resist. 2022;5(3):762-93.
93. Cui J, Dean D, Hornicek FJ, Chen Z, Duan Z. The role of extracelluar matrix in osteosarcoma progression and metastasis. J Exp Clin Cancer Res. 2020;39(1):178.
94. Dang H, Wu W, Wang B, Cui C, Niu J, Chen J, et al. CXCL5 Plays a Promoting Role in Osteosarcoma Cell Migration and Invasion in Autocrine- and Paracrine-Dependent Manners. Oncol Res. 2017;25(2):177-86.
95. Chao CC, Lee CW, Chang TM, Chen PC, Liu JF. CXCL1/CXCR2 Paracrine Axis Contributes to Lung Metastasis in Osteosarcoma. Cancers (Basel). 2020;12(2).
96. Jiang H, Wang X, Miao W, Wang B, Qiu Y. CXCL8 promotes the invasion of human osteosarcoma cells by regulation of PI3K/Akt signaling pathway. Apmis. 2017;125(9):773-80.
97. Yang D, Liu J. Neutrophil Extracellular Traps: A New Player in Cancer Metastasis and Therapeutic Target. J Exp Clin Cancer Res. 2021;40(1):233.
98. Ohms M, Möller S, Laskay T. An Attempt to Polarize Human Neutrophils Toward N1 and N2 Phenotypes in vitro. Front Immunol. 2020;11:532.
99. Tang H, Xie J, Du YX, Tan ZJ, Liang ZT. Osteosarcoma neutrophil extracellular trap network-associated gene recurrence and metastasis model. J Cancer Res Clin Oncol. 2024;150(2):48.
100. Khare T, Bissonnette M, Khare S. CXCL12-CXCR4/CXCR7 Axis in Colorectal Cancer: Therapeutic Target in Preclinical and Clinical Studies. Int J Mol Sci. 2021;22(14).
101. Janssens R, Struyf S, Proost P. The unique structural and functional features of CXCL12. Cell Mol Immunol. 2018;15(4):299-311.
102. Shi Y, Riese DJ, 2nd, Shen J. The Role of the CXCL12/CXCR4/CXCR7 Chemokine Axis in Cancer. Front Pharmacol. 2020;11:574667.
103. Kusuma I, Yapson GYA, Nolan J, Wiratnaya IGE, Supadmanaba IGP. Clinicopathological and prognostic significance of CXCR4 expression in osteosarcoma: a meta-analysis. Biomedicine (Taipei). 2022;12(4):34-43.
104. Twenhafel L, Moreno D, Punt T, Kinney M, Ryznar R. Epigenetic Changes Associated with Osteosarcoma: A Comprehensive Review. Cells. 2023;12(12).
105. Katsianou MA, Andreou D, Korkolopoulou P, Vetsika E-K, Piperi C. Epigenetic Modifications in Osteosarcoma: Mechanisms and Therapeutic Strategies. Life [Internet]. 2025; 15(8).
106. Velletri T, Xie N, Wang Y, Huang Y, Yang Q, Chen X, et al. P53 functional abnormality in mesenchymal stem cells promotes osteosarcoma development. Cell Death Dis. 2016;7(1):e2015.
107. Czarnecka AM, Synoradzki K, Firlej W, Bartnik E, Sobczuk P, Fiedorowicz M, et al. Molecular Biology of Osteosarcoma. Cancers (Basel). 2020;12(8).
108. Bousquet M, Noirot C, Accadbled F, Sales de Gauzy J, Castex MP, Brousset P, et al. Whole-exome sequencing in osteosarcoma reveals important heterogeneity of genetic alterations. Annals of Oncology. 2016;27(4):738-44.
109. Shen Y, Huang S, Chen G, Wang G, Sui L. Involvement of TP53 in osteosarcoma - challenges and prospects. Front Oncol. 2025;15:1605080.

110. Kleinerman RA, Schonfeld SJ, Tucker MA. Sarcomas in hereditary retinoblastoma. Clin Sarcoma Res. 2012;2(1):15.
111. Ottaviani G, Jaffe N. The Etiology of Osteosarcoma. In: Jaffe N, Bruland OS, Bielack S, editors. Pediatric and Adolescent Osteosarcoma. Boston, MA: Springer US; 2010. p. 15-32.
112. Chen X, Bahrami A, Pappo A, Easton J, Dalton J, Hedlund E, et al. Recurrent Somatic Structural Variations Contribute to Tumorigenesis in Pediatric Osteosarcoma. Cell Reports. 2014;7(1):104-12.
113. Bartholf DeWitt S, Hoskinson Plumlee S, Brighton HE, Sivaraj D, Martz EJ, Zand M, et al. Loss of ATRX promotes aggressive features of osteosarcoma with increased NF-κB signaling and integrin binding. JCI Insight. 2022;7(17).
114. Koelsche C, Schrimpf D, Tharun L, Roth E, Sturm D, Jones DTW, et al. Histone 3.3 hotspot mutations in conventional osteosarcomas: a comprehensive clinical and molecular characterization of six H3F3A mutated cases. Clinical Sarcoma Research. 2017;7(1):9.
115. Shao YW, Wood GA, Lu J, Tang QL, Liu J, Molyneux S, et al. Cross-species genomics identifies DLG2 as a tumor suppressor in osteosarcoma. Oncogene. 2019;38(2):291-8.
116. Chen X, Bahrami A, Pappo A, Easton J, Dalton J, Hedlund E, et al. Recurrent somatic structural variations contribute to tumorigenesis in pediatric osteosarcoma. Cell Rep. 2014;7(1):104-12.
117. Zheng C, Tang F, Min L, Hornicek F, Duan Z, Tu C. PTEN in osteosarcoma: Recent advances and the therapeutic potential. Biochimica et Biophysica Acta (BBA) - Reviews on Cancer. 2020;1874(2):188405.
118. Zhao J, Dean DC, Hornicek FJ, Yu X, Duan Z. Emerging next-generation sequencing-based discoveries for targeted osteosarcoma therapy. Cancer Letters. 2020;474:158-67.
119. Yan T, Wunder JS, Gokgoz N, Gill M, Eskandarian S, Parkes RK, et al. COPS3 amplification and clinical outcome in osteosarcoma. Cancer. 2007;109(9):1870-6.
120. Liu S, Chen Z. The Functional Role of PMP22 Gene in the Proliferation and Invasion of Osteosarcoma. Med Sci Monit. 2015;21:1976-82.
121. van Dartel M, Cornelissen PWA, Redeker S, Tarkkanen M, Knuutila S, Hogendoorn PCW, et al. Amplification of 17p11.2∼p12, including PMP22, TOP3A, and MAPK7, in high-grade osteosarcoma. Cancer Genetics and Cytogenetics. 2002;139(2):91-6.
122. Urban W, Krzystańska D, Piekarz M, Nazar J, Jankowska A. Osteosarcoma's genetic landscape painted by genes' mutations. Acta Biochim Pol. 2023;70(3):671-8.
123. Barøy T, Kresse SH, Skårn M, Stabell M, Castro R, Lauvrak S, et al. Reexpression of LSAMP inhibits tumor growth in a preclinical osteosarcoma model. Molecular Cancer. 2014;13(1):93.
124. Sayles LC, Breese MR, Koehne AL, Leung SG, Lee AG, Liu HY, et al. Genome-Informed Targeted Therapy for Osteosarcoma. Cancer Discov. 2019;9(1):46-63.
125. Xie X, Bian Y, Li H, Yin J, Tian L, Jiang R, et al. A Comprehensive Understanding of the Genomic Bone Tumor Landscape: A Multicenter Prospective Study. Front Oncol. 2022;12:835004.
126. Rickel K, Fang F, Tao J. Molecular genetics of osteosarcoma. Bone. 2017;102:69-79.
127. Carter JM, Inwards CY, Jin L, Evers B, Wenger DE, Oliveira AM, et al. Activating GNAS Mutations in Parosteal Osteosarcoma. The American Journal of Surgical Pathology. 2014;38(3).
128. Salinas-Souza C, De Andrea C, Bihl M, Kovac M, Pillay N, Forshew T, et al. GNAS mutations are not detected in parosteal and low-grade central osteosarcomas. Mod Pathol. 2015;28(10):1336-42.
129. Rubio-San-Simón A, Wilson W, Sironi G, le Deley M-C, Palmerini E, Gaspar N, et al. Prognostic factors in patients with relapsed high-grade osteosarcoma: a systematic review. British Journal of Cancer. 2025.
130. Prudowsky ZD, Yustein JT. Recent Insights into Therapy Resistance in Osteosarcoma. Cancers [Internet]. 2021; 13(1).
131. Nakano K. Challenges of Systemic Therapy Investigations for Bone Sarcomas. International Journal of Molecular Sciences [Internet]. 2022; 23(7).

132. Liang H, Cui M, Tu J, Chen X. Advancements in osteosarcoma management: integrating immune microenvironment insights with immunotherapeutic strategies. Frontiers in Cell and Developmental Biology. 2024;Volume 12 - 2024.
133. Nørregaard KS, Jürgensen HJ, Gårdsvoll H, Engelholm LH, Behrendt N, Søe K. Osteosarcoma and Metastasis Associated Bone Degradation-A Tale of Osteoclast and Malignant Cell Cooperativity. Int J Mol Sci. 2021;22(13).
134. Tulotta C, Lefley DV, Moore CK, Amariutei AE, Spicer-Hadlington AR, Quayle LA, et al. IL-1B drives opposing responses in primary tumours and bone metastases; harnessing combination therapies to improve outcome in breast cancer. npj Breast Cancer. 2021;7(1):95.
135. Coleman RE, Croucher PI, Padhani AR, Clézardin P, Chow E, Fallon M, et al. Bone metastases. Nature Reviews Disease Primers. 2020;6(1):83.
136. Di Paolo NC, Shayakhmetov DM. Interleukin 1α and the inflammatory process. Nat Immunol. 2016;17(8):906-13.
137. Guo C, Yang XG, Wang F, Ma XY. IL-1α induces apoptosis and inhibits the osteoblast differentiation of MC3T3-E1 cells through the JNK and p38 MAPK pathways. Int J Mol Med. 2016;38(1):319-27.
138. Kim JH, Jin HM, Kim K, Song I, Youn BU, Matsuo K, et al. The mechanism of osteoclast differentiation induced by IL-1. J Immunol. 2009;183(3):1862-70.
139. Kamolmatyakul S, Chen W, Yang S, Abe Y, Moroi R, Ashique AM, et al. IL-1alpha stimulates cathepsin K expression in osteoclasts via the tyrosine kinase-NF-kappaB pathway. J Dent Res. 2004;83(10):791-6.
140. Janiszewski T, Kołt S, Ciastoń I, Vizovisek M, Poręba M, Turk B, et al. Investigation of osteoclast cathepsin K activity in osteoclastogenesis and bone loss using a set of chemical reagents. Cell Chem Biol. 2023;30(2):159-74.e8.
141. Tanabe N, Maeno M, Suzuki N, Fujisaki K, Tanaka H, Ogiso B, et al. IL-1 alpha stimulates the formation of osteoclast-like cells by increasing M-CSF and PGE2 production and decreasing OPG production by osteoblasts. Life Sci. 2005;77(6):615-26.
142. Watari K, Shibata T, Kawahara A, Sata K, Nabeshima H, Shinoda A, et al. Tumor-derived interleukin-1 promotes lymphangiogenesis and lymph node metastasis through M2-type macrophages. PLoS One. 2014;9(6):e99568.
143. Kuan EL, Ziegler SF. A tumor-myeloid cell axis, mediated via the cytokines IL-1α and TSLP, promotes the progression of breast cancer. Nat Immunol. 2018;19(4):366-74.
144. León X, Bothe C, García J, Parreño M, Alcolea S, Quer M, et al. Expression of IL-1α correlates with distant metastasis in patients with head and neck squamous cell carcinoma. Oncotarget. 2015;6(35):37398-409.
145. Eder C. Mechanisms of interleukin-1β release. Immunobiology. 2009;214(7):543-53.
146. Sonomoto K, Yamaoka K, Oshita K, Fukuyo S, Zhang X, Nakano K, et al. Interleukin-1β induces differentiation of human mesenchymal stem cells into osteoblasts via the Wnt-5a/receptor tyrosine kinase-like orphan receptor 2 pathway. Arthritis Rheum. 2012;64(10):3355-63.
147. Hengartner N-E, Fiedler J, Ignatius A, Brenner RE. IL-1β Inhibits Human Osteoblast Migration. Molecular Medicine. 2013;19(1):36-42.
148. Nakamura I, Jimi E. Regulation of Osteoclast Differentiation and Function by Interleukin-1. Vitamins & Hormones. 74: Academic Press; 2006. p. 357-70.
149. Cao Y, Jansen ID, Sprangers S, Stap J, Leenen PJ, Everts V, et al. IL-1β differently stimulates proliferation and multinucleation of distinct mouse bone marrow osteoclast precursor subsets. J Leukoc Biol. 2016;100(3):513-23.
150. Polzer K, Joosten L, Gasser J, Distler JH, Ruiz G, Baum W, et al. Interleukin-1 is essential for systemic inflammatory bone loss. Ann Rheum Dis. 2010;69(1):284-90.
151. Han ZP, Liu DB, Wu LQ, Li Q, Wang ZG, Zang XF. IL-1β secreted by macrophage M2 promotes metastasis of osteosarcoma via NF-κB/miR-181α-5p/RASSF1A/Wnt pathway. Transl Cancer Res. 2020;9(4):2721-33.

152. Wang W, Wang Z, Chen S, Zang X, Miao J. Interleukin-1β/nuclear factor-κB signaling promotes osteosarcoma cell growth through the microRNA-181b/phosphatase and tensin homolog axis. J Cell Biochem. 2019;120(2):1763-72.
153. Eyre R, Alférez DG, Santiago-Gómez A, Spence K, McConnell JC, Hart C, et al. Microenvironmental IL1β promotes breast cancer metastatic colonisation in the bone via activation of Wnt signalling. Nat Commun. 2019;10(1):5016.
154. Holen I, Lefley DV, Francis SE, Rennicks S, Bradbury S, Coleman RE, et al. IL-1 drives breast cancer growth and bone metastasis in vivo. Oncotarget. 2016;7(46):75571-84.
155. Landuzzi L, Ruzzi F, Pellegrini E, Lollini PL, Scotlandi K, Manara MC. IL-1 Family Members in Bone Sarcomas. Cells. 2024;13(3).
156. He Y, Liang X, Meng C, Shao Z, Gao Y, Wu Q, et al. Genetic polymorphisms of interleukin-1 beta and osteosarcoma risk. Int Orthop. 2014;38(8):1671-6.
157. Riches DWH, Chan ED, Winston BW. CHAPTER 7 - TNF-α-induced Regulation and Signalling in Macrophages. Immunobiology. 1996;195(4):477-90.
158. Ranta V, Orpana A, Carpén O, Turpeinen U, Ylikorkala O, Viinikka L. Human vascular endothelial cells produce tumor necrosis factor-alpha in response to proinflammatory cytokine stimulation. Crit Care Med. 1999;27(10):2184-7.
159. Mehta AK, Gracias DT, Croft M. TNF activity and T cells. Cytokine. 2018;101:14-8.
160. Hess K, Ushmorov A, Fiedler J, Brenner RE, Wirth T. TNFalpha promotes osteogenic differentiation of human mesenchymal stem cells by triggering the NF-kappaB signaling pathway. Bone. 2009;45(2):367-76.
161. Kitaura H, Kimura K, Ishida M, Kohara H, Yoshimatsu M, Takano-Yamamoto T. Immunological reaction in TNF-α-mediated osteoclast formation and bone resorption in vitro and in vivo. Clin Dev Immunol. 2013;2013:181849.
162. Mori T, Sato Y, Miyamoto K, Kobayashi T, Shimizu T, Kanagawa H, et al. TNFα promotes osteosarcoma progression by maintaining tumor cells in an undifferentiated state. Oncogene. 2014;33(33):4236-41.
163. Ross SH, Cantrell DA. Signaling and Function of Interleukin-2 in T Lymphocytes. Annu Rev Immunol. 2018;36:411-33.
164. Sun H, Zhao Y, Wang K, Zhu L, Dong J, Zhao J, et al. Low dose IL-2 suppress osteoclastogenesis in collagen-induced arthritis via JNK dependent pathway. Immunity, Inflammation and Disease. 2020;8(4):727-35.
165. Guma SR, Lee DA, Yu L, Gordon N, Hughes D, Stewart J, et al. Natural killer cell therapy and aerosol interleukin-2 for the treatment of osteosarcoma lung metastasis. Pediatr Blood Cancer. 2014;61(4):618-26.
166. Meazza C, Cefalo G, Massimino M, Daolio P, Pastorino U, Scanagatta P, et al. Primary metastatic osteosarcoma: results of a prospective study in children given chemotherapy and interleukin-2. Med Oncol. 2017;34(12):191.
167. Khapli SM, Mangashetti LS, Yogesha SD, Wani MR. IL-3 Acts Directly on Osteoclast Precursors and Irreversibly Inhibits Receptor Activator of NF-κB Ligand-Induced Osteoclast Differentiation by Diverting the Cells to Macrophage Lineage1. The Journal of Immunology. 2003;171(1):142-51.
168. Mangi MH, Newland AC. Interleukin-3 in hematology and oncology: current state of knowledge and future directions. Cytokines Cell Mol Ther. 1999;5(2):87-95.
169. Barhanpurkar AP, Gupta N, Srivastava RK, Tomar GB, Naik SP, Joshi SR, et al. IL-3 promotes osteoblast differentiation and bone formation in human mesenchymal stem cells. Biochemical and Biophysical Research Communications. 2012;418(4):669-75.
170. Gupta N, Barhanpurkar AP, Tomar GB, Srivastava RK, Kour S, Pote ST, et al. IL-3 Inhibits Human Osteoclastogenesis and Bone Resorption through Downregulation of c-Fms and Diverts the Cells to Dendritic Cell Lineage. The Journal of Immunology. 2010;185(4):2261-72.
171. Yogesha SD, Khapli SM, Wani MR. Interleukin-3 and Granulocyte-Macrophage Colony-stimulating Factor Inhibits Tumor Necrosis Factor (TNF)-α-induced Osteoclast Differentiation by

Down-regulation of Expression of TNF Receptors 1 and 2*. Journal of Biological Chemistry. 2005;280(12):11759-69.
172. Yogesha SD, Khapli SM, Srivastava RK, Mangashetti LS, Pote ST, Mishra GC, et al. IL-3 inhibits TNF-alpha-induced bone resorption and prevents inflammatory arthritis. J Immunol. 2009;182(1):361-70.
173. Ehrlich LA, Chung HY, Ghobrial I, Choi SJ, Morandi F, Colla S, et al. IL-3 is a potential inhibitor of osteoblast differentiation in multiple myeloma. Blood. 2005;106(4):1407-14.
174. Dr. Feyen JHM, di Padova FE, Trechsel U, Elford P. Interleukin-6 is produced by bone and modulated by parathyroid hormone. Journal of Bone and Mineral Research. 1989;4(4):633-8.
175. Girasole G, Jilka RL, Passeri G, Boswell S, Boder G, Williams DC, et al. 17 beta-estradiol inhibits interleukin-6 production by bone marrow-derived stromal cells and osteoblasts in vitro: a potential mechanism for the antiosteoporotic effect of estrogens. J Clin Invest. 1992;89(3):883-91.
176. O'Brien SA, Zhu M, Zhang W. The Importance of IL-6 in the Development of LAT-Mediated Autoimmunity. The Journal of Immunology. 2015;195(2):695-705.
177. Palmisano B, Riminucci M, Karsenty G. Interleukin-6 signaling in osteoblasts regulates bone remodeling during exercise. Bone. 2023;176:116870.
178. Ishimi Y, Miyaura C, Jin CH, Akatsu T, Abe E, Nakamura Y, et al. IL-6 is produced by osteoblasts and induces bone resorption. J Immunol. 1990;145(10):3297-303.
179. Löwik CW, van der Pluijm G, Bloys H, Hoekman K, Bijvoet OL, Aarden LA, et al. Parathyroid hormone (PTH) and PTH-like protein (PLP) stimulate interleukin-6 production by osteogenic cells: a possible role of interleukin-6 in osteoclastogenesis. Biochem Biophys Res Commun. 1989;162(3):1546-52.
180. Palmqvist P, Persson E, Conaway HH, Lerner UH. IL-6, leukemia inhibitory factor, and oncostatin M stimulate bone resorption and regulate the expression of receptor activator of NF-kappa B ligand, osteoprotegerin, and receptor activator of NF-kappa B in mouse calvariae. J Immunol. 2002;169(6):3353-62.
181. Kudo O, Sabokbar A, Pocock A, Itonaga I, Fujikawa Y, Athanasou NA. Interleukin-6 and interleukin-11 support human osteoclast formation by a RANKL-independent mechanism. Bone. 2003;32(1):1-7.
182. Yoshitake F, Itoh S, Narita H, Ishihara K, Ebisu S. Interleukin-6 directly inhibits osteoclast differentiation by suppressing receptor activator of NF-kappaB signaling pathways. J Biol Chem. 2008;283(17):11535-40.
183. Rahmadiani N, Norahmawati E, Endharti AT, Hambalie AO, Isma SPP. PD-L1, STAT3, IL6, and EGFR Immunoexpressions in High-Grade Osteosarcoma. Adv Orthop. 2024;2024:9036225.
184. Pillai M, Torok-Storb B, Iwata M. Expression and function of IL-7 receptors in marrow stromal cells. Leuk Lymphoma. 2004;45(12):2403-8.
185. Aguila HL, Mun SH, Kalinowski J, Adams DJ, Lorenzo JA, Lee SK. Osteoblast-specific overexpression of human interleukin-7 rescues the bone mass phenotype of interleukin-7-deficient female mice. J Bone Miner Res. 2012;27(5):1030-42.
186. Kim JH, Sim JH, Lee S, Seol MA, Ye SK, Shin HM, et al. Interleukin-7 Induces Osteoclast Formation via STAT5, Independent of Receptor Activator of NF-kappaB Ligand. Front Immunol. 2017;8:1376.
187. Hui X, Farooq MA, Chen Y, Ajmal I, Ren Y, Xue M, et al. A novel strategy of co-expressing CXCR5 and IL-7 enhances CAR-T cell effectiveness in osteosarcoma. Front Immunol. 2024;15:1462076.
188. Kitaura H, Marahleh A, Ohori F, Noguchi T, Shen WR, Qi J, et al. Osteocyte-Related Cytokines Regulate Osteoclast Formation and Bone Resorption. Int J Mol Sci. 2020;21(14).
189. Fong YC, Maa MC, Tsai FJ, Chen WC, Lin JG, Jeng LB, et al. Osteoblast-derived TGF-beta1 stimulates IL-8 release through AP-1 and NF-kappaB in human cancer cells. J Bone Miner Res. 2008;23(6):961-70.

190. Bendre MS, Montague DC, Peery T, Akel NS, Gaddy D, Suva LJ. Interleukin-8 stimulation of osteoclastogenesis and bone resorption is a mechanism for the increased osteolysis of metastatic bone disease. Bone. 2003;33(1):28-37.
191. Liu T, Ma Q, Zhang Y, Wang X, Xu K, Yan K, et al. Self-seeding circulating tumor cells promote the proliferation and metastasis of human osteosarcoma by upregulating interleukin-8. Cell Death Dis. 2019;10(8):575.
192. Iyer SS, Cheng G. Role of interleukin 10 transcriptional regulation in inflammation and autoimmune disease. Crit Rev Immunol. 2012;32(1):23-63.
193. Xiong Y, Yan C, Chen L, Endo Y, Sun Y, Zhou W, et al. IL-10 induces MC3T3-E1 cells differentiation towards osteoblastic fate in murine model. J Cell Mol Med. 2020;24(1):1076-86.
194. Xu LX, Kukita T, Kukita A, Otsuka T, Niho Y, Iijima T. Interleukin-10 selectively inhibits osteoclastogenesis by inhibiting differentiation of osteoclast progenitors into preosteoclast-like cells in rat bone marrow culture system. J Cell Physiol. 1995;165(3):624-9.
195. Nastasi N, Pasha A, Bruno G, Subbiani A, Pietrovito L, Leo A, et al. Blockade of IL-10 Signaling Ensures Mifamurtide Efficacy in Metastatic Osteosarcoma. Cancers (Basel). 2023;15(19).
196. Maier R, Ganu V, Lotz M. Interleukin-11, an inducible cytokine in human articular chondrocytes and synoviocytes, stimulates the production of the tissue inhibitor of metalloproteinases. J Biol Chem. 1993;268(29):21527-32.
197. Hill PA, Tumber A, Papaioannou S, Meikle MC. The Cellular Actions of Interleukin-11 on Bone Resorption in Vitro. Endocrinology. 1998;139(4):1564-72.
198. Kespohl B, Schumertl T, Bertrand J, Lokau J, Garbers C. The cytokine interleukin-11 crucially links bone formation, remodeling and resorption. Cytokine & Growth Factor Reviews. 2021;60:18-27.
199. Girasole G, Passeri G, Jilka RL, Manolagas SC. Interleukin-11: a new cytokine critical for osteoclast development. J Clin Invest. 1994;93(4):1516-24.
200. Liu T, Ma Q, Zhang Y, Ke S, Yan K, Chen X, et al. Interleukin-11 receptor α is overexpressed in human osteosarcoma, and near-infrared-labeled IL-11Rα imaging agent could detect osteosarcoma in mouse tumor xenografts. Tumour Biol. 2015;36(4):2369-75.
201. Lewis VO, Ozawa MG, Deavers MT, Wang G, Shintani T, Arap W, et al. The interleukin-11 receptor alpha as a candidate ligand-directed target in osteosarcoma: consistent data from cell lines, orthotopic models, and human tumor samples. Cancer Res. 2009;69(5):1995-9.
202. Liu J, Cao S, Kim S, Chung EY, Homma Y, Guan X, et al. Interleukin-12: an update on its immunological activities, signaling and regulation of gene expression. Curr Immunol Rev. 2005;1(2):119-37.
203. Ruiz C, Pérez E, García-Martínez O, Díaz-Rodríguez L, Arroyo-Morales M, Reyes-Botella C. Expression of cytokines IL-4, IL-12, IL-15, IL-18, and IFNgamma and modulation by different growth factors in cultured human osteoblast-like cells. J Bone Miner Metab. 2007;25(5):286-92.
204. Nagata N, Kitaura H, Yoshida N, Nakayama K. Inhibition of RANKL-induced osteoclast formation in mouse bone marrow cells by IL-12: involvement of IFN-gamma possibly induced from non-T cell population. Bone. 2003;33(4):721-32.
205. Yoshimatsu M, Kitaura H, Fujimura Y, Kohara H, Morita Y, Yoshida N. IL-12 Inhibits Lipopolysaccharide Stimulated Osteoclastogenesis in Mice. J Immunol Res. 2015;2015:214878.
206. Yoshimatsu M, Kitaura H, Fujimura Y, Eguchi T, Kohara H, Morita Y, et al. IL-12 inhibits TNF-α induced osteoclastogenesis via a T cell-independent mechanism in vivo. Bone. 2009;45(5):1010-6.
207. Zhou Z, Lafleur EA, Koshkina NV, Worth LL, Lester MS, Kleinerman ES. Interleukin-12 up-regulates Fas expression in human osteosarcoma and Ewing's sarcoma cells by enhancing its promoter activity. Mol Cancer Res. 2005;3(12):685-91.
208. de Vries JE. The role of IL-13 and its receptor in allergy and inflammatory responses. J Allergy Clin Immunol. 1998;102(2):165-9.
209. Onoe Y, Miyaura C, Kaminakayashiki T, Nagai Y, Noguchi K, Chen QR, et al. IL-13 and IL-4 inhibit bone resorption by suppressing cyclooxygenase-2-dependent prostaglandin synthesis in osteoblasts. J Immunol. 1996;156(2):758-64.

210. Karamikheirabad M, Zhang J, Ahn AR, Park HS, Park SH, Moon YJ, et al. IL-13Rα2 Is Involved in Resistance to Doxorubicin and Survival of Osteosarcoma Patients. Pharmaceuticals (Basel). 2024;17(11).
211. Perera PY, Lichy JH, Waldmann TA, Perera LP. The role of interleukin-15 in inflammation and immune responses to infection: implications for its therapeutic use. Microbes Infect. 2012;14(3):247-61.
212. Takeda H, Kikuchi T, Soboku K, Okabe I, Mizutani H, Mitani A, et al. Effect of IL-15 and natural killer cells on osteoclasts and osteoblasts in a mouse coculture. Inflammation. 2014;37(3):657-69.
213. Feng S, Madsen SH, Viller NN, Neutzsky-Wulff AV, Geisler C, Karlsson L, et al. Interleukin-15-activated natural killer cells kill autologous osteoclasts via LFA-1, DNAM-1 and TRAIL, and inhibit osteoclast-mediated bone erosion in vitro. Immunology. 2015;145(3):367-79.
214. Lollini PL, Palmieri G, De Giovanni C, Landuzzi L, Nicoletti G, Rossi I, et al. Expression of interleukin 15 (IL-15) in human rhabdomyosarcoma, osteosarcoma and Ewing's sarcoma. Int J Cancer. 1997;71(5):732-6.
215. Rebhun RB, York D, Cruz SM, Judge SJ, Razmara AM, Farley LE, et al. Inhaled recombinant human IL-15 in dogs with naturally occurring pulmonary metastases from osteosarcoma or melanoma: a phase 1 study of clinical activity and correlates of response. Journal for ImmunoTherapy of Cancer. 2022;10(6):e004493.
216. Xu S, Cao X. Interleukin-17 and its expanding biological functions. Cell Mol Immunol. 2010;7(3):164-74.
217. Huang H, Kim HJ, Chang EJ, Lee ZH, Hwang SJ, Kim HM, et al. IL-17 stimulates the proliferation and differentiation of human mesenchymal stem cells: implications for bone remodeling. Cell Death & Differentiation. 2009;16(10):1332-43.
218. Kim HJ, Seo SJ, Kim J-Y, Kim Y-G, Lee Y. IL-17 promotes osteoblast differentiation, bone regeneration, and remodeling in mice. Biochemical and Biophysical Research Communications. 2020;524(4):1044-50.
219. Min HK, Kim S, Lee JY, Kim KW, Lee SH, Kim HR. IL-18 binding protein suppresses IL-17-induced osteoclastogenesis and rectifies type 17 helper T cell / regulatory T cell imbalance in rheumatoid arthritis. J Transl Med. 2021;19(1):392.
220. Yoshimura N, Kariya R, Shimada M, Tateyama M, Matsunaga H, Shibata Y, et al. The IL-17-IL-17RA axis is required to promote osteosarcoma progression in mice. Sci Rep. 2023;13(1):21572.
221. Dinarello CA. Overview of the IL-1 family in innate inflammation and acquired immunity. Immunol Rev. 2018;281(1):8-27.
222. Udagawa N, Horwood NJ, Elliott J, Mackay A, Owens J, Okamura H, et al. Interleukin-18 (interferon-gamma-inducing factor) is produced by osteoblasts and acts via granulocyte/macrophage colony-stimulating factor and not via interferon-gamma to inhibit osteoclast formation. J Exp Med. 1997;185(6):1005-12.
223. Cornish J, Gillespie MT, Callon KE, Horwood NJ, Moseley JM, Reid IR. Interleukin-18 is a novel mitogen of osteogenic and chondrogenic cells. Endocrinology. 2003;144(4):1194-201.
224. Liu S, Liu Y-p, Lv Y, Yao J-L, Yue D-m, Zhang M-y, et al. IL-18 Contributes to Bone Cancer Pain by Regulating Glia Cells and Neuron Interaction. The Journal of Pain. 2018;19(2):186-95.
225. Nakamura Y, Yamada N, Ohyama H, Nakasho K, Nishizawa Y, Okamoto T, et al. Effect of interleukin-18 on metastasis of mouse osteosarcoma cells. Cancer Immunol Immunother. 2006;55(9):1151-8.
226. Hoffman C, Park SH, Daley E, Emson C, Louten J, Sisco M, et al. Interleukin-19: a constituent of the regulome that controls antigen presenting cells in the lungs and airway responses to microbial products. PLoS One. 2011;6(11):e27629.
227. Dai Z, Chen Y, He E, Wang H, Guo W, Wu Z, et al. Interleukin-19 promotes bone resorption by suppressing osteoprotegerin expression in BMSCs in a lipopolysaccharide-induced bone loss mouse model. Bone Joint Res. 2023;12(11):691-701.

228. Tsubaki M, Takeda T, Matsuda T, Yamamoto Y, Higashinaka A, Yamamoto K, et al. Interleukin 19 suppresses RANKL-induced osteoclastogenesis via the inhibition of NF-κB and p38MAPK activation and c-Fos expression in RAW264.7 cells. Cytokine. 2021;144:155591.
229. He Y, Luo W, Liu Y, Wang Y, Ma C, Wu Q, et al. IL-20RB mediates tumoral response to osteoclastic niches and promotes bone metastasis of lung cancer. J Clin Invest. 2022;132(20).
230. Wegenka UM. IL-20: Biological functions mediated through two types of receptor complexes. Cytokine & Growth Factor Reviews. 2010;21(5):353-63.
231. Hsu YH, Chen WY, Chan CH, Wu CH, Sun ZJ, Chang MS. Anti-IL-20 monoclonal antibody inhibits the differentiation of osteoclasts and protects against osteoporotic bone loss. J Exp Med. 2011;208(9):1849-61.
232. Furukawa S, Moriyama M, Miyake K, Nakashima H, Tanaka A, Maehara T, et al. Interleukin-33 produced by M2 macrophages and other immune cells contributes to Th2 immune reaction of IgG4-related disease. Scientific Reports. 2017;7(1):42413.
233. Saidi S, Bouri F, Lencel P, Duplomb L, Baud'huin M, Delplace S, et al. IL-33 is expressed in human osteoblasts, but has no direct effect on bone remodeling. Cytokine. 2011;53(3):347-54.
234. Lima ILA, Macari S, Madeira MFM, Rodrigues LFD, Colavite PM, Garlet GP, et al. Osteoprotective Effects of IL-33/ST2 Link to Osteoclast Apoptosis. The American Journal of Pathology. 2015;185(12):3338-48.
235. Wang S, Zhao G, Zhao S, Qiao Y, Yang H. The Effects of Interleukin-33 (IL-33) on Osteosarcoma Cell Viability, Apoptosis, and Epithelial-Mesenchymal Transition are Mediated Through the PI3K/AKT Pathway. Med Sci Monit. 2020;26:e920766.
236. Armour KJ, Smith NW, Brown BL, Dobson PR. Interleukin-1 beta induces the synthesis of adenylyl cyclase in Swiss 3T3 fibroblasts and MG-63 osteosarcoma cells. Biochem Biophys Res Commun. 1995;212(2):293-9.
237. Dedhar S. Regulation of expression of the cell adhesion receptors, integrins, by recombinant human interleukin-1 beta in human osteosarcoma cells: inhibition of cell proliferation and stimulation of alkaline phosphatase activity. J Cell Physiol. 1989;138(2):291-9.
238. Dedhar S. Signal transduction via the beta 1 integrins is a required intermediate in interleukin-1 beta induction of alkaline phosphatase activity in human osteosarcoma cells. Exp Cell Res. 1989;183(1):207-14.
239. Lee S-K, Gardner AE, Kalinowski JF, Jastrzebski SL, Lorenzo JA. RANKL-stimulated osteoclast-like cell formation in vitro is partially dependent on endogenous interleukin-1 production. Bone. 2006;38(5):678-85.
240. Malik A, Kanneganti TD. Function and regulation of IL-1α in inflammatory diseases and cancer. Immunol Rev. 2018;281(1):124-37.
241. Atkins E, Wood WB, Jr. Studies on the pathogenesis of fever. II. Identification of an endogenous pyrogen in the blood stream following the injection of typhoid vaccine. J Exp Med. 1955;102(5):499-516.
242. Zhang W, Borcherding N, Kolb R. IL-1 Signaling in Tumor Microenvironment. In: Birbrair A, editor. Tumor Microenvironment: The Role of Interleukins – Part A. Cham: Springer International Publishing; 2020. p. 1-23.
243. Tu S, Bhagat G, Cui G, Takaishi S, Kurt-Jones EA, Rickman B, et al. Overexpression of interleukin-1beta induces gastric inflammation and cancer and mobilizes myeloid-derived suppressor cells in mice. Cancer Cell. 2008;14(5):408-19.
244. Achyut BR, Angara K, Jain M, Borin TF, Rashid MH, Iskander ASM, et al. Canonical NFκB signaling in myeloid cells is required for the glioblastoma growth. Sci Rep. 2017;7(1):13754.
245. Atlas THP. IL-1b RNA tissue specificity 2023 [
246. Sen R, Baltimore D. Multiple nuclear factors interact with the immunoglobulin enhancer sequences. Cell. 1986;46(5):705-16.
247. Sen R, Baltimore D. Inducibility of κ immunoglobulin enhancer-binding protein NF-κB by a posttranslational mechanism. Cell. 1986;47(6):921-8.

248. Wang J, Du B. Hsa_circRNA_092488 Exacerbates the Progression of Deep Vein Thrombosis Through the NLRP3/NFkB Signaling Pathway. Turk J Haematol. 2025.
249. Itoh G, Takagane K, Fukushi Y, Kuriyama S, Umakoshi M, Goto A, et al. Cancer-associated fibroblasts educate normal fibroblasts to facilitate cancer cell spreading and T-cell suppression. Mol Oncol. 2022;16(1):166-87.
250. Liu T, Zhang L, Joo D, Sun SC. NF-κB signaling in inflammation. Signal Transduct Target Ther. 2017;2:17023-.
251. Monaco C, Paleolog E. Nuclear factor κB: a potential therapeutic target in atherosclerosis and thrombosis. Cardiovascular Research. 2004;61(4):671-82.
252. Brand K, Page S, Walli AK, Neumeier D, Baeuerle PA. Role of nuclear factor-kappa B in atherogenesis. Exp Physiol. 1997;82(2):297-304.
253. Caster DJ, Powell DW. Precision Targeting of NF-κB Signaling in Lupus Nephritis. Lupus (Los Angel). 2020;6(1).
254. Montano H, Allen IC, Reilly CM. The path less traveled: the non-canonical NF-κB pathway in systemic lupus erythematosus. Front Immunol. 2025;16:1588486.
255. Liao H, Zheng J, Lu J, Shen HL. NF-κB Signaling Pathway in Rheumatoid Arthritis: Mechanisms and Therapeutic Potential. Mol Neurobiol. 2025;62(6):6998-7021.
256. Mukherjee T, Kumar N, Chawla M, Philpott DJ, Basak S. The NF-κB signaling system in the immunopathogenesis of inflammatory bowel disease. Sci Signal. 2024;17(818):eadh1641.
257. Baldwin AS, Jr. The NF-kappa B and I kappa B proteins: new discoveries and insights. Annu Rev Immunol. 1996;14:649-83.
258. Ghosh G, Wang VY. Origin of the Functional Distinctiveness of NF-κB/p52. Front Cell Dev Biol. 2021;9:764164.
259. Hayden MS, Ghosh S. Regulation of NF-κB by TNF family cytokines. Semin Immunol. 2014;26(3):253-66.
260. de Jesús TJ, Ramakrishnan P. NF-κB c-Rel Dictates the Inflammatory Threshold by Acting as a Transcriptional Repressor. iScience. 2020;23(3):100876.
261. Baeuerle PA, Baltimore D. A 65-kappaD subunit of active NF-kappaB is required for inhibition of NF-kappaB by I kappaB. Genes Dev. 1989;3(11):1689-98.
262. Migliazza A, Lombardi L, Rocchi M, Trecca D, Chang C-C, Antonacci R, et al. Heterogeneous Chromosomal Aberrations Generate 3' Truncations of the NFKB2/lyt-10 Gene in Lymphoid Malignancies. Blood. 1994;84(11):3850-60.
263. Blank V, Kourilsky P, Israël A. Cytoplasmic retention, DNA binding and processing of the NF-kappa B p50 precursor are controlled by a small region in its C-terminus. Embo j. 1991;10(13):4159-67.
264. Liou HC, Nolan GP, Ghosh S, Fujita T, Baltimore D. The NF-kappa B p50 precursor, p105, contains an internal I kappa B-like inhibitor that preferentially inhibits p50. Embo j. 1992;11(8):3003-9.
265. Hoffmann A, Natoli G, Ghosh G. Transcriptional regulation via the NF-κB signaling module. Oncogene. 2006;25(51):6706-16.
266. Dobrzanski P, Ryseck RP, Bravo R. Differential interactions of Rel-NF-kappa B complexes with I kappa B alpha determine pools of constitutive and inducible NF-kappa B activity. Embo j. 1994;13(19):4608-16.
267. Ishimaru N, Kishimoto H, Hayashi Y, Sprent J. Regulation of naive T cell function by the NF-κB2 pathway. Nature Immunology. 2006;7(7):763-72.
268. de Wit H, Dokter WH, Koopmans SB, Lummen C, van der Leij M, Smit JW, et al. Regulation of p100 (NFKB2) expression in human monocytes in response to inflammatory mediators and lymphokines. Leukemia. 1998;12(3):363-70.
269. Matsusaka T, Fujikawa K, Nishio Y, Mukaida N, Matsushima K, Kishimoto T, et al. Transcription factors NF-IL6 and NF-kappa B synergistically activate transcription of the inflammatory cytokines, interleukin 6 and interleukin 8. Proc Natl Acad Sci U S A. 1993;90(21):10193-7.

270. Yu H, Lin L, Zhang Z, Zhang H, Hu H. Targeting NF-κB pathway for the therapy of diseases: mechanism and clinical study. Signal Transduction and Targeted Therapy. 2020;5(1):209.
271. Ishikawa H, Carrasco D, Claudio E, Ryseck RP, Bravo R. Gastric hyperplasia and increased proliferative responses of lymphocytes in mice lacking the COOH-terminal ankyrin domain of NF-kappaB2. J Exp Med. 1997;186(7):999-1014.
272. Bours V, Franzoso G, Azarenko V, Park S, Kanno T, Brown K, et al. The oncoprotein Bcl-3 directly transactivates through κB motifs via association with DNA-binding p50B homodimers. Cell. 1993;72(5):729-39.
273. Basak S, Behar M, Hoffmann A. Lessons from mathematically modeling the NF-κB pathway. Immunol Rev. 2012;246(1):221-38.
274. Hoffmann A, Levchenko A, Scott ML, Baltimore D. The IkappaB-NF-kappaB signaling module: temporal control and selective gene activation. Science. 2002;298(5596):1241-5.
275. Mulero MC, Huxford T, Ghosh G. NF-κB, IκB, and IKK: Integral Components of Immune System Signaling. In: Jin T, Yin Q, editors. Structural Immunology. Singapore: Springer Singapore; 2019. p. 207-26.
276. Prescott JA, Balmanno K, Mitchell JP, Okkenhaug H, Cook SJ. IKKα plays a major role in canonical NF-κB signalling in colorectal cells. Biochem J. 2022;479(3):305-25.
277. Fitzgerald KA, McWhirter SM, Faia KL, Rowe DC, Latz E, Golenbock DT, et al. IKKepsilon and TBK1 are essential components of the IRF3 signaling pathway. Nat Immunol. 2003;4(5):491-6.
278. Lee KJ, Lee H, Joo CH. Negative Regulation of IKKε-Mediated IRF7 Phosphorylation by HSP70. J Immunol. 2020;204(9):2562-74.
279. Polley S, Passos Dario O, Huang D-B, Mulero Maria C, Mazumder A, Biswas T, et al. Structural Basis for the Activation of IKK1/α. Cell Reports. 2016;17(8):1907-14.
280. Zhang J, Zhang R, Li W, Ma XC, Qiu F, Sun CP. IκB kinase β (IKKβ): Structure, transduction mechanism, biological function, and discovery of its inhibitors. Int J Biol Sci. 2023;19(13):4181-203.
281. Page A, Ortega A, Alameda JP, Navarro M, Paramio JM, Saiz-Pardo M, et al. IKKα Promotes the Progression and Metastasis of Non-Small Cell Lung Cancer Independently of its Subcellular Localization. Comput Struct Biotechnol J. 2019;17:251-62.
282. Liu T, Zhang L, Joo D, Sun S-C. NF-κB signaling in inflammation. Signal Transduction and Targeted Therapy. 2017;2(1):17023.
283. Hai ping P, Feng bo T, Li L, Nan hui Y, Hong Z. IL-1β/NF-kb signaling promotes colorectal cancer cell growth through miR-181a/PTEN axis. Archives of Biochemistry and Biophysics. 2016;604:20-6.
284. Le Negrate G. Viral interference with innate immunity by preventing NF-κB activity. Cell Microbiol. 2012;14(2):168-81.
285. Kajino T, Ren H, Iemura S-i, Natsume T, Stefansson B, Brautigan DL, et al. Protein Phosphatase 6 Down-regulates TAK1 Kinase Activation in the IL-1 Signaling Pathway*. Journal of Biological Chemistry. 2006;281(52):39891-6.
286. Adli M, Merkhofer E, Cogswell P, Baldwin AS. IKKalpha and IKKbeta each function to regulate NF-kappaB activation in the TNF-induced/canonical pathway. PLoS One. 2010;5(2):e9428.
287. Sun SC. The noncanonical NF-κB pathway. Immunol Rev. 2012;246(1):125-40.
288. Xiao G, Harhaj EW, Sun S-C. NF-κB-Inducing Kinase Regulates the Processing of NF-κB2 p100. Molecular Cell. 2001;7(2):401-9.
289. Xiao G, Fong A, Sun S-C. Induction of p100 Processing by NF-κB-inducing Kinase Involves Docking IκB Kinase α (IKKα) to p100 and IKKα-mediated Phosphorylation*. Journal of Biological Chemistry. 2004;279(29):30099-105.
290. Sun SC. The non-canonical NF-κB pathway in immunity and inflammation. Nat Rev Immunol. 2017;17(9):545-58.
291. Weih DS, Yilmaz ZB, Weih F. Essential role of RelB in germinal center and marginal zone formation and proper expression of homing chemokines. J Immunol. 2001;167(4):1909-19.

292. Lu X, Chen Q, Liu H, Zhang X. Interplay Between Non-Canonical NF-κB Signaling and Hepatitis B Virus Infection. Front Immunol. 2021;12:730684.
293. Mackay F, Mackay CR. The role of BAFF in B-cell maturation, T-cell activation and autoimmunity. Trends Immunol. 2002;23(3):113-5.
294. Ryu HM, Park SG, Yea SS, Jang WH, Yang YI, Jung G. Gene expression analysis of primary normal human hepatocytes infected with human hepatitis B virus. World J Gastroenterol. 2006;12(31):4986-95.
295. Davis JL, Cox L, Shao C, Lyu C, Liu S, Aurora R, et al. Conditional Activation of NF-κB Inducing Kinase (NIK) in the Osteolineage Enhances Both Basal and Loading-Induced Bone Formation. J Bone Miner Res. 2019;34(11):2087-100.
296. McIntosh K, Khalaf YH, Craig R, West C, McCulloch A, Waghmare A, et al. IL-1β stimulates a novel, IKKα -dependent, NIK -independent activation of non-canonical NFκB signalling. Cell Signal. 2023;107:110684.
297. Li R, Shi Y, Zhao S, Shi T, Zhang G. NF-κB signaling and integrin-β1 inhibition attenuates osteosarcoma metastasis via increased cell apoptosis. International Journal of Biological Macromolecules. 2019;123:1035-43.
298. Gong T, Su X, Xia Q, Wang J, Kan S. Expression of NF-κB and PTEN in osteosarcoma and its clinical significance. Oncol Lett. 2017;14(6):6744-8.
299. Zhong C, Yang D, Zhong L, Xie W, Sun G, Jin D, et al. Single-cell and bulk RNA sequencing reveals Anoikis related genes to guide prognosis and immunotherapy in osteosarcoma. Scientific Reports. 2023;13(1):20203.
300. Wang Y, Qin D, Gao Y, Zhang Y, Liu Y, Huang L. Identification of therapeutic targets for osteosarcoma by integrating single-cell RNA sequencing and network pharmacology. Front Pharmacol. 2022;13:1098800.
301. Tang QL, Xie XB, Wang J, Chen Q, Han AJ, Zou CY, et al. Glycogen synthase kinase-3β, NF-κB signaling, and tumorigenesis of human osteosarcoma. J Natl Cancer Inst. 2012;104(10):749-63.
302. Tissue expression of CHUK - Summary - The Human Protein Atlas. [Available from: https://www.proteinatlas.org/ENSG00000213341-CHUK/tissue.
303. Colomer C, Pecharroman I, Bigas A, Espinosa L. Targeting IKKα kinase to prevent tumor progression and therapy resistance. Cancer Drug Resist. 2020;3(3):482-90.
304. Anzalone G, Albano GD, Montalbano AM, Riccobono L, Bonanno A, Gagliardo R, et al. IL-17A-associated IKK-α signaling induced TSLP production in epithelial cells of COPD patients. Exp Mol Med. 2018;50(10):1-12.
305. Leopizzi M, Cocchiola R, Milanetti E, Raimondo D, Politi L, Giordano C, et al. IKKα inibition by a glucosamine derivative enhances Maspin expression in osteosarcoma cell line. Chem Biol Interact. 2017;262:19-28.
306. Huang W-C, Hung M-C. Beyond NF-κB activation: nuclear functions of IκB kinase α. Journal of Biomedical Science. 2013;20(1):3.
307. Colomer C, Margalef P, Villanueva A, Vert A, Pecharroman I, Solé L, et al. IKKα Kinase Regulates the DNA Damage Response and Drives Chemo-resistance in Cancer. Mol Cell. 2019;75(4):669-82.e5.
308. Liao Y, Hua Y, Li Y, Zhang C, Yu W, Guo P, et al. CRSP8 promotes thyroid cancer progression by antagonizing IKKα-induced cell differentiation. Cell Death Differ. 2021;28(4):1347-63.
309. Lv S, Wang F, Wang K, Fan Y, Xu J, Zheng J, et al. IκB kinase α: an independent prognostic factor that promotes the migration and invasion of oral squamous cell carcinoma. Br J Oral Maxillofac Surg. 2020;58(3):296-303.
310. Dejardin E, Bonizzi G, Bellahcène A, Castronovo V, Merville MP, Bours V. Highly-expressed p100/p52 (NFKB2) sequesters other NF-kappa B-related proteins in the cytoplasm of human breast cancer cells. Oncogene. 1995;11(9):1835-41.
311. Wang H, Zhang M, Xu X, Hou S, Liu Z, Chen X, et al. IKKα mediates UVB-induced cell apoptosis by regulating p53 pathway activation. Ecotoxicol Environ Saf. 2021;227:112892.

312. Luo J-L, Tan W, Ricono JM, Korchynskyi O, Zhang M, Gonias SL, et al. Nuclear cytokine-activated IKKα controls prostate cancer metastasis by repressing Maspin. Nature. 2007;446(7136):690-4.
313. Kwak YT, Li R, Becerra CR, Tripathy D, Frenkel EP, Verma UN. IkappaB kinase alpha regulates subcellular distribution and turnover of cyclin D1 by phosphorylation. J Biol Chem. 2005;280(40):33945-52.
314. Michalides R, van Tinteren H, Balkenende A, Vermorken JB, Benraadt J, Huldij J, et al. Cyclin A is a prognostic indicator in early stage breast cancer with and without tamoxifen treatment. Br J Cancer. 2002;86(3):402-8.
315. Gautschi O, Ratschiller D, Gugger M, Betticher DC, Heighway J. Cyclin D1 in non-small cell lung cancer: a key driver of malignant transformation. Lung Cancer. 2007;55(1):1-14.
316. Chen S, Li L. Degradation strategy of cyclin D1 in cancer cells and the potential clinical application. Front Oncol. 2022;12:949688.
317. Musgrove EA, Caldon CE, Barraclough J, Stone A, Sutherland RL. Cyclin D as a therapeutic target in cancer. Nat Rev Cancer. 2011;11(8):558-72.
318. Ka Ho H, Plevin R, Mackay S, Paul A. 193 A Novel First in Class IKK Alpha Inhibitor Abrogates Endothelial Cell Nuclear Factor Kappa B Signalling and Inflammatory Protein Expression. Heart. 2014;100(Suppl 3):A107-A.
319. Kenkre JS, Bassett J. The bone remodelling cycle. Ann Clin Biochem. 2018;55(3):308-27.
320. Hadjidakis DJ, Androulakis, II. Bone remodeling. Ann N Y Acad Sci. 2006;1092:385-96.
321. Garbe LR, Monges GM, Pellegrin EM, Payan HL. Ultrastructural study of osteosarcomas. Hum Pathol. 1981;12(10):891-6.
322. Kort WJ, Hülsmann WC, Stehman TEM. Modulation of metastatic ability by inhibition of cholesterol synthesis. Clinical & Experimental Metastasis. 1989;7(5):517-23.
323. Feng J, Zhang J, Chen Y. Prognostic value of a glycolysis and cholesterol synthesis related gene signature in osteosarcoma: implications for immune microenvironment and personalized treatment strategies. Oncologie. 2024;26(2):301-10.
324. Li Y, Xian M, Yang B, Ying M, He Q. Inhibition of KLF4 by Statins Reverses Adriamycin-Induced Metastasis and Cancer Stemness in Osteosarcoma Cells. Stem Cell Reports. 2017;8(6):1617-29.
325. Tsushima H, Tang YJ, Puviindran V, Hsu SC, Nadesan P, Yu C, et al. Intracellular biosynthesis of lipids and cholesterol by Scap and Insig in mesenchymal cells regulates long bone growth and chondrocyte homeostasis. Development. 2018;145(13).
326. Xu S, Tang C. Cholesterol and Hedgehog Signaling: Mutual Regulation and Beyond. Front Cell Dev Biol. 2022;10:774291.
327. Yao Z, Han L, Chen Y, He F, Sun B, kamar S, et al. Hedgehog signalling in the tumourigenesis and metastasis of osteosarcoma, and its potential value in the clinical therapy of osteosarcoma. Cell Death & Disease. 2018;9(6):701.
328. Nagao-Kitamoto H, Nagata M, Nagano S, Kitamoto S, Ishidou Y, Yamamoto T, et al. GLI2 is a novel therapeutic target for metastasis of osteosarcoma. Int J Cancer. 2015;136(6):1276-84.
329. Xu F, Yan J, Peng Z, Liu J, Li Z. Comprehensive analysis of a glycolysis and cholesterol synthesis-related genes signature for predicting prognosis and immune landscape in osteosarcoma. Front Immunol. 2022;13:1096009.
330. Feng J, Zhang J, Chen Y. Prognostic value of a glycolysis and cholesterol synthesis related gene signature in osteosarcoma: implications for immune microenvironment and personalized treatment strategies. Oncologie. 2023;26(2):301-10.
331. Gibbs RA. The Human Genome Project changed everything. Nat Rev Genet. 2020;21(10):575-6.
332. Gullapalli RR, Desai KV, Santana-Santos L, Kant JA, Becich MJ. Next generation sequencing in clinical medicine: Challenges and lessons for pathology and biomedical informatics. J Pathol Inform. 2012;3:40.

333. Parums DV. Editorial: Twenty Years On from Sequencing the Human Genome, Personalized/Precision Oncology Prepares to Meet the Challenges of Checkpoint Inhibitor Therapy. Med Sci Monit. 2023;29:e940911.
334. Mohammadi MM, Bavi O. DNA sequencing: an overview of solid-state and biological nanopore-based methods. Biophys Rev. 2022;14(1):99-110.
335. Hood L, Rowen L. The Human Genome Project: big science transforms biology and medicine. Genome Med. 2013;5(9):79.
336. Bentley DR. The Human Genome Project--an overview. Med Res Rev. 2000;20(3):189-96.
337. Chatterjee B, Roy P, Sarkar UA, Zhao M, Ratra Y, Singh A, et al. Immune Differentiation Regulator p100 Tunes NF-κB Responses to TNF. Front Immunol. 2019;10:997.
338. Eggers LF, Schwudke D. Liquid Extraction: Folch. In: Wenk MR, editor. Encyclopedia of Lipidomics. Dordrecht: Springer Netherlands; 2016. p. 1-6.
339. Sun SC. Non-canonical NF-κB signaling pathway. Cell Res. 2011;21(1):71-85.
340. Craig R, McIntosh K, Ho Ho K, McCulloch A, Riley C, Lawson C, et al. IL-1β stimulates a novel axis within the NFκB pathway in endothelial cells regulated by IKKα and TAK-1. Biochem Pharmacol. 2025;232:116736.
341. Guo Q, Jin Y, Chen X, Ye X, Shen X, Lin M, et al. NF-κB in biology and targeted therapy: new insights and translational implications. Signal Transduction and Targeted Therapy. 2024;9(1):53.
342. Takeda K, Takeuchi O, Tsujimura T, Itami S, Adachi O, Kawai T, et al. Limb and Skin Abnormalities in Mice Lacking IKKα. Science. 1999;284(5412):313-6.
343. Pasparakis M, Luedde T, Schmidt-Supprian M. Dissection of the NF-κB signalling cascade in transgenic and knockout mice. Cell Death & Differentiation. 2006;13(5):861-72.
344. Liang C, Zhang M, Sun S-C. β-TrCP binding and processing of NF-κB2/p100 involve its phosphorylation at serines 866 and 870. Cellular Signalling. 2006;18(8):1309-17.
345. Moser B, Hochreiter B, Basílio J, Gleitsmann V, Panhuber A, Pardo-Garcia A, et al. The inflammatory kinase IKKα phosphorylates and stabilizes c-Myc and enhances its activity. Mol Cancer. 2021;20(1):16.
346. García-García VA, Alameda JP, Fernández-Aceñero MJ, Navarro M, García-Escudero R, Page A, et al. Nuclear versus cytoplasmic IKKα signaling in keratinocytes leads to opposite skin phenotypes and inflammatory responses, and a different predisposition to cancer. Oncogene. 2025;44(3):165-78.
347. Craig R, McIntosh K, Ho Ho K, McCulloch A, Riley C, Lawson C, et al. IL-1β stimulates a novel axis within the NFκB pathway in endothelial cells regulated by IKKα and TAK-1. Biochemical Pharmacology. 2025;232:116736.
348. Riley C, Ammar U, Alsfouk A, Anthony NG, Baiget J, Berretta G, et al. Design and Synthesis of Novel Aminoindazole-pyrrolo[2,3-b]pyridine Inhibitors of IKKα That Selectively Perturb Cellular Non-Canonical NF-κB Signalling. Molecules. 2024;29(15).
349. Sun W, Ge N, Yu Y, Burlingame S, Li X, Zhang M, et al. Phosphorylation of Thr-516 and Ser-520 in the kinase activation loop of MEKK3 is required for lysophosphatidic acid-mediated optimal IkappaB kinase beta (IKKbeta)/nuclear factor-kappaB (NF-kappaB) activation. J Biol Chem. 2010;285(11):7911-8.
350. Chen TC, Lin KT, Chen CH, Lee SA, Lee PY, Liu YW, et al. Using an in situ proximity ligation assay to systematically profile endogenous protein-protein interactions in a pathway network. J Proteome Res. 2014;13(12):5339-46.
351. Ridder DA, Urbansky LL, Witzel HR, Schindeldecker M, Weinmann A, Berndt K, et al. Transforming Growth Factor-β Activated Kinase 1 (Tak1) Is Activated in Hepatocellular Carcinoma, Mediates Tumor Progression, and Predicts Unfavorable Outcome. Cancers (Basel). 2022;14(2).
352. Widmann C, Sather S, Oyer R, Johnson GL, Dreskin SC. In vitro activity of MEKK2 and MEKK3 in detergents is a function of a valine to serine difference in the catalytic domain. Biochimica et Biophysica Acta (BBA) - Protein Structure and Molecular Enzymology. 2001;1547(1):167-73.

353. Du K, Zhang X, Qin Y, Ma H, Bing C, Deng S, et al. MAP3K13-232aa encoded by circMAP3K13 enhances cisplatin-induced pyroptosis by directly binding to IKKα in gastric adenocarcinoma. Cell Death Dis. 2025;16(1):667.
354. Li Y, Yang J-Y, Xie X, Jie Z, Zhang L, Shi J, et al. Preventing abnormal NF-κB activation and autoimmunity by Otub1-mediated p100 stabilization. Cell Research. 2019;29(6):474-85.
355. Marinis JM, Hutti JE, Homer CR, Cobb BA, Cantley LC, McDonald C, et al. IκB kinase α phosphorylation of TRAF4 downregulates innate immune signaling. Mol Cell Biol. 2012;32(13):2479-89.
356. Xu X, Zhang C, Xu H, Wu L, Hu M, Song L. Autophagic feedback-mediated degradation of IKKα requires CHK1- and p300/CBP-dependent acetylation of p53. Journal of Cell Science. 2020;133(22):jcs246868.
357. Totomoch-Serra A, Marquez MF, Cervantes-Barragán DE. Sanger sequencing as a first-line approach for molecular diagnosis of Andersen-Tawil syndrome. F1000Res. 2017;6:1016.
358. Gao J, Wu H, Shi X, Huo Z, Zhang J, Liang Z. Comparison of Next-Generation Sequencing, Quantitative PCR, and Sanger Sequencing for Mutation Profiling of EGFR, KRAS, PIK3CA and BRAF in Clinical Lung Tumors. Clin Lab. 2016;62(4):689-96.
359. Rabbani B, Nakaoka H, Akhondzadeh S, Tekin M, Mahdieh N. Next generation sequencing: implications in personalized medicine and pharmacogenomics. Mol Biosyst. 2016;12(6):1818-30.
360. Roh SW, Abell GC, Kim KH, Nam YD, Bae JW. Comparing microarrays and next-generation sequencing technologies for microbial ecology research. Trends Biotechnol. 2010;28(6):291-9.
361. McCombie WR, McPherson JD, Mardis ER. Next-Generation Sequencing Technologies. Cold Spring Harb Perspect Med. 2019;9(11).
362. Mahajan MC, McLellan AS. Whole-Exome Sequencing (WES) for Illumina Short Read Sequencers Using Solution-Based Capture. Methods Mol Biol. 2020;2076:85-108.
363. Liu L, Li Y, Li S, Hu N, He Y, Pong R, et al. Comparison of next-generation sequencing systems. J Biomed Biotechnol. 2012;2012:251364.
364. van Dijk EL, Auger H, Jaszczyszyn Y, Thermes C. Ten years of next-generation sequencing technology. Trends in Genetics. 2014;30(9):418-26.
365. Koteluk O, Bielicka A, Lemańska Ż, Jóźwiak K, Klawiter W, Mackiewicz A, et al. The Landscape of Transmembrane Protein Family Members in Head and Neck Cancers: Their Biological Role and Diagnostic Utility. Cancers (Basel). 2021;13(19).
366. Rocha SF, Schiller M, Jing D, Li H, Butz S, Vestweber D, et al. Esm1 modulates endothelial tip cell behavior and vascular permeability by enhancing VEGF bioavailability. Circ Res. 2014;115(6):581-90.
367. Goettsch C, Rauner M, Sinningen K, Helas S, Al-Fakhri N, Nemeth K, et al. The osteoclast-associated receptor (OSCAR) is a novel receptor regulated by oxidized low-density lipoprotein in human endothelial cells. Endocrinology. 2011;152(12):4915-26.
368. Kung CP, Khaku S, Jennis M, Zhou Y, Murphy ME. Identification of TRIML2, a novel p53 target, that enhances p53 SUMOylation and regulates the transactivation of proapoptotic genes. Mol Cancer Res. 2015;13(2):250-62.
369. Avan P, Le Gal S, Michel V, Dupont T, Hardelin JP, Petit C, et al. Otogelin, otogelin-like, and stereocilin form links connecting outer hair cell stereocilia to each other and the tectorial membrane. Proc Natl Acad Sci U S A. 2019;116(51):25948-57.
370. Kanasaki H, Tselmeg M, Oride A, Sukhbaatar U, Hara T, Kyo S. Pulsatile kisspeptin effectively stimulates gonadotropin-releasing hormone (GnRH)-producing neurons. Gynecol Endocrinol. 2017;33(9):721-7.
371. Manganas LN, Durá I, Osenberg S, Semerci F, Tosun M, Mishra R, et al. BASP1 labels neural stem cells in the neurogenic niches of mammalian brain. Scientific Reports. 2021;11(1):5546.
372. Chen LJ, Liu HY, Xiao ZY, Qiu T, Zhang D, Zhang LJ, et al. IGF2BP3 promotes the progression of colorectal cancer and mediates cetuximab resistance by stabilizing EGFR mRNA in an m(6)A-dependent manner. Cell Death Dis. 2023;14(9):581.

373. Xu Y, Guo Z, Peng H, Guo L, Wang P. IGF2BP3 promotes cell metastasis and is associated with poor patient survival in nasopharyngeal carcinoma. J Cell Mol Med. 2022;26(2):410-21.
374. Karataeva AR, Klaassen RV, Ströder J, Ruiperez-Alonso M, Hjorth JJ, van Nierop P, et al. C-terminal interactors of the AMPA receptor auxiliary subunit Shisa9. PLoS One. 2014;9(2):e87360.
375. Schoonderwoerd MJA, Goumans MTH, Hawinkels L. Endoglin: Beyond the Endothelium. Biomolecules. 2020;10(2).
376. Hodge JM, Kirkland MA, Aitken CJ, Waugh CM, Myers DE, Lopez CM, et al. Osteoclastic potential of human CFU-GM: biphasic effect of GM-CSF. J Bone Miner Res. 2004;19(2):190-9.
377. Docherty LE, Rezwan FI, Poole RL, Turner CL, Kivuva E, Maher ER, et al. Mutations in NLRP5 are associated with reproductive wastage and multilocus imprinting disorders in humans. Nat Commun. 2015;6:8086.
378. Zhuang H, Chen X, Wang Y, Huang S, Chen B, Zhang C, et al. Identification of LIPH as an unfavorable biomarkers correlated with immune suppression or evasion in pancreatic cancer based on RNA-seq. Cancer Immunol Immunother. 2022;71(3):601-12.
379. Li Y, Zhou X, Zhang Q, Chen E, Sun Y, Ye D, et al. Lipase member H is a downstream molecular target of hypoxia inducible factor-1α and promotes papillary thyroid carcinoma cell migration in BCPAP and KTC-1 cell lines. Cancer Manag Res. 2019;11:931-41.
380. Tantisira KG, Silverman ES, Mariani TJ, Xu J, Richter BG, Klanderman BJ, et al. FCER2: a pharmacogenetic basis for severe exacerbations in children with asthma. J Allergy Clin Immunol. 2007;120(6):1285-91.
381. Chen LH, Kuo WH, Tsai MH, Chen PC, Hsiao CK, Chuang EY, et al. Identification of prognostic genes for recurrent risk prediction in triple negative breast cancer patients in Taiwan. PLoS One. 2011;6(11):e28222.
382. Gatla HR, Zou Y, Uddin MM, Singha B, Bu P, Vancura A, et al. Histone Deacetylase (HDAC) Inhibition Induces IκB Kinase (IKK)-dependent Interleukin-8/CXCL8 Expression in Ovarian Cancer Cells. J Biol Chem. 2017;292(12):5043-54.
383. Singha B, Gatla HR, Manna S, Chang TP, Sanacora S, Poltoratsky V, et al. Proteasome inhibition increases recruitment of IκB kinase β (IKKβ), S536P-p65, and transcription factor EGR1 to interleukin-8 (IL-8) promoter, resulting in increased IL-8 production in ovarian cancer cells. J Biol Chem. 2014;289(5):2687-700.
384. Prescott JA, Cook SJ. Targeting IKKβ in Cancer: Challenges and Opportunities for the Therapeutic Utilisation of IKKβ Inhibitors. Cells. 2018;7(9).
385. Goto A, Okado K, Martins N, Cai H, Barbier V, Lamiable O, et al. The Kinase IKKβ Regulates a STING- and NF-κB-Dependent Antiviral Response Pathway in Drosophila. Immunity. 2018;49(2):225-34.e4.
386. Carayol N, Chen J, Yang F, Jin T, Jin L, States D, et al. A Dominant Function of IKK/NF-κB Signaling in Global Lipopolysaccharide-induced Gene Expression *. Journal of Biological Chemistry. 2006;281(41):31142-51.
387. Park S-H, Liu Z, Sui Y, Helsley RN, Zhu B, Powell DK, et al. IKKβ Is Essential for Adipocyte Survival and Adaptive Adipose Remodeling in Obesity. Diabetes. 2016;65(6):1616-29.
388. Liu B, Wang Y, Wu Y, Cheng Y, Qian H, Yang H, et al. IKKβ regulates the expression of coagulation and fibrinolysis factors through the NF-κB canonical pathway in LPS-stimulated alveolar epithelial cells type II. Exp Ther Med. 2019;18(4):2859-66.
389. Nedeva IR, Vitale M, Elson A, Hoyland JA, Bella J. Role of OSCAR Signaling in Osteoclastogenesis and Bone Disease. Front Cell Dev Biol. 2021;9:641162.
390. Braakman I, Hebert DN. Protein folding in the endoplasmic reticulum. Cold Spring Harb Perspect Biol. 2013;5(5):a013201.
391. Morgens DW, Deans RM, Li A, Bassik MC. Systematic comparison of CRISPR/Cas9 and RNAi screens for essential genes. Nat Biotechnol. 2016;34(6):634-6.
392. Lawrence T, Bebien M. IKKalpha in the regulation of inflammation and adaptive immunity. Biochem Soc Trans. 2007;35(Pt 2):270-2.

393. Friedrich M, Pohin M, Jackson MA, Korsunsky I, Bullers SJ, Rue-Albrecht K, et al. IL-1-driven stromal–neutrophil interactions define a subset of patients with inflammatory bowel disease that does not respond to therapies. Nature Medicine. 2021;27(11):1970-81.
394. Brabcová E, Kolesár L, Thorburn E, Stříž I. Chemokines induced in human respiratory epithelial cells by IL-1 family of cytokines. Folia Biol (Praha). 2014;60(4):180-6.
395. Okabe H, Beppu T, Ueda M, Hayashi H, Ishiko T, Masuda T, et al. Identification of CXCL5/ENA-78 as a factor involved in the interaction between cholangiocarcinoma cells and cancer-associated fibroblasts. Int J Cancer. 2012;131(10):2234-41.
396. Liu Y, Mei J, Gonzales L, Yang G, Dai N, Wang P, et al. IL-17A and TNF-α Exert Synergistic Effects on Expression of CXCL5 by Alveolar Type II Cells In Vivo and In Vitro. The Journal of Immunology. 2011;186(5):3197-205.
397. Kolmus K, Van Troys M, Van Wesemael K, Ampe C, Haegeman G, Tavernier J, et al. β-agonists selectively modulate proinflammatory gene expression in skeletal muscle cells via non-canonical nuclear crosstalk mechanisms. PLoS One. 2014;9(6):e90649.
398. Si J, Wang C, Zhang D, Wang B, Zhou Y. Osteopontin in Bone Metabolism and Bone Diseases. Med Sci Monit. 2020;26:e919159.
399. Zoch ML, Clemens TL, Riddle RC. New insights into the biology of osteocalcin. Bone. 2016;82:42-9.
400. Vimalraj S, Arumugam B, Miranda PJ, Selvamurugan N. Runx2: Structure, function, and phosphorylation in osteoblast differentiation. Int J Biol Macromol. 2015;78:202-8.
401. Simpson S, Dunning MD, de Brot S, Grau-Roma L, Mongan NP, Rutland CS. Comparative review of human and canine osteosarcoma: morphology, epidemiology, prognosis, treatment and genetics. Acta Vet Scand. 2017;59(1):71.
402. Liu Q, Li A, Tian Y, Wu JD, Liu Y, Li T, et al. The CXCL8-CXCR1/2 pathways in cancer. Cytokine Growth Factor Rev. 2016;31:61-71.
403. Kastner L, Kandalaft W, Mahant AM, Crimella J, Hakim S, Peng XP, et al. Cytokine Profiling of Children, Adolescents, and Young Adults Newly Diagnosed with Sarcomas Demonstrates the Role of IL-1β in Osteosarcoma Metastasis. Cancers (Basel). 2025;17(18).
404. Hoffmann A, Cheng G, Baltimore D. NF-κB: master regulator of cellular responses in health and disease. Immunity & Inflammation. 2025;1(1):2.
405. Chow LQ, Eckhardt SG. Sunitinib: from rational design to clinical efficacy. J Clin Oncol. 2007;25(7):884-96.
406. Habanjar O, Diab-Assaf M, Caldefie-Chezet F, Delort L. 3D Cell Culture Systems: Tumor Application, Advantages, and Disadvantages. Int J Mol Sci. 2021;22(22).
407. Duval K, Grover H, Han LH, Mou Y, Pegoraro AF, Fredberg J, et al. Modeling Physiological Events in 2D vs. 3D Cell Culture. Physiology (Bethesda). 2017;32(4):266-77.
408. Berman SD, Calo E, Landman AS, Danielian PS, Miller ES, West JC, et al. Metastatic osteosarcoma induced by inactivation of Rb and p53 in the osteoblast lineage. Proc Natl Acad Sci U S A. 2008;105(33):11851-6.
409. McArdle AJ, Menikou S. What is proteomics? Arch Dis Child Educ Pract Ed. 2021;106(3):178-81.
410. Manzoni C, Kia DA, Vandrovcova J, Hardy J, Wood NW, Lewis PA, et al. Genome, transcriptome and proteome: the rise of omics data and their integration in biomedical sciences. Brief Bioinform. 2018;19(2):286-302.
411. Hegde PS, White IR, Debouck C. Interplay of transcriptomics and proteomics. Current Opinion in Biotechnology. 2003;14(6):647-51.
412. Kwon YW, Jo H-S, Bae S, Seo Y, Song P, Song M, et al. Application of Proteomics in Cancer: Recent Trends and Approaches for Biomarkers Discovery. Frontiers in Medicine. 2021;Volume 8 - 2021.

413. Thompson A, Schäfer J, Kuhn K, Kienle S, Schwarz J, Schmidt G, et al. Tandem mass tags: a novel quantification strategy for comparative analysis of complex protein mixtures by MS/MS. Anal Chem. 2003;75(8):1895-904.
414. Navarrete-Perea J, Yu Q, Gygi SP, Paulo JA. Streamlined Tandem Mass Tag (SL-TMT) Protocol: An Efficient Strategy for Quantitative (Phospho)proteome Profiling Using Tandem Mass Tag-Synchronous Precursor Selection-MS3. J Proteome Res. 2018;17(6):2226-36.
415. Chua XY, Mensah T, Aballo T, Mackintosh SG, Edmondson RD, Salomon AR. Tandem Mass Tag Approach Utilizing Pervanadate BOOST Channels Delivers Deeper Quantitative Characterization of the Tyrosine Phosphoproteome. Mol Cell Proteomics. 2020;19(4):730-43.
416. Erdjument-Bromage H, Huang FK, Neubert TA. Sample Preparation for Relative Quantitation of Proteins Using Tandem Mass Tags (TMT) and Mass Spectrometry (MS). Methods Mol Biol. 2018;1741:135-49.
417. Zecha J, Satpathy S, Kanashova T, Avanessian SC, Kane MH, Clauser KR, et al. TMT Labeling for the Masses: A Robust and Cost-efficient, In-solution Labeling Approach. Mol Cell Proteomics. 2019;18(7):1468-78.
418. Dunphy K, Dowling P. Chapter 11 - Profiling of the phosphoproteome using tandem mass tag labeling. In: Meleady P, editor. Proteomics Mass Spectrometry Methods: Academic Press; 2024. p. 163-72.
419. Franceschi C, Garagnani P, Parini P, Giuliani C, Santoro A. Inflammaging: a new immune-metabolic viewpoint for age-related diseases. Nat Rev Endocrinol. 2018;14(10):576-90.

Appendix

Appendix 1

```
#Set working directory
setwd("C:/Users/kirst/OneDrive - University of Strathclyde/PhD/Kirsty
Seq/RNA seq Data Oct 2024")
getwd()

#Load libraries
library("ggplot2")
library("dplyr")
library("ggrepel")
library("ggthemes")
library("topGO")
library("org.Hs.eg.db")
library("AnnotationDbi")

#Set themes
theme_Publication <- function(base_size=14, base_family="helvetica") {

  (theme_foundation(base_size=base_size, base_family=base_family)
   + theme(plot.title = element_text(face = "bold",
                                     size = rel(1.2), hjust = 0.5),
           text = element_text(),
           panel.background = element_rect(colour = NA),
           plot.background = element_rect(colour = NA),
           panel.border = element_rect(colour = NA),
           axis.title = element_text(face = "bold",size = rel(1)),
           axis.title.y = element_text(angle=90,vjust =2),
           axis.title.x = element_text(vjust = -0.2),
           axis.text = element_text(),
           axis.line = element_line(colour="black"),
           axis.ticks = element_line(),
           panel.grid.major = element_line(colour="#f0f0f0"),
           panel.grid.minor = element_blank(),
           legend.key = element_rect(colour = NA),
           legend.position = "bottom",
           legend.direction = "horizontal",
           legend.key.size= unit(0.2, "cm"),
           legend.margin = unit(0, "cm"),
           legend.title = element_text(face="italic"),
           plot.margin=unit(c(10,5,5,5),"mm"),

strip.background=element_rect(colour="#f0f0f0",fill="#f0f0f0"),
           strip.text = element_text(face="bold")
   ))

}

scale_fill_Publication <- function(...){
  library(scales)
  discrete_scale("fill","Publication",manual_pal(values                    =
c("#386cb0","#fdb462","#7fc97f","#ef3b2c","#662506","#a6cee3","#fb9a99","
#984ea3","#ffff33")), ...)

}

scale_colour_Publication <- function(...){
  library(scales)
```

```
  discrete_scale("colour","Publication",manual_pal(values                  =
c("#386cb0","#fdb462","#7fc97f","#ef3b2c","#662506","#a6cee3","#fb9a99","
#984ea3","#ffff33")), ...)

}

#Load datasets
df1<- read.csv("Differential_expression_analysis_table.csv")
df2<- read.csv("Differential_expression_analysis_table[1].csv")
df3<- read.csv("Differential_expression_analysis_table[2].csv")
df4<- read.csv("Differential_expression_analysis_table[3].csv")
df5<- read.csv("Differential_expression_analysis_table[4].csv")
df6<- read.csv("Differential_expression_analysis_table[5].csv")
df7<- read.csv("Differential_expression_analysis_table[6].csv")
df8<- read.csv("Differential_expression_analysis_table[7].csv")
df9<- read.csv("Differential_expression_analysis_table[8].csv")

#Filter datasets
# Create a list of data frames
dfs <- list(df1, df2, df3, df4, df5, df6, df7, df8, df9)


#Map UNIPROT names
map_ensembl_to_uniprot <- function(df) {
  # Extract unique ENSEMBL IDs from the data frame
  unique_ids <- unique(df$ID)

  # Perform the mapping using AnnotationDbi::select
  mapping <- tryCatch({
    AnnotationDbi::select(org.Hs.eg.db,
                          keys = unique_ids,
                          columns = c("ENSEMBL", "UNIPROT"),
                          keytype = "ENSEMBL")
  }, error = function(e) {
    message("Error in mapping: ", e)
    return(data.frame(ENSEMBL = character(0), UNIPROT = character(0))) #
Return an empty data frame in case of error
  })

  # Merge the original data frame with the mapping
  # This assumes ENSEMBL IDs are unique in the original df; if not, you
might need a different merging strategy
  df_merged <- merge(df, mapping, by.x = "ID", by.y = "ENSEMBL", all.x =
TRUE)

  # Rename the UNIPROT column to Accession
  names(df_merged)[names(df_merged) == "UNIPROT"] <- "Accession"

  return(df_merged)
}

# Apply the mapping function to each data frame
df_list_mapped <- lapply(dfs, map_ensembl_to_uniprot)

# If you need them back as individual variables
list2env(setNames(df_list_mapped, paste0("df", 1:9)), envir = .GlobalEnv)

# Create a list to store filtered data frames
filtered_list <- list()
df_up_list <- list()
df_down_list <- list()
```

```
# Loop through each data frame
for (i in seq_along(dfs)) {
  # Remove duplicate rows based on all columns to avoid repetition
  dfs[[i]] <- distinct(dfs[[i]])
  # Extract unique ENSEMBL gene IDs
  unique_ids <- unique(dfs[[i]]$ID)

  # Use select() from AnnotationDbi to get the mappings
  mapping <- AnnotationDbi::select(org.Hs.eg.db,
                                   keys = unique_ids,
                                   columns = c("ENSEMBL", "UNIPROT"),
                                   keytype = "ENSEMBL")

  # Merge the mappings back to the original dataframe
  dfs[[i]] <- merge(dfs[[i]], mapping, by.x = "ID", by.y = "ENSEMBL", all.x
= TRUE)

  # Drop rows where UniProt ID is NA (Adjust column name if necessary)
  dfs[[i]] <- filter(dfs[[i]], !is.na(UNIPROT))

  #  Filter  rows  where  padj  <=  0.05  and  (log2FoldChange  <  -1  or
log2FoldChange > 1)
  filtered_list[[i]] <- dfs[[i]] %>%
    filter(padj <= 0.05, (log2FoldChange < -1 | log2FoldChange > 1))

  # Filter for upregulated genes: padj <= 0.05 and log2FoldChange > 1
  df_up_list[[i]] <- dfs[[i]] %>%
    filter(padj <= 0.05, log2FoldChange > 1)

  # Filter for downregulated genes: padj <= 0.05 and log2FoldChange < -1
  df_down_list[[i]] <- dfs[[i]] %>%
    filter(padj <= 0.05, log2FoldChange < -1)
}

# Access the filtered data frames for each original data frame
df1_filtered <- filtered_list[[1]]
df2_filtered <- filtered_list[[2]]
df3_filtered <- filtered_list[[3]]
df4_filtered <- filtered_list[[4]]
df5_filtered <- filtered_list[[5]]
df6_filtered <- filtered_list[[6]]
df7_filtered <- filtered_list[[7]]
df8_filtered <- filtered_list[[8]]
df9_filtered <- filtered_list[[9]]

df1_up <- df_up_list[[1]]
df2_up <- df_up_list[[2]]
df3_up <- df_up_list[[3]]
df4_up <- df_up_list[[4]]
df5_up <- df_up_list[[5]]
df6_up <- df_up_list[[6]]
df7_up <- df_up_list[[7]]
df8_up <- df_up_list[[8]]
df9_up <- df_up_list[[9]]

df1_down <- df_down_list[[1]]
df2_down <- df_down_list[[2]]
df3_down <- df_down_list[[3]]
df4_down <- df_down_list[[4]]
df5_down <- df_down_list[[5]]
```

```
df6_down <- df_down_list[[6]]
df7_down <- df_down_list[[7]]
df8_down <- df_down_list[[8]]
df9_down <- df_down_list[[9]]

# Creat lists of dataframes:
dfs_filtered    <-    list(df1_filtered,    df2_filtered,    df3_filtered,
df4_filtered,  df5_filtered,  df6_filtered,  df7_filtered,  df8_filtered,
df9_filtered)
dfs_up <- list(df1_up, df2_up, df3_up, df4_up, df5_up, df6_up, df7_up,
df8_up, df9_up)
dfs_down  <-  list(df1_down,  df2_down,  df3_down,  df4_down,  df5_down,
df6_down, df7_down, df8_down, df9_down)
dfs <- list(df1,df2, df3, df4, df5, df6, df7, df8, df9)

#Write csv files for Cytoscape analysis
# Define titles for your files
df_titles <- c(
  "IKKa KO 24 hours stimulated to IKKa KO 8 hours stimulated",
  "IKKa KO 8 hours stimulated to IKKa KO unstimulated",
  "IKKa KO 24 hours stimulated to IKKa KO unstimulated",
  "IKKa KO 8 hours stimulated to WT 8 hours stimulated",
  "WT 24 hours stimulated to WT 8 hours stimulated",
  "IKKa 24 hours stimulated to WT 24 hours stimulated",
  "IKKa KO unstimulated to WT unstimulated",
  "WT 8 hours stimulated to WT unstimulated",
  "WT 24 hours stimulated to WT unstimulated"
)

# Loop through the upregulated dataframes
setwd("C:/Users/kirst/OneDrive  -  University  of  Strathclyde/PhD/Kirsty
Seq/RNA seq Data Oct 2024/Upregulated data")
for (i in seq_along(df_up_list)) {
  # Replace spaces with underscores, then remove any remaining non-
alphanumeric characters (keeping underscores)
  filename_up <- paste0(gsub(" ", "_", df_titles[i]), "_upregulated.csv")
  write.csv(df_up_list[[i]], filename_up, row.names = FALSE)
}
# Loop through the downregulated dataframes
setwd("C:/Users/kirst/OneDrive  -  University  of  Strathclyde/PhD/Kirsty
Seq/RNA seq Data Oct 2024/Downregulated data")
for (i in seq_along(df_down_list)) {
  filename_down    <-    paste0(gsub("    ",    "_",    df_titles[i]),
"_downregulated.csv")
  write.csv(df_down_list[[i]], filename_down, row.names = FALSE)
}

#============ VOLCANO PLOT ===========
# Set working directory
setwd("C:/Users/kirst/OneDrive  -  University  of  Strathclyde/PhD/Kirsty
Seq/RNA seq Data Oct 2024/Volcano plots automated")

# Plot titles
VolcanoPlots_titles <- c("IKKa KO 24 hours stimulated to IKKa KO 8 hours
stimulated",
                         "IKKa  KO  8  hours  stimulated  to  IKKa  KO
unstimulated",
                         "IKKa  KO  24  hours  stimulated  to  IKKa  KO
unstimulated",
                         "IKKa  KO  8  hours  stimulated  to  WT  8  hours
stimulated",
```

```
                          "WT 24 hours stimulated to WT 8 hours stimulated",
                          "IKKa 24 hours stimulated to WT 24 hours
stimulated",
                          "IKKa KO unstimulated to WT unstimulated",
                          "WT 8 hours stimulated to WT unstimulated",
                          "WT 24 hours stimulated to WT unstimulated")

# Loop through each dataframe and generate a volcano plot
for (i in seq_along(dfs)) {
  df <- dfs[[i]]

  # Ensure that padj is numeric, and handle non-numeric values
  df$padj <- as.numeric(df$padj)  # Force conversion to numeric (will
introduce NAs for non-numeric values)

  # Remove rows where padj is NA
  df <- df[!is.na(df$padj), ]

  # Create a unique identifier for each point (combination of
log2FoldChange and padj)
  df <- df %>%
    group_by(log2FoldChange, padj) %>%
    slice_head(n = 1) %>%
    ungroup()

  # Rank genes by padj and select the top 20
  top20_genes <- df %>%
    arrange(padj) %>%
    slice_head(n = 20) %>%
    pull(Gene.name)

  # Update the dataframe to include a label for the top 20 most significant
genes
  df$label <- ifelse(df$Gene.name %in% top20_genes,
as.character(df$Gene.name), NA)

  # Calculate the maximum -log10(padj) value for setting y-axis limit
  max_y_value <- max(-log10(df$padj), na.rm = TRUE)

  # If max_y_value is NA or negative, skip this plot
  if (is.na(max_y_value) || max_y_value <= 0) {
    message(paste("Skipping dataset", i, "due to invalid -log10(padj)
values."))
    next
  }

  # Add a buffer to the max value for aesthetic purposes
  adjusted_max_y <- max_y_value * 1.1

  # Generate the volcano plot
  volcano_plot <- ggplot(df, aes(x = log2FoldChange, y = -log10(padj))) +
    geom_point(aes(color = case_when(
      log2FoldChange < -1 & padj <= 0.05 ~ "blue",
      log2FoldChange > 1 & padj <= 0.05 ~ "#6600CC",
      TRUE ~ "grey50"
    )), alpha = 0.5, size = 2) +
    scale_color_identity() +
    xlim(c(-7, 7)) +
    ylim(c(0, adjusted_max_y)) +
    labs(title = paste("Volcano Plot -", VolcanoPlots_titles[i]),
         x = "Log2 Fold Change",
```

```
          y = "-log10(P-value)") +
    geom_hline(yintercept = 1.3, linetype = "dashed", color = "black") +
    geom_vline(xintercept = c(-1, 1), linetype = "dashed", color = "black")
+
    geom_text_repel(aes(label = label, color = case_when(
      log2FoldChange < -1 & padj <= 0.05 & !is.na(label) ~ "blue",
      log2FoldChange > 1 & padj <= 0.05 & !is.na(label) ~ "#6600CC",
      TRUE ~ NA_character_
    )), na.rm = TRUE, max.overlaps = Inf) +
    theme_Publication() +
    theme(legend.position = "none")

  print(volcano_plot)

  # Save the plot with spaces in the filename
  file_name <- paste0(VolcanoPlots_titles[i], ".png") # Keep the original
title with spaces
  ggsave(file_name, plot = volcano_plot, device = "png", width = 10, height
= 6, dpi = 300)
}


#==== GENE ONTOLOGY ====
# Define a function for GO enrichment analysis
performGOEnrichment <- function(interestDF, allGenesDataFrame, geneColumn
= "ID") {
  # Create a named vector for all genes, marking genes of interest with 1,
others with 0
  geneList      <-      ifelse(allGenesDataFrame[[geneColumn]]      %in%
interestDF[[geneColumn]], 1, 0)
  names(geneList) <- allGenesDataFrame[[geneColumn]]

  # Convert to factor with two levels
  geneList <- factor(geneList, levels = c(0, 1))

  # Define selection function for genes of interest
  selection <- function(x) x == 1

  # Setup the enrichment object
  allGO2genes <- annFUN.org(
    whichOnto = "MF", #Change BP, CC or MF
    feasibleGenes = NULL,
    mapping = "org.Hs.eg.db",
    ID = "ensembl"
  )
  GOdata <- new(
    "topGOdata",
    ontology = "MF",
    allGenes = geneList,
    annot = annFUN.GO2genes,
    GO2genes = allGO2genes,
    geneSel = selection,
    nodeSize = 5
  )

  # Perform gene enrichment
  results.fisher <- runTest(GOdata, algorithm = "classic", statistic =
"fisher")
  goEnrichment <- GenTable(
    GOdata,
    fisher = results.fisher,
```

```
    orderBy = "fisher",
    topNodes = 100
  )

  goEnrichment$fisher <- as.numeric(goEnrichment$fisher)
  goEnrichment <- goEnrichment[goEnrichment$fisher < 0.05, ]
  goEnrichment <- goEnrichment[, c("GO.ID", "Term", "fisher")]

  return(goEnrichment)
}

# Create a list to store the GO enrichment results for each comparison
go_enrichment_results <- list()

# Loop through the datasets
for (i in seq_along(dfs_down)) {
  # Call your function with the corresponding filtered dataset and its
background dataset
  go_enrichment_results[[i]]     <-     performGOEnrichment(dfs_down[[i]],
dfs[[i]], geneColumn = "ID")
}

# go_enrichment_results now contains the GO enrichment analysis results
for each pair


# Plot Enriched Results
setwd("C:/Users/kirst/OneDrive  -  University  of  Strathclyde/PhD/Kirsty
Seq/RNA    seq    Data    Oct    2024/Gene    Ontology/Gene    Ontology
downregulated/Molecular Function")
df_titles <- c("IKKa KO 24 hours stimulated to IKKa KO 8 hours stimulated
- Downregulated",
               "IKKa  KO  8  hours  stimulated  to  IKKa  KO  unstimulated  -
Downregulated",
               "IKKa  KO  24  hours  stimulated  to  IKKa  KO  unstimulated  -
Downregulated",
               "IKKa  KO  8  hours  stimulated  to  WT  8  hours  stimulated  -
Downregulated",
               "WT  24  hours  stimulated  to  WT  8  hours  stimulated  -
Downregulated",
               "IKKa  24  hours  stimulated  to  WT  24  hours  stimulated  -
Downregulated",
               "IKKa KO unstimulated to WT unstimulated - Downregulated",
               "WT 8 hours stimulated to WT unstimulated - Downregulated",
               "WT 24 hours stimulated to WT unstimulated - Downregulated")

# Loop through the GO enrichment results
for (i in seq_along(go_enrichment_results)) {
  ntop <- 20
  ntop <- min(ntop, nrow(go_enrichment_results[[i]]))

  ggdata <- go_enrichment_results[[i]][1:ntop,]

  # Remove rows where Term is NA
  ggdata <- ggdata[!is.na(ggdata$Term), ]

  # Remove duplicate terms
  ggdata <- ggdata[!duplicated(ggdata$Term), ]

  # Use only the Term column for labels, without adding numbers
```

```
  ggdata$UniqueTerm <- factor(ggdata$Term, levels = rev(unique(ggdata$Term)))

  gg1 <- ggplot(ggdata, aes(x = UniqueTerm, y = -log10(fisher), size = -log10(fisher), fill = -log10(fisher))) +
    expand_limits(y = 1) +
    geom_point(shape = 21) +
    scale_size(range = c(2.5, 12.5)) +
    scale_fill_continuous(low = '#00CCFF', high = '#6600CC') +
    xlab('') + ylab('Enrichment score') +
    labs(
      title = paste(df_titles[i], "GO Molecular Function"), # Remember to change BP, CC or MF
      subtitle = "Top 20 terms ordered by Fisher's exact test p value",
      caption = "Cut-off lines drawn at equivalents of p=0.05, p=0.01, p=0.001"
    ) +
    geom_hline(yintercept = c(-log10(0.05), -log10(0.01), -log10(0.001)),
               linetype = c("dotted", "longdash", "solid"),
               colour = c("black", "black", "black"),
               linewidth = c(0.5, 1.5, 3)) +
    theme_bw(base_size = 24) +
    theme(
      legend.position = 'right',
      plot.title = element_text(angle = 0, size = 16, face = 'bold', vjust = 1),
      plot.subtitle = element_text(angle = 0, size = 14, face = 'bold', vjust = 1),
      plot.caption = element_text(angle = 0, size = 12, face = 'bold', vjust = 1),
      axis.text.x = element_text(angle = 45, size = 12, face = 'bold', hjust = 1),
      axis.text.y = element_text(angle = 0, size = 12, face = 'bold', vjust = 0.5),
      axis.title = element_text(size = 12, face = 'bold'),
      axis.line = element_line(colour = 'black'),
      legend.key = element_blank(),
      legend.text = element_text(size = 14, face = "bold"),
      title = element_text(size = 14, face = "bold")
    ) +
    coord_flip()

  # Print the plot
  print(gg1)

  # Use the original title with spaces as the filename
  filename <- paste0(df_titles[i], ".png") # Keep spaces in the title

  # Specify desired width and height in inches for the plot
  width_inches <- 15 # Example width
  height_inches <- 9 # Example height, adjust as needed

  # Save the plot with spaces in the filename
  ggsave(filename, plot = gg1, device = "png", width = width_inches, height = height_inches, dpi = 300)
}


#==== HEATMAPS ====
library(pheatmap)
```

```
# Set working directory for saving heatmaps
setwd("C:/Users/kirst/OneDrive - University of Strathclyde/PhD/Kirsty
Seq/RNA seq Data Oct 2024/Heatmaps/Downregulated")

# df_titles contains your custom titles for each dataframe
df_titles <- c("IKKa KO 24 hours stimulated to IKKa KO 8 hours stimulated
- Downregulated",
               "IKKa KO 8 hours stimulated to IKKa KO unstimulated -
Downregulated",
               "IKKa KO 24 hours stimulated to IKKa KO unstimulated -
Downregulated",
               "IKKa KO 8 hours stimulated to WT 8 hours stimulated -
Downregulated",
               "WT 24 hours stimulated to WT 8 hours stimulated -
Downregulated",
               "IKKa 24 hours stimulated to WT 24 hours stimulated -
Downregulated",
               "IKKa KO unstimulated to WT unstimulated - Downregulated",
               "WT 8 hours stimulated to WT unstimulated - Downregulated",
               "WT 24 hours stimulated to WT unstimulated - Downregulated")

# Loop through the list of dataframes and their corresponding titles
for (i in 1:length(dfs_down)) {
  current_df <- dfs_down[[i]]

  # Ensure uniqueness by keeping only the first occurrence of each ID
  current_df <- current_df %>%
    distinct(ID, .keep_all = TRUE)

  # Rank genes by padj and select the top 20 most significant
  top20_genes <- current_df %>%
    arrange(padj) %>% # Sort by padj in ascending order (most significant
first)
    slice_head(n = 20) # Select the top 20 genes

  # Select the numeric columns (excluding log2FoldChange, pvalue, and padj)
  numeric_data <- top20_genes[, c(5:10)]  # Adjust column indices as needed

  # Ensure all selected columns are numeric
  numeric_data <- numeric_data[, sapply(numeric_data, is.numeric)]

  # Set row names as the gene names instead of IDs
  rownames(numeric_data) <- top20_genes$Gene.name

  # Remove rows with NA, NaN, or Inf values
  numeric_data <- na.omit(numeric_data)

  # Check if numeric_data is empty, skip plotting if there are no valid
numeric columns
  if (ncol(numeric_data) == 0 || nrow(numeric_data) == 0) {
    message(paste("No numeric data available for heatmap:", df_titles[i]))
    next
  }

  heatmap_title <- paste("Heatmap of", df_titles[i])

  # Dynamically create the filename for saving the plot
  plot_filename <- paste0(df_titles[i], ".png")  # Add PNG extension

  # Print and save the heatmap with the specified filename
  pheatmap(numeric_data,
```

```
            scale = "row",
            clustering_distance_rows = "euclidean",
            clustering_distance_cols = "euclidean",
            clustering_method = "complete",
            show_rownames = TRUE,  # Show row names (gene names)
            show_colnames = FALSE,
            main = heatmap_title,
            width = 12,
            cluster_rows = FALSE,    # Do not cluster rows to keep sorted
order
            cluster_cols = FALSE,   # Do not cluster columns (treatments)
            filename = plot_filename) # Dynamically save the plot as a PNG
}

#==== PRINCIPAL COMPONENT ANALYSIS (PCA) =====
library(ggplot2)
library(ggrepel)

# Set the working directory where plots will be saved
setwd("C:/Users/kirst/OneDrive  -  University  of  Strathclyde/PhD/Kirsty
Seq/RNA seq Data Oct 2024/PCAs")

# Titles for each dataset (in the right order)
df_titles <- c("IKKa KO 24 hours stimulated to IKKa KO 8 hours stimulated",
               "IKKa KO 8 hours stimulated to IKKa KO unstimulated",
               "IKKa KO 24 hours stimulated to IKKa KO unstimulated",
               "IKKa KO 8 hours stimulated to WT 8 hours stimulated",
               "WT 24 hours stimulated to WT 8 hours stimulated",
               "IKKa 24 hours stimulated to WT 24 hours stimulated",
               "IKKa KO unstimulated to WT unstimulated",
               "WT 8 hours stimulated to WT unstimulated",
               "WT 24 hours stimulated to WT unstimulated")

# Loop through the list of datasets and apply PCA
for (i in 1:length(dfs_up)) {
  current_df <- dfs_up[[i]]

  # Select only the columns 5 to 10 representing the two treatments
  numeric_data <- current_df[, c(5:10)]  # Exclude the first 4 columns

  # Ensure all selected columns are numeric
  numeric_data  <-  numeric_data[,  sapply(numeric_data,  is.numeric)]    #
Filter numeric columns

  # Check if the numeric data has any valid rows and columns
  if (ncol(numeric_data) == 0 || nrow(numeric_data) == 0) {
    message(paste("No numeric data available for PCA in dataset:", i))
    next
  }

  # Remove rows with NA, NaN, or Inf values
  numeric_data <- na.omit(numeric_data)

  # Transpose the matrix for PCA (samples as rows, genes as columns)
  data_matrix <- as.matrix(numeric_data)
  data_matrix <- t(data_matrix)

  # Perform PCA
  pca <- prcomp(data_matrix, scale = TRUE)
```

```
  # Adjust treatment labels: columns 5-7 as first label, 8-10 as second
label
  treatment_labels       <-       c(rep(colnames(current_df)[5],       3),
rep(colnames(current_df)[8], 3))
  treatment_labels <- gsub("\\.", " ", treatment_labels)  # Replace dots
with spaces

  # Label repetitions as "1," "2," and "3"
  repetition_labels <- rep(c("1", "2", "3"), 2)

  # Create a dataframe for the PCA results, including the treatment
information
  pca_data <- data.frame(Sample = repetition_labels,
                         PC1 = pca$x[, 1],
                         PC2 = pca$x[, 2],
                         Treatment  =  factor(treatment_labels,  levels  =
unique(treatment_labels)))

  # Dynamically create filenames for saving the plots
  pca_plot_filename <- paste0(df_titles[i], "_PCA.png")
  scree_plot_filename <- paste0(df_titles[i], "_Scree.png")

  # Generate a ggplot 2D PCA plot for clustering of treatments with points
and labels
  pca_plot <- ggplot(data = pca_data, aes(x = PC1, y = PC2, label = Sample,
color = Treatment)) +
    geom_point(size  =  3)  +   # Add points for treatments, colored by
Treatment
    geom_text_repel(size = 4) +  # Add labels, avoiding overlaps
    scale_color_manual(values    =    c("blue",    "red"),    labels    =
unique(treatment_labels)) +  # Define colors and labels
    xlab(paste("PC1 - ", round(100 * summary(pca)$importance[2, 1], 1),
"%", sep = "")) +
    ylab(paste("PC2 - ", round(100 * summary(pca)$importance[2, 2], 1),
"%", sep = "")) +
    theme_Publication() +  # Apply your custom theme
    ggtitle(df_titles[i])

  # Save the PCA plot
  ggsave(pca_plot_filename, plot = pca_plot, device = "png", width = 10,
height = 6, dpi = 300)

  # Make a scree plot with principal component labels
  pca_var <- pca$sdev^2
  pca_var_per <- round(pca_var / sum(pca_var) * 100, 1)

  # Create scree plot
  png(scree_plot_filename, width = 1000, height = 600)
  barplot(pca_var_per, main = paste("Scree Plot -", df_titles[i]),
          xlab  =  "Principal  Component",  ylab  =  "Percent  Variation",
names.arg = paste0("PC", 1:length(pca_var_per)))
  dev.off()

  # Get the top 10 contributing genes to PC1
  loading_scores <- pca$rotation[, 1]  # PC1 loading scores
  gene_scores <- abs(loading_scores)    # Get the magnitudes
  gene_score_ranked <- sort(gene_scores, decreasing = TRUE)
  top_10_genes  <-  names(gene_score_ranked[1:10])    #  Top  10  genes
contributing to PC1

  cat("Top 10 genes contributing to PC1 for Dataset", i, ":\n")
```

```
  print(top_10_genes)

  cat("Loading scores for top 10 genes:\n")
  print(pca$rotation[top_10_genes, 1])  # Show loading scores for the top
10 genes
}
```